UNIVERSITY OF CALIFORNIA SAN DIEGO

Metabolite Mediators of Inflammation and Immunity

A dissertation submitted in partial satisfaction of the requirements for the degree

Doctor of Philosophy

in

Biomedical Sciences

by

Ian T. Mathews

Committee in charge:

Professor Mohit Jain, Chair
Professor Sonia Sharma, Co-Chair
Professor Edward Dennis
Professor Ananda Goldrath
Professor Silvio Gutkind
Professor Scott Lippman

2020

The Dissertation of Ian T. Mathews is approved, and it is acceptable in quality and form for publication on microfilm and electronically:

_____

_____

_____

_____

_____

Co-Chair

_____

Chair

University of California San Diego

2020

DEDICATION

to Chris Robinson,

and the wisdom in bringing your own traffic cone

EPIGRAPH

But Sisyphus teaches the higher fidelity that negates the gods and raises rocks. He too concludes that all is well. This universe henceforth without a master seems to him neither sterile nor futile. Each atom of that stone, each mineral flake of that night filled mountain, in itself forms a world. The struggle itself toward the heights is enough to fill a man's heart. One must imagine Sisyphus happy.

Albert Camus

TABLE OF CONTENTS

LIST OF FIGURES

LIST OF TABLES

ACKNOWLEDGEMENTS

Towards the completion of this dissertation, I would like to emphatically thank my advisers Sonia Sharma and Mohit Jain for their continuous edits, moral support, and examples of unerring work ethic. I would also like to acknowledge and deeply thank my partner Samanatha Durfee, my friends Dylan Bacon, Caite Lagers, Staci Fikel, Madison Klug, and Shay Veeder for their noble attempts at keeping my life balanced and occasionally restful.

Chapter 1 is a reprint in its entirety of “Cellular sensing of extracellular purine nucleosides triggers an innate IFN-β response”, by Dhanwani, Rekha; Takahashi, Mariko; Mathews, Ian T; Lenzi, Camille; Romanov, Artem; Watrous, Jeramie D; Pieters, Bartijn; Hedrick, Catherine C; Benedict, Chris; Linden, Joel; Nilsson, Roland; Jain, Mohit; Sharma, Sonia. Science Advances, July 2020. The dissertation author was a co-primary author on this publication.

Chapter 2 is in its entirety a manuscript in preparation, “Circulating linoleoyl-lysophosphatidylcholine is protective in immune checkpoint blockade toxicity”, by Mathews, Ian T; Henglin, Mir; Liu, Mingyue; Mercader, Kysha; Campbell, Allison; Tiwari, Saumya; Dao, Khoi; Quach, Lily; Nguyen, Thien-Tu Catherine; Zheng, Pan; Cheng, Susan; Jain, Mohit; Sharma, Sonia. The dissertation author will be the primary author on this publication.

Chapter 3 is in its entirety a manuscript in preparation, “Bile acid glucosides are predictors of immune checkpoint inhibitor response and promote anti-tumor immunity”, by Mathews, Ian T; Segota, Igor; Henglin, Mir; Mercader, Kysha; Tiwari, Saumya; Palmero, Amelia; Ding, Jeff; Dao, Khoi; Campbell, Allison; Cheng, Susan; Jain, Mohit; Sharma, Sonia.The dissertation author will be the primary author on this publication.

VITA

2014 Bachelor of Sciences, Arizona State University

2020 Doctor of Philosophy, University of California San Diego

Publications

“The Src homology 3 domain-containing guanine nucleotide exchange factor is overexpressed in high-grade gliomas and promotes tumor necrosis factor-like weak inducer of apoptosis-fibroblast growth factor-inducible 14-induced cell migration and invasion via tumor necrosis factor receptor-associated factor 2”. Journal of Biological Chemistry, vol 288, pg 21887-21896, June 2013.

“Implications of Rho GTPase Signaling in Glioma Cell Invasion and Tumor Progression”. Frontiers in Oncology, October 2013.

“Mcl-1 mediates TWEAK/Fn14-induced non-small cell lung cancer survival and therapeutic response.” Molecular Cancer Research, vol 12(4), pg 550-559, April 2014.

“Propentofylline inhibits glioblastoma cell invasion and survival by targeting the TROY signaling pathway”. Journal of Neurooncology, vol 126(3), pg 397-404, February 2016.

“SGEF Is Regulated via TWEAK/Fn14/NF-κB Signaling and Promotes Survival by Modulation of the DNA Repair Response to Temozolomide”. Molecular Cancer Research, vol 14(3), pg 302-312, March 2016.

“Identification of aurintricarboxylic acid as a selective inhibitor of the TWEAK-Fn14 signaling pathway in glioblastoma cells”. Oncotarget, vol 8(7), pg 12234-12246, February 2017.

“HORMA Domain Proteins and a Trip13-like ATPase Regulate Bacterial cGAS-like Enzymes to Mediate Bacteriophage Immunity”. Molecular Cell, vol 77(4), pg 709-722, February 2020.

“Structure and Mechanism of a Cyclic Trinucleotide-Activated Bacterial Endonuclease Mediating Bacteriophage Immunity”. Molecular Cell, vol 77(4), pg 723-733, February 2020.

“Bacterial SAVED/CARF-family effectors respond to 3′–5′ and 2′–5′-linked nucleotide signals in CBASS antiviral immunity” Cell. July 2020.

“Cellular sensing of extracellular purine nucleosides triggers an innate IFN-β response” Science Advances, July 2020.

Fields of Study

Major Field: Biology

Studies in Cancer Cell Biology
Professors Nhan L. Tran and Michael Berens

Studies in Cancer Immunology
Associate Professor Sonia Sharma

Major Field: Chemistry

ABSTRACT OF THE DISSERTATION

Metabolites as Modulators of Inflammation and Immunity

by

Ian T. Mathews
Doctor of Philosophy in Biomedical Sciences
University of California San Diego, 2020

Professor Mohit Jain, Chair
Professor Sonia Sharma, Co-Chair

Immune checkpoint blockade (ICB) monoclonal antibodies are a breakthrough class of immune-activating therapies for the treatment of advanced solid tumors. Limitations on clinical response to ICB include aspects of immunity: i) intrinsic to the tumor, ii) extrinsic to the tumor and derived from peripheral immune fitness and environmental immunomodulatory factors, and iii)

involved in development of therapeutic toxicity. Here, I approach these limitations to ICB response through the measurement and functional characterization of endogenous and exogenous metabolites, effector molecules in the energetic and signaling determinants of immunity.

In studying the determinants of successful intratumoral immune activation, I describe a unique metabolic dysregulation which propagates infection-free induction of type-I interferons, key cytokines in cellular immunity. Cells depleted of ADA2, a purine metabolic enzyme, bear diminished reserved of s-adenosyl methionine, a key cofactor in DNA methylation and repression of genomic endogenous retroviral elements (ERVs). Under alleviated repression, ERVs are expressed and sensed by cell-intrinsic viral sensing machinery, producing type-I interferon induction. This mechanism of purine metabolic reprogramming can be used to significantly alter the inflammatory profile of a tumor towards ICB responsiveness.

In complement, I studied the systemic progression of ICB toxicity, a multi-organ collection of ICB-induced autoimmunity which causes therapeutic termination independent of tumor responsiveness. Loss of two circulating lipid metabolites, LPC (18:2) and LPC (16:0), is observed in patients who develop both ICB-induced and traditional autoimmunity. Supplementation of LPC (18:2) in mice ameliorates deleterious inflammation of chemical or ICB origin via negative regulation of circulating neutrophils, effector myeloid cells in the inflammatory response. This protective effect occurred without impacting anti-tumor immunity, suggesting other pro-resolution metabolites in circulation may similarly regulate toxicity without limiting ICB efficacy.

Finally, I sought to characterize mechanisms of reported influences by the commensal gut microbiome on tumor ICB responsiveness via measurement of microbially derived metabolites in circulation, and their value as response predictive features. I characterize a class of dihydroxy-bile acid glycosides which predict ICB response and are positively regulated by previously characterized response-associated gut microbes. Cumulatively, these observations represent

three approaches to addressing the clinical limitations of ICB interventions through metabolic characterization and reprogramming.

Introduction

Cancer and the Immune System

Immune recognition of neoplastic cells has been a considered paradigm in cancer biology since the early 20th century, coming about contemporaneously with, and partially predicated on, early discoveries on the genetic etiology of cancer. The first postulate in cancer immune recognition is generally attributed to Paul Ehrlich, a German immunologist whose career was best highlighted by notable clinical research in antisera to diptheria and the establishment of the first chemotherapeutic to syphilis (a discovery which also first coined the term “chemotherapy”). Ehrlich came to cancer research late in his career late, in an amusingly contemporary situation of reduced funding for his basic research in immunology intersected by general calls and direct requests of Ehrlich’s by German elites to devote more research to cancer.

At the turn of the century, Ehrlich was a relative outsider to ongoing research in human malignancy. In the late 1800’s to early 1900’s, discoveries in developmental biology and embryology helped couch the mechanisms of cancer development in mechanisms of inheritance, where the genetic material of individual cells randomly accrued errors during cell division, giving rise to malignant cells. Ehrlich, with his background in host response to pathogens and heavily influenced by the work of colleague Robert Koch, hypothesized that these mistakes in cell division would happen “in an overwhelming frequency,” often enough to require recognition and regulation in a process akin to an antimicrobial response. He wrote[1]:

> In the enormously complicated course of fetal and post-fetal development, aberrant cells become unusually common. Fortunately, in the majority of people, they remain completely latent thanks to the organism's positive mechanisms.

Empirical evidence to support this hypothesis would remain elusive for most of the next century; Ehrlich’s own mixed results in immunizing mice with attenuated malignant cells would prove emblematic of the difficulty in experimentally validating what would eventually be called the

hypothesis of cancer immunosurveillance. In fact, greater understanding of adaptive immune recognition of tissue allografts in the early-mid 20th century actively challenged tumor immune surveillance experiments like Ehrlich's as recognition of allogenic tissue, rather than tumor-specific antigens[2]. Not until syngeneic tumor models were developed on long-term inbred mouse lineages was it evident that malignant cells themselves were immunogenic[3,4]. Immunity against syngeneic tumors in mice formed the cornerstone of the cancer immunosurveillance hypothesis, as formed by Sir Macfarlane Burnet and Lewis Thomas[4]. Burnet and Thomas separately postulated the evolutionary root of adaptive cellular immunity observed in allograft rejection was in fact recognition of malignant cells[5], and recognition of tumor-specific antigens occurred throughout the lives of vertebrate animals, preventing disease progression[6]. The correlates of this hypothesis – namely that immunocompromised hosts, unable to effectively eliminate malignant cells, would develop neoplasia more frequently, and that mature tumors in competent hosts somehow overcame this negative selection – would be contested for the remainder of the 20th century.

Experimental Immunosurveillance

Key experiments in mice, undertaken in the period between 1960 through 1980, were seemingly conclusive in their refutation of the cancer immunosurveillance hypothesis. Following Burnet and Thomas, researchers attempted to test whether animals with impaired adaptive immunity developed malignancies more frequently than immunocompetent animals, particularly spontaneous and chemically induced tumors. In rodent models of immunosuppression using anti-lymphocyte serum, no differences in chemically induced tumor incidence were observed[7,8], and inconsistent responses were reported by sex and strain in mice who underwent thymectomy as newborns[9-11]. Extensive testing of spontaneous and chemically induced tumor incidence in the newly developed athymic nude mouse model, while limited to a single mouse strain later found to be metabolically problematic for titration of the carcinogen methylcholantrene (MCA)[12,13],

nonetheless appeared to firmly refute specific tumor immune recognition. Athymic CBA/H mice displayed no difference in tumor induction by MCA[14-16], and had no increased tumor incidence by 7 months of age[14,17,18]. Cumulatively, these studied questioned the import, if not the existence, of an immune-mediated check on neoplastic development.

Support for immunosurveillance resurged as mouse models of immunodeficiency became more nuanced, and our knowledge of cell-based immunity expanded. The role of T-cell mediated immunity was more directly tested in the 1990's and early 2000's, in which signaling via interferon-gamma (IFN-γ) and production of perforin were interrupted and mice were challenged with syngenetic tumors. Tumors developed in mice treated with IFN-γ neutralizing antibody were faster growing and more immunogeneic[19]; similarly, tumors from IFN-γ receptor, α subunit deficient mice were more tumorigenic and immune activating[20]. Loss of the downstream transcription factor STAT1, itself critical for effective T-cell activation, similarly produced more frequent and fast-growing tumors in MCA-treated mice[19]. These were amongst the first substantive rebuffs of the disappointing results in early athymic rodent models of tumorigenesis, reopening the door for the demonstration of an immunosurveillance component to tumor development.

In an analogous fashion, other groups sought to determine whether cytotoxic T-cell effector function, like T-cell activation, was necessary for the immunosurveillance phenotypes observed in mice. Genetic depletion of *Prf1*, the gene which in mice encodes the cytolytic protein perforin released by cytotoxic T-cells, led to higher rates of MCA-induced[21] or spontaneous[22,23] tumors. Of note, it was in comparison of perforin and IFN-γ deficiencies in mice side-by-side where the functional relevance to tumor immunosurveillance of natural killer (NK) and natural killer T (NKT) cells became more apparent[24].

NK cells were first characterized in the 1970's for their cytotoxic activity against syngenetic or allogeneic tumor neoantigen[25-27] or oncogenic viral antigen[28,29], observed in several mammalian

systems including both humans and mice. Natural cell immunity, the cytotoxic effect against aberrant syngeneic target cells observed in *ex vivo* cytotoxicity assays, have credence to a antitumor immune phenotype independent of T-cells or lytic actions of macrophages. of A firm definition of these populations, necessary for their detailed study in immunosurveillance, was elusive for much of the subsequent decades, however. Without these, the ability to rigorously test the effects of NK cells in immunosurveillance furthered the field's stagnation.

In time, surface marker validation in mice and in humans allowed for the definitive identification of NK populations, contemporaneously with directed IFN-γ pathway knockout studies in mice[30,31]. Characterization of these cells helped add nuance to a few of the persistent critiques of immunosurveillance, particularly around the negative results of athymic mice. Identification of NK populations with and without T-cell receptors which persist in athymic mice[32] helped explain persistent immune recognition of tumors despite T- and B-cell deficiency in neonatal thymectomy. In addition, the synergistic, non-overlapping effects on anti-tumor immunity of IFN-γ and perforin knockout mice is partially explained by the existence of NK cells, which also release perforin in their cytotoxic actions, but are predominantly IFN-γ secreting cells and show greater dependence on Type-I Interferon (IFN-α/β) in their function[21,23,24].

An iterative expansion of knowledge around natural and cell-mediated immunity proved less revelatory in its support of the immunosurveillance hypothesis than the experiments which followed the development of RAG-deficient mice. RAG-1 and RAG-2 are recombination activating genes expressed exclusively in the immune compartment, and are critical to the maturation of T- and B-cell antigen-specific receptors[33]. Unlike previous attempts to interrupt V(D)J recombination, notably DNA-PKcs knockout in mice, RAG-1/2 restriction to the lymphocytic compartment minimized the compounding factor of diminished DNA double-stranded break repair in tumorigenesis[34,35]. Genetic depletion of either RAG-1 or RAG-2 leads to complete depletion of T-, B-, and NKT-cells[33], and in these mice, both MCA-induced and spontaneous tumors of varied

histologies developed more frequently than co-housed wild type controls[36]. Of note, there is evidence RAG-1/2 knockout is incomplete in its ablation of tumor immunosurveillance; mice deficient in both RAG-2 and STAT1 (RkSk) developed spontaneous breast tumors not observed in single knockouts or wild-type controls[36]. RAG-$2^{-/-}$ mice also retain NK cell-mediated tumor immunosurveillance, supported by the observation that RAG-$2^{-/-}$ crossed with $\gamma c^{-/-}$ mice develop MCA-induced sarcomas at greater frequency than RAG-$2^{-/-}$ deficiency alone[37].

Efforts to experimentally test the tumor immunosurveillance hypotheses of Burnet and Thomas produced an image of tumor maturation alongside selection by the adaptive and innate immune systems. Cumulatively, these critical experiments support a more comprehensive program of immunosurveillance in rodents than originally respected, including both αβ and γδ T-cells[38], NK cells, and NKT cells. Nascent tumors experience unique combinations of lymphocytic and myeloid selective pressures inherent to their original tissue niches. This concept, where mature tumors are the product of a diverse collection of imperfectly selective pressures from the immune system, was coined by Robert Schreiber and others as cancer immunoediting[39], and will prove critical to the utilization and honing of immunotherapy to treat human tumors.

Immunoediting in Human Tumor Development

Central to the concept of immunoediting is the correlate that selective pressure from the immune system “sculpts” nascent tumors during neoplastic development. Tumors derived from nude[40], severe combined immunodeficiency (SCID)[41], or RAG-1/2 deficient[36] mice support this idea, as they are more immunogenic and are frequently rejected when transplanted to same-strain, immunocompetent hosts. Whether this process shapes the immunogenicity of human tumors, or indeed whether immunosurveillance meaningfully occurred in humans, was more difficult to definitively establish. First, the components of cell-mediated and natural immunity evidenced in rodent models are conserved in humans[39,42]. Natural experiments to test the immunosurveillance hypothesis in a manner analogous to RAG-1/2 deficiency in mice is limited

to retrospective studies of immunosuppressed individuals (secondary) or congenital immunodeficiency (primary). The first multi-cohort studies of patients from 1960-1990 of induced immunosuppression following organ transplant, here using cytostatic agents (cyclophosphamide, azathioprine)[43,44], supported immunosurveillance in humans but with an important etiological asterisk. A striking majority of tumors which presented with higher frequency in transplant patients have known viral etiology, including sarcomas and carcinomas caused by HPV, HSV-8, and Epstein-Barr virus. AIDS patients often presented with the same classes of cancers, particularly Karposi sarcoma[45]. These first observations supported that immunosuppressed individuals were more susceptible to oncogenic viruses, but lacked definitive evidence for increased tumors of non-viral etiology. Later retrospectives focused particularly on cancers without known viral origin; three main clinical data repositories (the Cincinnati Transplant Tumor Registry (CTTR) in the US, the Nordic Renal Transplant Registry (NRTR) in Denmark, Finland, Norway, and Sweden, and the Australian and New Zealand Transplant Registry (ANTR)), reported solid tumor incidence at 2-25 times the normal population rate in transplant patients[43,46-49]. Of note, at least one study suggested the relative increased risk of cancer was higher among patients who received transplants in their youth rather than later in life[47], and the strength and duration of secondary immunodeficiency appear to directly correlate with incident cancer risk[50]. Increased non-viral tumor incidence was confirmed in non-white populations, though significant variability in risk profiles exist between races, including in non-skin malignancies[51]. Retrospective evidence of non-viral cancer risk in immunosuppressed patients is contemporaneously well-established.

Cancer risk from primary immunodeficiencies, or congenital immunodeficiency, is comparatively more challenging to study than secondary immunodeficiencies largely due to the relative paucity of cases. One larger cohort from the Immunodeficiency Cancer Registry, which highlighted 145 mixed-presentation primary immunodeficiencies who developed cancers, of which SCID patients were only nine, indicated these where primarily lymphocytic in origin[52].

Collation of this and other, smaller clinical retrospectives promote that primary immunodeficiencies do indeed produce tumors more frequently than the general population, but that the number of such cases are marginally less frequent than patients undergoing secondary immunodeficiencies[53,54]. More recently, the larger United States Immune Deficiency Network (USIDNET) registry effectively confirmed a modest higher incidence in primary immunodeficiency, though predominantly in men, and predominantly in patients with common variable immunodeficiencies (CVID)[55]. Unlike SCID patients, patients with CVID experience intermittent immunoinsufficiency secondary to depleted immunoglobulin in circulation[56]. These patients sproadically develop autoimmune-like inflammatory disorders secondary to increased frequency of bacterial and viral infections[56,57]. These patients also develop malignancies at a higher frequency, developing gastric cancers and hematological malignancies, particularly Hodgkin's lymphoma[58,59]. SCID patients, though a less frequent primary immunodeficiency and develop cancer less frequently than CVID patients, also appear to experience cancer at higher rates than the normal population[52,53,55]. One potential interpretation of this seeming paradox – individuals with incomplete immunodeficiencies appear to have a higher frequency cancer incidence than individuals with more complete immunodeficiencies – may lie in the complex role inflammation plays in tumorigenesis.

Critical to immunoediting in humans is the dual role of the immune system in tumor development; both the immunosurveillance role T-, NK-, and NKT-cells play in selecting against immunostimulatory clones, but also in the formation of a tumor-promoting inflammatory niche. The role of co-opted myeloid immune cells in the tumor microenvironment is of particular importance to immune escape. Both classical[60,61] and non-classical[62] monocytes are cytolytic against malignant cells, and home to primary and metastatic tumors in a CX3CR1/CCR2-dependent manner for this purpose[63-65]. Once these monocyte populations reach tumors, however, they differentiate into many of the myeloid-derived populations which frequently promote

tumorigenesis and immune evasion by providing a cytokine-dependent inflammatory signal, boosting tumor growth and dampening anti-tumor cytolytic activity.

Tumor-associated macrophages (TAMs) are a well-characterized example[66] of the multitude of myeloid-derived intratumoral populations, which include neutrophils of varied maturity[67], mature and pre-dendritic cells, undifferentiated monocytes, and the heterogenous myeloid-derived suppressor cell (MDSC) populations. TAMs are seeded intratumorally by monocytes in early malignancies, but are a self-sustaining population following differentiation and during tumor development[68,69]. Clinically, TAM cellularity inversely correlates with overall patient survival[70,71]. This effect appears to be hypoxia-inducible factor (HIF)/cAMP response element modulator (CREM)-dependent in TAMs, spurred by the low-pH, low oxygen environment within tumors[72-74]. In conjunction with low basal activity of the NFκB and STAT3 transcription factors, TAMs produce a profile of inflammatory regulatory cytokines and prostaglandins for sustained, tumor-promoting paracrine signaling[75]. TAMs coordinate the proliferation of cancer cells in their release and processing of EGF, FGF, PDGF, and TGFβ[76-79], they reshape the stromal and vascular microenvironment towards tumor progression through the release of VEGF and multiple matrix metalloproteinases[80-84], and they promote chemotherapeutic resistance in cancer cells, predominantly through anti-apoptotic signaling downstream of IL6 production[85].

The tumor-promoting properties of TAMs are synergistic with, and derived from, their role in tumor-promoting, low-level inflammation. The characteristics of TAMs described above are predominantly those of M2-polarized macrophages, one pole on a phenotypic spectrum observed in TAMs between immune-activating M1-macrophages and immunosuppressive M2-macrophages. Multiple excellent reviews of these polarizations in tissue-resident macrophages have been produced elsewhere[80,86,87], as well as manuscripts covering the plasticity of the M1/M2 distinction and the challenges in effectively identifying these (perhaps overly simplified) classes as distinct populations *in vivo*[88,89]. M2-polarized macrophages are often generalized as

immunosuppressive. Production of IL10 and TGFβ are central to this characterization; M2-macrophages release IL10 and TGFβ to recruit $CD4^+$ regulatory T-cells (Treg)[90] and blunt the expansion of cytolytic $CD8^+$ T-cells[91]. IL10 in particular may promote new monocyte differentiation to M2-like macrophages intratumorally, rather than cytolytic cells or anti-tumor dendritic cells[92]. Critical, however, are TAM cell-cell interaction mechanisms in antigen presentation, and their regulation of cytotoxic T-, NK-, and NKT-cell activity.

Human tumors frequently shed the components of cytotoxic adaptive immunity developed as antiviral mechanisms during tumorigenesis. Some neoplastic cells, including in breast, colorectal, prostate, and melanoma tumors, have been reported to lose one or more of the three HLA subunits which make up MHC-I in humans[93,94]. Normal and malignant cells expressing MHC-I regularly present self-antigen for recognition by $CD8^+$ T-cells, a process with high enough sequence resolution that mutant epitopes can be recognized as cancer neoantigens and induce T-cell activation with some fidelity[95]. Therefore, the loss of antigen presentation in MHC-I downregulation is a direct means of immunoevasion by malignant cells. NK-cells likely play a role of elevated importance in this context; MHC-I/II recruitment to cell surfaces in tumors is directly related to IFN-γ[96,97], but inversely correlated with NKG2D ligand expression on tumor cells[98,99], indicating NK-mediated immunosurveillance against cells depleting MHC-I. Indeed, NK-cell cytolytic action is increased against cells with diminished MHC surface expression[98].

Here we see antigen presentation as a critical example of the synergistic, occasionally counter-intuitive roles different immune cells play within the tumor microenvironment. There's evidence M2-like TAMs upregulate the non-canonical HLA family member HLA-E and HLA-G, while downregulating classical HLA-A, -B, and -C similarly to neoplastic cells[93]. The function of these noncanonical HLAs are distinctly immunosuppressive. Macrophage HLA-G interacts with the costimulatory molecule ILT2 on T-cells, blunting T-cell priming[100-102]. Similarly, NK-cells become anergic in response to macrophage HLA-E binding of NKG2D on the NK-cell surface[101]

in a manner analogous to MIC-NKG2D interactions leading to NK priming[103]. This concept – competition for a stimulatory molecule on a cytolytic cell during antigen presentation – is crucial to the adaptive immune receptor family at the heart of modern cancer immunotherapy: the B7 family of coinhibitory receptors, more broadly known as the immune checkpoint.

The Immune Checkpoint and Checkpoint Blockade Therapy

Both the cell-based and humoral arms of the human adaptive immune response involve the immune synapse, the interface between an antigen presenting cell and a putative antigen recognizing cell. B-cells, αβ and γδ T-cells, NK- and NKT-cells alike form an immune synapse when interacting with MHC or MHC-like antigen presentation complexes on a target cell. In cancer immunosurveillance, a simplified version of the immune synapse is between the antigen presenting cell bearing a tumor neoantigen epitope and a cytolytic $CD8^+$ T cell with an αβ T cell receptor specific for that epitope. In this synapse, two cell-cell interactions are necessary. First, the T-cell receptor must recognize and bind the epitope-bound MHC-II on the antigen presenting cell. One could consider this interaction as the determinant of the response's magnitude – successful epitope recognition predicates a response from the T-cell, and a particularly immunogenic antigen may induce a more robust immune response. But the direction, whether the cell is primed for effector function or pushed towards senescence after recognizing antigen, is determined by the second interaction with the antigen presenting cell. T-cell priming following antigen recognition is propagated by a costimulatory signal, most canonically CD28 on the T-cell surface interacting with CD80/CD86 on the antigen presenting cell. Both signals induce a STAT1-dependent signal transduction platform which in turn induces expansion and cytolytic activity[19], in this case against cells bearing the cancer neoantigen being presented.

Like antigen presentation, costimulatory signals come in many different colors and shades for different contexts of priming at the immune synapse. Three families of costimulatory molecules relevant to CD8 T-cell activation had been broadly characterized by the turn of the 21st century:

CD2-, LFA1-, and CD28-interacting receptors[104]. CD2 is an immunoglobulin-like cell adhesion molecule[105] on cytotoxic T-cells and NK-cells which binds APC-expressed LFA3. Costimulation experiments with human peripheral lymphocytes indicate CD2-LFA3 interaction appears to be of particular importance in memory T-cell activation and long-term function[106-108]. LFA1, a CD11/CD18 integrin heterodimer (αLβ2), is broadly expressed on T lymphocytes and recognizes APC-expressed ICAM family adhesion receptors[109]. LFA1 acts as a costimulatory molecule predominantly by being an anchor, spatially organizing the TCR-MHC interface[110] through dynamic actin polymerization and myosin contraction, stereotactically stabilizing the immune synapse[111,112] (a valuable review of the spatial dynamics of the immune synapse can be found here[113]). In fact, LFA1 is not a mutually exclusive coactivator of T-cell function; LFA1-ICAM interactions promote the spatial organization and stability of CD28-CD80/86 costimulation by the same mechanism: constructing a peripheral supramolecular activation cluster at the immune synapse[114,115] There is some evidence of mutual exclusivity between $CD28^+$ and $CD2^+$ T-cells[107], however; CD28 is another immunoglobulin-like coactivator, though predominantly expressed on naïve and effector CD8s, suggesting costimulatory molecules may contribute to T-cell fate determination and immunological memory. Loss of CD28 is a sign of repeated antigen stimulation, often associated with T-cell senescence[116]; expansion of these $CD28^-$ $CD8^+$ T-cells is a feature of aging and associated pathological inflammation[117]. Of these three costimulatory molecules expressed by T-cells, CD28 is by far the most well-studied, especially in the context of cellular immunity and cancer.

CD28 binds either of two B7 ligand family members on APCs, CD80 or CD86, to produce the necessary costimulatory signal at the immune synapse for T-cell activation. To do this, CD28 competes with the coinhibitory receptor CTLA4, the first such receptor to be exploited as a clinical target in the treatment of solid tumors and a quintessential example of what is commonly referred to as the immune checkpoint. When CTLA4-CD80/CD86 interactions predominate at a T-cell –

APC immune synapse over CD28, this clonality is suppressed from expansion, and the T-cell becomes senescent. While the predominant mechanism of CTLA4-mediated coinhibitory action is not established, it is generally accepted that both a signal transduction-derived and a sterically-derived mechanism occur in blunting T-cell activity, both of which directly interfere with CD28 function. When bound to CD80/CD86, CTLA4 interacts directly with PP2A serine/threonine phosphatase and indirectly with the tyrosine phosphatase SHP2[118], though the functional relevance of SHP2 interaction is questionable beyond sequestering SHP2 from CD28[119]. PP2A function following recruitment to CTLA is better understood: CTLA4 inhibits AKT-mediated glycolytic function via recruitment and activation of PP2A[120]. PP2A phosphatase recruitment also may blunt IL2 production[121] downstream of CD28 activty[122]. Sterically, CTLA4 acts as a competitive inhibitor of CD28, binding CD80/CD86 with greater affinity than CD28[123]. There's evidence which indicates CTLA4-CD80/86 interaction can sequester the B7 ligands via endocytosis in *trans*, and that this occurs only upon successful TCR engagement[124].

CTLA4 was first characterized as a CD80/CD86-recognizing T-cell restricted receptor in humans during the 1980's[125,126]; its affinity for B7 family ligands and expression on antigen mature T-cells originally promoted CTLA4 as a costimulatory CD28 analogue[127,128]. These included at least one study where CTLA4-blocking antibodies, the eventual therapeutic modality used to boost anti-tumor immunity years later, indicated CTLA4 inhibition could actually boost T-cell proliferation *in vitro*[127,128] In 1994, Walunas *et al* provided the definitive experiment on CTLA4 function at the immune synapse, indicating that in the context of CD28 engagement, CTLA4-CD80/CD86 interaction blocks T-cell expansion[129]. This experiment, in combination with later studies tied to the mechanisms of coinhibitory signaling behind CTLA4 activation and the consistent observation of CTLA4 induction upon CD28 activation, cemented the principal role of CTLA4 as a rheostat on T-cell activation, tuning down CD28-mediated expansion when necessary to avoid action against self-tissue. CTLA4 became the first molecule to be characterized as a

member of the homeostatic immune checkpoint, showing resurgent anti-tumor immunity *in vivo* when blocked[130].

Influencing costimulatory signals towards boosting immune activation has been a stated ambition of clinical oncologists and cancer-focused immunologists since at least the 1990's. Their interests came to fruition with the development of Ipilimumab, the first therapeutics targeting the immune checkpoint with demonstrable clinical efficacy in cancer patients, in 2000[131]. Ipilumumab is a humanized, IgG1 isotype monoclonal antibody targeting CTLA4 – specifically, it was found Ipilimumab interacts with a CD80/CD86-facing β-sheet on the extracellular domain of CTLA4, sterically blocking coinhibitory action[132]. The first trials conducted by ipilimumab developers Medarex, and later licensed to Bristol-Meyers Squibb, were in metastatic melanoma, and produced modest results[133]. The toxicity profile for Ipilimumab was of particular concern as clinicians considered whether and how to use this new class of anti-cancer agent: even in small pre-trial studies, immune related adverse events (irAE) were more common than anti-tumor response[131,133,134]. Dosing and irAE mitigation for ipilimumab was matured over the next several years such that in 2010, where other CTLA4-targeting agents, most prominently tremelimumab, failed in Phase III clinical trials of advanced melanoma[135], ipilimumab was successful[136]. Of note, while this trial offered a modest 23% response rate and 3.6 month median survival benefit for ipilimumab, evidence arose from these and future studies of durable long-term benefits for most responders[136,137]. Potential for a sustained anti-tumor immunological memory after termination of ipilimumab opened the door to treating advanced solid tumors with a wider array of immune checkpoint targeting therapies.

Through that door walked monoclonal antibodies targeting PD1/PD-L1 interactions, a therapeutic class which rapidly outshone ipilimumab for its comparatively infrequent rate of irAE development[138]. Like CTLA4, PD1 is a B7 family receptor expressed on T-cells, though PD1 recognized the ligands PD-L1 and PD-L2. PD1 also recruits SHP2 upon activation and blunts

CD28-derived, Akt-mediated glycolytic expansion, though this is dependent on phosphorylation of PD1's ITIM/ITSM domains[120,139,140]. Immune checkpoint contextualization for PD1 has some important distinctions from CTLA4, however. For starters, while CTLA4 is T-cell restricted in its expression and is the dominant immune checkpoint receptor in tertiary lymph nodes[141,142], PD1 is expressed on T-, B-, and NK-cells[143,144], which recognize a dynamically expressed PD-L1 ligand on tumor cells to similar immunosuppressive effect[145,146]. Unlike CTLA4, which predominantly regulates $CD4^+$ T-helper cells and regulatory T-cells (Treg) (a leading candidate for the cause of its comparatively high irAE incidence profile[147]), PD1 utilization is more broad, and its repression is more beneficial to the expansion of exhausted $CD8^+$ effector T-cells in the tumor microenvironment[148,149]. These observations of CTLA4 and PD1 partial exclusivity in their immunosuppressive roles promoted the development of PD1-targeting therapeutics as complementary, and potentially superior, immune checkpoint blockers.

It is perhaps not surprising then when nivolumab and pembrolizumab, both IgG4 isotype monoclonal antibodies against PD1, were tested in metastatic melanoma or lung adenocarcinoma, they consistently induced anti-tumor response at comparable or superior levels to ipilimumab monotherapy, and induced Grade III/IV (severe) irAEs with less frequency[150,151]. Of note, the nature and intensity of irAEs developed on PD1-targeting blockade were often in distinct organ systems than ipilimumab[138,152]; while both treatments induced skin and gastrointestinal inflammation with some regularity, conditions like hypophysitis and pneumonitis were almost entirely target-specific. Differential irAE profiles lent credence to the theory, supported in part by *in vivo* PD1 and CTLA suppression comparative studies of autoimmune development[139,153], which purported the two coinhibitory molecules served nonredundant roles in suppressing anti-self immunity. Evidence for PD1 and CTLA4 exclusivity has expanded as ipilumumab, nivolumab, and pembrolizumab's indication has expanded to less severe tumors of broader histology. Nivolumab and pembrolizumab, owing to their lower toxicity profile, are as of 2016 first-line therapies for the

treatment of metastatic melanoma and non-small cell lung carcinoma[154,155], but all three are being tested as potential therapeutics in the treatment of a diverse array of solid tumors. Importantly, the treatment of advanced solid tumors is increasingly moving towards ipilimumab + anti-PD1 combination therapy, where strong evidence for synergistic response has been observed in advanced melanoma[156,157] and increasingly NSCLC[150]. Response rates in melanoma can reach nearly 60 percent for combination ipilimumab/nivolumab[156], an unprecedented advance in the treatment of this hyperaggressive malignancy. Nonetheless, the compounding nature of irAE development in combination therapy[158] measured against a persistently unresponsive population of immune checkpoint blockade patients firmly defines the horizon on a rapidly developing immune oncology field.

I will conclude this section on the immune checkpoint by introducing the next generation of immune checkpoint targeting therapies, many of which are in clinical or pre-clinical development. There are numerous excellent reviews in this space[159-161], but for the purposes of introducing clinical approaches to overcoming continued unresponsiveness to immune checkpoint inhibition, I will briefly summarize the alternative targets approach here.

Broadly, next-generation immune checkpoint inhibitors fall into two categories: those targeting other coinhibitory molecules (B7-H3, BTLA, LAG3, TIM3, TIGIT, VISTA), and those which act as activators of costimulatory molecules (OX40, 41BB, GITR, ICOS). The former holds a similar level of promise to what preclinical research into PD1 inhibition produced for CTLA4 exclusivity. The CD4 homologue LAG3, for instance, had broad lymphocytic distribution, expressed on $CD8^+$, $CD4^+$ helper T-cells[162] and consistently by regulatory T-cells[163], but specifically recognizes the cellular immune antigen presentation complex MHC-II as its ligand. MHC-II recognition may suggest a $CD8^+$ restricted functionality, but significant evidence from *in vivo* studies indicate LAG3 targeted antibodies which do not interrupt its interaction with MHC-II still powerfully block its coinhibitory action[162,164], potentially via Treg repression intratumorally.

Significant research on the direct function of LAG3 may be required to fully understand the indication of its targeting antibodies, but its synergistic function with PD1 in T-cell anergy[165,166] and tumor rejection[167] remain promising. Indeed, the non-overlapping nature of blocking PD1 and BTLA[168], TIM3[169], TIGIT[170], or other coinhibitory molecules in combination[165] indicate the stacking phenomenon observed in CTLA4/PD1 combination therapy is a useful model to pursue additional immune checkpoint blockade responsiveness.

Induced activation of costimulatory molecules, including receptors like 41BB, GITR, ICOS, and OX40, is similarly synergistic with suppression of coinhibition[171-174]. Like CD28, these costimulatory receptors detect cognate ligands on antigen presenting cells towards immune activation, and can be induced to this effect through agonist-like antibody interactions. The CD28 homologue ICOS is a particularly interesting case study of costimulatory agonism in combination with coinhibitory blockade, particularly with ipilimumab. Clinical evidence of ICOS upregulation on tumor-infiltrating effector T-cells following anti-CTLA4 treatment[174] coincides nicely with the preclinical observation of ICOS/CTLA4 synergy[175]. Early phase clinical trials exist for all of these costimulatory agonists, though early data does suggest the irAE profiles involved would require significant tuning of dose and combination PD1/CTLA4 regimens.

Cumulatively, the immune checkpoint is the culmination of over a century of establishing, overturning, and re-establishing the role for the immune system as a check on neoplasia. Immune checkpoint inhibitors are a breakthrough class of immunotherapies for the treatment of advanced solid tumors. In the wake of the immune checkpoint's still fresh clinical successes, we are considering the new and challenging indications for unresponsiveness, in order to better understand how tumors adapt to existing immune checkpoint blockade.

Factors Limiting Immune Checkpoint Blockade Response

The best objective response to immune checkpoint blockade to date was observed in advanced melanoma with combinatory ipilimumab and nivolumab. The Phase III study of this

combination against ipilimumab or nivolumab alone reported a 58 percent survival rate at three years post-initiation[156], which by any previously established endpoint metric in the treatment of advanced melanoma is definitively fantastic. In examination of this cohort, there are key observations to be made around responsiveness and the selection criteria for this study. First, treatment-associated irAE in the nivolumab plus ipilimumab arm of CheckMate 067 were among the highest reported for an immune checkpoint-based therapy. Of these patients, 59 percent of patients acquired severe (Grade III/IV) irAE, and 39 percent of patients were forced to discontinue therapy do to the severity of their irAE. Second, patients were genetically profiled prior to starting therapy, where *BRAF* V600 mutational status, a common oncogenic driver mutation in melanoma with direct correlates to higher tumor infiltrating lymphocyte (TIL) proportions[176,177] and a higher neoantigen load[176]. Approximately 33 percent of each arm were BRAF V600 mutant, a characteristic which proved to be one of the best predictors of responsiveness to nivolumab and ipilimumab combination, particularly in comparison to nivolumab alone. Finally, patients were specifically selected who had not received previous immunotherapy; in a prior phase I trial of concurrent ipilimumab plus nivolumab or nivolumab patients previously given ipilimumab, there were objective response differences between the groups. Patients who received sequential treatment had at 20 percent objective response rate, compared to the 40 percent rate observed in the concurrent cohort[178]. Concurrent therapy may be more beneficial because of a stronger, more acute immune induction in this regimen compared to sequentially given immune checkpoint blockade, but it may also be evidence for a resistance mechanism by which patients previously treated with immunotherapy are less responsive to new blockade treatment writ-large. Those who designed the study took these factors into account as potential influencing factors for how patients may or may not respond to immune checkpoint blockade.

Here, my dissertation will outline in Chapters 1, 2, and 3 different approaches taken to boosting response to immune checkpoint blockade that consider three paradigms of limitation to

response, including tumor-intrinsic factors, tumor-extrinsic factors, and factors which regulate irAE progression as a response-limiting outcome.

Tumor Intrinsic Response Factors

Significant translational research efforts have been applied to understanding what a responsive tumor looks like compared to an unresponsive tumor prior to giving immunotherapy. The dichotomous comparison approach to understanding response has clear utility in understanding the intratumoral immune landscape for responders versus non-responders, but it also has basis in the logistics of clinical oncology. Tumor biopsies at baseline are common practice in the age of targeted therapies, often secondary to surgical tumor resection as intervention but increasingly as a minimally invasive diagnostic measure, and are predominantly used for baseline genetic profiling. In melanoma, whether patients receive BRAF-targeting therapies dabrafenib or vemurafenib is dependent on determining BRAF mutational status[155]; similar considerations are made for EGFR mutations and erlotinib/gefitinib treatment in lung carcinoma[154]. Whole genome and transcriptome studies on population-level, multi-institutional cohorts can come from the same biopsies, producing resources like The Cancer Genome Atlas (TCGA) datasets where robust outcome associations can be tested[179]. It's from tumor biopsy sequencing datasets that some of the first tumor-intrinsic hypotheses around immune checkpoint blockade responsiveness were tested.

An early observation in clinical immune checkpoint blockade (ICB) response studies was on mutational burden and neoantigen incidence. A well-supported correlate in ICB efficacy is, given the immune checkpoint acts predominantly at the immune synapse in cellular immunity, that anti-tumor immunity must recognize tumor-specific epitopes. Candidate epitopes fall into two camps: tumor antigens as ectopically expressed self-antigens, where proteins normally restricted to certain organs and cell types are inappropriately expressed by tumors, or full-scale neoantigens, where nonsynonymous mutations in the tumor genome are reflected as non-self

antigens in their cognate proteins. Due to the nature of T-cell maturation, central tolerance at the thymus of organ-specific self antigens make the contribution of ectopically expressed wild-type genes as immunogenic in cancer unlikely. Therefore, characterizing immunogenicity from neoantigens and how neoantigens were derived is critically important in understanding tumor intrinsic response factors. Neoepitope availability appears to be a baseline requirement – tumors with low mutational burden are weakly responsive to immune checkpoint blockade, most likely owing to the lack of new epitopes of any immunogenic character to be recognized[180,181].

Identifying the character of neoantigen remains challenging but nonetheless central to predicting tumor responsiveness with greater accuracy. Identifying putative neoantigens can partially be performed *in silico*[95], detecting tumor nonsynonymous mutations within the exome, cross-referencing against transcriptome data to monitor whether these neoepitopes make their way into transcript. An active area of research involves scoring these candidate neoantigens on likely immunogenicity, a multiparametric score which integrates empirical observations of what previously immunogenic neoantigens look like[182-184], including through machine learning-based structural recognition[185] or immunoprecipitation of MHC and mass spectrometry-based detection of bound antigen[186].

These methods are exceptionally good at identifying neoepitopes based on presentation character, but accurately predicting the immunogenicity, and beyond that responsiveness to immune checkpoint blockade, of tumors remains challenging. The first reason is incredibly familiar in oncology: tumor clonality. It is predicted that 92 percent of MHC-II presented neoantigens are derived from passenger mutations; from MHC-I, nearly all neoantigens are passenger[95]. Initial responses to immunotherapy likely don't require ubiquitous mutations, as long as a sufficient number of cells bear neoantigens to be recognized by newly revitalized cytotoxic T-cells. The dream of immunologic memory secondary to immune checkpoint blockade is hampered significantly, however, if a class of neoantigens is not recognized which is either a driver mutation

and therefore more necessary to tumor recurrence, or is ubiquitously expressed by enough clonal populations in the tumor to be effectively discriminatory. Indeed, what studies exist of longitudinal patient tumor biopsies indicate the neoantigen repitore is actively edited over the course of therapy. Further, TCGA data mining for putative neoantigens indicates neoantigen frequency is less in mature tumors than would be predicted by chance[187], indicating immunogenic neoantigens are actively selected against in a likely tumor extrinsic manner. There are even preclinical data which suggest neoantigen repression occurs in a manner intrinsic to the malignant cell, via epigenetic repression of immunogenic neoantigen expression[188]. Collectively, these observations indicate neoantigen profiles are actively remodeled during tumor progression and on therapy in a manner which to which clinicians must actively adapt. Currently, heroic efforts are underway to make longitudinal neoantigen profiling from serial biosampling[189] and even cell-free tumor DNA in circulation[190,191] more accessible and informative, and even to develop personalized vaccines around patient-specific neoantigen profiles.

An important caveat of neoantigen profiling is the enormity of factors beyond the immune synapse which dictate a successful immune response. Clinical data indicating tumors with high mutational load and high neoantigen abundance can still be unresponsive to immune checkpoint blockade support the conclusion that when mature tumors do not actively repress the expression of their neoantigens, they promote an immunosuppressive microenvironment. Tumor associated macrophages (TAMs) were discussed earlier in this context for their immunosuppressive capacity; after recruitment to the tumor microenvironment, anti-tumor monocytes differentiate to TGFβ, IL10, and growth factor producing macrophages which promote tumorigenesis[66,80]. Of note here is the ordering of events. M2-like macrophages help coordinate an inflammatory, immunosuppressive niche in the tumor microenvironment, but the queues which promote their differentiation from monocytes and polarization towards M2-like macrophages and dendritic cells are themselves immunosuppressive. Monocytes may differentiate in response to direct interaction

of monocytic CD11b with CD90 expressed on malignant cells[192], but are further driven towards a more protumoral phenotype through sensing a low oxygen, acidic environment[72-74,84]. M2-like TAMs contribute to the metabolic tumor niche even further as high expressors of arginase and indolamine-2,3-dioxygenase (IDO), catabolic enzymes which limit extracellular pools of arginine and tryptophan, respectively[82,193,194]. Development of an immunosuppressive tumor microenvironment is iterative and highly responsive to challenge by cellular immunity.

An intriguing corollary to this observation is the dependency of immunosuppression in the tumor microenvironment to the magnitude of cellular immune activation. Induction of macrophage-derived IDO, the expression of PD-L1, and even the CCL22-dependent recruitment of Treg cells to the tumor microenvironment has been linked to $CD8^+$ T-cell production of IFNγ upon activation[195], analogous to $CD8^+$ T-cell pressure-dependent epigenetic repression of neoantigen expression[188]. Anthropomorphically, it's in the interest of mature tumors to adopt immunosuppressive mechanisms like these to limit intratumoral effector T cell function; clinical evidence is modest but consistent for the dependence of non-anergic effector T cells in the tumor microenvironment on immune checkpoint inhibition[196,197] and overall survival[149,198]. Anergy is key here – $CD8^+$ T-cells expressing PD-L1 (often used as a proxy for exhausted or anergic effector cells) do not have the same clinical correlates[149]. Similarly, the ratio of $CD8^+$ effectors to Tregs appears to be critical in identifying responsive tumors[198,199] Indeed, some of the same microenvironmental determinants of effector T-cell expansion, including available amino acid, free fatty acid, and glucose, drive Treg recruitment and suppressor function[200-202].

More broadly, the cellular profile of a tumor (and the metabolic determinants thereof) can be observed as phenotypically distinct in the clinic. Dichotomous comparisons of responder vs non-responder tumor transcriptomes have been utilized to understand what gene expression patterns are unique to responsive tumors. Recent studies employing this approach will often identify hits in two broad classifications of gene functions. The first, associated with effector

function, will frequently identify genes important to antigen presentation, recognition, and clonal expansion as differentially expressed between baseline response categories. MHC presentation[203], IFNγ, TCF7, and EOMES$^+$ signatures (associated with effector memory CD8$^+$ T-cells)[204], and increasingly antiviral type-I interferon signaling[205,206]. The stories told by these transcriptomic surveys, while not overlapping in distinct genes, indicate immune checkpoint blockade is most successful in tumors with immunological memory for tumor neoantigen, and have the capacity to reawaken effector memory populations in the tumor following treatment with a PD1-blocking antibody. Further, the synergistic nature of type-I interferon induction with *in vivo* studies of ICB efficacy[207-209] indicate responsive tumors more successfully engage cellular innate immunity than non-responsive tumors.

The second important transcript-level determinant of ICB responsiveness is around genes controlling genomic stability. Deficiencies in BRCA1 and BRCA2, both regulators of DNA double stranded break repair, tend to associate with more responsive tumors[210]. Mismatch repair genes more broadly are overexpressed in responsive tumors[211,212]. Interestingly, the hereditary condition Lynch syndrome, where microsatellite instability and subsequent progression to colon carcinoma is relatively common[213], frequently bear more ICB-responsive tumors[212]. Several research initiatives into boosting tumor genomic instability, and therefore ICB responsiveness, are underway. Among the most compelling are efforts to utilize conventional chemotherapy and radiotherapy to promote additional antigenicity out of tumors. Early clinical studies indicate genotoxic stress boosts CD8$^+$ T-cell reactivity and IFNγ production[214-216], important priming characteristics of an effective immune checkpoint blockade outcome.

In summary, approaches to improving immune checkpoint blockade response which address the limits imposed by tumor intrinsic factors seek to characterize and boost the immunogenicity of tumor neoantigens, to promote genomic instability, and to limit the cellular and

microenvironmental suppressive nature of tumors by inducing type-I interferons and blunting TAM/Treg cytokine production.

Tumor Extrinsic and Environmental Response Factors

Returning once again to CheckMate-067[156] for insights on what makes an ICB-responsive tumor, there are two easily overlooked outcomes in the ipilimumab plus nivolumab arm that are worth consideration here. The first is on age – patients over the age of 65 were much less likely to respond positively to combination therapy over nivolumab alone. There are some pretty clear assumptions that can be made to explain this observation, not the least of which being older melanoma patients tend to have poor survival rates compared to younger patients independent of therapy[217]. Additionally, there's growing evidence immune fitness decreases as we age. Experimentally, the loss of Tet2 and DNMT3A models the loosening grip of epigenetic regulation our cells hold as we age, and these mice tend to develop more severe and long-lasting deleterious inflammation following challenge[218-221]. The unwinding with age of immunosurveillance against human cytomegalovirus, for most individuals a lifelong asymptomatic infection[222], is emblematic of the kind of relaxed immunity that, in part, makes older individuals more susceptible to developing tumors. Because the comorbidities which make irAE progression a therapy-termination outcome are more frequent in elderly individuals[223], better understanding the age-associated factors in tumor extrinsic immune responses is critical. Currently, no comprehensive age-based comparison study exists for ICB determinants.

The second outcome easily overlooked in CheckMate-067 is perhaps even more galling than the ever-encroaching specter of old age. Of the factors recorded by Matson *et al* in this study, the single factor which most strongly associates with overall survival on combination ipilimumab and nivolumab was actually the site location. CheckMate-067 was a multi-institutional study, conducted at 137 sites in 21 different countries, though a plurality of cases were in the United States[156]. For some reason, for patients receiving treatment in the United States, receiving

combination therapy was twice as beneficial as nivolumab alone, while European patients hardly saw any comparative benefit at all[156]. Confounding variables notwithstanding, what is markedly different about treating melanoma in Europe compared to the United States?

Here, environmental factors likely play a role. When tumor-intrinsic factors are unlikely to be substantially different from one region or another – in CheckMate-067, European melanomas are unlikely to be different enough from American melanomas to elicit an effect of that magnitude – the host's own immune fitness is likely to play a role. Indeed, there's evidence for both seasonal and genetic influences on immune function[224,225]. Similarly, geographical differences exist in autoimmune condition prevalence, with regional differences in sarcoidosis and systemic lupus erythamatosis, among other conditions[226,227]. Unfortunately, the etiology of environmental differences is difficult to trace in many cases. Seasonal differences in immune fitness have some clear derivations – many viral infections, both global and endemic, have seasonal patterns, with the flu being the most high-profile seasonal infection. Given that a massive proportion of tumor-reactive cytotoxicity is not directed at tumor neoantigens but rather viral epitopes from repeated infections like those from influenza exposure[228], the frequency and magnitude of these seasonal exposures may very well dictate immune checkpoint blockade response. Similarly, allergen exposure is heavily tied to the pollination seasons of local plant-life, and can effect aspects of immunity distant to the mucosa; allergen-targeting IgE and IgG levels have been shown to directly regulate effector T-cell counts in the periphery[229]. Allergen exposure has the potential to effect the proliferation of tumor-reactive T-cells, but also the prevalence of autoreactive T-cell clones that may expand in ICB-irAE progression[230,231].

A plausible mechanism by which environmental influences may impact ICB response are those derived from variable Vitamin D production in different seasons and regions. Vitamin D3 can be directly metabolized by dendritic cells and other immune cells into biologically active 1,25(OH)(2)D(3)[232-234], where it can be recognized by the nuclear receptor VDR. VDR activation

secondary to 1,25(OH)(2)D(3) inhibits T-cell proliferation[235,236], particularly $CD45RO^+$ memory T-cells[237], and promotes Treg expansion[238,239]. D3 metabolites can act directly on dendritic cells as well, blocking their maturation and antigen presentation function[240,241]. On top of effective antigen presentation being critical to immunotherapy response targeting the immune synapse like ICB, the evidence suggests impaired dendritic cell maturation may blunt effective ICB response by promoting IL10-induced anergy in nearby naïve T-cells[209,242]. Cumulatively, these studies indicate vitamin D is an incredibly potent negative regulator of cellular immunity; its metabolites via VDR signaling likely determine the clonal expansion of numerous neoantigen-reactive T cell populations during tumorigenesis.

Ultimately, many of the environmental influences on the immune system are reflected in differences within the gut microbiome, the collection of commensal microbes living in the gastrointestinal tract. The microbiome has an associatively profound, but mechanistically undercharacterized, impact on immune checkpoint blockade. In three landmark studies, response to anti-PD1 and anti-CTLA4-based immune checkpoint blockade could be categorized by baseline 16S or metagenomic sequencing of the gut microbiome[243-245]. In some cases, individual microbial families or species can be identified as differentially abundant in responsive patients[246], and adoptive transfer of stool from responsive patients to germ-free mice can boost response to checkpoint blockade[246]. This latter experiment in particular indicates a causal, rather than passenger, role for the microbiome in checkpoint blockade response, though these early studies did not establish the mechanism by which microbial influences on distant melanomas or lung carcinomas may occur. Orthogonal attempts to dissect these influences are frequently gut-centric; the gut microflora play a key role in colorectal cancer progression from colitis *in vivo* by promoting TLR-mediated inflammation at sites of colitic damage, for instance[247], in a manner which likely impacts colitis-induced colorectal cancer treatment outcomes compared to *de novo* CRCs.

One particularly compelling mechanism by which the gut microbiome influenced a distal malignancy was outlined by Ma *et al* in 2019[248] in what proved to be an exemplar of microbially derived metabolites impacting anti-tumor immunity. In it, Ma *et al* utilized an antibiotic depletion mechanism to study the microbiome's impact on the inflammatory state of liver neoplasia. What they found was the proportion of primary to secondary bile acids returning from the gut to the liver via the enterohepatic loop was passively being sensed by the liver stellate endothelial cells (LSEC) in the portal vasculature. When gut microbes are present to hydrolyze bile acids to secondary bile acids, LSECs function normally and the liver tumors grow unprovoked. Without bacteria, and therefore bacterial hydrolase activity, primary bile acids accumulate in the portal vein and are sensed by LSECs. LSECs express and release CXCL16 into the portal vein and into the liver. CXCL16 sensing causes recruitment of $CCR6^{+}$ NKT cells in the liver, which actively clear malignant cells[248]. These data introduce a key paradigm in the influence of the microbiome on distal sites – microbially-derived or influenced metabolites are sensed by somatic cells and the immune system towards unique functional outcomes.

Tumor-extrinsic features of immunosuppression and limits on immune checkpoint blockade response are inherently more challenging to study than tumor-intrinsic features. Determining causality is difficult when processes like lifelong viral infections, allergens, and microbiome influences are not easy to translate to an *in vivo* model system. Characterizing the sensors of environmental stimuli in the immune system and further employing human biosampling wherever possible will be key to expanding our still limited understanding of factors away from the tumor itself.

Immune Checkpoint Inhibitor Toxicity as a Limit on Response

In CheckMate-067, our lodestone phase III trial, toxicity was incredibly high, and yet seemingly never more of an acceptable outcome. Overall survival at three years to combination ipilimumab and nivolumab therapy was 58 percent; immune related adverse events (irAEs) which

led to treatment discontinuation was 39 percent. To an extent, these data can be interpreted as a race to remission. The magnitude of immune stimulus induced by combination therapy was such that nearly every patient either survived to the end of the three-year observation period, or ended treatment because of toxicity. Clinicians could only hope to reach tumor regression endpoints before their patients' toxicities (96 percent in the combination arm had some kind of irAE) became too severe or ran into a comorbidity. In many ways, mitigating irAE severity without limiting ICB efficacy is the next, distant horizon in the application of immune checkpoint blockade we must reach before immune activation can be stimulated further.

Immune related adverse events (irAEs) are a heterogeneous collection of autoinflammatory conditions[138]. They can affect most every organ system, and their severity can vary widely within that same organ. Gastrointestinal involvement is the classical example of irAEs that can progress from mild diarrhea or uncomfortable stools (a Grade I or II presentation), all the way to ulcerating, painful colitis (a Grade IV). Grade III and IV irAEs can range from colitis to pneumonitis to hypophysitis, but ultimately the conclusion of the patient's treatment team will come down to comorbidities. For the most part, ICB is still used to treat mostly advanced melanomas and lung carcinomas, both death sentences without serious interventions. A patient will choose to stay on therapy if they can, even after developing Grade III/IV symptoms (in CheckMate-067, 59 percent of patients developed Grade III/IV irAEs, but only 30 percent of patients discontinued therapy because of their severe irAEs). Having a comorbidity in an irAE-effected system can be devastating, however, and the patient may have no choice but to withdraw from treatment to recover.

ICB, still an actively investigational class of therapeutics, is typically administered without anti-inflammatory drugs that may blunt efficacy. In some cases, anti-TNF monoclonal antibodies or glucocorticoids are given to stave off the worst of the toxicity symptoms, though the limited studies on this subject bear mixed results. The dose and breath of time required to effectively

mitigate gastrointestinal irAE begins exposing patients to infection risk from immunosuppression[249], with at least one retrospective study suggesting infliximab treatment may have done more harm than good in ICB outcomes[250].

While treatment options for irAE symptomology are limited (and potentially contraindicated), predictive modalities are getting some attention. Circulating factors including the proportion of neutrophils vs lymphocytes have demonstrated reproducible predictive correlations in immune checkpoint blockade (we even confirm these results ourselves in Chapter 2). An early expansion of a more broad cohort of TCR clonalities is also associated with irAE progression in ipilimumab-treated patients[251], though it's unclear by which mechanisms some individuals see the broad repertoire expansion while some do not. Additionally, at least one study has identified gut microbes at baseline with association to gastrointestinal irAE development[252], indicating the microbiome may play a role in colitis development. The success of stool transplants in ICB-induced colitis in humans does indicate gut microbes can have a regulatory role on at least intestinal inflammation[253].

Cumulatively, these studies indicate the clinical research community has reached an impasse on irAE mitigation. Without tractable techniques for treating toxicity independently of ICB efficacy, and assuming stool transplants are not as effective in treating non-colonic irAE, toxicity will remain a common barrier to bettering immunotherapy response. Importantly, many of the next generation immune checkpoint inhibitors are showing progressive irAE development at higher rates than PD1 or even CTLA4 targeting therapies; this is particularly the case for costimulatory receptors like OX40, where creative solutions to administration may be necessary[161,254]

Metabolites as Effectors of Immunity

In covering the determinants of immune checkpoint inhibitor response, research has focused on the necessary factors for T-cell expansion following activation at the immune synapse, and the tumor microenvironment as a niche which actively controls these factors as a means of

immunosuppression. Often, the determinants of T-cell activation are metabolites, small molecules that are the diverse foundational units to the macromolecular structures of our cells. Differential regulation of metabolites is often focused on indirectly in the study of the immune checkpoint – commonly, metabolic pathways are enriched in responder or non-responder dichotomous transcriptomics analyses. These studies limit the scope in which metabolic reprogramming is considered in immune checkpoint blockade modulation, and lead to outcomes where, when therapeutics like indolame-2,3-dioxygenase (IDO) inhibitor epacadostat fail in Phase III clinical trials[255], the field lacks an obvious next set of metabolic enzymes worth targeting.

Here, we'll review metabolites with immunoregulatory properties, including metabolites with important energetic functions for the maintenance and expansion of active lymphocyte populations, as well as metabolites which act as second messenger/signaling metabolites. While these categories can often overlap (the IDO product kynurenines being ironic examples of one such overlap), they segregate metabolites between the nutrient sensing and cytokine/costimulatory sensing roles of effector T cells

Energetic Determinants of Immunity

As previously discussed, the acidic and low-oxygen niche of the budding tumor microenvironment is a foundation-setting event in the develop of a mature neoplasia. From the actions of CREM and HIF1α, respectively[74,84,200,256], tumor cells orchestrate Treg and M2-like TAM recruitment production of TGFβ and other immunosuppressive cytokines, and importantly the upregulation of glycolysis[73]. Both expanding T-cells and neoplastic cells rely heavily on glycolysis and excrete lactate – in fact, competition for free glucose within the tumor is one of the most central competitions within the tumor microenvironment. Effector T-cells are highly dependent on mammalian target of rapamycin (mTOR) signaling as a metabolic checkpoint before antigen-primed expansion[257]. When neoplastic cells outcompete T-cells for glucose, activated T-cells fail to expand, glycolysis is stalled, and IFNγ production is reduced, all in an mTOR-dependent

manner[257]. Interestingly, there's interplay between glycolysis and immune checkpoint efficacy – ICB treatment boosts glycolysis and restores IFNγ production from T-cells, but blocking of PD-L1 on tumor cells specifically *down*regulates glycolysis in neoplastic cells, also in an mTOR-dependent manner[257,258]. Metabolic competition in this and many ways is both a determinant of and a product of immune checkpoint blockade outcomes.

Amino acid consumption is another competitive front between T-cells and cancer. Of the ten essential amino acid (phenylalanine, valine, threonine, tryptophan, isoleucine, methionine, histidine, arginine, leucine, and lysine), two amino acids are frequently characterized as competitive in the tumor microenvironment. The first is arginine, a classic dependency for rapidly proliferating cells, particularly effector T-cell proliferation and maturation. T-cells can metabolize arginine to produce energetic polyamines and nitric oxide, an important component of cytolytic T-cell action[259,260]. Further, arginine is a necessary component for TCR-zeta chain maturation, without which IFNγ production and T-cell proliferation is significantly impaired[194]. Mature tumors adapt to this dependency by recruiting TAMs, which express high levels of the enzyme arginase; TAMs release arginase into the extracellular space and catabolize free arginine into ornithine and urea, thereby limiting a necessary T-cell energetic metabolite and further increasing the acidity of the tumor microenvironment[194,260]. Arginase inhibition is synergistic with immune checkpoint inhibition in preclinical tumor models[261], though pharmacological inhibitors have not been successfully tested in combination with immune checkpoint blockade. IDO serves an analogous function to arginase in its catabolic action on free tryptophan[262], though the immunosuppressive action of IDO is likely dependent on both depriving T-cells of additional tryptophan and the production of tryptophan's immunomodulatory catabolites, the kynurenine metabolites[263]. Kynurenine and its metabolite kynurenic acid are ligands for the nuclear aryl hydrocarbon receptor[264]. Binding aryl hydrocarbon receptor drives peripheral $CD4^+$ differentiation to Tregs, and reduces immunogenic signaling during antigen presentation of dendritic cells[265,266]. The

multifaceted nature of IDO-mediated immunosuppression makes the clinical failure of its combination with pembrolizumab particularly disappointing, though preclinical evidence gives us clues to why combination treatment may not have been effective. IDO1 is a type-I and type-II interferon inducible gene[193,195], indicating tumors not already expressing these cytokines in some abundance prior to starting combination therapy may not have had enough IDO1 expressed for a synergistic effect with pembrolizumab.

Finally, a critical and underappreciated metabolic roadblock for a successful immune checkpoint blockade-induced effect is the availability of free fatty acids and triglycerides for β-oxidation, a critical energetic process for the maintenance of central memory and effector memory T-cells[201,267,268]. Following antigen recognition, $CD8^+$ cells deficient in fatty acid oxidation gene expression fail to produce memory populations and are lost entirely by 6 weeks[267]. On the other hand, PPAR-γ induction of β-oxidation genes promotes anti-tumoral action of PD1 blockade[269], though it's unclear from this study whether fatty acid oxidation was useful for $CD8^+$ memory T-cell expansion or if it frontloaded the energetic needs of naïve T-cells which also utilize free fatty acids via β-oxidation. Fatty acid utilization is a critical example of overlap between energetic and signaling function, considering the fate tumor myeloid cells typically have for free fatty acids.

Bioactive Signaling Metabolites

Fatty acids are stored in the plasma membranes of cells via esterification and metabolized as necessary for the cell's energetic needs. However, in some cases, these same fatty acids can be processed by intracellular oxygenases and isomerases to form a diverse array of bioactive signaling lipids. The eicosanoid family, named for the 20-carbon chain length of the common progenitor arachidonic acid, is a collection of oxylipins that are released by cells for a diverse array of immunoregulatory functions[270]. Arachidonic-derived prostaglandins and leukotrienes are pernicious signaling molecules; two chemically related eicosanoids can be a potent vasoconstrictor[271] or vasodilator[272]; they can be GPCR-dependent inducers of inflammation[273,274]

or GPCR-dependent pro-resolution signaling molecules[275]. The functional complexity of these lipids is in no way limited by their structural modularity, a (usually) enzymatic process called class-switching by which eicosanoids can subsume entirely new signaling roles to adapt to changing inflammatory contexts[273,276].

Broad generalizations of eicosanoids are still possible, however – polyunsaturated fatty acids like arachidonic acid are first liberated from membrane phospholipid by the activity of phospholipase A2. From there, the free fatty acid's fate is determined by which oxygenase it sees next. COX1 and COX2 are the most pleiotropic and generally (far from exclusively) produce pro-inflammatory prostaglandins. COX is the target of non-steroidal anti-inflammatory (NSAID) therapies like aspirin, which has the unusual pharmacological effect of irreversibly inhibiting COX1 and promoting the acetylation of COX2[277]. Acetylated COX2 shunts its enzymatic activity to the production of the intermediate prostaglandin 15(R)-HETE, which is then metabolized by 5-lipoxygenase (5-LOX) to produce leukotrienes, mediators of leukocyte recruitment and bronchochonstriction[278]. Additional chemical diversity is provided by 8-, 12-, and 15-LOX, which synthesize additional immunoregulatory lipoxins[279,280]. Eicosanoids broadly signal through GPCRs and PPAR nuclear receptors[269,279,281].

Eicosanoids have only been characterized superficially in their role at the immune synapse and in immune checkpoint inhibitor outcomes. COX inhibition promotes anti-PD1 efficacy *in vivo*, potentially for the immunosuppessive character of prostaglandin E2 (PGE2) on type-I interferon production[282,283], or by suppression of NK-mediated conventional dendritic cell recruitment to the tumor microenvironment[284]. There's additional evidence that dendritic cell-derived PGE2 coordinates a more immunosuppressive microenvironment through higher Treg to Th-17 cellularity ratios[285].

Beyond eicosanoids there are a wealth of bioactive signaling lipids, including most lysolipids[286-288], endocannabinoids[289,290], and sphingolipids[291,292]. There's even an additional layer

of potential signaling diversity – lysophosophoethanolamines and lysophosphocholines can be metabolized by COX to produce eicosanoid-like lysolipids with uncharacterized signaling function[293]. Bioactive signaling lipids are a wealth of functional regulators of inflammation which have yet to be effectively characterized in immune checkpoint blockade outcomes.

Chapter 1: Reprogramming Purine Metabolism to Boost Tumor STING/Type-I Interferon

Cellular sensing of extracellular purine nucleosides triggers an innate IFNβ response

Authors

Rekha Dhanwani[1,†], Mariko Takahashi[1,†], Ian T. Mathews[1,2,3,†], Camille Lenzi[1], Artem Romanov[1], Jeramie D. Watrous[2,3], Bartijn Pieters[1], Catherine C. Hedrick[1], Chris A. Benedict[1], Joel Linden[1,3], Roland Nilsson[4,5], Mohit Jain[2,3], Sonia Sharma[1,*]

Affiliations

[1] La Jolla Institute for Immunology, La Jolla, CA 92037, USA.

[2] Department of Medicine, University of California, San Diego, La Jolla, CA, USA.

[3] Department of Pharmacology, University of California, San Diego, La Jolla, CA 92093, USA.

[4] Cardiovascular Medicine Unit, Department of Medicine, Karolinska Institutet, Karolinska University Hospital, SE-17176, Stockholm, Sweden.

[5] Center for Molecular Medicine, Karolinska Institutet, Karolinska University Hospital, SE-17176, Stockholm, Sweden.

[†]These authors contributed equally to this work.

[*]Corresponding author, soniasharma@lji.org (S.S.)

Abstract

Mechanisms coupling immune-stimulatory DNA danger signals in the extracellular environment to innate sensing pathways in the cytosol are poorly understood. Here we identify a novel immune-metabolic axis by which cells respond to purine nucleosides and trigger a type I Interferon β response. We find that depletion of ADA2, an ecto-enzyme that catabolizes extracellular dAdo to dIno, or supplementation of dAdo or dIno stimulates IFNβ. Under conditions of reduced ADA2 enzyme activity, dAdo is transported into cells and undergoes catabolysis by the cytosolic isoenzyme ADA1, driving intracellular accumulation of dIno. dIno is a functional

innate immune-metabolite that interferes with the methionine cycle by inhibiting SAM synthetase. Inhibition of SAM-dependent cellular *trans*-methylation drives epigenomic hypomethylation and over-expression of immune-stimulatory endogenous retroviral elements that induce IFNβ by engaging cytosolic dsRNA sensors. We uncovered a novel cellular signaling pathway that responds to extracellular DNA-derived metabolites, coupling nucleoside catabolism by adenosine deaminases to cellular IFNβ production.

MAIN TEXT

Introduction

Innate immunity is a universal cellular response to pathogenic threats. Upon sensing infection, damage, or genotoxic stress, susceptible cells activate innate immune signaling cascades such as the IFNβ axis. IFNβ is a pleiotropic cytokine that signals via the type I interferon receptor (IFNAR) to exert autocrine and paracrine effects on cellular growth, apoptosis, and immune cell activation, ultimately playing an essential role in propagation and resolution of the inflammatory response[294]. IFNβ is produced during the course of infection, neoplastic transformation, cancer immunotherapy, and auto-immune disease due to cellular recognition of atypical or mis-localized nucleic acids, which is precipitated by intrinsic and extrinsic sensing mechanisms[295,296]. Cell-intrinsic RNA or DNA ligands derive from internalized viruses and bacteria, or from host-cellular sources such as damaged mitochondria, stalled replication forks, or endogenous retroviral elements encoded within the genome. Inside the cell, these aberrant nucleic acids are recognized by cytoplasmic sensors such as retinoic acid-inducible gene-I (RIG-I), melanoma differentiation-associated protein 5 (MDA5) or cyclic GMP-AMP synthetase (cGAS). Engagement of innate cytosolic sensors in turn activates key signaling adaptor proteins including mitochondrial antiviral signaling (MAVS) or stimulator of interferon genes (STING), which drive IFNβ production.

How extracellular nucleic acids engage cytosolic sensors is incompletely understood. Mammalian DNA is a damage-associated molecular pattern (DAMP) with immune-stimulatory activity that largely depends upon recognition by internal sensors [297]. Specialized phagocytic cells, including monocytes, macrophages and dendritic cells, may engulf extracellular DNA fragments to access the cytosolic machinery. However, it is unclear how non-phagocytic or stromal cells respond to extracellular DNA danger signals, or whether extracellular DNA-derived metabolites generated by the activity of endonucleases and other nucleic acid modifying enzymes can act in an extrinsic or paracrine manner to modulate the innate immune response.

Here we describe a novel cellular response to the extracellular purine nucleoside dAdo, which stimulates IFNβ and an IFNβ-driven innate immune response in a paracrine manner. We show that loss of extracellular ADA2 enzyme activity in stromal endothelial cells drives increased cellular uptake of extracellular dAdo. Upon transport into the cell, dAdo is catabolized by the cytosolic isoenzyme ADA1 to yield dIno, which specifically accumulates inside ADA2-depleted cells. dIno is a functional immune-metabolite that perturbs cellular metabolic reactions which suppress expression of endogenous retroviral elements, immune-stimulatory molecules that directly engage innate cytosolic sensors for dsRNA. Our novel results suggest that metabolism of extracellular DNA or nucleoside danger signals, which are released during ischemia, infection and tumor growth, is a key regulatory checkpoint during physiological inflammation. These regulatory mechanisms are likely abolished in human metabolic syndromes such as ADA2 or Purine Nucleoside Phosphorylase (PNP) deficiency diseases, which manifest as profound immunological dysregulation characterized by systemic inflammation and inappropriate induction of IFNβ as well as other innate pro-inflammatory cytokines.

Results

Loss of ADA2 triggers spontaneous IFNβ production

Gene mutations in molecules of the innate cytosolic sensing machinery drive systemic inflammatory diseases in humans due to excessive IFNβ production [298]. We reasoned that new mechanistic insights into innate immune sensing and molecular triggers of inflammation could be gained by examining functionally uncharacterized disease-associated genes. Search of the Online Mendelian Inheritance in Man (OMIM) database identified thirty-eight syndromes of systemic inflammation resulting from a single, sequence-verified gene mutation (**Table S1.1**). To examine whether these candidate genes regulate IFNβ pathway activation, *in situ* immunofluorescence was used to assess inducible nuclear translocation of the transcription factor Interferon Regulatory Factor 3 (IRF3) [299], which directly *trans*-activates the IFNβ promoter locus. Upon transfection with immune-stimulatory poly (dA:dT) DNA, IRF3 translocation and IFNβ mRNA levels were quantified in primary human umbilical vein endothelial cells (HUVEC) and other endothelial-lineage cells (**Figure S1.1A-B**). Forward genetic screening in HUVEC confirmed STING and Three Prime Repair Exonuclease I (TREX1), an inhibitor of DNA sensing through STING, as positive and negative regulators of IRF3/IFNβ, respectively. Results identify ADA2 as a new negative regulator of IRF3 activation (**Table S1.1** and **Figure. 1.1A**).

To ascertain whether loss of ADA2 drives spontaneous IRF3 activation in the absence of exogenous stimulation, phosphorylation of IRF3 and auto-phosphorylation of the IRF3 kinase TBK1 were examined in ADA2 knockdown cells. Western blotting with phospho-specific antibodies demonstrated spontaneous phosphorylation of IRF3 and TBK1 in siADA2-treated or siTREX1-treated cells compared to a control, non-targeting siRNA (**Figure 1.1B**). IFNβ mRNA levels were also spontaneously elevated in ADA2-depleted cells (**Figure 1.1C**), and were further

enhanced upon infection with human cytomegalovirus, a β-herpesvirus that induces a robust cellular IFNβ response [299]. Induction of an IFNβ-stimulated gene signature in unstimulated siADA2-treated cells was observed using whole-genome transcriptome analysis (**Figure 1.1D**). Differentially expressed transcripts in this dataset included genes encoding pro-inflammatory cytokines, chemokines, and innate immune response proteins (**Figure 1.1E**). These findings are concordant with previous observations that IFN-associated gene expression signatures are detectable in peripheral blood cells from ADA2-deficient patients [300]. Application of a neutralizing antibody for IFNβ confirmed autocrine/paracrine IFNβ-driven signaling in ADA2-depleted cells (**Figure 1.1F**). Together, results establish ADA2 as an inhibitor of spontaneous IFNβ production.

Human endothelial cells express functional ADA2

We next sought to determine the mechanism by which ADA2 regulates innate immunity. Human ADA1 and ADA2 are isoenzymes that catalyze the irreversible deamination of adenosine (Ado) and deoxyadenosine (dAdo) to inosine (Ino) and deoxyinosine (dIno), respectively [301,302]. *ADA2* mRNA transcripts are broadly expressed in human immune cells [303](**Figure S1.2A**), and were detected in the monocytic cell line U937 as well as multiple primary human endothelial lineage cells by qRT-PCR (**Figure 1.2A**) and RNAseq in HUVEC (**Figure S1.2B**). A prior report failed to detect intracellular ADA2 protein or enzyme activity in HUVEC [304]. However, ADA2 is an ecto-enzyme possessing a classical signal peptide [305], and extracellular ADA2 protein was detectable in cultured supernatants of U937 and human endothelial cells by ELISA (**Figure 1.2B**) and western blotting (**Figure 1.2C**). In HUVEC, siADA2 reduced ADA2 mRNA levels by ~75 % with no cross-reactivity against ADA1 (**Figure S1.2C**). Similarly, siADA1 reduced ADA1 mRNA levels by ~90%, with no cross-reactivity towards ADA2 (**Figure S1.2D**). Analysis of deaminase activity, measured through *de novo* conversion of ^{15}N-labeled dAdo to dIno by mass spectrometry, demonstrated that >90% of intracellular ADA activity measured in HUVEC whole

cell lysate was specifically reduced by ADA1 depletion, and unaffected by ADA2 depletion (**Figure 1.2D**). In contrast, extracellular ADA activity measured in HUVEC supernatant was reduced >75% by specific depletion of ADA2, with ADA1 accounting for a minority of extracellular activity (**Figure 1.2D**), recapitulating results obtained in human plasma [306]. To confirm ADA2-specific activity in HUVEC supernatants, dAdo to dIno conversion was measured in the presence of ADA2 siRNA and 50 μM erythro-9-(2-hydroxy-3-nonyl)adenine (EHNA) to selectively inhibit ADA1 activity (**Figure S1.2E**). Together, experiments demonstrate functional expression of extracellular ADA2 by HUVEC.

ADA2 and dAdo are paracrine modulators of IFNβ

To examine whether extracellular ADA2 activity regulates IFNβ, enzyme add-back experiments were performed in ADA2-depleted cells using recombinant ADA proteins. Addition of rADA2 inhibited spontaneous induction of *IFNβ*, *CCL5*, and *CXCL10* mRNA in siADA2-treated HUVEC (**Figure 1.2E**). Notably, rescue effects accompanied reconstitution of extracellular ADA activity to wild type levels, and were inhibited by pentostation, a general inhibitor of adenosine deaminase activity. Prior reports suggest that extracellular ADA2 may function independently of its enzyme activity by exerting growth factor-like effects on cells [301,305]. To confirm involvement of ADA enzyme activity in immune activation, rADA1 was added to ADA2-depleted cells, resulting in rescue of cytokine expression and extracellular ADA activity (**Figure 1.2E**). Given the essential role of extracellular purine nucleoside deaminase activity in suppressing expression of innate cytokines, U937 cells were supplemented with exogenous nucleosides and innate immune responses examined. Supplementation of dAdo specifically induced IFNβ (**Figure 2F**), suggesting that both ADA2 and dAdo act in a paracrine manner to modulate cellular innate responses.

Accordingly, co-culture of siADA2-treated HUVEC with untreated U937 cells provoked spontaneous IFNβ production in bystander U937 cells (**Figure 1.2G**), confirming paracrine or non-cell autonomous effects of ADA2 in HUVEC.

Loss of ADA2 drives intracellular dAdo catabolism and accumulation of dIno

Extracellular Ado and dAdo are bioactive molecules that signal to immune cells during pathological inflammation [307,308]. Ado and dAdo are released into the microenvironment in an autocrine/paracrine fashion or produced upon degradation of extracellular nucleic acids. Ado, but not dAdo, primarily signals via G-protein coupled purinergic adenosine receptors (AdoR) (**Figure 1.3A**), which elicit pleiotropic immune-modulatory effects. Alternatively, dAdo may be transported into cells via the action of nucleoside transporters. Vascular endothelial cells express relatively high levels of equilibrative nucleoside transporters (ENT) (**Figure 1.3B**) that enable rapid and efficient clearance of dAdo from the blood [309], and may render these cells particularly sensitive to the effects of ADA2 deficiency and dysregulation of extracellular dAdo metabolism. Accordingly, incubation of HUVEC with ^{15}N-labeled dAdo resulted in rapid cellular uptake and equilibration of intracellular and extracellular dAdo pools within 5 minutes (**Figure 1.3C**). Pre-treatment with dipyridamole (DPM), a pharmacological inhibitor of ENT-mediated dAdo transport, reduced expression of the IFNβ and the IFNβ-driven gene signature in ADA2-depleted cells (**Figure 1.3D**). Results indicate that cellular nucleoside transport of dAdo is essential for IFNβ production driven by reduced ADA2 enzyme activity.

Once taken up by cells, dAdo is metabolized through intracellular purine salvage and/or degradation pathways [308] (**Figure 1.4A**), which may yield downstream effector molecules that influence innate signaling. To assess potential intracellular fates of consumed extracellular dAdo, global mass spectrometry-based metabolomics was performed [310]. Comprehensive analysis of

metabolites revealed intracellular accumulation of dIno and its downstream catabolite hypoxanthine in ADA2-depleted cells relative to control cells (**Figure 1.4B-C**), while other purine metabolites including dAdo and Ado were not changed (**Figure S1.3A**). These results show that loss of ADA2 activity dysregulates cellular purine catabolism, and imply a compensatory mechanism by which extracellular dAdo is catabolized inside the cell. Consistent with this, addition of extracellular ^{15}N-labeled dAdo drove rapid intracellular accumulation of labeled dIno product in ADA2-depleted cells (**Figure 1.4C**). Intracellularly, dIno is produced from consumed dAdo by ADA1 (**Figure 1.4A**). Depletion of ADA1 in ADA2-knockdown cells suppressed both IFNβ expression and dIno production, demonstrating a functional role for ADA1 in producing intracellular dIno in the setting of ADA2 deficiency (**Figure 1.4D and Fig. S1.3B-C**). In contrast, increasing intracellular dIno pools by silencing its catabolic enzyme PNP, or silencing the cellular enzyme deoxy-cytidine kinase (dCK), an alternative enzyme for intracellular metabolism of dAdo (**Figure 1.4A**), increased IFNβ levels (**Figure 1.4D and Fig. S1.3C**). Consistent with these observations, supplementation of exogenous dIno, but not Ino or hypoxanthine, was sufficient to trigger IFNβ mRNA production (**Figure 1.4E and Fig. S1.3D**), supporting a novel functional role for dIno in the cellular innate immune response. Notably, the immune-stimulatory effect of exogenous dIno was sensitive to DPM (**Figure S1.3D**), and was enhanced by pre-treatment with 9-deazaguanine (**Figure 1.4E)**, which inhibits intracellular and extracellular catabolism of dIno by PNP. Data show that dIno accumulates intracellularly in ADA2-depleted cells due to the activity of ADA1, and functions as an immune-metabolite that is both necessary and sufficient for IFNβ induction.

dIno inhibits the cellular methionine cycle via S-Adenosylmethionine synthetase

We next sought to determine the mechanism by which dIno acts as an immune-metabolite and functional regulator of innate immune signaling. Intracellularly, nucleosides and their

analogues or metabolites interface with multiple cellular processes including *trans*-methylation [311]. Loss of ADA2 was associated with steady-state reduction in relative levels of L-cystathionine, a downstream metabolite in the methionine cycle (**Figure S1.4A**). To further examine methionine metabolism, time-course stable isotope tracing was performed with U-^{13}C-methionine [312,313]. Intracellular methionine metabolite pools were fully labeled within minutes of exposure to extracellular label, while S-adenosyl-methionine (SAM) and its downstream metabolite S-adenosylhomocysteine (SAH) acquired labeling over time (**Figure S1.4B**). The methionine M+4 mass isotopomer was consistently measured at ~2 % (**Figure S1.4C**), suggesting a truncated cycle with little re-methylation of homocysteine into methionine. Upon ADA2 depletion, SAM and SAH pools exhibited slower labeling over time relative to controls, and model-based metabolic flux analysis [312] revealed impaired cycle flux through the SAM synthetase (MAT) and methyl-transferase (MT) reactions (**Figure 1.4F**). *In vitro* enzyme activity assays demonstrated that dIno, and to a lesser extent dAdo but not the nucleoside cytidine, directly inhibited MAT activity (**Figure 1.4G**). Accordingly, pharmacological inhibition of MAT using cycloleucine induced IFNβ (**Figure 1.4H**), phenocopying the effects of ADA2 deficiency or dIno accumulation and suggesting a role for MAT inhibition in the immune-stimulatory effects of dIno. The MAT product SAM serves as a methyl donor for multiple enzymatic reactions, including DNA methyl-transferase (DNMT)-dependent methylation of genomic cytosine bases (**Figure 1.4F**). Accordingly, inhibition of DNMT using 5-azacytidine induced IFNβ (**Figure 1.4H**). To examine the status of genomic *trans*-methylation in ADA2-depleted cells, labeled methionine was used to monitor incorporation of methyl groups onto cytosine residues in genomic DNA. Control cells steadily accumulated labeled methyl-cytosine, reaching ~20-25 % of genomic methyl-cytosine over 72 hours. In contrast, cells depleted of ADA2 or DNMT (**Figure 1.4I**) as well as dIno-supplemented cells (**Figure S1.4D**) all demonstrated reduced *de novo* DNA methylation as early as 24 hours after the addition of label. These data demonstrate that dIno directly inhibits the activity of MAT and the methionine/SAM

cycle, with subsequent reduction of genomic DNA *trans*-methylation upon loss of ADA2 or supplementation with dIno.

Induction of methylation-sensitive endogenous retrovirus elements triggers IFNβ

Endogenous retrovirus elements (ERV) encode a diverse family of germline immune-stimulatory dsRNA-like molecules whose dynamic expression is particularly sensitive to genomic DNA hypomethylation. Over-expression of ERV in cells is directly linked to IFNβ production due to engagement of innate immune dsRNA sensing pathways [314,315]. Indeed, loss-of-function studies confirmed that the cytosolic dsRNA sensors RIG-I and MDA5 as well as the dsRNA signaling adaptor MAVS drive spontaneous IFNβ production upon depletion of ADA2 (**Figure 1.5A and Figure S1.5A**). Analysis of transcriptomic data obtained in ADA2-depleted cells to specifically examine expression of long terminal repeat (LTR)-containing genomic sequences, which comprise a large portion ERV elements, revealed over-expression of >30 LTR-containing ERV-like molecules (**Figure 1.5B**). Furthermore, *ERVFRD-1* and *ERVK28* genes were highly induced after supplementation with dIno or depletion of ADA2 (**Figure 1.5C-D**). Importantly, augmented expression of ERV in dIno-treated cells (**Figure 1.5C**, 24H) or ADA2-depleted cells (**Figure 1.5D**, 24-48H) was detectable prior to induction of IFNβ mRNA (**Figure S1.5B,** 72H) and occurred independently of autocrine/paracrine IFNβ-driven signaling (**Figure 1.5E and S1.5F**). To confirm immune-stimulatory effects of ERV, transcript variants of *ERVK28* were over-expressed in HUVEC, resulting in spontaneous induction of *IFNβ*, *CCL5* and *CXCL10* (**Figure 1.5F**). Results demonstrate that over-expression of immune-stimulatory ERV in ADA2-depleted cells drives the IFNβ response.

Discussion

Here we report for the first time a new cellular strategy for triggering IFNβ production by extracellular dAdo (**Figure 1.6**). Loss of the ecto-enzyme ADA2 or direct supplementation of exogenous dAdo drives cellular transport and catabolism by the cytosolic enzyme ADA1, driving *de novo* dIno production and dIno accumulation inside ADA2-depleted cells. dIno is a functional immune-metabolite that directly inhibits the cellular methionine cycle at the level of MAT, thereby suppressing cellular *trans*-methylation reactions. Genomic hypomethylation provokes over-expression of immune-stimulatory ERV transcripts, including *ERVK28* and *ERVFRD-1*, which trigger IRF3 activation and IFNβ. Thus, purine nucleoside regulation by ADA2 and other enzymes of extracellular DNA metabolism is likely an important determinant of IFNβ and IFNβ-driven gene expression in inflammatory microenvironments, where inappropriate release and accumulation of cell-free DNA and its nucleoside by-products accompanies infection, ischemic injury, and tumor growth.

The ADA2/ADA1 axis controls bio-activity of purine nucleoside metabolites

Results presented here show for the first time that cellular innate immunity is triggered by a unique immune-metabolic axis that balances competing, compartmentalized adenosine deaminase activities in the extracellular and cytosolic spaces. Differential effects of ADA2 and ADA1 depletion on IFNβ expression in HUVEC underscores the complex nature of bio-active purines in modulating immune cells and inflammation. In the extracellular space, Ado exerts pleiotropic effects upon innate and adaptive immune cells from signals generated via purinergic G-protein coupled receptors or ligand-gated ion channels [307]. Due to broad expression of the A2A and A2B adenosine receptor isoforms (AdoR) in the immune compartment, Ado exerts predominantly anti-inflammatory effects on cells. Here we show for the first time that extracellular dAdo exerts a pro-inflammatory effect due to triggering of cellular IRF3 activation, IFNβ production, and an IFNβ-driven innate immune response that up-regulates an array of pro-inflammatory cytokines, chemokines and signaling proteins (**Figure 1.1D**). Ultimately, the

magnitude, duration, and outcome of immune-suppressive and immune-stimulatory purine signals at a given immunological niche will depend upon metabolic activities of cellular purine salvage or degradation enzymes, as well as ecto-nucleases and ecto-nucleotidases such as DNAse I, CD39 and CD73 that catalyze Ado and dAdo production from cell-free RNA or DNA in circulation. These enzymes are the key targets for modulating the purine pathway and thus developing novel strategies for immune-therapy.

In HUVEC, ADA activities are compartmentalized such that ADA2 accounts for >75% of extracellular activity, and ADA1 accounts for all intracellular activity (**Figure 1.2D**). Extracellular activity in HUVEC conditioned supernatants accurately reflects human plasma, where total circulating ADA activity measured in healthy individuals correlates with the ADA2-specific activity [306,316]. Indeed, median ADA1 activity measured in normal human plasma accounts for ~25% [306], recapitulating results obtained here using gene-specific siRNAs. Despite data from multiple studies demonstrating that ADA2 accounts for the majority of extracellular ADA activity measured in human plasma, it has nonetheless been postulated that ADA2 plays a minimal role regulating purine metabolism *in vivo*. This is variously attributed to the particular biochemical properties of ADA2, putative growth factor-like properties of ADA2 and lack of Ado/dAdo elevation in DADA2 patient plasma. Importantly, data obtained using rADA2 and rADA1 proteins (**Figure 1.2E**) or dAdo supplementation (**Figure 1.2F**) unequivocally demonstrate that ADA enzymatic activity regulates IFNβ expression. Regarding the biochemistry of ADA2, many early studies reporting enzyme reaction rate and substrate affinity were obtained using purified protein preparations that are highly unstable [302], and may have underestimated the actual enzyme activity *in vivo*. Further, ADA2 activity assays in plasma and cell-conditioned supernatants typically use relatively high nucleoside concentrations (e.g. 1 mM), however our results were fully recapitulated at a range of dAdo concentrations as low as 100 nM (I Mathews and S Sharma, *unpublished results*). Notably, ADA2 exhibits a broadly-optimal pH range compared to ADA1

[301,302], suggesting it may be particularly suited to pathological conditions when release of lactic acid or reduced blood flow/hypoxia drive pH down, significantly affecting normal metabolic activities and potentially impairing ADA1. Indeed, circulating ADA2 activity is specifically increased upon HIV infection [317], chronic hepatitis [318], rheumatoid arthritis [319] and tuberculosis [320], and has repeatedly been proposed as a diagnostic tool or surrogate bio-marker for multiple human inflammatory diseases. Our new mechanistic insights regarding cellular innate immunity provide a key missing component in our understanding of ADA2 as a functional regulator of immunity rather than a passive bio-marker of inflammation.

While ADA2 possesses a signal peptide that directs trafficking through classical protein secretion pathways, intracellular protein stores are selectively retained in the cytoplasm of myeloid cells and mobilized upon cellular stimulation. In contrast to endothelial cells examined, in which intracellular ADA2 protein [304] and enzyme activity (**Figure 1.2D**) is undetectable, monocytes and macrophages retain ADA2 inside cells [304]. Upon cellular stimulation with phorbol esters and calcium ionophore, intracellular stores of ADA2 are acutely mobilized into the extracellular space [321], likely contributing to increased ADA2 activity observed *in vivo* in human plasma. Transcriptional profiles obtained from unbiased analysis of human hematopoietic cell subsets [303] revealed broad expression of ADA2 mRNA in many immune cell types (**Figure S1.2A**), where regulated retention and release of ADA2 might be at play during the course of physiological inflammation *in vivo*. Elucidating the specific signals that regulate inducible ADA2 activity during inflammation will require developing an appropriate multi-cellular, immune-competent system in which ADA1 and ADA2 expression and compartmentalization are conserved.

Extrinsic sensing of DNA danger signals

Like ADA2, extracellular accumulation of bio-active nucleosides also occurs during inflammation, due to acute damage to cells and tissues [307]. Driving local concentrations of

extracellular nucleotides and nucleosides well above their homeostatic levels in circulation could exceed the catabolic capacity of ADA2 enzyme activity, pushing cellular equilibrium in favor of nucleoside uptake by the vascular endothelium and other cells. Indeed, both Ado and dAdo typically display a half-life of seconds in circulation due to rapid and efficient uptake by vascular endothelial cells [309], which express relatively high levels of nucleoside transporters (**Figure 1.3B**) and may confer particular sensitivity to the functional effects of ADA2 deficiency and extracellular dAdo.

Acute elevations of extracellular ATP and Ado up to micromolar concentrations has been quantified *in vivo* upon ischemia in the brain [322] and heart [323]. Extracellular accumulation of dAdo is less well documented, however a recent unbiased metabolic characterization of myocardial infarction in humans showed that sustained plasma elevations of dAdo occured during the reperfusion phase of ischemic tissue [324], when the bulk of vascular injury and inflammation occurs. Interestingly, ischemia/reperfusion injury provokes a robust innate type I Interferon response [325], which is likely to be impacted by the dAdo-dependent mechanism reported here. In the solid tumor microenvironment, chronic elevation of Ado at micromolar concentrations plays a critical role in modulating tumor-infiltrating immune cells [326]. dAdo is also elevated in tumor interstitial fluid from mouse B16 melanomas relative to serum concentrations (I Mathews and S Sharma, *unpublished results*). Notably, induction of ERV in tumors drives a protective anti-tumor IFNβ response[314] associated with increased survival[315], suggesting that enhanced dAdo uptake may play a protective role in the tumor microenvironment by boosting tumor immune surveillance.

Cell-free DNA also accumulates in circulation during pathological inflammation [297], and dAdo may be produced upon breakdown of extracellular DNA by circulating DNAse I [327]. This is particularly relevant for infections and other pathological processes that stimulate the formation of neutrophil extracellular traps (NETs), a unique form of cell death in which decondensed chromatin is released into the extracellular environment by activated neutrophils. Interestingly, a

recent study reported enhanced NETosis in cells from DADA2 patients, which was linked to increased Ado signaling via adenosine receptors expressed on neutrophils [328]. Thus, it is likely that increased NETosis, subsequent release of cellular DNA coupled and dysregulated dAdo metabolism in ADA2 patients could synergize to drive innate cytokine responses in DADA2 patients. This is of relevance for microbial infections in which excessive neutrophil activation drives pathogenic inflammation, such as the novel coronavirus COVID-19 which drives excessive NETosis and cytokine-driven pathogenic inflammation in the human lung [329].

Clarifying the cellular and molecular mechanisms governing extracellular DNA-DAMP signaling will be necessary to understand how protective or pathogenic inflammatory signals are initiated, propagated and amplified during the course of an inflammatory episodes. In this regard, specialized myeloid cells can sense and respond to immune-stimulatory DNA triggers using both cell-intrinsic and cell-extrinsic mechanisms. This signaling diversity enables these specialized cells to report intrinsic inflammatory provocations or amplify extrinsic signals. Accordingly, here we show that monocytic cells respond to paracrine effects of ADA2 and dAdo by triggering IFNβ. Whether non-phagocytic or stromal cells can sense external DNA-DAMP triggers, allowing them to amplify inflammation in response to external innate ligands, is unclear. Our results in HUVEC establish purine nucleosides as broadly-acting immune-stimulatory agents of sterile inflammation, and implicate cellular sensing of extracellular purines as a unique modality enabling non-specialized cells to fulfill a specialized innate immune function by responding to DNA-DAMP signals originating from distal cell damage. This is relevant to the as-yet incomplete understanding of the origins of innate inflammatory signals in human autoimmune disease and vasculitis, and our data suggest that stromal cells of the vascular endothelium are initiators of inflammatory signals rather than bystanders.

ADA2 deficiency disease

Our novel results linking reduced ADA2 ecto-enzyme activity and dysregulated purine nucleoside signaling to spontaneous IFNβ production may expand our understanding of the complex and seemingly conflicting patho-biology of ADA2 deficiency disease (DADA2), a poorly understood immunological disease affecting several hundred patients worldwide, primarily children. Many patients with DADA2, whose clinical diagnosis is contingent upon specific reduction of serum ADA2 enzyme activity or loss-of-function mutations in the *ADA2* gene [304,330], experience clinical symptoms ranging from multi-organ vascular inflammation of brain, skin, and kidneys to primary immune-deficiency due to bone marrow failure. Our data show that ADA2 deficiency exerts paracrine effects on the immune response that directly relate to dysregulated dAdo/dIno metabolism. Notably, extracellular accumulation of dAdo was not observed in ADA2-deficient HUVEC nor was it required for spontaneous IFNβ induction (**Figure 1.3B**). Rather, ENT and ADA1-dependent production of dIno, dysregulation of genomic DNA methylation and ERV induction drove cellular IFNβ production. DADA2 patients do not exhibit steady-state elevations of dAdo in blood [304], however intracellular measurements of purines and ERV have not been reported in myeloid and stromal cells from these individuals. Further, since steady-state levels of dAdo measured in systemic circulation do not necessarily reflect localized or dynamic changes in dAdo levels in inflamed tissues or organs, development of an appropriate *in vivo* or multi-cellular system will be required to accurately assess effects of ADA2 deficiency on dynamic changes in dAdo levels.

Striking similarities exist between ADA2 deficiency disease and other metabolic syndromes of purines in humans; approximately one third of patients harboring loss-of-function mutations in PNP, the enzyme that catabolizes dIno, present with elevated levels of dIno and autoimmune manifestations [331]. These include systemic lupus erythematosus, a disease of multi-organ autoinflammation and vasculitis, in which elevated type I IFN production is causally implicated. Recently, an unbiased genetic analysis of human SLE identified missense single nucleotide

polymorphisms in the coding region of the *PNP* locus, which correlated in a dose-dependent manner to low PNP expression, low PNP enzyme activity and high circulating levels of IFN [332]. The mechanism of IFN up-regulation is unknown, but may interface with the novel mechanism described here. The overlapping immunological manifestations of DADA2 and PNP deficiency disease, which run the spectrum of immune deficiency to autoimmunity, support overlapping immune-modulatory mechanisms involving purine nucleosides.

The functional significance of IFNβ in the patho-biology of DADA2 or PNP deficiency disease is not well understood. Notably, IFNβ-driven signaling promotes immune cell activation and drives additional inflammatory cytokines, including TNF. Notably, elevated TNF is not detectable in the serum in DADA2 patients, however its functional relevance in driving vascular inflammation in DADA2 arises from the clinical observation that inhibitors of TNF effectively control symptoms of inflammatory vasculopathy and prevent strokes [333]. Importantly, both IFNβ and TNF are functional drivers of pathology in systemic lupus erythematosus [334]. In macrophages, TNF induces low levels of IFNβ, and autocrine TNF signaling synergizes with autocrine IFNβ signaling to enhance the expression of pro-inflammatory genes. Notably, neither control nor ADA2-depleted HUVEC do not express detectable levels of TNF, either at baseline or in response to innate ligands and virus infection (R. Dhanwani and S. Sharma, *unpublished results*). However, our data support a paracrine effect for IFNβ produced by vascular endothelium in driving TNF expression in macrophages. Imbalanced macrophage polarization towards the pro-inflammatory M1 macrophage phenotype is characteristic of DADA2 disease by [304], and M1 macrophages are a primary source of TNF *in vivo*. IFNβ-driven signaling actually drives M1 polarization, through activation of the transcription factor STAT1 and up-regulation of M1-promoting cytokines CXCL10 and CXCL9 [335]. Thus, our data support a model whereby spontaneous IFNβ produced by vascular endothelium can drive down TNF production by M1 macrophages.

A primary limitation of our study is an absence of *in vivo* corroboration that ADA2 deficiency or extracellular purine nucleosides drive IFNβ production in stromal and immune cells. This is compounded by the lack of conservation of ADA2 in the mouse, and the heterogenous nature of DADA2 disease, which likely affects many different cell types due to autocrine/paracrine activities of ADA2 and purine nucleosides as well as the variable nature of extracellular purine accumulation. Future studies centered on studying other regulatory enzymes of purine nucleoside metabolism using mouse models of tumor growth, infection or ischemia, as well as studies of both stromal and immune cells isolated from DADA2 patients undergoing acute manifestations of inflammatory disease will be required to further understand the complex balance between the pro-inflammatory and anti-inflammatory activities of purine nucleosides in human disease.

Figure 1.1: Loss of ADA2 triggers spontaneous IFNβ production.

A) siRNA screen of 38 human disease genes in HUVEC (Table S1), quantifying IRF3 nuclear translocation upon poly (dA:dT) DNA treatment (200 ng/mL for 3h). Averaged ranked Z score for each gene-specific siRNA oligonucleotide pool is represented. STING, TREX1 and ADA2 scores are indicated in red (n=3 technical replicates for n=3 biological replicates, >200 single cells per technical replicate). (B) Western blot analysis of siControl, siADA2 or siTREX-transfected HUVEC lysates (35 ug/lane). Image J quantification of the intensity ratio between phospho-IRF3/pan IRF3 and phospho-TBK1/TBK in unstimulated cells is shown in bar graphs. (C) IFNβ mRNA levels, measured by qRT-PCR, in siControl, siADA2 or siTREX1-transfected HUVEC upon treatment with vehicle or infection with hCMV (MOI=1 for 3h) (n=3 technical replicates). (D) Differential gene expression between siControl and siADA2-transfected HUVEC, measured by polyA+-enriched RNAseq (n=3 biological replicates) and REACTOME pathway analysis of the ADA2-specific genes. Red and blue dots denote genes significantly up or down- regulated > 2-fold. (E) Expression levels of IRF3-driven or IFNβ-driven genes, measured by qRT-PCR, in siControl, siADA2 or siTREX1-transfected HUVEC upon mock or hCMV infection (MOI=1 for 3h). (F) Expression levels of IRF3-driven or IFNβ-driven genes, measured by qRT-PCR, in siControl, or siADA2-transfected HUVEC treated with IFNβ-neutralizing antibody (10, 20, and 40 U/mL) (n=3 technical replicates). All results were replicated in three independent experiments. Values presented as mean +/- standard deviation. *, $P<0.05$; **, $P<0.01$; ***$P<0.001$.

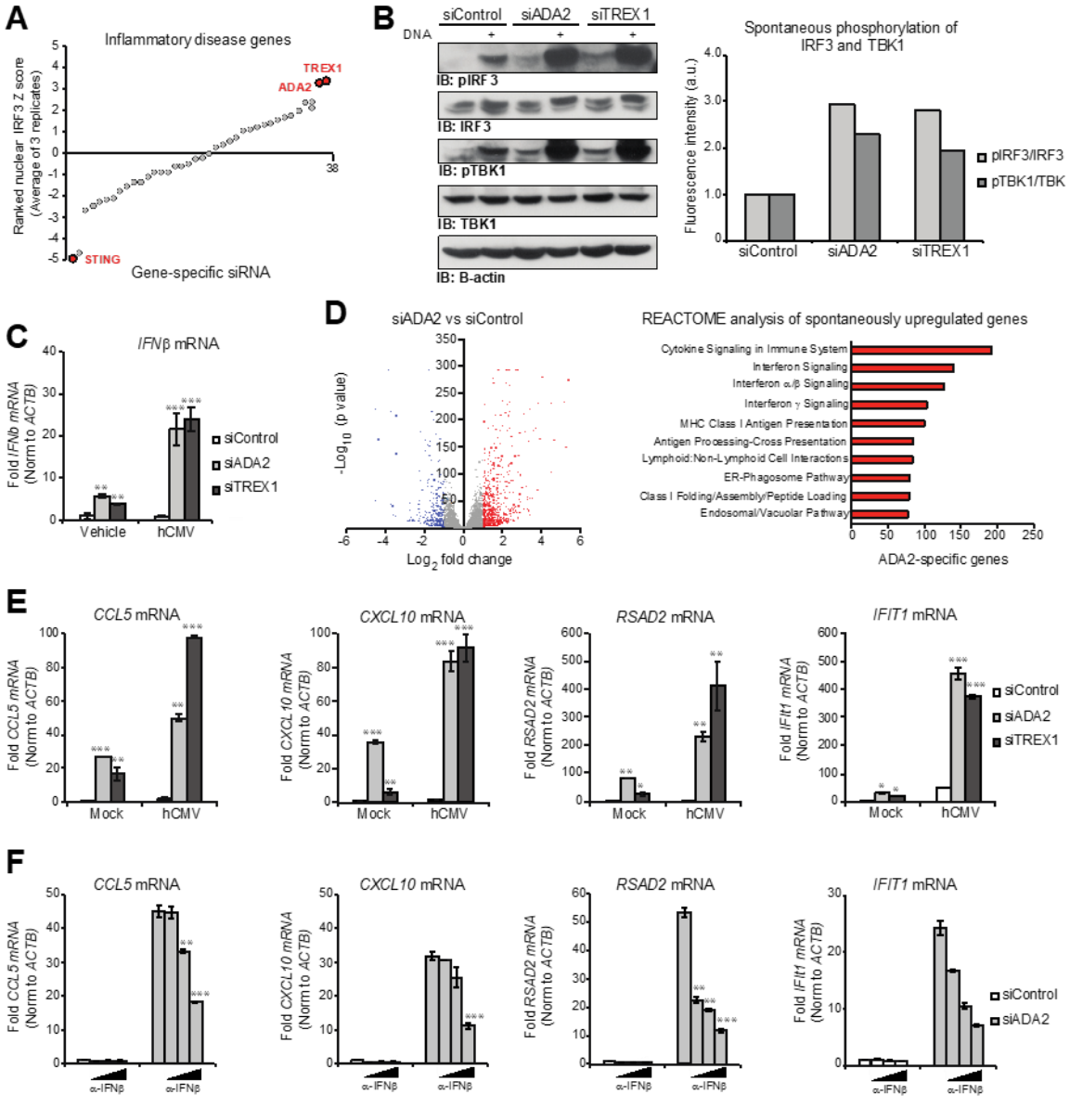
A
Inflammatory disease genes
Ranked nuclear IRF3 Z score (Average of 3 replicates)
TREX1
ADA2
STING
38
Gene-specific siRNA
B
siControl
siADA2
siTREX1
DNA
IB: pIRF3
IB: IRF3
IB: pTBK1
IB: TBK1
IB: B-actin
Spontaneous phosphorylation of IRF3 and TBK1
Fluorescence intensity (a.u.)
pIRF3/IRF3
pTBK1/TBK
siControl
siADA2
siTREX1
C
IFNβ mRNA
Fold IFNb mRNA (Norm to ACTB)
siControl
siADA2
siTREX1
Vehicle
hCMV
D
siADA2 vs siControl
-Log10 (p value)
Log2 fold change
REACTOME analysis of spontaneously upregulated genes
Cytokine Signaling in Immune System
Interferon Signaling
Interferon α/β Signaling
Interferon γ Signaling
MHC Class I Antigen Presentation
Antigen Processing-Cross Presentation
Lymphoid:Non-Lymphoid Cell Interactions
ER-Phagosome Pathway
Class I Folding/Assembly/Peptide Loading
Endosomal/Vacuolar Pathway
ADA2-specific genes
E
CCL5 mRNA
CXCL10 mRNA
RSAD2 mRNA
IFIT1 mRNA
Fold CCL5 mRNA (Norm to ACTB)
Fold CXCL10 mRNA (Norm to ACTB)
Fold RSAD2 mRNA (Norm to ACTB)
Fold IFIt1 mRNA (Norm to ACTB)
siControl
siADA2
siTREX1
Mock
hCMV
F
CCL5 mRNA
CXCL10 mRNA
RSAD2 mRNA
IFIT1 mRNA
Fold CCL5 mRNA (Norm to ACTB)
Fold CXCL10 mRNA (Norm to ACTB)
Fold RSAD2 mRNA (Norm to ACTB)
Fold IFIt1 mRNA (Norm to ACTB)
siControl
siADA2
α-IFNβ

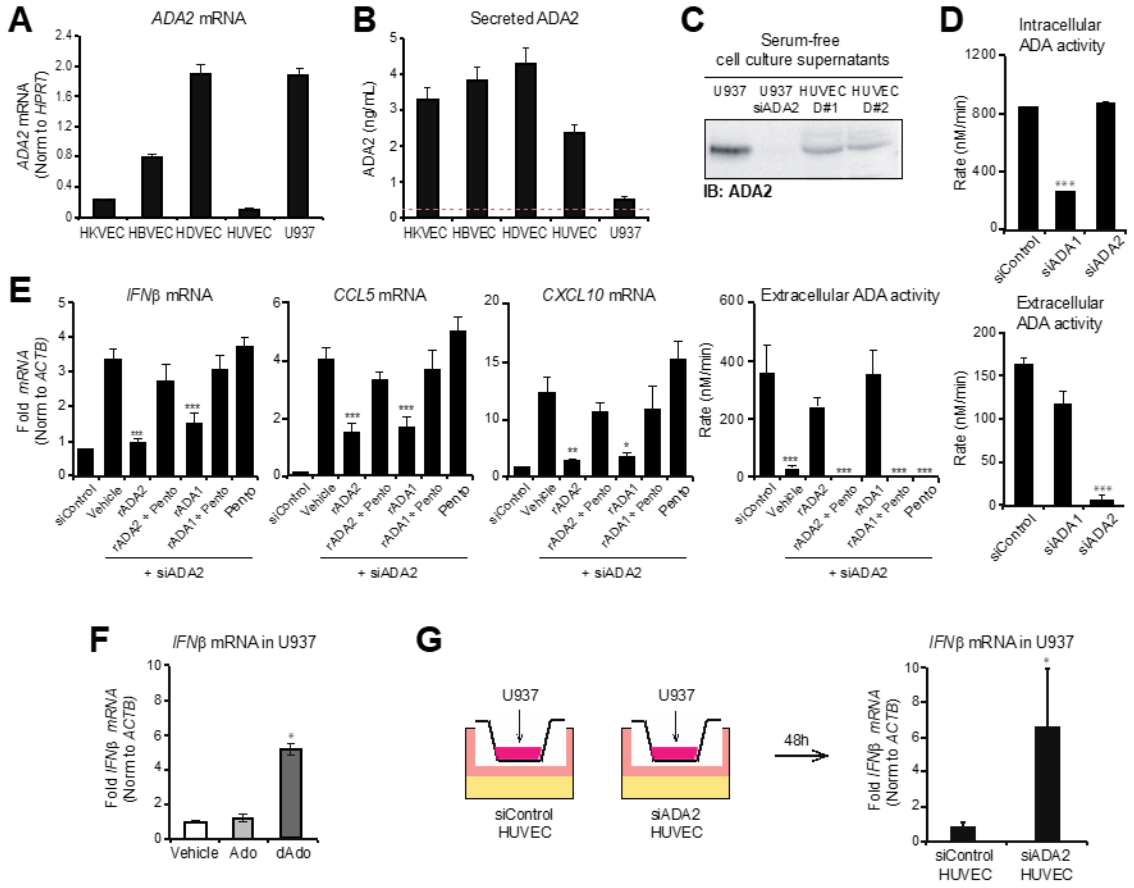

Figure 1.2: Extracellular ADA2 and dAdo are paracrine modulators of IFNβ.
(A) ADA2 mRNA levels, measured by qRT-PCR, in primary endothelial cells and U937 monocytic cells (n=3 technical replicates). (B) Secreted ADA2 protein, measured by ELISA, in primary endothelial cells and U937 monocytic cells (n=3 technical replicates). (C) Secreted ADA2 protein, assessed by western blotting of serum-free cell conditioned supernatants, from HUVEC and U937 monocytic cells. (D) Adenosine deaminase activity, measured by de novo conversion of 1 mM isotopically-labelled dAdo to dIno in whole cell lysates (intracellular) or cell conditioned supernatants (extracellular) from siControl, siADA1 or siADA2-transfected HUVEC. Values are normalized to cell number and protein concentration (n=5 technical replicates). (E) Expression levels of IRF3-driven or IFNβ-driven genes, measured by qRT-PCR, and extracellular ADA activity, measured by de novo conversion of 1 mM isotopically-labelled dAdo to dIno in cell conditioned supernatants, from siControl or siADA2-transfected HUVEC supplemented with rADA1 or rADA2, pre-treated with vehicle or pentostatin (10 □M for 30 min). Activity values are normalized to cell number and protein concentration (n=5 technical replicates). (F) IFNβ mRNA, measured by qRT-PCR, in U937 monocytic cells supplemented with adenosine (Ado) or deoxyadenosine (d-Ado) (100 uM for 48h) (n=3 technical replicates). (G) IFNβ mRNA levels, measured by qRT-PCR, in U937 co-cultured in TransWell inserts with siControl or siADA2-treated HUVEC for 48h (n=3 technical replicates). All results were replicated in three independent experiments. Values presented as mean +/- standard deviation. *, P<0.05; **, P<0.01; ***P<0.001.

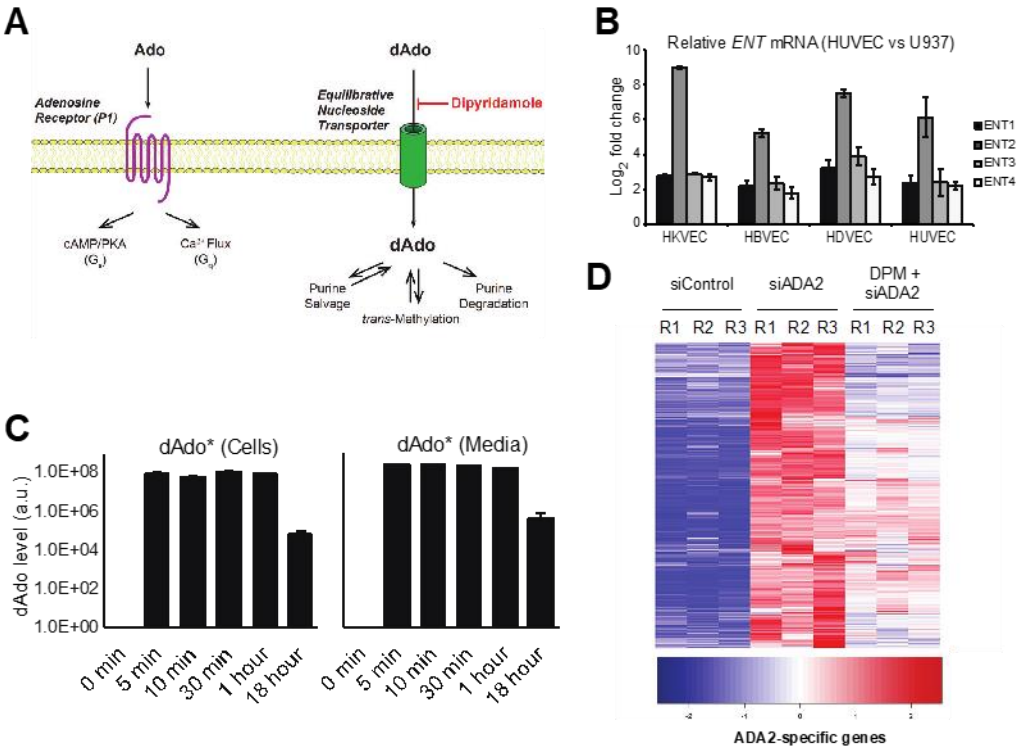

Figure 1.3: Cellular nucleoside transport is required for induction of IFNβ upon depletion of ADA2. (A) Schematic representation of extracellular Ado receptor signaling and dAdo uptake/intracellular metabolism. (B) Equilibrative Nucleoside Transporter (ENT) mRNA levels, measured by qRT-PCR, in HUVEC and U937 (n=3 technical replicates). (C) Extracellular and intracellular levels of isotope-labelled dAdo, measured by LC-MS/MS (n=5 biological replicates). (D) Differential gene expression in siControl, siADA2 or siADA2/DPM-treated (40 μM for 48h) HUVEC, measured by polyA+ RNAseq (n=3 biological replicates). All results were replicated in three independent experiments. Values presented as mean +/- standard deviation. *, P<0.05; **, P<0.01; ***P<0.001.

Figure 1.4: Loss of ADA2 drives intracellular dAdo catabolism and accumulation of dIno.
A) Intracellular metabolic pathways of purine degradation (ADA1, Adenosine Deaminase 1; PNP, Purine Nucleoside Phosphorylase; HPRT, Hypoxanthine Phosphoribosyltransferase) and purine salvage (ADK, Adenosine Kinase; dCK, deoxyCytidine Kinase; 5'-NT, 5'-nucleotidase). (B) Relative levels and concentrations of small molecule polar metabolites, measured by LC-MS/MS quantification of siControl or siADA2-transfected HUVEC (n=5 biological replicates). (C) de novo accumulation of 15N-dAdo labeled dIno, measured by LC-MS/MS quantification of siControl or siADA2-treated HUVEC (n=5 biological replicates). (D) IFNβ mRNA levels, measured by qRT-PCR, in HUVEC transfected with siRNAs targeting ADA2 and ADA1, PNP, HPRT or DCK. (D) IFNβ mRNA levels, measured by qRT-PCR, in HUVEC supplemented with dIno (500 μM for 24h) or (E) pre-treated with the PNP inhibitor 9-deazaguanine (100 □M for 30 minutes) prior to dIno supplementation (500 μM for 24h) (n=3 technical replicates). (F) Flux analysis of the methionine/SAM cycle, measured by LC-MS/MS quantification of U-13C-methionine labeled methionine, SAM, and S-Adenosyl homocystein (SAH), in siControl or siADA2-treated HUVEC (n=5 biological replicates). (G) MAT enzyme activity, measured by LC-MS/MS quantification of SAM, in HUVEC lysates supplemented with nucleosides (n=3 technical replicates). (H) IFNβ mRNA levels, measured by qRT-PCR, in HUVEC pre-treated with cycloleucine (MAT inhibitor, 20 mM for 30 minutes) or 5-azacytidine (DNMT inhibitor, 500 nM for 30 minutes) (n=3 technical replicates). (I) de novo DNA methylation, measured by LC-MS/MS quantification of U-13C-methionine labeled 2'-deoxy-5-methylcytidine in siControl, siADA2 or siDNMT1-treated HUVEC (n=3 biological replicates). Values are represented as the percentage of total label incorporation. All results were replicated in three independent experiments. Values presented as mean +/- standard deviation. ND, not detectable. *, P<0.05; **, P<0.01; ***P<0.001.

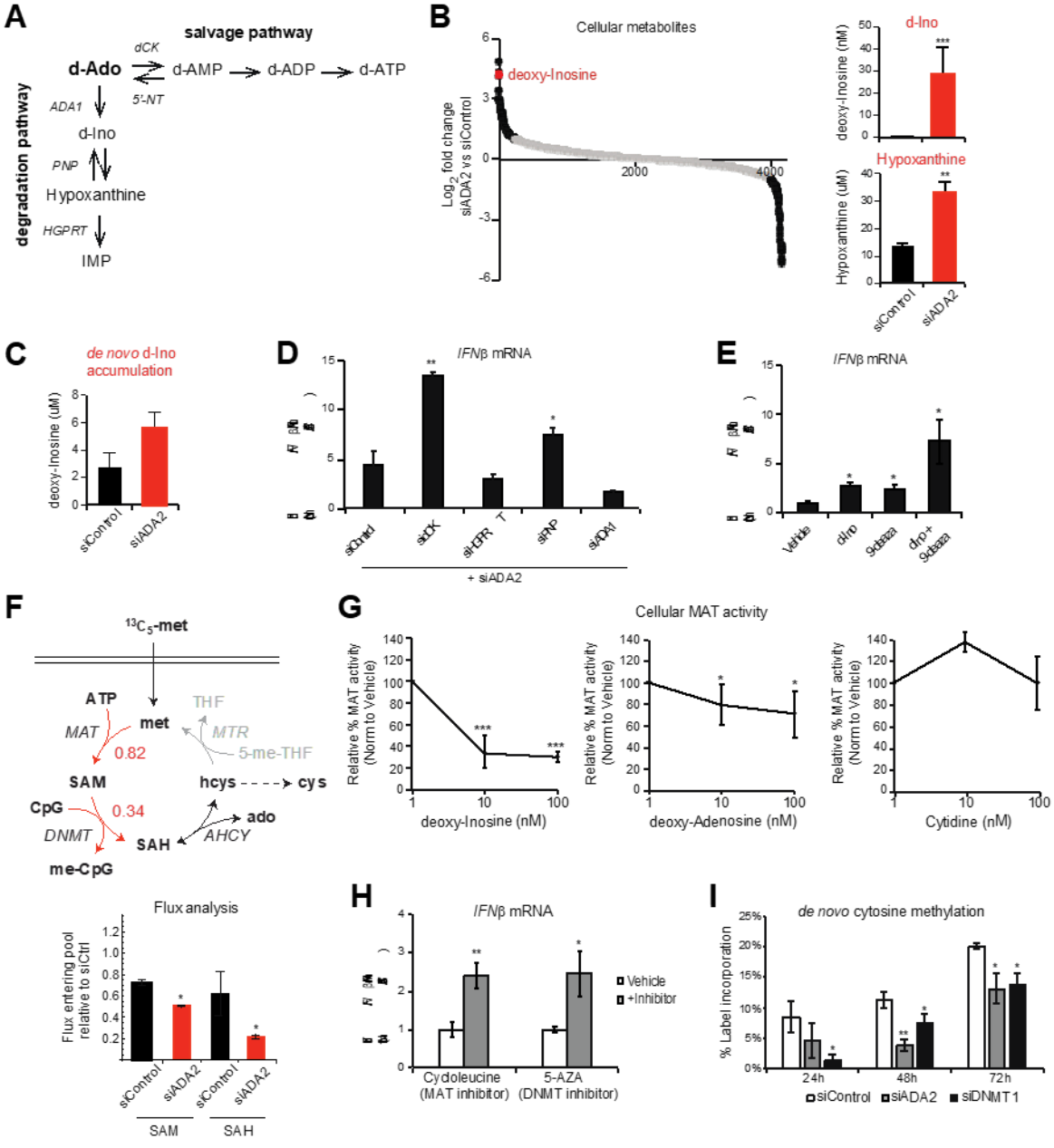
A
salvage pathway
d-Ado
dCK
d-AMP
d-ADP
d-ATP
5'-NT
ADA1
d-Ino
PNP
Hypoxanthine
HGPRT
IMP
degradation pathway
B
Cellular metabolites
deoxy-Inosine
Log2 fold change siADA2 vs siControl
d-Ino
deoxy-Inosine (nM)
Hypoxanthine
Hypoxanthine (uM)
siControl
siADA2
C
de novo d-Ino accumulation
deoxy-Inosine (uM)
D
IFNβ mRNA
siControl
siCK
siHPRT
siPNP
siADK1
+ siADA2
E
IFNβ mRNA
Vehicle
dIno
Sydstaza
dIno+ Sydstaza
F
13C5-met
ATP
met
THF
MAT
MTR
0.82
5-me-THF
SAM
hcys
cys
CpG
0.34
ado
DNMT
SAH
AHCY
me-CpG
Flux analysis
Flux entering pool relative to siCtrl
siControl
siADA2
SAM
SAH
G
Cellular MAT activity
Relative % MAT activity (Norm to Vehicle)
deoxy-Inosine (nM)
deoxy-Adenosine (nM)
Cytidine (nM)
H
IFNβ mRNA
Vehicle
+Inhibitor
Cycloleucine (MAT inhibitor)
5-AZA (DNMT inhibitor)
I
de novo cytosine methylation
% Label incorporation
24h
48h
72h
siControl
siADA2
siDNMT1

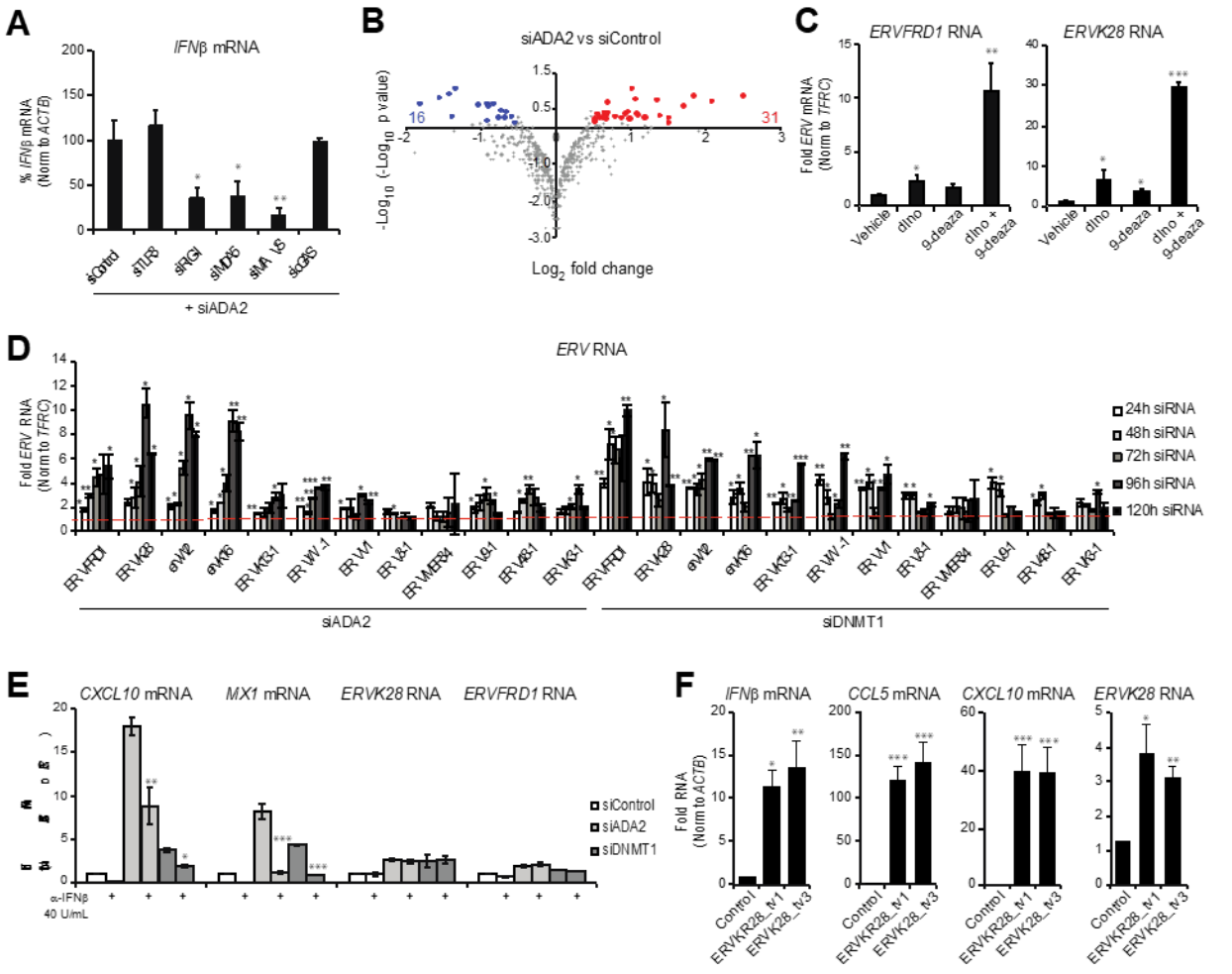

Figure 1.5: Induction of methylation-sensitive endogenous retrovirus elements triggers cytosolic dsRNA signaling and IFNβ production.
(A) IFNβ mRNA levels, measured by qRT-PCR, in HUVEC transfected with siRNAs targeting ADA2 and innate sensing molecules (n=3 technical replicates). (B) Differential expression of LTR-containing ERV genes between siControl and siADA2-transfected HUVEC, measured by polyA+ enriched RNAseq (n=3 biological replicates). Red and blue dots denote ERV significantly up or down-regulated > 1.5-fold. (C) mRNA levels of ERVFRD1 and ERVK28, measured by qRT-PCR, in HUVEC supplemented for 24h with dIno (500 □M) or pre-treated for 30 minutes with the PNP inhibitor 9-deazaguanine (100 □M) prior to dIno supplementation for 24h (n=3 technical replicates). (D) mRNA levels of endogenous retrovirus elements (ERV) at 24-120 hours, measured by qRT-PCR, in siADA2 or siDNMT1-transfected HUVEC (n=3 technical replicates). (E) mRNA levels of ISG and ERV, measured by qRT-PCR, in siADA2-transfected HUVEC treated with anti-IFNβ neutralizing antibody (40 U/mL) (n=3 technical replicates). (F) ERV, IFNβ, CCL5 and CXCL10 mRNA levels, measured by qRT-PCR, in HUVEC transfected with control plasmid or plasmids encoding ERVK28 transcript variants. Values presented as mean +/- standard deviation. *, P<0.05; **, P<0.01; ***P<0.001.

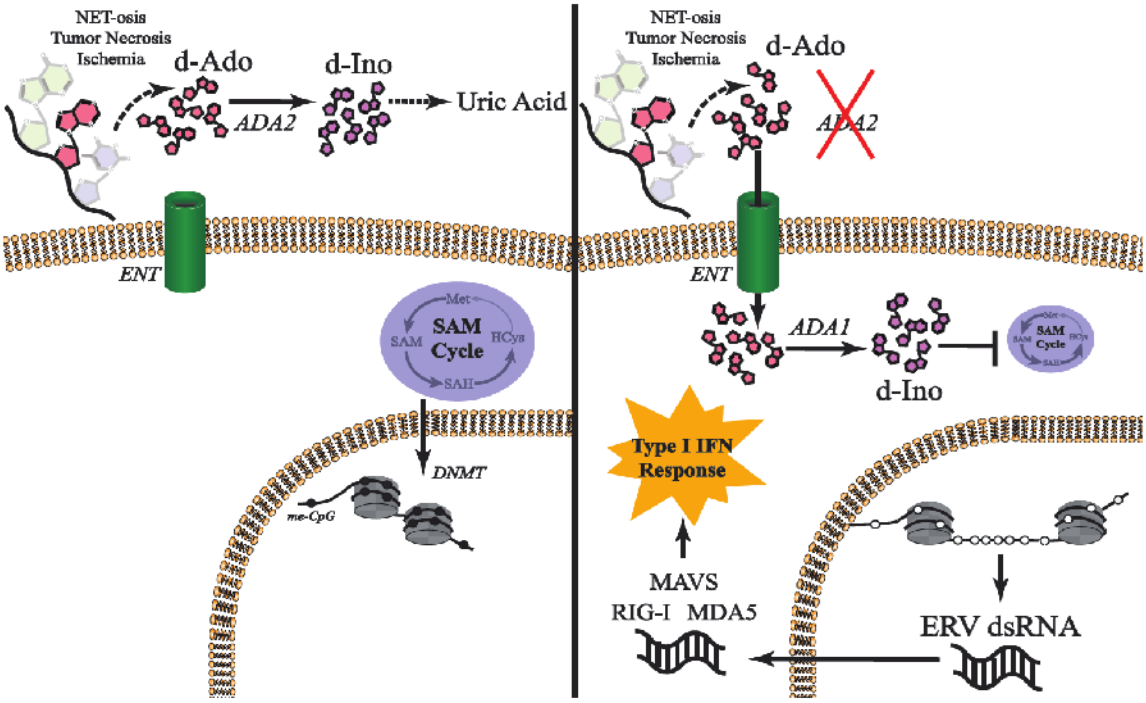

Figure 1.6: Cellular sensing of extracellular purine nucleosides triggers an innate immune response.
Loss of extracellular ADA2 activity or an excess of extracellular purine nucleosides drives uptake of dAdo and intracellular catabolism by ADA1, yielding dIno, an immuno-metabolite that directly inhibits MAT activity, the methionine cycle, and DNA methylation. Genomic hypomethylation drives up-regulation of ERVs, dsRNA molecules that engage cytosolic dsRNA sensors RIG-I and MDA5 via the signaling adaptor MAVS.

Supplementary Figures

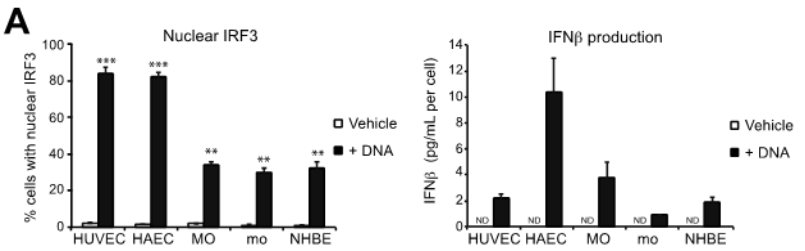

Figure S1.1: IRF3 translocation and IFNβ production in HUVEC.
(Left panel) IRF3 nuclear translocation in primary human endothelial cells (HUVEC, HAEC), PMA-treated U937 macrophage-like cells (MO), U937 monocytic cells (mo) and primary human bronchial epithelial cells (NHBE) treated with vehicle or poly dA:dT DNA (200 ng/mL for 3h) (n=3 technical replicates for n=3 biological replicates, >200 single cells per technical replicate). (Right panel) IFNβ secretion, measured by MSD assay, in cells treated with vehicle or poly dA:dT DNA (2—ng/mL for 3h) (n=3 technical replicates). All results were replicated in three independent experiments. Values presented as mean +/- standard deviation. ND, not detectable. *, P<0.05; **, P<0.01; ***P<0.001.

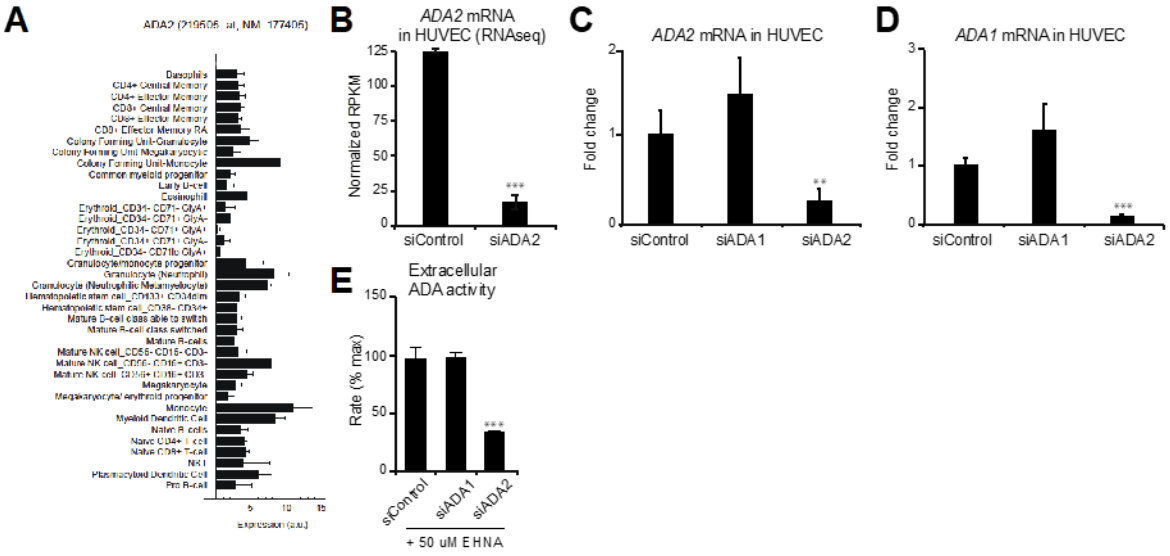

Figure S1.2: ADA2 mRNA is widely expressed in immune cells.
(A) Expression of ADA2 mRNA levels in human immune cells, derived from the GSE24759 microarray series matrix. All results were replicated in three independent experiments. Values presented as mean +/- standard deviation. (B) ADA2 mRNA levels, measured by qRT-PCR, in siRNA-transfected HUVEC (n=3 technical replicates). (C) ADA2 mRNA levels, measured by qRT-PCR, in HUVEC transfected with siControl, siADA1 or siADA2 siRNA. (D) ADA1 mRNA levels, measured by qRT-PCR, in HUVEC transfected with siControl, siADA1 or siADA2 siRNA. (E) Extracellular ADA activity, measured by de novo conversion of 1 mM isotopically-labelled dAdo to dIno in cell conditioned supernatant, from siControl or siADA2-transfected HUVEC pre-treated with vehicle or EHNA (50 uM for 30 min). Values are normalized to cell number and protein concentration (n=5 technical replicates) (n=5 technical replicates).

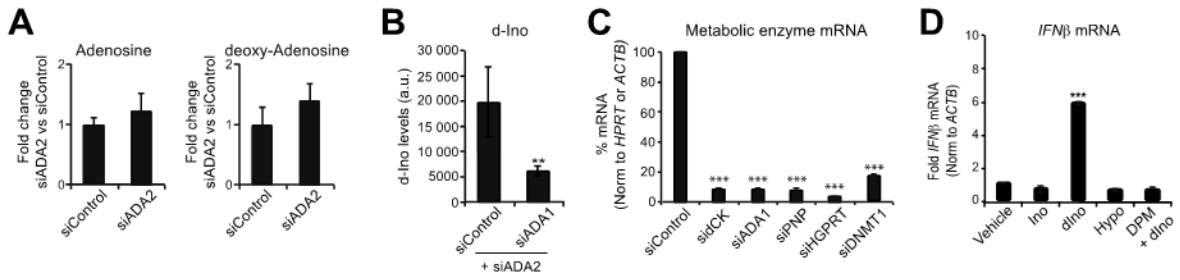

Figure S1.3: dIno is a functional immune-metabolite for IFNβ production.
(A) Fold change in purine metabolites, measured by LC-MS/MS quantification, of siControl or siADA2-transfected HUVEC (n=5 biological replicates). (B) dIno levels, measured by LC-MS/MS quantification of HUVEC treated with siADA2 and siControl or siADA1 (n=5 biological replicates). (C) mRNA levels of metabolic enzymes in the purine salvage, purine degradation and SAM pathways, measured by qRT-PCR in siRNA-treated HUVEC (n=3 technical replicates). (D) IFNβ mRNA levels, measured by qRT-PCR, in HUVEC supplemented for 24h with nucleosides (n=3 technical replicates). All results were replicated in three independent experiments. Values presented as mean +/- standard deviation. ND, not detectable. *, P<0.05; **, P<0.01; ***P<0.001.

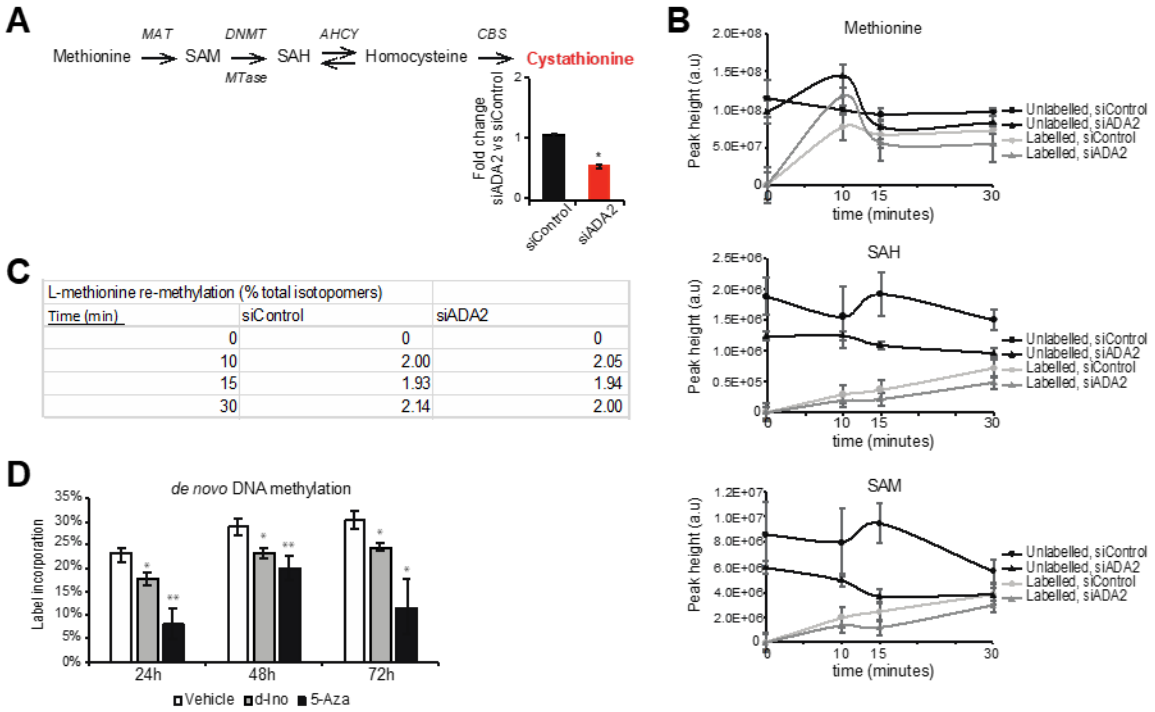

Figure S1.4: Flux analysis of the cellular methionine/SAM cycle and genomic methylcytosine. (A) Linear representation of cellular methionine/SAM pathway metabolism, and fold change of L-cystathionine, measured by LC-MS/MS, in siControl or siADA2-transfected HUVEC lysates (n=5 biological replicates). (B) Labeling of intracellular methionine, SAM and SAH pools, measured by LC-MS/MS (n=5 biological replicates). (C) Methionine re-methylation, measured by quantification of the methionine M+4 mass isotopomer using LC-MS/MS (n=5 biological replicates). (D) de novo DNA methylation, measured using LC-MS/MS quantification of isotope-labeled 2'-deoxy-5-methylcytidine in HUVEC treated for 24h with d-Ino (500 □M) or 5-AZA (50 □M) (n=3 biological replicates). All results were replicated in three independent experiments. Values presented as mean +/- standard deviation. ND, not detectable. *, P<0.05; **, P<0.01; ***P<0.001.

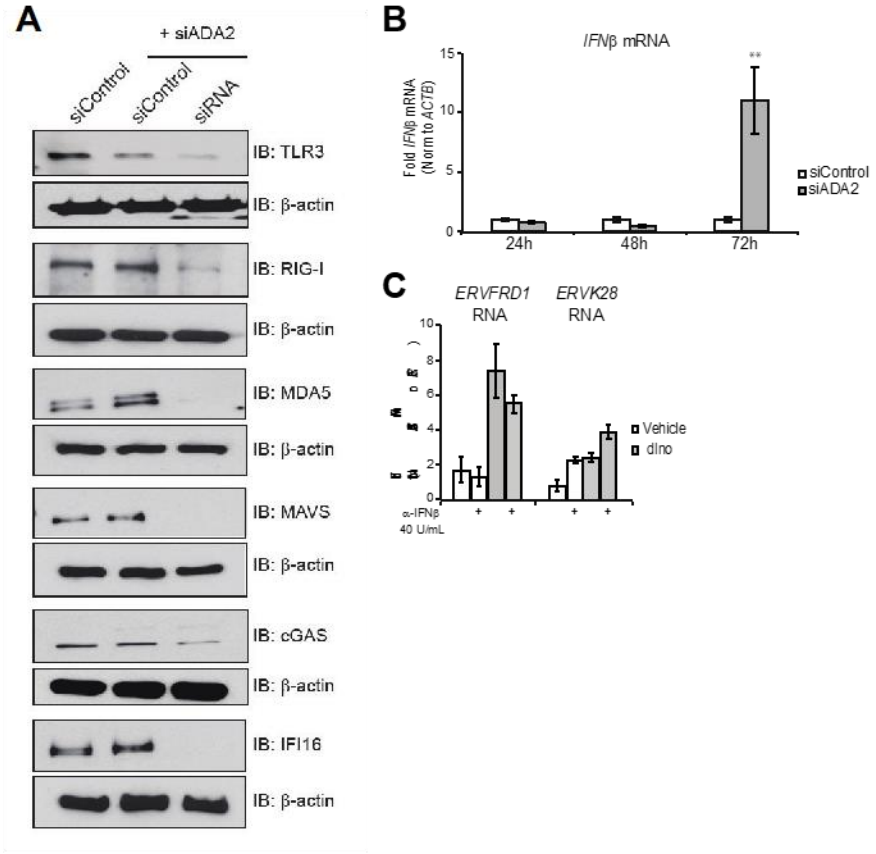

Figure S1.5: Protein levels of innate sensors and IFNβ expression.
(A) Western blotting of innate signaling molecules in siRNA-treated HUVEC. (B) IFNβ mRNA levels, measured by qRT-PCR, in siControl or siADA2-treated HUVEC (n=3 technical replicates). (C) ERV mRNA levels, measured by qRT-PCR, in HUVEC pre-treated with anti-IFNβ neutralizing antibody (40 U/mL) prior to stimulation with vehicle or dIno (500 □M) + 9-deazaguanine (100 µM) (n=3 technical replicates). All results were replicated in three independent experiments. Values presented as mean +/- standard deviation. ND, not detectable. *, P<0.05; **, P<0.01; ***P<0.001.

Table S1.1: 38 rare diseases of systemic inflammation with sequence-verified single gene mutations.
Information was obtained from the Online Mendelian Inheritance in Man (OMIM) database by searching for symptoms of vasculitis. Results of the siRNA screen in HUVEC are represented as Z scores.

OMIM	Gene_ID	Clinical Syndrome	Clinical Presentation	Organs affected	Inheritance	Z score
118450	JAG1	Alagille syndrome; ALGS1	Bile duct reduction (cholestasis) cardiac disease, skeletal abnormalities, ocular abnormalities, facial phenotype	Liver, heart, lungs, eyes, kidneys, bones, nervous system	AD	2
610205	NOTCH2	Alagille syndrome; ALGS2	Bile duct reduction (cholestasis) cardiac disease, skeletal abnormalities, ocular abnormalities, facial phenotype	Liver, heart, lungs, eyes, kidneys, bones, nervous system	AD	-2.7
125310	NOTCH3	Cerebral arteriopathy with subcortical infarcts and leukoencephalopathy	Characterized by relapsing strokes with neuropsychiatric symptoms (migraine, strokes, and white matter lesions)	CNS, small arterial vessels of the brain	AD	-2.1
152700	PTPN22	Systemic lupus erythematosus	Glomerulonephritis, dermatitis, thrombosis, vasculitis, seizures, and arthritis	Heart, lung, kidneys, limbs, skin, CNS	AD	-2.5
152700	FCGR2A	Lupus nephritis	Glomerulonephritis, dermatitis, thrombosis, vasculitis, seizures, and arthritis	Heart, lung, kidneys, limbs, skin, CNS	AD	-0.6
152700	FCGR2B	Systemic lupus erythematosus	Glomerulonephritis, dermatitis, thrombosis, vasculitis, seizures, and arthritis	Heart, lung, kidneys, limbs, skin, CNS	AD	-0.1
152700	CTLA4	Systemic lupus erythematosus	Glomerulonephritis, dermatitis, thrombosis, vasculitis, seizures, and arthritis	Heart, lung, kidneys, limbs, skin, CNS	AD	-1.1
152700 192315 225750	TREX1	Systemic lupus erythematosus Retinal vasculopathy with cerebral leukodystrophy Aicardi-Goutieres syndrome 1	-Glomerulonephritis, dermatitis, thrombosis, vasculitis, seizures, and arthritis -Progressive loss of vision, stroke, motor impairment, and cognitive decline -Cerebral atrophy, leukodystrophy, intracranial calcifications, chronic cerebrospinal fluid (CSF) lymphocytosis	Heart, lung, kidneys, limbs, skin, CNS CNS, retina; systemic vascular involvement CNS, retina; systemic vascular involvement	AD AD AD, AR	3.7
152700	DNASE1	Systemic lupus erythematosus	Glomerulonephritis, dermatitis, thrombosis, vasculitis, seizures, and arthritis	Heart, lung, kidneys, limbs, skin, CNS	AD	1.4
612952	SAMHD1	Aicardi-Goutieres syndrome 5	Developmental delay, poor feeding, irritability, or abnormal neurologic signs, leukodystrophy and calcifications in the basal ganglia or periventricular regions	Brain, skin	AR	0.5
162200	NF1	Neurofibromatosis, type 1	Café-au-lait spots (pigmented birthmarks), Lisch nodules in the eye, fibromatous tumors of the skin	Eye and skin	AD	-0.9
182410 615688	CECR1	Sneddon syndrome Polyarteritis nodosa, chilhood on-set; PAN	Livedo reticularis, cerebrovascular disease Ischemic strokes, recurrent fever, elevated acute-phase proteins, myalgias, and inflammatory vasculitis	Livedo racemosa (skin), heart, CNS Vascular system: skin, nervous system, kidney, GI tract	AR AR	3.6
186580	NOD2/CARD 15	Blau syndrome; BLAUS	Uveitis, synovitis, cranial neuropathies	Early-onset sarcoidosis; joints, skin, eyes	AD	0.3
216550	VPS13B	Cohen syndrome	Facial dysmorphism, microcephaly, truncal obesity, intellectual disability, progressive retinopathy, and intermittent congenital neutropenia	Retinopathy, neutropenia	AR	1.3

225760	FLVCR2	Proliferative vasculopathy and hydranencephaly-hydrocephaly syndrome	Hydranencephaly, diffuse ischemic lesions of the brain stem, spinal cord calcifications	CNS, retina	AR	0.2
607151	RNF213	Moyamoya disease; MYMY2	Bilateral internal carotid artery stenosis (narrowing) and abnormal collateral vessels	Vascular system		1
614042 613834	ACTA2	Moyamoya disease; MYMY3 Multisystemic smooth muscle dysfunction syndrome	Aortic disease, cerebral vascular abnormalities	Smooth muscle, lungs, vasculature	AD	-4.7
615750	GUCY1A3	Moyamoya disease; MYMY6	Severe achalasia, ischemic strokes	Vascular system	AR	-0.3
277400	MMACHC	Combined methylmalonic aciduria and homocystinuria	Developmental, hematologic, neurologic, metabolic, ophthalmologic, and dermatologic clinical findings	Vascular system, GI tract, kidneys, CNS	AR	1.7
309400	ATP7a	Menkes disease	Copper deficiency	Cardiovascular, bones, skin, CNS	XLR	-0.3
600142	HTRA1/PRSS 11	Cerebral arteriopathy with subcortical infarcts and leukoencephalopathy; CARASIL	Alopecia, spondylosis, and progressive motor dysfunction and dementia	Nervous system, spine	AR	1.1
602473	ETHE1	Ethylmalonic encephalopathy	Neurodevelopmental delay and regression, recurrent petechiae, orthostatic acrocyanosis, and chronic diarrhea	Brain, gastrointestinal tract, and peripheral vessels	AR	0.7
603075	HMCN1	Age-related macular degeneration-1; ARMD1	Progressive degeneration of photoreceptors and underlying RPE cells in the retina	Eyes	AD	1.5
603075	CFHR3	Age-related macular degeneration-1; ARMD1	Progressive degeneration of photoreceptors and underlying RPE cells in the retina	Eyes	AD	-2.3
603075	CFHR1	Age-related macular degeneration-1; ARMD1	Progressive degeneration of photoreceptors and underlying RPE cells in the retina	Eyes	AD	-1.4
603075	PLEKHA1	Age-related macular degeneration-1; ARMD1	Progressive degeneration of photoreceptors and underlying RPE cells in the retina	Eyes	AD	-0.5
603075	APOE	Age-related macular degeneration-1; ARMD1	Progressive degeneration of photoreceptors and underlying RPE cells in the retina	Eyes	AD	2.3
605714	APP	Cerebral amyloid angiopathy	Cerebral hemorrhage, ischemic lesions, and progressive dementia	Degenerative vascular changes, cerebral blood vessel walls	AD	-2.2
611773	COL4A1	Hereditary angiopathy with nephropathy, aneurysms, and muscle cramps	Retinal arterial tortuosities, intraretinal hemorrhages	Systemic vasculopathy; retina	AD	1.7
612199	CTC1/C17orf 68	Cerebroretinal microangiopathy with calcifications and cysts	Intracranial calcifications, leukodystrophy, and brain cysts, resulting in spasticity, ataxia, dystonia, seizures, and cognitive decline	Eyes, vascular system, heart, GI tract	AR	-1.8
612852	IL1RN	Sterile multifocal osteomyelitis with periostitis and pustulosis, OMPP	Pustulosis	Bones, sepsis, immunodeficiency, skin	AR	-0.9
613835	CRB1	Leber congenital amaurosis 8	Vision loss, nystagmus, and severe retinal dysfunction	Retinal dystrophy		-0.6
610333	RNASEH2A	Aicardi-Goutieres syndrome 4	Systemic		AR	-1.5
610181	RNASEH2B	Aicardi-Goutieres syndrome 2	Progressive neurodegeneration, Intracranial calcification primarily affecting the basal ganglia, microcephaly	Brain	AR	-1.4
610329	RNASEH2C	Aicardi-Goutieres syndrome 3	Extreme irritability, intermittent fever, chilblains,	Brain	AR	-0.9

			progressive microcephaly, spasticity, dystonia, and profound psychomotor retardation, white matter abnormalities, intracerebral calcifications, and cerebral atrophy			
615010	ADAR1	Aicardi-Goutieres syndrome 6	intracranial calcification and severe developmental delay, leukodystrophy	Brain	AR	1.2
615846	IFIH1	Aicardi-Goutieres syndrome 7	Microcephaly, spastic-dystonic tetraparesis, lack of speech	Brain	AD	2.4
615934	STING	STING-associated vasculopathy, onset in infancy; SAVI	Autoinflammatory vasculopathy, leading to severe skin lesions	Skin, lungs	AD	-4.9

Table S1.2: siRNA oligonucleotide sequences. Sequences correspond to siGenome oligonucleotide pools.

Gene Symbol	Entrez ID	siRNA Sequences
ADA2	51816	GGAAGUAGCUCAGAAGUUU, CAAGGAAGCUCUGAUGAUC, GCCAAAGGCUUGUCCUAUG, UCGCAGAAUCCAUCCGAAU
ADA2 (si OTP pool)	51816	UCGCAGAAUCCAUCCGAAU, GCCCAAAGCUAGUUAGUAC, CUUCCACGCCGGAGAAACA, GUGCCAAAGGCUUGUCCUA
ADA1	100	GAAACCAUCUUAUACUAUG, GGACACUGAUUACCAGAUG, UCAAAAGGAUCGCCUAUGA, GGACAUGGGCUUUACUGAA
ADA1 (si OTP pool)	100	GGGCUCGGCCGAAGUAGUA, CAAGUUUGACUACUACAUG, GGACAUGGGCUUUACUGAA, CCAAAGAGGGCGUGGUGUA
DCK	1633	CCAGAGACAUGCUUACAUA, GCAGGGAAGUCAACAUUUG, UGAAUUGGAUGGAAUCAUU, GAGACAGAGUGGACAAUUU
TREX1	11277	CAGAACACGGCCCAAGGAA, GCGCAUGGGCGUCAAUGUU, CCUUCUGUGUGGAUAGCAU, AGGACCAAGCCAAGACCAU
TMEM173	340061	GCACCUGUGUCCUGGAGUA, GGUCAUAUUACAUCGGAUA, GCAUCAAGGAUCGGGUUUA, ACAUUCGCUUCCUGGAUAA
PNP	4860	GCAAUAAUCUGUGGUUCUG, GCACGGCACUGUGGACUUC, UGAAAGGUUUGGAGAUCGU, GAUCUUUGACUACGGUGAA
HPRT	3251	GAUAUGCCCUUGACUAUAA, GUUUAUUCCUCAUGGACUA CUAUUGACAUCGCCAGUAA, GACUGAACGUCUUGCUCGA
MAVS	57506	AAGUAUAUCUGCCGCAAUU, GCUGUGAGCUAGUUGAUCU, CAAGAGACCAGGAUCGACU, AGAAUGAGUAUAAGUCCGA
DNMT1	1786	GGAAGAAGAGUUACUAUAA, GAGCGGAGGUGUCCCAAUA, GGACGACCCUGACCUCAAA, GAACGGUGCUCAUGCUUAC
TLR3	7098	GAAGCUAUGUUUGGAAUUA,GAUCAUCGAUUUAGGAUUG, GAAGAGGAAUGUUUAAAUC, CAACAUAGCCAACAUAAAU
DDX58	23586	CAGAAGAUCUUGAGGAUAA, GCACAGAAGUGUAUAUUGG, AGACAUGGGUAUAGAGUUA, CAACCGAUAUCAUUUCUGA
IFIH1	64135	GAGAAUAACUCAUCAGAAU, GAAAUCAUCUGCAAAUGUG, GGAAAUGAAUCAGGUGUAA, GAAUAACCCAUCACUAAUA
MB21D1	115004	GAAGAAACAUGGCGGCUAU, GAAGAGAAAUGUUGCAGGA, GUAAGGAAUUUCUGACAAA, CAACACUCGUGCAUAUUAC

Table S1.3: Taqman and SYBR Green primers for qRT-PCR of mRNA. Catalogue numbers and sequences are listed.

Gene symbol	Taqman probe ID
ADA2	Hs00602615_m1
DCK	Hs01040726_m1
IFN-b	Hs01077958_s1
HPRT	Hs02800695_m1
SLC29A4	Hs00928283_m1
SLC29A3	Hs00217911_m1
SLC29A2	Hs00155426_m1
SLC29A1	Hs01085704_g1
ADA	Hs01110945_m1
PNP	Hs01002926_m1
TREX1	Hs03989617_s1
DNMT1	Hs00945875_m1
CCL5	Hs00982282_m1
CXCL10	Hs01124252_g1
RSAD2	Hs00369813_m1

Gene	Forward Primer	Reverse Primer
IFN-b	GCTTGGATTCCTACAAAGAAGCA	ATAGATGGTCAATGCGGCGTC
IFIT1	TTGATGACGATGAAATGCCTGA	CAGGTCACCAGACTCCTCAC
HPRT	CCTGGCGTCGTGATTAGTGAT	AGCACACAGAGGGCTACAATG
ACTIN-B	TGAAGTGTGACGTGGACATC	GGAGGAGCAATGATCTTGAT

Table S1.4: Taqman and SYBR Green primers for qRT-PCR of ERV. Catalogue numbers and sequences are listed.

ERV gene	Taqman probe ID
ERVFRD1	Hs01942443_s1
ERVK13-1	Hs01393565_g1
ERVW-1	Hs01926764_u1
ERVV-1	Hs00708335_s1
ERV3-1	Hs04184598_s1
ERVMER34	Hs01038117_m1
ERV9-1	Hs04972165_g1
ERVH48-1	Hs05577546_g1
ERVK3-1	Hs03028028_s1

ERV gene	Primer sequence
ERVK28-1	CTGCCCACTAGGAGACTTAAT, GCCTCAGTATCTCCTTCCTTTC
ERVW-2	GCTACAAATGGTTCTTCAAATGGAG, ACAAGGGCTAGCAGGCT
ERVK16	TTTGACTGAAGTATTAAAAGGTGT, GTGACTGCAATTAATCCCATAATC

Materials and Methods

Experimental design: The objective of this research is to examine novel molecular mechanisms regulating the innate immune IFNβ response using controlled laboratory experiments. To identify novel gene and protein regulators of IFNβ, we optimized and implemented loss-of-function RNAi screening for activation of the transcription factor IRF3 in primary human vascular endothelial cells. Among 38 candidates associated with systemic inflammation and vasculitis in humans, the metabolic enzyme ADA2 was identified as a novel negative regulator of spontaneous IFNβ production. Subsequent transcriptomic, metabolic, and functional experiments were performed to examine the effects of ADA2 deficiency and purine nucleoside supplementation in triggering IFNB via activation of cytosolic nucleic acid sensing pathways. **Study design:** Sample size (n) for each experimental group is described in each figure legend, and was determined based on the optimal number to generate statistically significant data. No data were excluded. All experimental findings were independently replicated three times. Outliers were identified at the beginning of the study. Samples were randomized by position on plates, microplates and flow cells, or temporally randomized on the mass spectrometer. For siRNA screening, qRT-PCR, RNAseq, and mass spectrometry, research subjects (e.g. cell culture supernatants or lysates) were analyzed in a blinded manner using numerical keys.

Antibodies and reagents: Recombinant ADA1 (93985) was purchased from Sigma, and recombinant ADA2 (7518-AD) from R&D Systems. ADA2 antibody (HPA007888) was purchased from Sigma; β-actin antibody (MAB8929) from R&D; TLR3 antibody (sc-32232) from Santa Cruz; cGAS antibody (AP10510c) from Abgent; DDX58/RIG-I (ab45428), MAVS (ab31334) and IFI16 (ab55328) antibodies from Abcam; IFIH1/MDA5 antibody (21775-1-AP) from Proteintech; phospho-IRF3 (Ser396) (4947S), phospho-TBK1 (Ser172) (5483S), TBK1 (3013S), and IRF3 (4302S) antibodies from Cell Signaling Technologies; human IFNβ neutralizing antibody (31401-

1) was purchased from PBL interferon source; 2'-deoxyadenosine, adenosine, dipyridamole, EHNA, 5-azacytidine, and 9-deazaguanine from Sigma; pentostatin from Cayman Chemicals; cycloleucine from MP biomedicals; 2'-deoxyinosine, inosine and hypoxanthine from Alfa Aeser. ELISA kit for ADA2 quantification in cell culture supernatants was purchased from Cloud Clone Corp. poly (dA:dT) DNA was purchased from Invivogen. poly (dA:dT) DNA (P0883) was purchased from Sigma.

Cells: Primary human cells were obtained from Lonza as single donor aliquots. Umbilical vascular endothelial cells (HUVEC) and aortic endothelial cells (HAEC) were maintained in EGM-2 Bulletkit growth media (Lonza) supplemented with 2 % hi-FBS. Dermal microvascular endothelial cells (HDVEC), brain microvascular endothelial cells (HBVEC), and kidney microvascular endothelial cells (HKVEC) were maintained in EBM-2MV Bulletkit growth media (Lonza) supplemented with hi-FBS. Normal bronchial epithelial cells (NHBE) were maintained in BEGM Bulletkit growth media (Lonza). U937 monocytes were obtained from ATCC and maintained in RPMI supplemented with hi-FBS. Purity of cell populations was verified >95 % by flow cytometry using the following markers: CD31 for endothelial cells (Biolegend 303121), EpCAM for epithelial cells (Biolegend 324207) and CD45 for U937 monocytes (Biolegend 103115). For activation of IRF3-driven responses, cells were transfected with poly dA:dT for 3 hours (200ng/mL) using LyoVec transfection reagent (Invivogen), or infected for 3 hours with hCMV MOLD (MOI=1). For IFNβ neutralizing experiments, cells were treated with 10-40 U/ml of anti-IFNβ neutralizing antibody for 72 hours.

Virus: hCMV clinical strain MOLD (a kind gift from Dr. Martin Raftery) was used. Stocks were prepared as previously described [299].

siRNA screening and transfections: siGenome siRNA oligonucleotide pools were purchased from Dharmacon, and transfections performed as previously described [299]. siRNA transfection in U937 was performed with Neon Transfection System 100 □l kit (Thermo Fisher Scientific). Cells were resuspended with R buffer (5 x 10^6 cells/ml) and electroporated with 100 nM siRNA at 1,400 V/10 ms/3 pulse. Following transfection with siRNA (30-40 nM), growth media was changed every 24 hours and cells were harvested after 72 hours unless otherwise specified. For the IRF3 screen, Z score was calculated for each gene-specific siRNA pool using mean and standard deviation values from triplicate wells compared to control, non-targeting siRNA (Dharmacon). Individual Z scores are listed in **Table S1**. siRNA sequences are listed in **Table S2**.

IRF3 immunostaining: IRF3 immunostaining was performed as described [299]. IRF3 antibody (sc-9082) was purchased from Santa Cruz Biotechnology; Alexa Fluor 647-conjugated anti-rabbit secondary antibody (111-604-144) from Jackson ImmunoResearch. DAPI was used to counter stain nuclei. Images were acquired at 10x magnification on ImageXpress Micro (Molecular Devices), and images were analyzed using the enhanced translocation module of MetaXpress (Molecular Devices). Individual cells were scored as positive for nuclear translocation if >70 % of IRF3 fluorescence was spatially correlated with nuclear probe. Each data point is representative of >200 cells.

Quantitative real-time PCR: Total RNA was extracted using Quick-RNA MiniPrep Plus kit (Zymo Research). 500 ng of RNA was used to synthesize complementary DNA using qScript cDNA synthesis kit (Quanta). Samples were diluted 10-fold and gene expression analyzed by on a CFX96 Touch Detection System (Bio-Rad) using FastStart SYBR Green Master Mix (Roche) or TaqMan Universal PCR Master Mix (ThermoFisher Scientific). Primer pair sequences and catalogue numbers for cellular mRNAs are listed in **Table S3**. Primer pair and catalogue numbers for ERV genes are listed in **Table S4**.

Western blotting: For western blotting of whole cell lysates, cells were lysed in 1X RIPA buffer (Cell Signaling Technologies), incubated on ice for 30 minutes and centrifuged at 10,000 rpm for 10 minutes. Protein concentration was quantified from cleared supernatants using BCA protein assay kit (Thermo Fisher Scientific). Equivalent amounts of lysate (30-50 ug) were boiled with 5x SDS sample buffer and resolved by 10 % SDS-PAGE, transferred to PVDF membrane (Thermo Fisher Scientific), blocked with 5 % milk and incubated with primary antibody (1:1000) at 4°C overnight. Blots were washed with TBST and incubated with HRP-conjugated secondary antibodies (1:7000) at room temperature for 1 hour. Signal was detected using Amersham ECL Prime (GE Healthcare). For western blotting of cultured supernatants to detect ADA2, HUVEC or U937 cells plated at 5 x 10^5 cells per well in 6-well plates in serum-free media were cultured for 48h prior to collecting supernatants. 2-6 mL of supernatant was filtered (0.45 □m filter 28413-312, VWR) and concentrated with Pierce Protein Concentrator PES 10K MWCO (88527, Thermo Fisher Scientific) at 5,000 rpm for 15 min to obtain 100-150 □L samples. Concentrated supernatants were incubated with 5x SDS sample buffer at 70C for 10 min and resolved by 10% SDS-PAGE as described above. ADA2 antibody was obtained from Sigma (HPA007888).

RNAseq: Total RNA was extracted from 1x10^5 cultured cells using the Quick-RNA MiniPrep samples should produce RIN^e scores above 9.0. For each sample, 500-1000 ng of total RNA was then prepared into an mRNA library using the Truseq Stranded mRNA Library Prep Kit (Illumina). Resulting libraries were then pooled at equimolar concentrations using Quant-iT PicoGreen dsDNA Assay Kit (Life Technologies) and were deep sequenced on an Illumina 2500 in Rapid Run Mode, producing between 10M and 90M single-end reads with lengths of 50 nt per sample. The single-end reads that passed Illumina filters were filtered for reads aligning to tRNA, rRNA, adapter sequences, and spike-in controls. The reads were then aligned to UCSC hg38 reference

genome using TopHat (v 1.4.1). DUST scores were calculated with PRINSEQ Lite (v0.20.3) and low-complexity reads (DUST > 4) were removed from the BAM files. The alignment results were parsed via SAMtools to generate SAM files. Read counts to each genomic feature were obtained with the htseq-count program (v 0.6.0) using the “union” option. After removing absent features (zero counts in all samples), the raw counts were then imported to R/Bioconductor package DESeq2 to identify differentially expressed genes among samples. DESeq2 normalizes counts by dividing each column of the count table (samples) by the size factor of this column. The size factor is calculated by dividing the samples by geometric means of the genes. This brings the count values to a common scale suitable for comparison. P-values for differential expression are calculated using binomial test for differences between the base means of two conditions. These p-values are then adjusted for multiple test correction using Benjamini Hochberg algorithm to control the false discovery rate. We considered genes differentially expressed between two groups of samples when the DESeq2 analysis resulted in an adjusted P-value of <0.05 and the fold-change in gene expression was 2-fold. Cluster analyses including principal component analysis (PCA) and hierarchical clustering were performed using standard algorithms and metrics. Hierarchical clustering was performed using complete linkage with Euclidean metric.

For analysis of ERV expression, the single-end reads that passed Illumina filters were filtered for reads aligning to tRNA, rRNA, adapter sequences, and spike-in controls. The reads were then aligned to the reference genome using TopHat (v 1.4.1) and alignment results parsed via SAMtools to generate SAM files. The uniquely and multi mapped reads were filtered from the bam files using MAPQ of 255 to filter uniquely mapped reads. Read counts to each repeat element were obtained by mapping the multi mapped reads to the each of the repeat classes and counting alignment for each repeat class (all the steps are part of the RepEnrich pipeline). After removing absent repeat elements (zero counts in all samples), the raw counts were then imported to R/Bioconductor package EdgeR differentially expressed genes among samples. The GLM

method within the EdgeR package was used to identify differentially expressed genes. We considered genes differentially expressed between two groups of samples when the EdgeR analysis resulted in an adjusted P-value of <0.05.

Recombinant ADA supplementation: HUVEC were seeded at $5x10^5$ cells/well in 6-well plates and incubated for 24 hours at 37°C 5 % CO_2. 24 hours post-transfection with siRNA, fresh growth media containing recombinant ADA1 (Sigma, 93985) or ADA2 (R&D Systems, 7518-AD) was added to wells (50-1000 ng/mL). Where indicated, pentostatin (10 □M) was added 1 hour prior to recombinant ADA2. 72 hours post-transfection cells were harvested and gene expression analysed by qRT-PCR.

Co-culture of HUVEC and U937: HUVECs ($1.4x10^5$) were plated in 24-well plates. 24h post-transfection with siRNA, media was changed into fresh EGM2, and wild type U937 ($1x10^5$ cells/200 ul RPMI 2 % FBS) were plated on polyester membrane Transwell clear inserts (0.4 □m) and co-cultured with HUVECs for an additional 48h prior to analysis of gene expression by qRT-PCR.

Metabolite extraction and LC-MS/MS: For cell sample preparation, $3x10^6$ HUVEC were lysed by aspirating in 80 % cold methanol, followed by three freeze-thaw cycles where samples were alternated between 40°C and -80°C baths in 30 second intervals. Lysates were then centrifuged at 4°C at 14,000 rpm for 10 minutes to remove cellular debris and supernatants dried using a Speed Vacuum system for two hours at 30°C before resuspension in an 80:20 ratio of methanol to water. For spent media samples, media was centrifuged at 14,000 rpm for one minute to remove cell debris before adding cold methanol at a ratio of 80:20 methanol to water. Cell and

media samples were placed at -20°C for 30 minutes to precipitate protein before centrifugation at 14,000 RPM for 10 minutes at 4°C. Each injection for LC-MS/MS analysis was equivalent to 80,000 cells or 0.5 uL of media. Liquid chromatography was performed with a Vanquish UHPLC system (Thermo Scientific), using a ZIC-pHILIC polymeric column (EMD Millipore) (150mm x 2.1mm, 5um). Mobile phases used were (A) 20 mM ammonium bicarbonate in water, pH 9.6, and (B) acetonitrile. Mobile phase gradients were as follows: 90 % B for first two 2 minutes followed by a linear gradient to 55 % B at 16 minutes, sustained for an additional 3 minutes before final re-equilibration for 11 minutes at 90 % B. Column temperature was 25°C, and mobile phase flow rate was 0.3 mL per minute. Detection was performed using a QExactive Orbitrap mass spectrometer with heated electrospray ionization source (Thermo Scientific). Sheath and auxiliary gas was high purity nitrogen at 40 au (arbitrary units) and 20 au, respectively. Tandem mass spectra were collected in both positive and negative ionization polarities. Ion transfer tube was set at 275°C, and vaporizer temperature was set to 350°C. CID MS2 was collected using stepped normalized collision energies of 15, 30 and 45 arbitrary units and isolation widths of +/- 0.5 mz. Peak heights from chromatograms corresponding to metabolites of interest were used for quantification. Indicated metabolites were detected as protonated/deprotonated ions of their monoisotopic masses and identities were confirmed by comparison to the MS1 and MS2 patterning of known standards under this LC-MS method.

Methionine labeling and SAM flux: EGM-2 medium with dialyzed serum containing 64 □M unlabeled methionine was supplemented with either 64 □M U-^{13}C-methionine (Cambridge Isotope laboratories Inc.; ^{13}C medium) or 64 □M unlabeled methionine (^{12}C medium). At time zero, cells cultured in ^{12}C medium were switched to ^{13}C medium, incubated for 10 or 30 minutes at 37°C, washed twice with ice cold PBS, extracted in 80 % cold methanol and analyzed with LC-MS as described above to obtain mass isotopomer distributions. Due to lack of remethylation of

homocysteine, SAM metabolism was modeled as a linear pathway from methionine → SAM → SAH, governed by the differential equations:

$$\dot{x}_{\mathrm{SAM}} / \mu_{\mathrm{SAM}} = x_{\mathrm{met}} - x_{\mathrm{SAM}}$$

$$\dot{x}_{\mathrm{SAH}} / \mu_{\mathrm{SAH}} = x_{\mathrm{SAM}} - x_{\mathrm{SAH}}$$

Where x_{SAM} and x_{SAH} are time-dependent mass isotopomer fractions with time derivatives $\dot{x}$, while x_{met} was considered constant; v is the flux through the linear pathway; and μ is the rate constant, related to the flux as $\mu \cdot c = v$, where c is the pool size (concentration) [312]. This model was fit to the $^{13}C_5$-methionine, $^{13}C_5$-SAM and $^{13}C_4$-SAH mass isotopomers at the 10- and 30-minute time points by minimizing the variance-weighted sum of square errors. The resulting observed χ^2 error was 3.95, which was acceptable at the 95% level. Confidence intervals for the parameters μ were obtained as previously described [336]. Change in flux was obtained as the ratio

$$v^{\mathrm{siADA2}} / v^{\mathrm{siCtrl}} = \mu^{\mathrm{siADA2}} c^{\mathrm{siADA2}} / (\mu^{\mathrm{siCtrl}} c^{\mathrm{siCtrl}})$$

and 95 % confidence intervals for this ratio were obtained from the corresponding confidence intervals for μ.

ADA and MAT activity: In vitro dAdo deamination assays were adapted from previously described methodology [304], by measuring *de novo* dIno and hypoxanthine production using LC-MS/MS. For extracellular activity, cultured HUVEC-conditioned EGM-2 supernatant was centrifuged at 1,500 RPM for 5 minutes to remove cellular debris. For intracellular activity, whole cell lysates were diluted to 10E5 cell equivalents per mL in cold PBS. Supernatant or lysate was incubated with 100 nM-1mM isotopically-labelled 2'-deoxyadenosine (15N5, Cambridge Isotope Laboratories) for 30 and 120 minutes at 37°C. Reactions were quenched using ice cold methanol

at a ratio of 80:20 methanol:reaction volume and centrifuged at 14,000 rpm for 10 minutes to remove protein. Supernatant was isolated, from which 2uL was injected for LC-MS/MS analysis. Quantification of deaminase activity was measured as nanomoles of isotopically-labeled dAdo and hypoxanthine produced per liter per minute. For quantification of extracellular, HUVEC-derived ADA activity, reaction rate in cell-free EGM-2 growth media was subtracted from rates in culture supernatant, and data were normalized to cell number and protein concentration. *In vitro* methionine adenosyl-transferase assays were performed by detection of isotopically-labeled s-adenosyl methionine by LC-MS/MS, as described above. Fresh cytoplasmic protein lysates were isolated from U937 monocytes. In tissue culture- treated 96 well low evaporation plates, 10 □g of lysate was incubated with 1mM U-^{13}C methionine, 1mM ATP, and nucleoside at indicated concentration. Reactions were buffered in 20 mM $MgSO_4$, 150 mM KCl, and 100 mM Tris, pH 7.4. After incubation for 30 minutes at 37°C, reactions were quenched using ice cold methanol at a ratio of 80:20 methanol:reaction volume. Samples were centrifuged at 14,000 rpm for 10 minutes to remove protein, and supernatants were dried using a Speed Vacuum concentrator system for two hours at 30°C. Samples were resuspended in 50 □L of 80:20 methanol to water, with 2 □L injected for LC-MS/MS. Quantification of methionine adenosyltranserase activity was measured via *m/z* 404.1611 chromatogram peak intensity, corresponding to the $M+H^+$ ion of 5-carbon U-^{13}C labeled S-adenosyl methionine and confirmed by diagnostic tandem mass spectra.

Quantification of labeled methyl-cytosine and labeled deoxyinosine: For labeled deoxyinosine, HUVEC were transfected with siRNA against the indicated target for 72 hours, followed by treatment with 85 □M U-^{15}N-2'-Deoxyadenosine (Cambridge Isotopes) for 5 minutes. Cells were lysed, and metabolite extraction with LC-MS/MS was performed as described. 2'-Deoxyinosine with full label incorporation (4^{15}N-2'-Deoxyinosine) was identified by diagnostic

MS/MS fragmentation pattern, and relative abundance was quantified by peak height. For labeled methyl-cytosine, HUVEC were transfected with siRNA against the indicated target for 72 hours. During this time, cells were incubated with U-^{13}C methionine (Cambridge Isotope Laboratories) at 64 □M, the equivalent concentration to endogenous levels in growth medium, for the indicated times. Following lysing, genomic DNA was isolated using the PureLink Genomic DNA Mini Kit (Invitrogen) and quantified before digestion with DNA Degradase I (Zymogen) kit according to the manufacturer's protocol. Product deoxynucleosides were mixed 1:2 with a 50 % acetonitrile, 50 % water + 40 mM ammonium bicarbonate solution. Each injection of digested genomic isolate was equivalent to 5 ng of DNA. Liquid chromatography was performed with a Vanquish UHPLC system (Thermo Scientific) using a ZIC-HILIC column (EMD Millipore) (150 x 1 mm, 5 µM). Metabolites were eluted following a gradient mobile phase of (A) 40 mM ammonium bicarbonate and (B) acetonitrile. The gradients were used as follows: 90 % B at start, immediately following a linear gradient to 0 % B over 2 minutes, and sustaining 0 % B for two additional minutes of detection before a final equilibration for 1 minute at 90 % B. Column temperature was 25°C, and mobile phase flow rate was 0.175 mL per minute. Detection was performed using a QExactve Orbitrap mass spectrometer (Thermo Scientific) as described above, with CID MS2 collected using stepped normalized collision energies of 30 and 45 arbitrary units. Peak heights from chromatograms corresponding to the M+1 isotopomer of 2'-deoxy-5-methylcytidine were used for quantification, subtracting peak height attributable to naturally occurring ^{13}C isotope.

ERV cloning: cDNAs for ERVK28 transcript 1 and 3 were ordered from IDT. cDNAs were amplified using the Phusion polymerase enzyme and specific primers that are flanked by EcoRI (forward: 5'-GCT**GAATTC**CAGGTATTGTAGGGG-3' for Transcript 1; forward: 5'-GCT**GAATTC**ATGAACCCATCGGAG-3' for Transcript 3. EcoRI sites in bold), and ApaI or XhoI restriction sites (reverse: 5′-GT**GGGCCC**TGCAAAATGGAGT-3′ for Transcript 1, ApaI site in bold.

Reverse 5'-G**CTCGAG**GCGCAGAATTTTTC-3' for Transcript 3, XhoI site in bold), respectively. The amplicons (308 bp for Transcript 1 and 457 bp for Transcript 3) were digested with EcoRI/ApaI and EcoRI/XhoI respectively, and were cloned in frame with Flag between the EcoRI and ApaI sites, or EcoRI and XhoI sites, respectively, in pcDNA3-Flag-TRAF6 (Addgene, #66929). Plasmids were produced in One Shot™ TOP10 bacteria, and constructs sequence verified.

ERV overexpression: For electroporation, $2x10^5$ HUVEC were transferred to a sterile 1.5 ml microcentrifuge tube, resuspended in 10 µl Buffer R, and mixed with 500 ng of pcDNA3-Flag vector. DNA electroporation was performed with the Neon Transfection System 10 µL kit (ThermoFisher Scientific) using the following settings: 1350 V, 30 ms, 2 pulses. After electroporation, cells from five 10 µL transfection reactions were added to the same well of a 6-well plate containing 2 mL of pre-warmed supplemented EGM-2 Bulletkit growth media (Lonza) without antibiotics. 24 hours after transfection, new media with antibiotics was added to the wells. 48 hours post-transfection, total RNA was extracted using Quick-RNA MiniPrep Plus kit (Zymo Research). 500 ng of RNA was used to synthesize complementary DNA using qScript cDNA synthesis kit (Quanta). Samples were diluted 6-fold and gene expression analyzed on a CFX96 Touch Detection System (Bio-Rad) using TaqMan Universal PCR Master Mix (ThermoFisher Scientific).

Statistical analysis: Data values are reported as mean +/- standard deviation, with differences determined using two-tailed Student's t-test, with Benjamini Hochberg adjustment for multiple comparisons. Regarding statistical calculations, normal data distribution was confirmed using controls or previously generated large-scale datasets (n>384) prior to analysis of experimental samples. All reported results were independently replicated using three independent experiments.

Acknowledgement

Chapter 1 is a reprint in its entirety of “Cellular sensing of extracellular purine nucleosides triggers an innate IFN-β response”, by Dhanwani, Rekha; Takahashi, Mariko; Mathews, Ian T; Lenzi, Camille; Romanov, Artem; Watrous, Jeramie D; Pieters, Bartijn; Hedrick, Catherine C; Benedict, Chris; Linden, Joel; Nilsson, Roland; Jain, Mohit; Sharma, Sonia. Science Advances, July 2020. The dissertation author was a co-primary author on this publication.

Chapter 2: Resolution of Immune Toxicity Using Bioactive Lipids

Circulating Linoleoyl-Lysophosphatidylcholine is Protective in Immune Checkpoint Blockade-Induced Toxic Inflammation

Ian T. Mathews[1,2], Mir Henglin[3], Mingyue Liu[4], Kysha Mercader[2], Serena J.D.W. Chee[5], Allison Campbell[6], Saumya Tiwari[2], Jeramie D. Watrous[2], Khoi Dao[2], Mahan Najhawan[2], Lily Quach[2], Thien-Tu Catherine Nguyen[2], Pandurangan Vijayanand[1], Sandip P Patel[2,7], Susan M. Kaech[2,8], Christian Ottensmeier[5], Roy Decker[6], Abijit Patel[6], Pan Zheng[4], Mihai Netea[9], Mitchell Kronenberg[1], Tao Long[2], Susan Cheng[3], Mohit Jain[2] and Sonia Sharma[1*]

[1]La Jolla Institute for Immunology, La Jolla, CA 92037

[2]School of Medicine, University of California San Diego, La Jolla CA 92093

[3]Cedars Sinai Medical Center, Los Angeles CA 90048

[4]Institute of Human Virology, University of Maryland, Baltimore, MD 21201

[5]University of Southampton, Southampton, United Kingdom

[6]Yale University, New Haven CT 06520

[7]Moores Cancer Center, University of California San Diego, La Jolla CA 92037

[8]Salk Institute for Biological Studies, La Jolla CA 92037

[9]Radboud University Medical Center, Nijmegen, the Netherlands

*correspondence: soniasharma@lji.org

Main

Development of toxic inflammation during immune checkpoint blockade (ICB), termed immune related adverse events (irAEs), severely limits the efficacy of cancer immunotherapy[337]. These complications are poorly managed in the clinic, in part because the molecular mechanisms that drive irAE progression and their relationship to ICB-driven tumor regression are not well understood. Here we describe a novel protective mechanism by which circulating bio-active lipids of the lysophosphatidylcholine (LPC) superfamily may suppress irAE progression in ICB-treated

patients. Plasma from patients with solid tumors undergoing anti-CTLA4 or anti-PD1 therapy was assessed using non-targeted liquid chromatography-tandem mass spectrometry. Reduced levels of linoleoyl-lysophosphatidylcholine LPC (18:2) correlated with the development of severe ICB-driven irAEs [-1.12 (CI -2.01-0.25) log(odds ratio)]. Acute loss of circulating LPC (18:2) was recapitulated in a humanized mouse model of anti-CTLA4-driven irAEs and in DSS-induced colitis, where supplementation of LPC (18:2) ameliorated colonic inflammation without affecting ICB-driven tumor regression. Lower LPC (18:2) levels was associated with higher levels of circulating neutrophils in healthy individuals and in ICB-treated patients, where circulating neutrophils accumulated in patients who developed severe irAEs. Further, LPC (18:2) supplementation depleted circulating neutrophil counts *in vivo.* Results uncover a novel regulatory mechanism by which circulating LPC (18:2) molecules specifically suppress systemic inflammation and irAEs during ICB therapy while preserving anti-tumor immunity, and suggest that LPC (18:2) supplementation can be applied as a strategy to improve clinical outcomes in cancer immunotherapy.

Resistance or unresponsiveness to chemotherapy is commonly observed in late stage tumors[338,339], and patients with advanced melanomas or lung carcinomas are increasingly treated with ICB therapy. Nivolumab or pembrolizumab, both PD1 targeting monoclonal antibodies, are indicated as standalone therapies in secondary regimens against advanced lung carcinomas[154], and as first-line therapies against advanced melanoma[155]. Ipilimumab, in large part due to its greater toxicity profile, has been relegated to a secondary regimen or is given in combination with nivolumab[155]. Combination therapy with nivolumab and ipilimumab demonstrates a three-year overall survival rate of 58 percent for stage III/IV melanoma[156] and 40 percent for treatment-naïve stage III/IV NSCLC[340]. Understanding the determinants of clinical ICB outcomes is currently of high significance and intense study. ICB-driven tumor regression has been linked to several factors, including tumor neoantigen incidence, peripheral markers of immune fitness, and

influences of the gut microbiome[244,246,341-344]. Less well understood are the determinants of ICB-driven irAEs. The success of ICB therapies, particularly those including ipilimumab, is held back by severe contraindicated immune toxicities that drive discontinuation of treatment[337]. For nivolumab plus ipilimumab therapy, the incidence of grade III/IV irAEs is reported to be 33-59 percent[150,156], with ~40 percent of cases leading to termination of treatment[156,345]. As novel combination therapies aimed at further increasing immune-stimulation and overall response to ICB are under active development, the incidence of ICB-driven irAEs is only expected to rise. Incomplete mechanistic understanding of ICB-driven irAEs, particularly in humans, means that therapeutic strategies aimed at dampening irAE toxicities without blunting ICB-driven tumor regression are currently lacking.

The multi-organ etiology of ICB-driven immune toxicities, which arise upon systemic administration of immune-stimulator agents, suggests that immune-modulatory molecules present in circulation may impact the progression of irAEs. Small molecule metabolites in the blood, in particular bio-active lipids with signaling function, drive specific states of inflammation and immunity[270,346] These include eicosanoids and other oxylipins with known inflammatory function in asthma and allergy[277,347-349], cystic fibrosis[281,350], and progression to heart failure[351,352], but also hundreds of chemically related metabolites which associate with inflammatory states, but serve unknown roles in inflammation[346]. We reasoned that circulating lipid metabolites could be used to discriminate between irAEs and tumor regression during ICB therapy. To uncover novel metabolite associations with ICB-driven irAEs, we performed measurements of circulating bio-active lipids with surrogate associations to development of irAEs in cancer patients undergoing ICB therapy. In total, 753 blood plasma samples from 150 patients were sampled across three distinct ICB cohorts (**Supplementary Table 1**). The discovery cohort, corresponding to melanoma patients treated with 3mg/kg ipilimumab (Cohort 1, n = 65)[353], displayed a total irAE incidence of 56.4 percent, of which 6.4 percent constituted severe grade III/IV irAEs. Blood sampling

corresponded to baseline and serial blood draws up to twelve weeks post-treatment, without significant sampling bias in age or sex demographics, or in tumor regression outcomes (**Supplementary Table 2**). This sampling window directly overlaps with clinically observed kinetics of irAE development following ipilimumab treatment[354]. Samples were analyzed using directed, nontargeted liquid chromatography mass spectrometry (LC-MS)[355], allowing for rapid simultaneous profiling and semi-quantitative ranking of thousands of unique bio-active lipid metabolites. The maximum absolute excursion, or change in abundance, of each LC-MS feature was associated with the severity of ipilimumab-derived irAEs.

5951 LC-MS features were ubiquitously detected in patient plasma, of which several were differentially expressed over time in association with irAE severity (**Fig 1a**). Within this subset, we focused on abundant features associated with severe grade III/IV irAEs. From a network analysis of targeted tandem mass spectral data[356], chemically-related irAE-associated features (**Extended Data 1a**) were identified against a library of chemical standards as palmitoyl-lysophosphatidylcholine (LPC (16:0)) and linoleoyl-lysophosphatidylcholine (LPC (18:2)) (**Fig 1b, Extended Data 1b**), monoacyl metabolites of membrane phosphocholines commonly found in healthy blood at micromolar levels[287]. LPCs comprise a super-family of bio-active second messenger molecules that function in immunity and inflammation[357]. In ipilimumab-treated patients with severe irAEs, we observed LPC (18:2) and LPC (16:0) levels significantly dropping over time (**Fig 1c**). This association was not observed for any other LPC species, or in chemically and metabolically related lysophosphatidylethanolamines(LPE), lysophosphatidylinositols (LPI), or lysophosphatidic acids (LPA) molecules (**Supplementary Table 2**). Importantly, neither LPC (18:2) nor LPC (16:0) excursions were significantly associated with RECIST 1.1 metrics of ipilimumab-driven tumor regression response in the patient cohort[358] (**Supplementary Table 2**), nor did baseline abundances of LPC exhibit any predictive value, although both lipids were modestly elevated at baseline in patients who developed severe irAEs (**Extended Data 1c**).

These data indicate that LPC (16:0) and LPC (18:2) are specifically depleted in patients who develop severe irAES upon treatment with ipilimumab, unique among all lysolipids measured in circulation.

Depletion of LPCs from circulation is reported in several inflammatory pathologies and in autoimmunity[359,360]. Loss of LPC (18:2) is observed in patients with systemic lupus erythematosus (SLE)[361] and during sepsis[286,291], and is a risk factor for development of Type-II Diabetes and myocardial infarction[351,362,363]. LPC (18:2) and LPC (16:0) abundance was measured in blood plasma from patients with prevalent autoimmune or chronic inflammatory conditions, including SLE, rheumatoid arthritis, and inflammatory bowel disease (FINRISK-2002, n = 158)[364]. Relative to healthy individuals, significantly lower LPC (18:2) and LPC (16:0) levels were observed in plasma from autoimmune patients (**Fig 1d**), suggesting that LPC levels are a marker of deleterious inflammation shared in common with ipilimumab-induced irAEs.

Clinical and preclinical evidence supports a mechanism of action for ipilimumab that is distinct from other ICB antibody therapies[137,345,365]. To test the generalizability of our observations to other ICB therapies and tumor types, we examined two orthogonal cancer patient cohorts (**Supplementary Table 1**). First, a community-acquired cohort with mixed solid tumors (Cohort 2, n = 32), contained patients treated with ipilimumab in combination with nivolumab, or with anti-PD1 therapies alone. In this cohort, reduction of LPC (18:2) and LPC (16:0) in patients who developed severe irAEs upon anti-PD1 monotherapies or ipilimumab plus nivolumab combination therapy (**Fig 2a-b, middle,** and **Extended Data 2**). Second, in a prospective Phase I pembrolizumab trial of advanced NSCLC and melanoma patients[366] (Cohort 3, n= 53), reduction of LPC (18:2) and LPC (16:0) was also observed in patients who developed severe treatment-associated irAEs (**Fig 2a-b, right**). The effect size of LPC (16:0) and LPC (18:2) excursion on ICB is calculated to be -2.26 (CI -0.86 - -3.72) and -1.12 (-0.25 - -2.01) log(odds ratio), respectively, for ICB-irAE associations (**Fig 2c**).

Together, data demonstrate that LPC (18:2) and LPC (16:0) are surrogate biomarkers of severe irAEs associated with ICB therapy. The inverse relationship between LPC abundance and irAEs led us to hypothesize that rather than passive biomarkers of ICB-driven irAEs, these bio-active molecules might play a functional role in deleterious inflammation. To further examine LPC *in vivo*, we utilized two relevant mouse models. First, an ICB-induced model of irAEs, employs humanized C57BL/6 mice expressing the *CTLA4* transgene ($CTLA4^{h/h}$). $CTLA4^{h/h}$ mice develop multi-organ immune toxicities from ipilimumab monotherapy or combination therapy with anti-PD1 within the same therapeutic window as tumor regression response[367]. The second model is dextran sulfate sodium (DSS)-induced colonic inflammation and colitis[368-370], a model in which CTLA4 plays a role in enhancing inflammation and T cell induction is modulatory[371,372], but is dispensable for pathogenesis[373]. Mass spectrometry analysis of terminal blood from ipilimumab and combination ICB-treated $CTLA4^{h/h}$ mice demonstrated reduction of LPC (18:2) and LPC (16:0) (**Fig 3a**), consistent with our findings in human cancer patients. In DSS-induced colitis, reduction of LPC (18:2) and (16:0) levels was also observed in terminal blood plasma **(Fig 3b**). Together, these results show that reduction in circulating LPC (18:2) and (16:0) is also observed in mouse models of ICB-driven irAEs and chemically-induced colitis.

Previous studies show that unsaturated 18-carbon LPCs are consistently depleted in the circulation of DSS-treated mice, and play a protective role in colitis[374]. Dietary supplementation of oleic acid (C18:1) or overexpression of liver stearoyl-CoA desaturase-1 in DSS-treated mice elicited protective effects, although it is unclear whether the effect is driven by LPC (18:2), LPC (18:1), or another oleic acid metabolite [374]. Compared to LPC 18:2, loss of LPC (16:0) was less pronounced in $CTLA4^{h/h}$ mice (Figure 3a). Furthermore, levels of LPC (18:2) were negatively correlated with a composite histological score of irAE severity in these mice (**Fig 3c**), while LPC (16:0) did not meet significance (**Extended Data 3a**). Based upon stronger association of LPC 18:2 and irAEs, $CTLA4^{h/h}$ mice were supplemented with LPC (18:2) and effects upon irAEs

examined. Exogenous LPC (18:2) was administered at physiological levels via intraperitoneal injection (**Extended Data 3b**) to CTLA4$^{h/h}$ mice prior to ICB treatment. The supplemented mice experienced a reduction in colonic inflammation and leukocytic infiltration (**Fig 3d, Extended Data 3c**), indicating reduced ICB-associated toxicity. In DSS-induced colitis, supplementation of LPC (18:2) significantly reduced weight loss and colonic shortening (**Extended Data 4a-b**)**,** reduced intestinal inflammation, and mitigated overall intestinal damage to crypt cells (**Fig 3d**). In contrast, administration of LPC (16:0) did not elicit protective effects against DSS-induced colon toxicity (**Extended Data 4c**), nor did saturated LPC (18:0), although the monounsaturated LPC (18:1) demonstrated a modest protective effect upon colon shortening (**Extended Data 4d**). Together, results show that circulating LPC (18:2) protects against colon inflammation.

How loss of circulating LPC (18:2) impacts immune function and irAEs is unclear. In general, putative mechanisms underlying ICB-driven irAEs may involve increased activity of autoreactive effector T-cells, higher auto-antibody titers, activation of innate immune cytokines, or complement-mediated damage to healthy stroma[337]. The parameters of systemic immunity can be examined by measuring immune cells, serum cytokines, and antibody titers, with population-level variance explained at least in part by circulating metabolite variation[225,375,376]. LPC (18:2) levels were measured in healthy human blood plasma from two large-scale, community-based cohorts[225,377] (**Supplementary Table 3**), where serum cytokines, serology, and 80 immune cell populations, measured using multi-color flow cytometry, were quantified in participants. Correlation between effector or proliferating lymphocyte populations and circulating LPC (18:2) was not observed in in healthy individuals (**Extended Data 5a**), nor was there an association between LPC (18:2) and immunoglobulin titer (**Extended Data 5b**). In the 500 Functional Genomes cohort (500FG, n=500), levels of LPC (18:2) were significantly inversely correlated with neutrophils and natural killer T (NKT) cells in the blood (**Fig 4a**). These results were validated in the FINRISK-2002 cohort (FINRISK-2002, n = 215), where clinical blood counts were used to

measure neutrophils and other polymorphonuclear myeloid cells (**Fig 4b**). Notably, circulating LPC (18:2) inversely correlated with serum IL-8, a key cytokine that drives neutrophil cellularity [378,379] (**Extended Data 5c-d**). Together, these results suggest that loss of circulating LPC (18:2) associates with aberrant innate immune activation in ICB-driven irAEs, specifically an increase in circulating neutrophils.

Acute neutrophilia in the blood is characteristic of infections or ischemic heart failure[380,381], while chronic PR3-neutrophilia produces vasculitis and is a feature of rheumatoid arthritis[382,383]. Notably, LPC (18:2) regulates neutrophil function by inducing neutrophil superoxide release[287,384]. Low neutrophil-to-lymphocyte ratio (NLR) ratios are a risk factor for ICB-driven irAEs at baseline[385,386], however neutrophil measurements in longitudinal blood samples of ICB-treated patients have not been reported, and the regulatory role of circulating neutrophils has not been studied in this context. Using blood panel analyses from ipilimumab-treated melanoma patients (Cohort 1), we observed increased neutrophil levels upon therapy in patients who developed severe irAEs (**Fig 4c**), in contrast to lymphocyte and monocyte excursions which did not demonstrate any relationship to immune toxicity (**Extended Data 6**). LPC (18:2) levels exhibited an inverse correlation with neutrophil counts in Cohorts 1 and 2 (**Fig 4d**), indicating that the negative association between blood levels of LPC (18:2) and neutrophils is maintained both in healthy individual and ICB-treated cancer patients. In $CTLA4^{h/h}$ mice treated with ipilimumab and anti-PD1, neutrophils accumulated in penultimate blood counts (**Extended Data 3d**); increased neutrophil counts have also been reported in peripheral blood[387,388] and colons[389] of DSS-treated mice. In mice acutely supplemented with LPC (18:2), as well as the monosaturated LPC (18:1), neutrophils in peripheral blood significantly diminished, whereas the saturated LPC (18:0) did not alter neutrophil levels (**Fig 4e**). These data suggest neutrophilia in ICB-irAE is conserved in mice, and neutrophil cellularity in the periphery is negatively regulated by circulating LPC (18:2).

Together, data support a functional role for LPC (18:2) as a protective metabolite modulator of deleterious inflammation during ICB therapy. In patients treated with ipilimumab or pembrolizumab, LPC (18:2) is consistently reduced in those who developed severe irAEs on therapy, independently of tumor responsiveness. Indeed, we find LPC (18:2) was maintained at consistent levels in anti-CTLA4/anti-PD1 treated C57BL/6 mice bearing B16 subcutaneous melanoma, and that LPC (18:2) supplementation mice had no discernible effect upon the tumor regression response to ICB treatment (**Extended Data 7a-b**).

In summary, we report a novel uncoupling of immune checkpoint blockade toxicity from anti-tumor efficacy via a functionally protective circulating lipid. Blood plasma LPC (18:2) levels deplete over the course of severe irAE progression, mimicking lower levels observed in other autoimmune and inflammatory pathologies. This observation builds on existing reports, where lower levels of circulating LPCs of varied acyl substitutions including LPC (18:2) are observed in prospective[351,363] and prevalent[291,361,390] blood sampling of inflammatory conditions.

The phenotypic ramifications of depleted LPCs in blood are not understood; we describe a previously uncharacterized relationship between circulating LPC (18:2), peripheral blood neutrophils, and irAE progression. Neutrophil accumulation on ipilimumab directly correlated with irAE severity, while both healthy and ICB-treated individuals with low LPC (18:2) levels had higher circulating neutrophil counts. LPCs are cAMP-dependent modulators of superoxide release in neutrophils[384] in an acyl saturation-dependent manner[287], but have not as yet been described as determinants of circulating neutrophil cellularity. We show LPC (18:2) supplementation *in vivo* rescues ICB- or chemically-induced symptoms of colitis, and negatively regulates peripheral blood neutrophil levels.

This study constitutes a useful contribution to our understanding of immune checkpoint blockade toxicity and the progression of severe irAE, specifically through the lens of bioactive lipid metabolites like LPC (18:2) as significant regulators of systemic immunity.

Figures

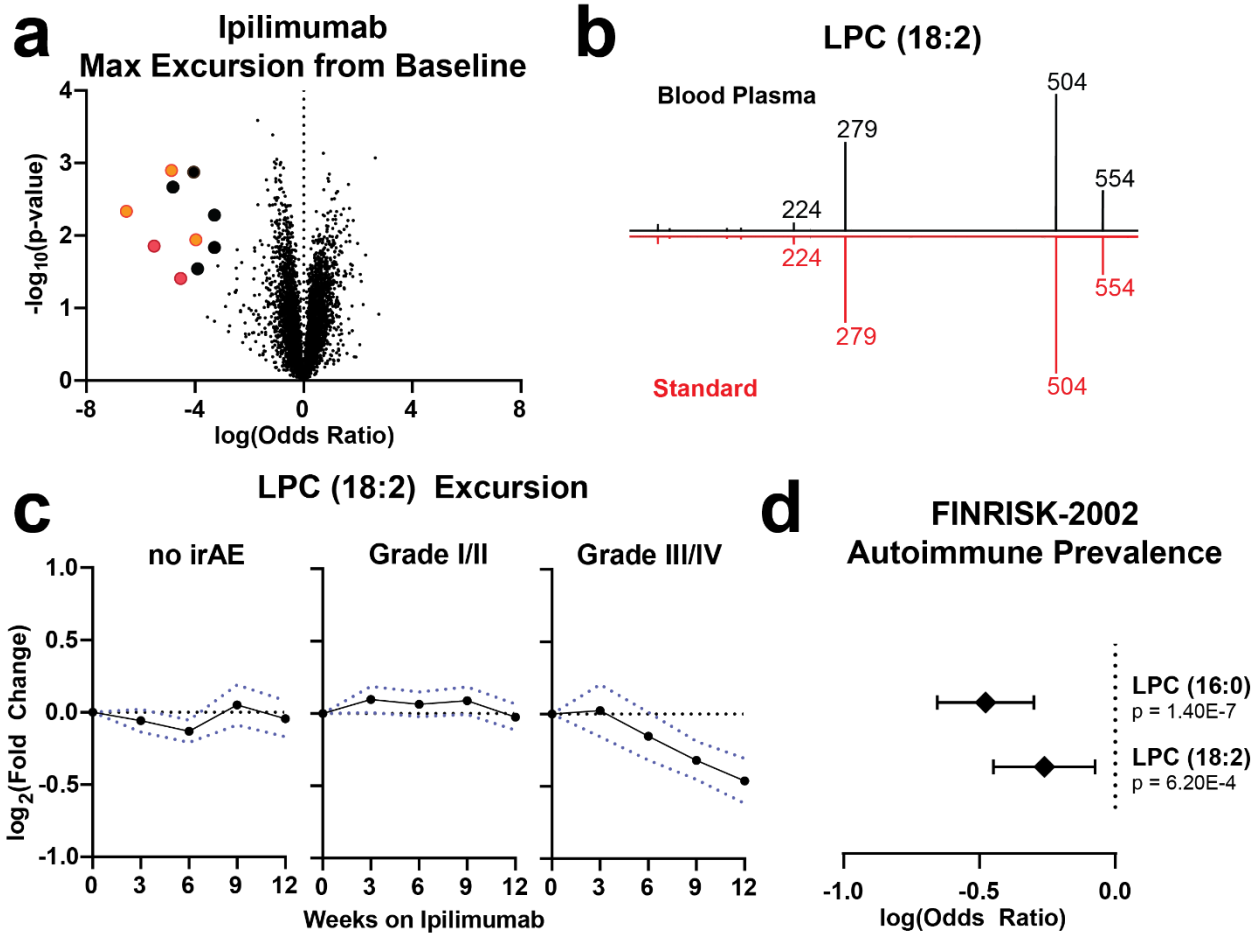

Figure 2.1: Identification of two circulating lysolipids depleted in ipilimumab toxicity and autoimmunity.

a) Volcano plot for irAE severity logistic regressions in ipilumumab treated melanoma patients (Cohort 1, n = 65) of 5951 ubiquitous bioactive lipid LC-MS features. Odds ratio normalized to a natural logarithm. b) Tandem mass spectra of *m/z* 554.3019, corresponding to LPC (18:2) [M+Cl^-]. c) Mean excursions of LPC (18:2) in Cohort 1, error = SEM. d) Natural log odds ratio of prevalent autoimmune pathologies in FINRISK-2002 (case: n = 158, control: n = 1712). Error = 95% CI.

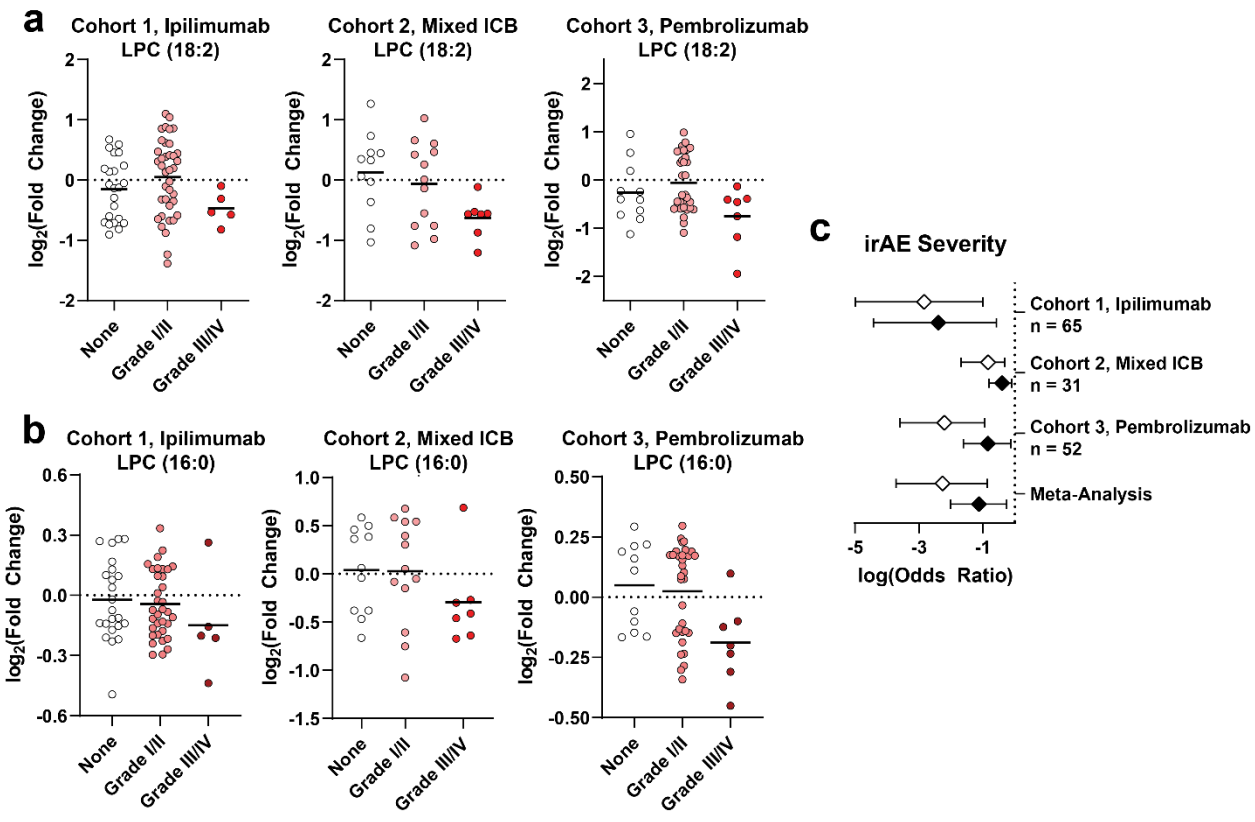

Figure 2.2: LPC (18:2) and LPC (16:0) loss is a conserved feature of ICB-irAE.

a-b) Maximum excursion of LPC (18:2) (a) and LPC (16:0) (b) in three cohorts of ICB-treated patients, bars = mean. C) Forest plots of natural log odds ratio of irAE severity for LPC (16:0) (open) and LPC (18:2) (closed). Error = 95% CI.

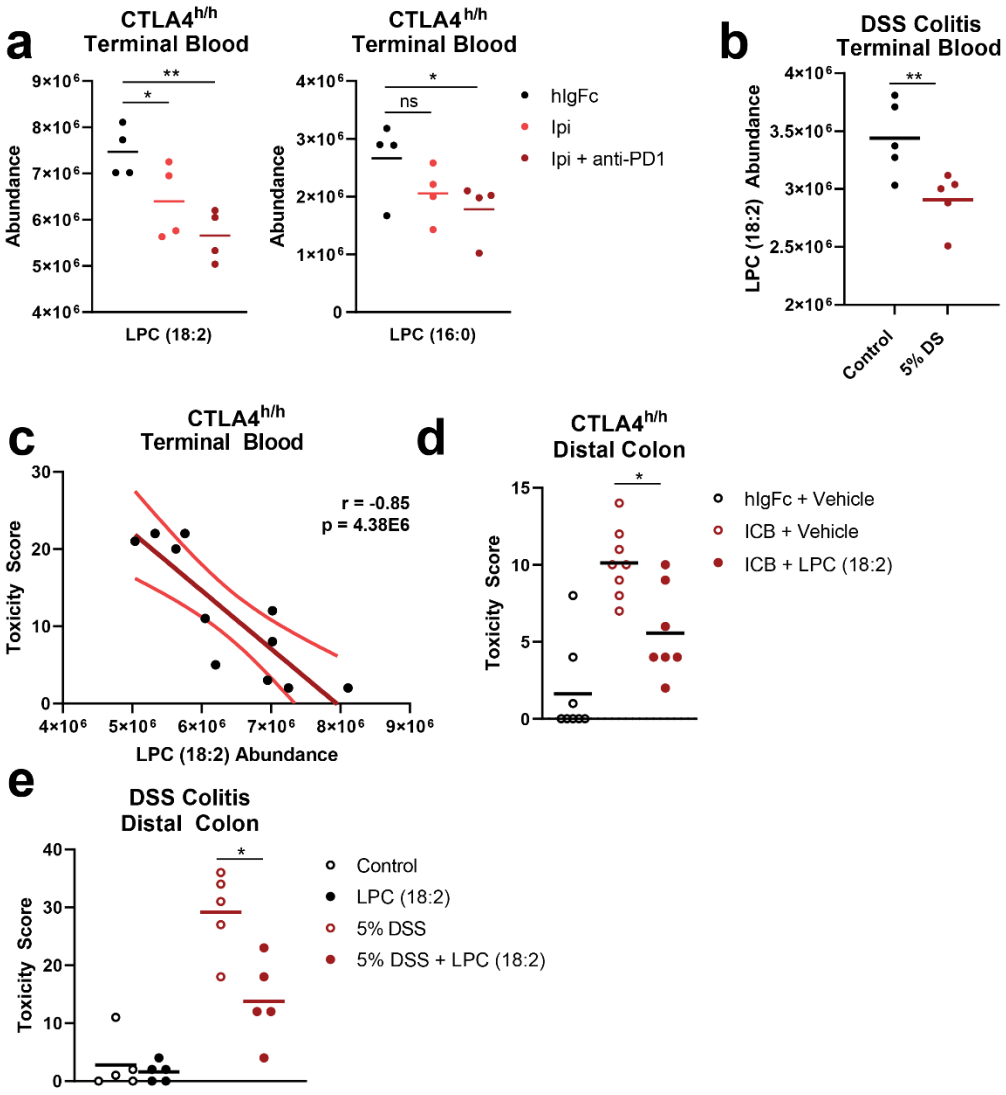

Figure 2.3: LPC (18:2) supplementation is protective in two models of colitis.

a) LPC (18:2) (left) and LPC (16:0) (right) abundance in terminal blood of CTLA4$^{h/h}$ C56BL/6 mice treated with 100 ug anti-human IgG1 isotype control (hIgFc), 100 ug ipilimumab (Ipi), or 100 ug ipilimumab + 100 ug anti-mouse PD1 monoclonal antibody (Ipi + anti-PD1). Antibody treatments were administered on Day 10, 13, 16, and 19. b) LPC (18:2) abundance in terminal blood of control and 5% w/v DSS-treated C56BL/6 mice. c) Scatter plot of composite toxicity score in CTLA4$^{h/h}$ mice with matched LPC (18:2) abundance in terminal blood. d) Toxicity score and representative H&E staining in distal colon of CTLA4$^{h/h}$ mice following intraperitoneal administration of 100 ug anti-human IgG1 isotype control (hIgFc) or 100 ug ipilimumab + 100 ug anti-mouse PD1 monoclonal antibody (ICB), dosed as above. LPC (18:2) was administered intraperitoneally at 25 mg/kg on Days 10, 13, 16, 19, 22, and 25. e) Toxicity score and representative H&E staining in distal colon of DSS-treated mice. LPC (18:2) was administered at 25 mg/kg on Days 0, 2, 4, and 6 of DSS treatment. Bars = mean value, significance: Student's T-Test, * = $p < 0.05$, ** = $p < 0.01$.

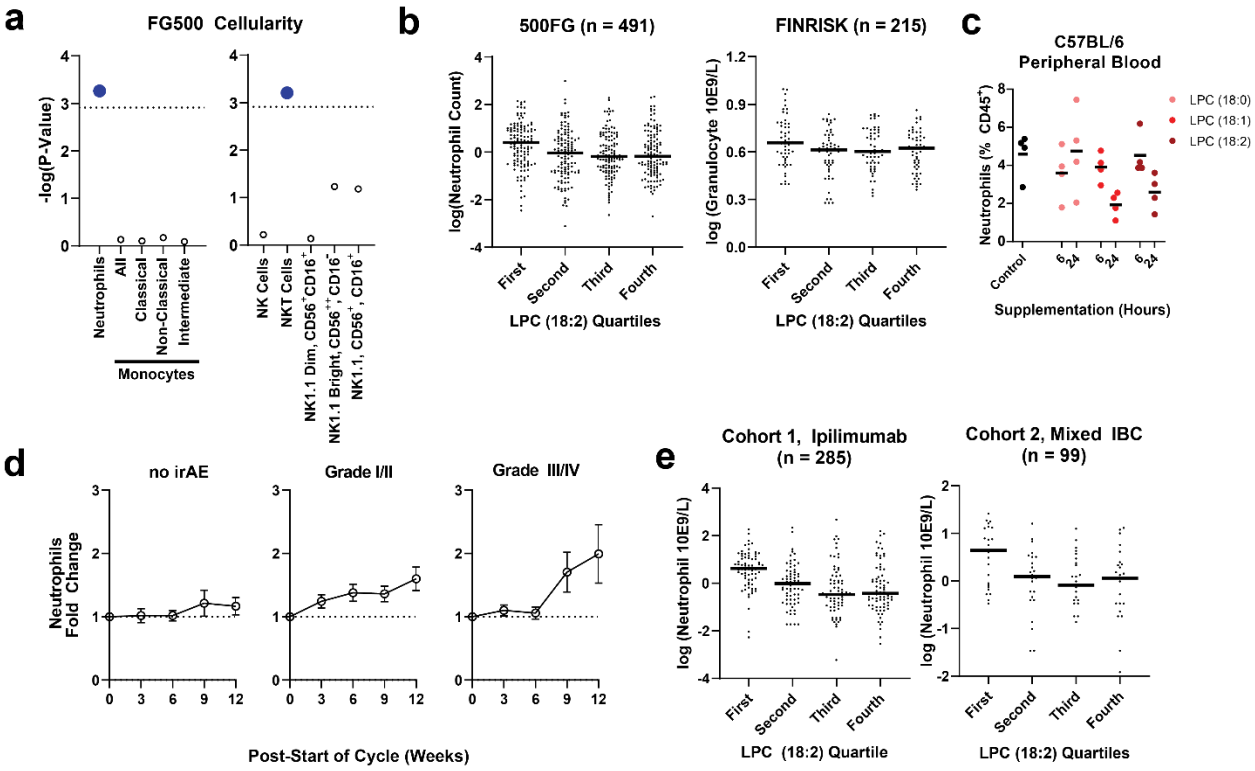

Figure 2.4: LPC (18:2) inversely correlates with neutrophil cellularity in circulation.

A) Significance of association by linear regression between LPC (18:2) and various myeloid (left) and natural killer cell (right) populations in matched blood from healthy individuals (500FG, n = 491, dotted line indicates p = 0.05 following Bonferroni multiple hypothesis correction). B) Quartiles of LPC (18:2) abundance and neutrophil counts as measured by multi-color flow cytometry (500FG, left) or by blood analyzer (FINRISK-2002, n = 215, right). Bars = mean. C) Fold change of neutrophil counts relative to baseline sampling in Cohort 1 ipilimumab treated melanoma patients. Error = SEM. D) Quartiles of LPC (18:2) abundance and neutrophil counts in ICB Cohort 1 and Cohort 2. Bars = mean. Significance is derived from linear regression including patient and timepoint as covariates to control for internal correlation.

Supplementary Figures

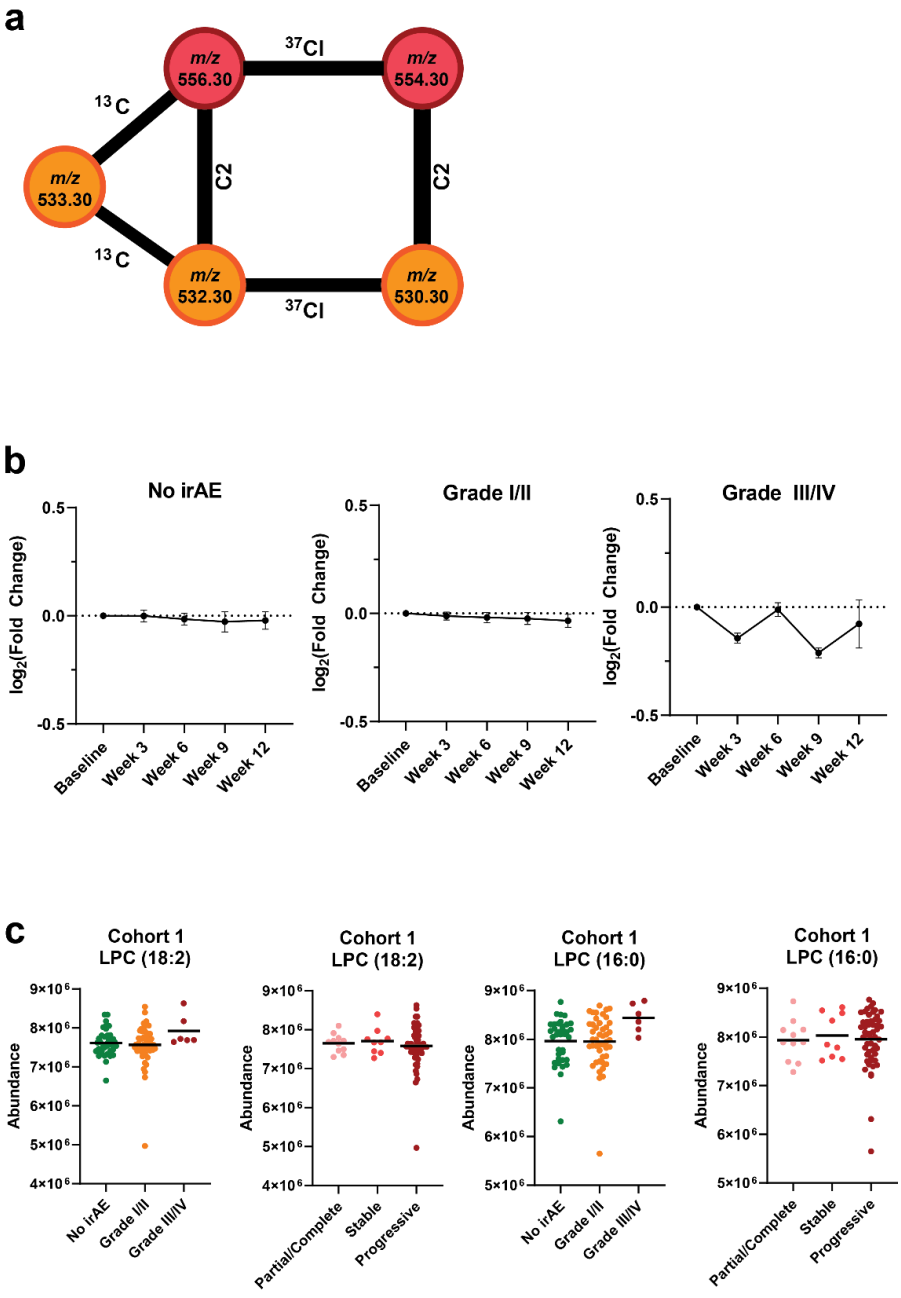

Figure S2.1: Chemically related LPC (18:2) and LPC (16:0) in ipilimumab patient outcomes.

a) Tandem mass spectral chemical network of 5 irAE-associated LC-MS features corresponding to [M+Cl$^-$] adducted LPC (18:2) and LPC (16:0). b) Excursion of LPC (16:0) in Cohort 1 ipilimumab treated patient blood plasma (n = 65). Error = SEM. c) Abundance of LPC (18:2) and LPC (16:0) in baseline sampling from Cohort 1.

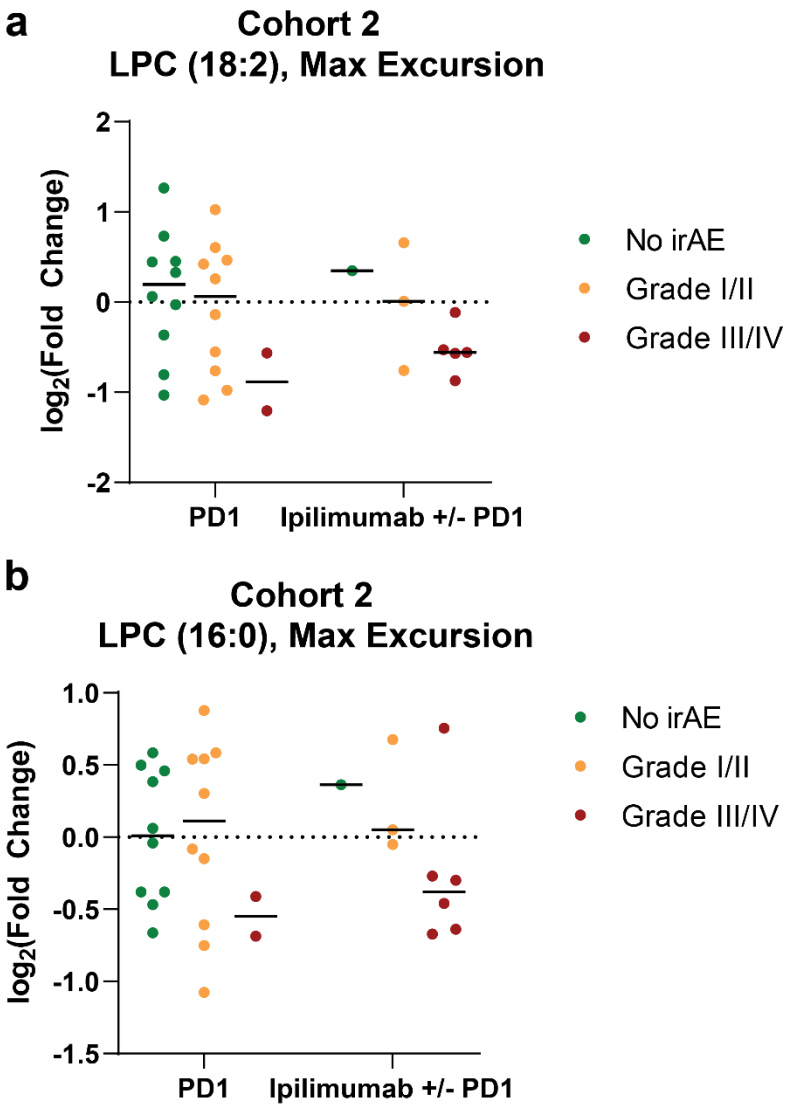

Figure S2.2: LPC (18:2) and LPC (16:0) excursion on different ICB treatments.

A-B) Maximum excursion of LPC (18:2) (A) and LPC (16:0) (B) in Cohort 2, broken out by anti-PD1 monotherapy or anti-PD1 combination ipilimumab.

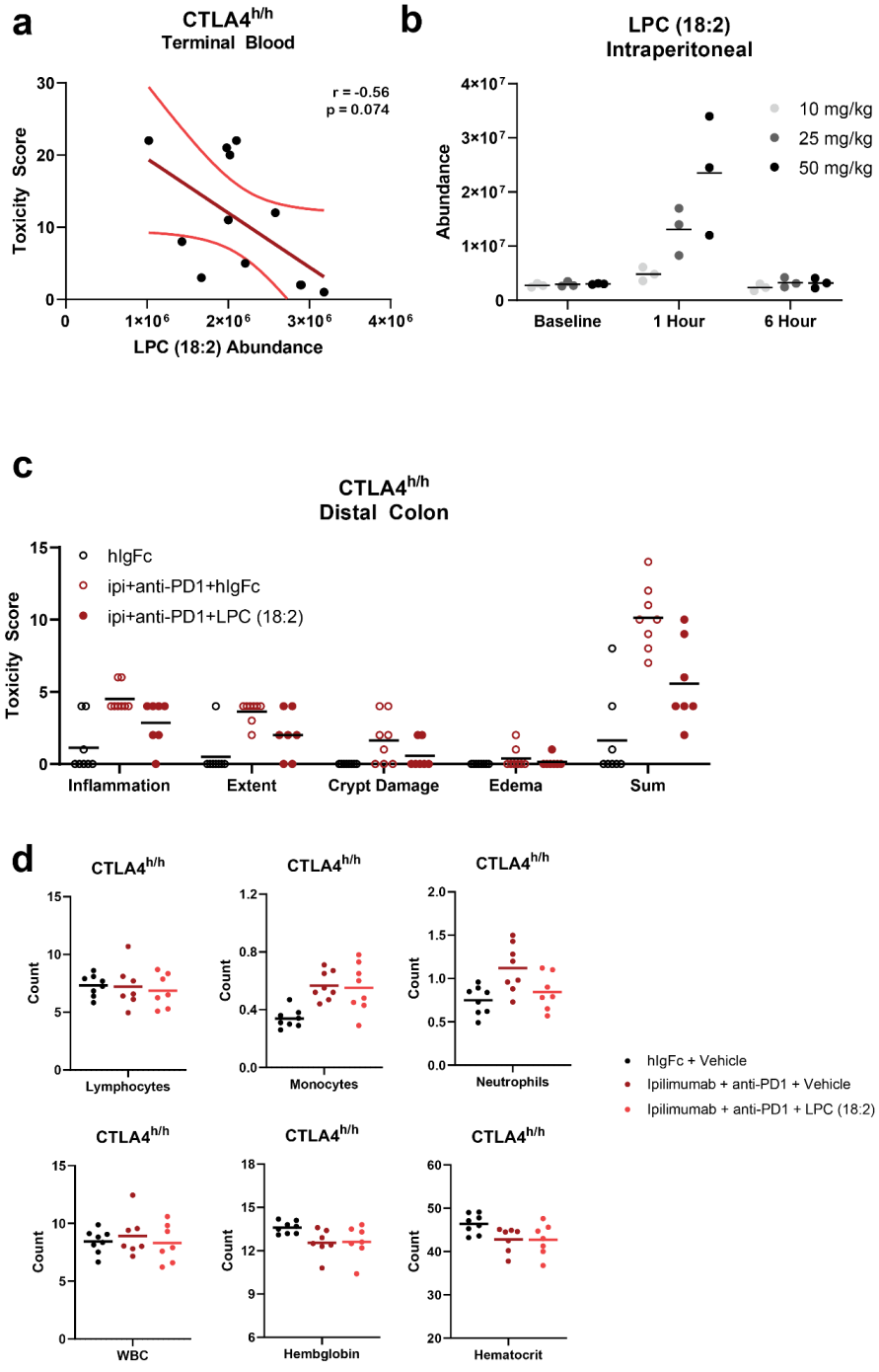

Figure S2.3: Loss and supplementation of LPCs in CTLA4 humanized mice.

A) Scatter plot of composite toxicity score in CTLA4$^{h/h}$ mice with matched LPC (16:0) abundance in terminal blood. Error = 95% CI. B) Blood plasma LPC (18:2) following single dose intraperitoneal supplementation in C57BL/6 mice. Bar = mean. C) Toxicity scoring by four criteria in CTLA4$^{h/h}$ mice. Bar = mean. D) Blood analysis by complete blood count in Day 41 CTLA4$^{h/h}$ mice.

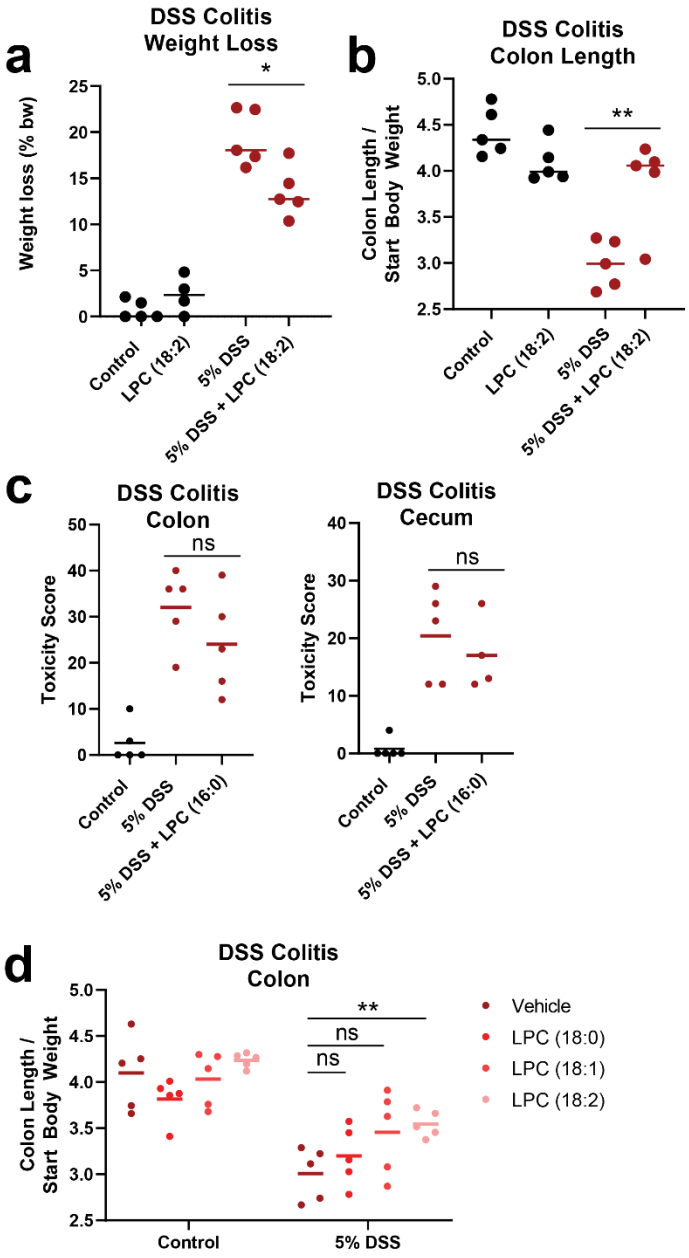

Figure S2.4: Loss and supplementation of LPCs in DSS-induced colitis.

A-B) Percent weight loss (A) and colon length relative to starting body weight (B) in 5% DSS treated mice following LPC (18:2) supplementation. C) Toxicity score in cecum and distal colon of 5% DSS treated mice following LPC (16:0) supplementation. D) Colon length relative to starting body weight in 5% DSS treated mice following supplementation with saturated and unsaturated C18-LPCs.

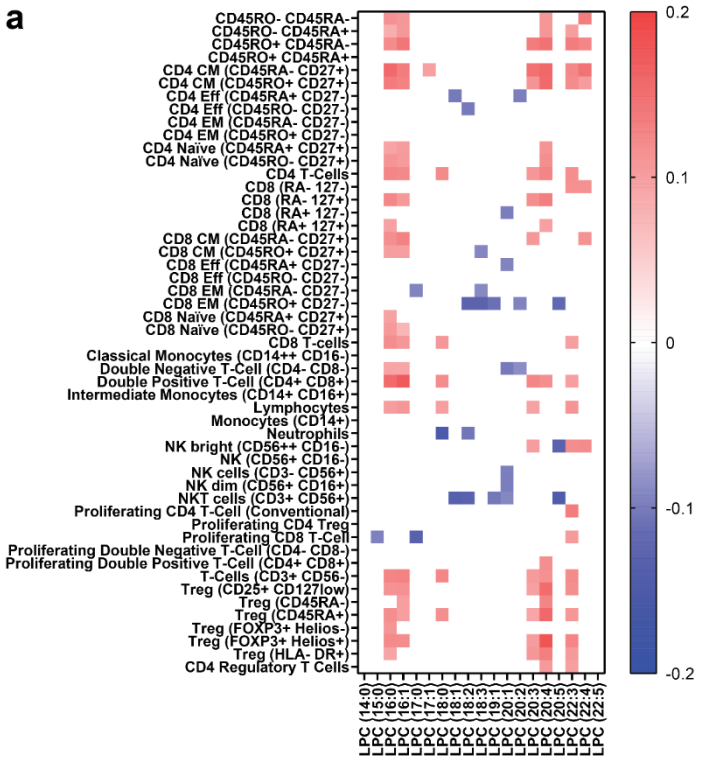

b

	Effect Size	Confidence Interval		p-value
IgA	0.05	-0.04	0.15	2.72E-01
IgG	-0.09	-0.18	0.01	9.00E-02
IgG1	-0.11	-0.21	-0.01	2.92E-02
IgG2	0.02	-0.08	0.12	7.04E-01
IgG3	-0.05	-0.15	0.05	3.44E-01
IgG4	0.03	-0.07	0.13	5.73E-01
IgM	-0.08	-0.18	0.02	1.17E-01

c

	Effect Size	Confidence Interval		p-value
IL-8	**-1.27**	**-2.20**	**-0.34**	**7.50E-03**
G-CSF	3.84	-1.56	9.25	1.63E-01
GM-CSF	3.08	-2.53	8.68	2.82E-01
M-CSF	-0.73	-2.44	0.99	4.06E-01

d

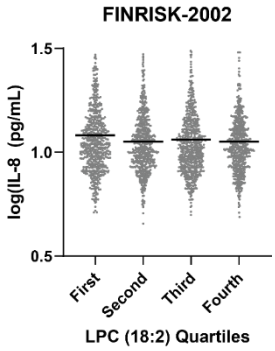

Figure S2.5: LPC and immune feature associations in 500FG and FINRISK 2002.

A) Heat map of LPC associations with immune cellularity by multi-color flow cytometry in 500FG (n = 488). Color = effect size with $p < 0.05$. B) Circulating LPC (18:2) associations by linear regression with serum immunoglobulin titers in 500FG (IgG [7.00-16.00 gram/Liter]; IgA [0.70-4.00 gram/Liter]; IgM [0.40-2.30 gram/Liter]; IgG1 [4.90-11.40 gram/Liter]; IgG2 [1.50-6.40 gram/Liter]; IgG3 [0.20-1.10 gram/Liter]; IgG4 [0.08-1.40 gram/Liter]. C) Circulating LPC (18:2) associations by linear regression with serum cytokines in FINRISK-2002 (n = 2500). D) Quartiles of circulating LPC (18:2) and serum interleukin-8 (IL-8) in FINRISK-2002.

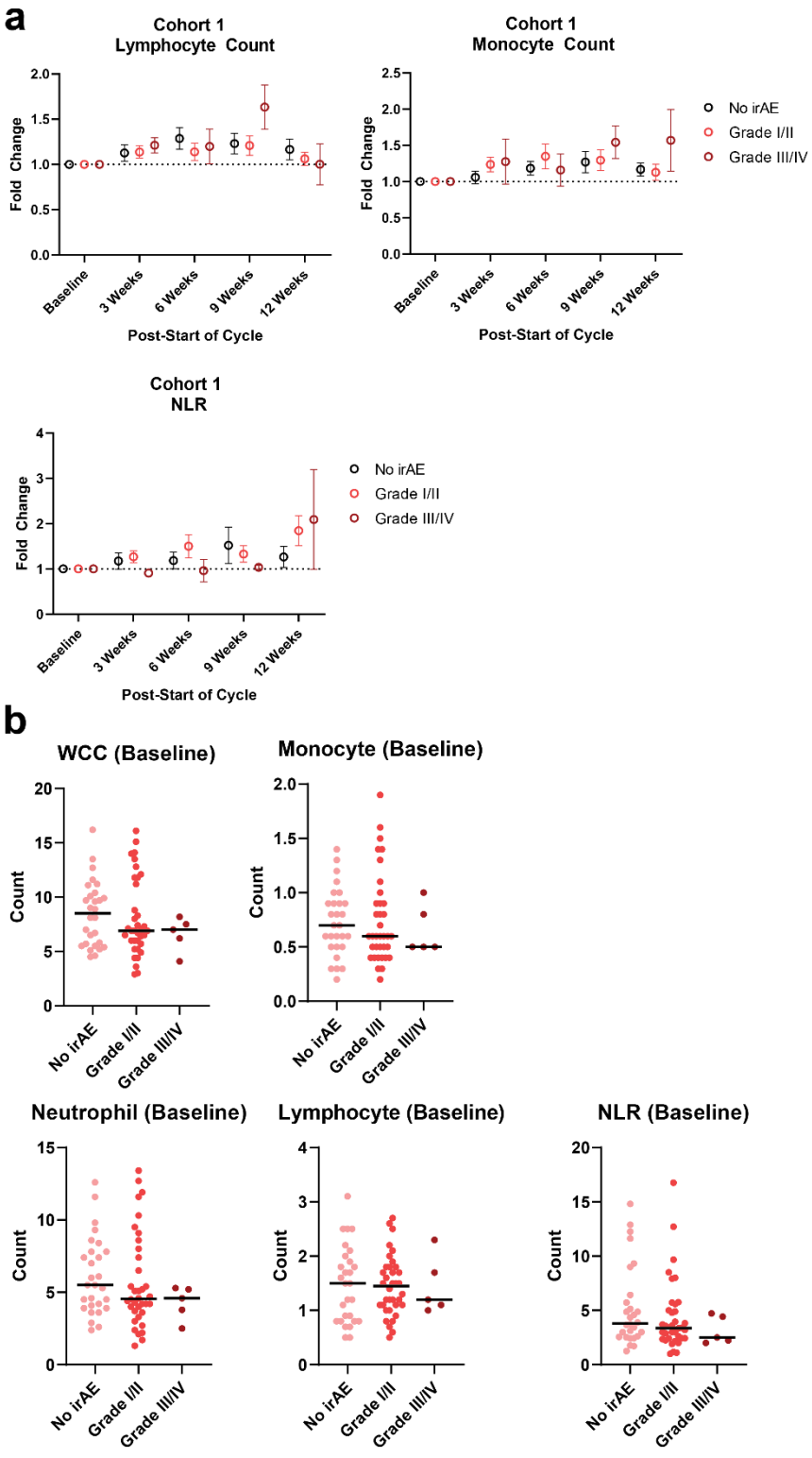

Figure S2.6: Blood immune cellularity in ipilimumab-treated melanoma patients.

A) Lymphocyte, monocyte, and neutrophil-to-lymphocyte ratio fold changes by blood analyzer in Cohort 1 ipilimumab-treated patients. Error = SEM B) Immune cell counts by blood analyzed in Cohort 1 baseline sampling. Bar = mean.

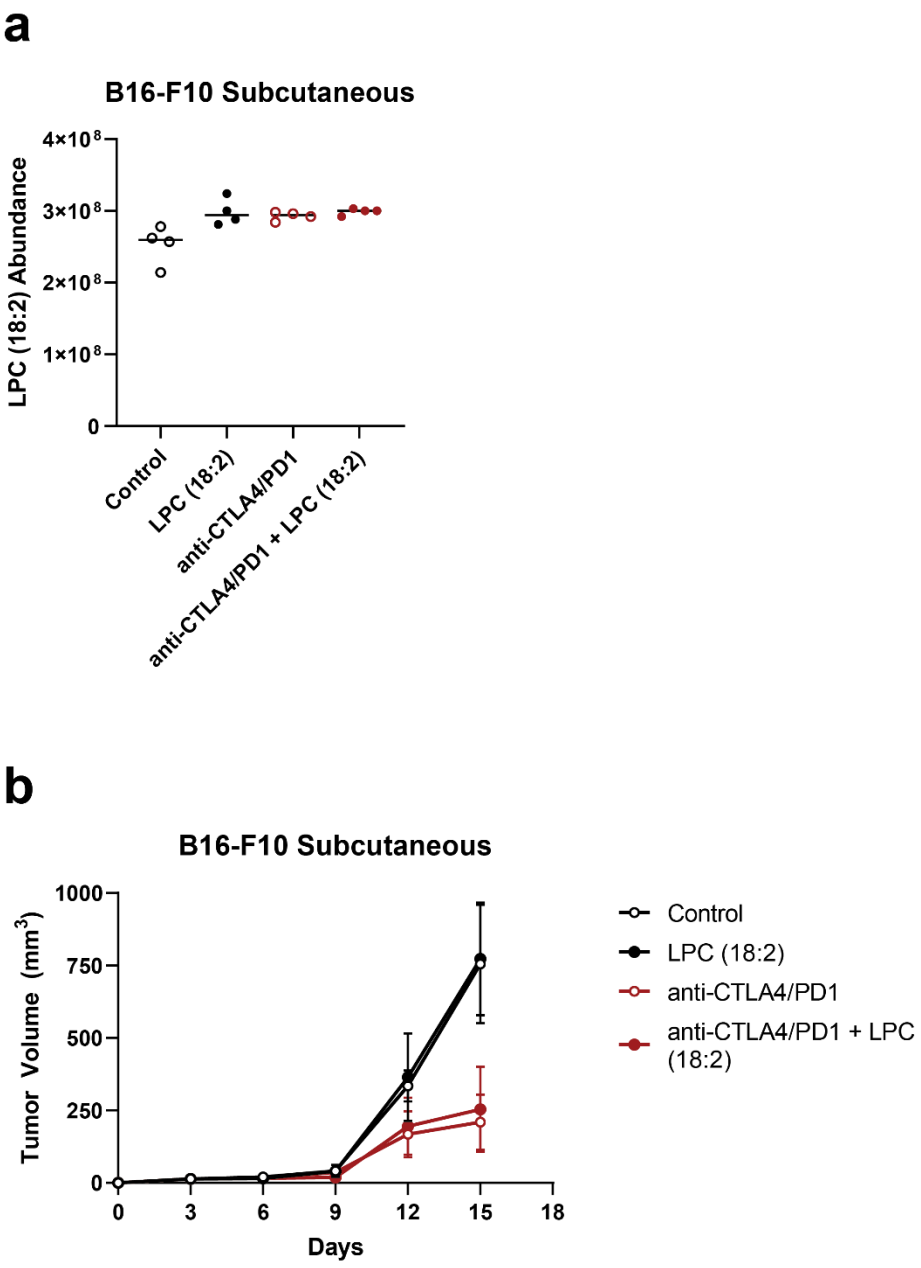

Figure S2.7: LPC (18:2) supplementation and ICB response in subcutaneous mouse melanoma.

A) LPC (18:2) abundance in terminal blood plasma from C57BL/6 mice bearing B16-F10 subcutaneous melanoma. B) B16-F10 tumor volume following LPC (18:2) supplementation and anti-mouse CTLA4 + anti-mouse PD1 intraperitoneal treatment.

Methods

Materials & Cell Lines

All LPCs (LPC (16:0), LPC (18:0), LPC (18:1), and LPC (18:2)) were purchased from Avanti Polar Lipids. Dextran sulfate sodium was purchased from Affymetrix. Autotaxin inhibitor PF-8380 was purchased from Tocris. Monoclonal anti-mouse CTLA4 (CD152) and anti-PD1 (CD279) antibody, as well as IgG2a isotype control antibody, were purchased from InVivoMAb. Clinical-grade ipilumumab was a kind donation from Dr. Sandip Patel (University of California San Diego, Moores Cancer Center). B16-F10 cells were a kind donation from the lab of Stephen Schoenberger (La Jolla Institute).

Cohort Information

Archived and de-identified blood plasma samples were obtained in accordance with the institutional review boards of each institute (University of Southampton, Yale University, University of California San Diego, FINRISK and 500FG IRB).

Bioactive Lipid Extraction from Blood Plasma

Na-EDTA or heparin prepared blood samples were thawed from storage at -80°C overnight in light-free conditions at 4°C. All extractions were performed in 96-well format. 20uL of each sample were mixed with 80uL of -20°C ethanol containing 20 deuterated standards to precipitate protein and extract lipid content. Samples were vortexed at 4°C and 500rpm for 15 minutes and centrifuged for 10 minutes to sediment protein content. From each supernatant, 65uL were taken and mixed with 350uL water in an Axygen 500uL retention v-bottom 96 well plate. To improve extraction, an additional 65uL of -20°C ethanol was added gently to the protein pellet, vortexed gently by hand for 15 seconds, and added to the same well.

Complete extracted sample volumes were loaded onto a Phenomenex Strata-X 10mg/mL polymeric solid phase extraction (SPE) 96-well plate pre-washed stepwise with 600uL methanol,

600uL ethanol, and equilibrated with 900uL water. Following gravity elution from each SPE well, 600uL of 9:1 water:methanol were added as a wash, pulled through slowly at 5mmHg, and then increased to 20mmHg for 45 seconds to fully dry each SPE. Bound metabolites enriched for bioactive lipids were then eluted in 450uL ethanol into a fresh 500ul Axygen v-bottom plate. Sample eluate was dried in a vacuum concentrator at 40°C until completely dried, before adding 50uL per well of 75:20:5 water:methanol:acetonitrile containing 10uM CUDA as resuspension solvent. Sample plates were vortexed at 500 RPM for 10 minutes at 4°C to fully resuspend metabolites, before transferring to 300uL glass inserts in a 96-well Greiner deep well plate and immediately sealed. Samples were then immediately analyzed via LC-MS/MS.

Liquid Chromatography-Tandem Mass Spectrometry

Directed, nontargeted liquid chromatography tandem mass spectrometry for the detection of bioactive lipid metabolites was performed as described previously[355]. LC-MS/MS was performed on a Thermo Vanquish UPLC system coupled to a Thermo QExactive Orbitrap mass spectrometer. Injection volume for each sample was 20uL onto a Phenomenex Kinetex C18 (1.7um particle size, 100 x 2.1 mm) column. Mobile phases were composed of; A: 70% water, 30% acetonitrile, 0.1% acetic acid, and B: 50% acetonitrile, 50% isopropanol, 0.02% acetic acid. Flow rate was a constant 0.375 mL/min, with gradient mobile phase as follows: 1% B from -1.00 minutes to 0.25 minutes, 1% to 55% B from 0.25 minutes to 5.00 minutes, 55% B to 99% B from 5.00 minutes to 5.50 minutes, and 99% B from 5.50 minutes to 7.00 minutes. Column temperature was 50°C, with a 50:25:25:0.1 water:acetonitrile:isopropanol:acetic acid needle was set to 5 seconds post-draw. Mass detection was performed with an equipped heated electrospray ionization (HESI) source with manually optimized source geometry[355]. Negative mode profile data was acquired for all samples, with sheath gas flow, aux gas flow, and sweep gas flow of 40, 15, and 2 units, respectively. Spray voltage was -3.5kV, and capillary and aux gas temperature were 265 and 350°C, respectively, with S-lens RF at 45. MS1 scan events were in a scan range of *m/z*

225-650, mass resolution of 17.5k, AGC of 1e6 and inject time of 50ms. To assist quantification and aligning intra- and inter-cohort chromatographic drift, tandem mass spectra were acquired using collision-induced dissociation (CID). Data independent acquisition (DIA) acquired in the following four mass windows: m/z 240.7–320.7, m/z 320.7–400.7, m/z 400.7–480.7, and m/z 480.7–560.7, with a mass resolution of 17.5, and AGC of 1e6, and an inject time of 40ms. Metabolite matching to LC-MS features was performed against an in-house library of bioactive lipids or by matching high quality tandem mass spectra against target features when identified.

LC-MS Data Handling

LC-MS peak identification was performed using deep neutral network-based classification as described previously[391]. Briefly, Thermo raw to mzXML file conversion was performed using MSconvert version 3.0.9393 (ProteoWizard), from which initial bulk LC-MS feature alignment was performed using in-house, R-based landmark identification and retention time correction. Chromatographic drift-corrected mzXML were then converted into composite raster image files including m/z and retention time windows bounding putative features. High-confidence features were then identified using a trained neutral network specific for this LC-MS/MS method. Semiquantitative comparisons of LC-MS features utilized peak height intensity values.

Animal Handling

Mice were exclusively of the C57BL/6 background, purchased originally from the Jackson Laboratory. Subcutaneous tumor modeling and dextran sulfate sodium experiments were performed on mice housed in pathogen-free conditions at the La Jolla Institute for Immunology (La Jolla, CA), while CTLA4$^{h/h}$ ICB-irAE experiments were performed at the Institute for Human Virology at University of Maryland (Baltimore, MD). All procedures involving mice were performed according to the respective Institutional Animal Care and Use Committee.

Dextran Sulfate Sodium-Induced Colitis Model

Colitis was induced in 9-12 week C57BL/6 using 5% dextran sulfate sodium (DSS) (Affymetrix) in drinking water. Same sex littermates were utilized; data from male mice, in which colitis was more robustly induced, are reported here, with results validated in female mice. Mice were given 5% DSS for 5 days, followed by two days on untreated water. Primary humane experimental endpoint was body weight loss in excess of 20% starting weight, measured daily. In some cases, mice were administered intraperitoneally with either control saline solution or indicated concentration of LPC. Severity of colitis was measured at experiment termination by body weight loss, colon length, and histological criteria (below).

Where indicated, blood was collected in EDTA-coated Eppendorf tubes from terminal mice by cardiac puncture, with cervical dislocation as secondary euthanasia. Blood was immediately centrifuged at 2000 RPM and 4°C for 20 minutes to collect blood plasma, which was stored at -80°C until analysis.

CTLA4 Humanized Mouse

Mice expressing human CTLA4 under the endogenous mouse *Ctla4* locus, backcrossed onto the C57BL/6 background, have been described previously[367]. Same sex littermate mice were used, with data from female mice where irAE presentation was most robust. Antibodies and LPC (18:2) were administered intraperitoneally at the indicated dose and time interval. Primary humane experimental endpoint was body weight loss in excess of 20%, measured every third day. Mice were humanely euthanized for toxicity scoring and blood plasma LC-MS analysis on Day 42.

Complete blood counts were collected on Day 41 (penultimate) of treatment from 50 uL of blood, collected in EDTA-coated Eppendorf tubes and analyzed by HEMAVET HV950 blood analyzer (Drew Scientific), according to manufacturer's protocol.

Histology

Multi-organ ICB toxicity scores in CTLA4$^{h/h}$ mice were generated from heart, lung, salivary gland, colon, and liver as described previously by Du *et al*[367].

Distal colon or cecum toxicity was determined from hemotoxilin and eosin stained tissues as described by Krause *et al*[392]*.* Briefly, cecum and distal colon samples were collected and fixed in zinc formalin (Medical Chemical Corporation) for at least 24 hours prior to paraffin embedding. Tissue was stained with hemotoxilin and eosin, and at least six representative 5um slices were collected from each tissue for embedding on slides. Image acquisition was performed on an Axioscan Z1 platform (Zeiss), using a 20x objective lens, utilizing the Zen 2.3 software automatic scan mode. Slides were blinded and then scored on a composite of the following criteria: inflammation (0 = none, 1 = mild, 2 = moderate, 3 = severe); infiltration (0 = none, 1 = mucosal or submucosal, 2 = mucosal and submucosal, 3 = transmural); crypt damage (0 = none, 1 = basal 1/3 damaged, 2 = basal 2/3 damaged, 3 = only surface epithelium intact, 4 = entire crypt and epithelium lost); and edema (0 = none, 1 = 1.5-2x submucosal thickness, 2 = >2x submucosal thickness).

Subcutaneous Tumor Modeling

C56BL/6 mice were used to model tumor growth and anti-tumor ICB efficacy. B16-F10 melanoma cells (1E6) were seeded in subcutaneous flanks in 9-12 week old mixed gender littermate mice. Tumor volume was measured as $(A \times B^2)/2$, where A = the largest and B = the smallest diameter by caliper. Primary humane experimental endpoint was body weight loss in excess of 20% or tumor volume in excess of 2000mm^3. Where indicated, 100 ug anti-mouse CTLA4 and 100 ug anti-mouse PD1 or 200 ug IgG2 isotype control antibody (InVivoMAb), or 25 mg/kg LPC (18:2), were administered intraperitoneally in 100 µL saline on Days 4, 7, 11, and 14 following tumor seeding.

Statistical Analysis

Associations between changes in bioactive lipid abundance and irAE severity were handled as ordinal logistic regressions between “none”, “Grade I/II”, and “Grade III/IV” groups; anti-tumor response associations were similarly handled as ordinal according to RECIST 1.1 metrics[358] of efficacy. Maximum excursion was treated as the largest absolute magnitude fold change of an LC-MS feature peak height relative to patient’s baseline sample following base-2 logarithmic transformation. Regressions included patient age and sex as covariates.

For continuous variables, including PBMC cellularity, linear regressions were performed against base-10 log transformed variables, with age, sex, and body mass index (BMI) as covariates.

Acknowledgements

We would like to acknowledge the Histology and Microscopy Core Facilities at the La Jolla Institute for their expertise in tissue handling and processing, in particular Dr. Zbigniew Mikulski, Katarzyna Dobaczewska, and Angela Denn. We would also like to acknowledge and thank the advice and guidance of Dr. Martina Dicker and Dr. Daniel Giles for their guidance on use of the dextran sulfate sodium model of colitis.

Author Information

Contributions: I.T.M., S.S., and M.J. conceived and designed the study. S.J.D.W.C., A.C., S.P.P., S.M.K., C.O., R.D., A.P., M.N. and P.V. collated the patient sampling and metadata, I.T.M., M.L, K.D., M.N., L.Q., and T.C.N. acquired and assembled the data. I.T.M., M.H., M.L., K.M., J.D.W., P.Z., M.K., and S.C. analyzed and interpreted the data. I.T.M, S.S., and M.J. wrote the manuscript.

Ethics Declarations

The authors have no conflicts of interest to declare.

Acknowledgements

Chapter 2 is in its entirety a manuscript in preparation, “Circulating linoleoyl-lysophosphatidylcholine is protective in immune checkpoint blockade toxicity”, by Mathews, Ian T; Henglin, Mir; Liu, Mingyue; Mercader, Kysha; Campbell, Allison; Tiwari, Saumya; Dao, Khoi; Quach, Lily; Nguyen, Thien-Tu Catherine; Zheng, Pan; Cheng, Susan; Jain, Mohit; Sharma, Sonia. The dissertation author will be the primary author on this publication.

Chapter 3: Microbial-Derived Metabolites as Immunotherapy Response Predictors

Bile Acid Glucosides are Predictors of Immune Checkpoint Inhibitor Response and Promote Anti-Tumor Immunity

Ian T. Mathews, Igor Segota, Mir Henglin, Kysha Mercader, Saumya Tiwari, Amelia Palmero, Jeff Ding, Mahan Najahawan, Khoi Dao, Serena JDW Chee, Allison Campbell, Pandurangan Vijayanand, Sandip P Patel, Susan M. Kaech, Christian Ottensmeier, Roy Decker, Abijit Patel, Mihai Netea, Susan Cheng, Tao Long, Mohit Jain, and Sonia Sharma

Abstract

Response to immune checkpoint blockade (ICB) in patients with solid tumors can be predicted by the abundance of certain gut commensal microbes. Whether and how these intestinal bacteria influence anti-tumor immunity is unknown. Here, we report the abundance of one gut microbe with previously identified positive association to anti-PD1 responsive, *Biffidobacterium longum*, associates with a broad array of metabolites in matched blood plasma. One such metabolite, a dihydroxy- bile acid, is positively associated with pembrolizumab response in a cohort of lung carcinoma patients. Chemically related bile acids are either PD1 or CTLA4 response predictive in cancer patients and exhibit strong correlates to effector and effector memory T-cell populations in healthy individuals. These observations support bile acid glucosides as liver and leukocyte-metabolized second messengers in microbiome influences on anti-tumor immunity.

The immune checkpoint is a colloquialism used to describe ligand-receptor pairs at the immune synapse which act as costimulatory or coinhibitory, “go vs no-go” signals following antigen recognition[393]. Immune checkpoint blockade interrupts coinhibitory signals by binding humanized, monoclonal antibodies to receptors like CTLA4 and PD1 on T-cells to blunt their anergic effect on primarily effector T-cells. Immunotherapy which combines CTLA4 and PD1-targeting therapies have shown particular clinical success; three year survival rate for ipilimumab

plus nivolumab combination therapy was 58 percent in Phase III clinical trial (CheckMate 067)[156]. Nevertheless, a persistent subgroup of solid tumors are unresponsive to ICB-based interventions without clear next steps in advancing intervention quality for these patients.

The determinants of immune checkpoint blockade response include the abundance, clonality, and immunogenic nature of tumor neoantigens[95,180,187], the correlated capacity for the cell to manage genomic instability[210-212,394]), and the prevalence and magnitude of anergy in tumor infiltrating lymphocytes[149,198,395,396]. Additionally, multiple groups have reported the gut microbiome, the collection of commensal bacteria and archaea detectable by metagenomic sequencing in stool, can distinguish responder from non-responder groups effectively in baseline sampling[244-246]. Key experiments in these studies, particularly the identification of species-level correlations and stool transplant *in vivo* support the hypothesis that members of the gut microbiome actively promote anti-tumor immunity and ICB response. Elucidating the mechanisms by which this effect may propagate can also serve as a means to critically examine this hypothesis.

One potential mechanism by which the gut microbiome may influence the immune system, specifically anti-tumor immunity at potentially distant tumor cites, is through the production of unique second messenger metabolites that influence immune function. The gut microflora orchestrates critical metabolic processes for which humans lack the relevant enzymes, particularly around nitrogen and sugar metabolism. Additionally, the gut microbiome produces unique lipid metabolites with potential immune signaling function[397], including compounds like short-chain fatty acids (SCFAs)[398,399] and odd-chain fatty acids[400]. A second tier of microbiome-influenced signaling metabolites include secondary metabolic products from host compounds, the most prominent being FXR/LXR signaling by bile acids[401,402]. Of note, microbially-influenced metabolites can be absorbed through the intestinal villi and make their way to the liver and wider circulation, potentially influencing distant processes.

To evaluate microbially-influenced metabolites in circulation, we utilized patient sampling from the longitudinal FINRISK-2002 study, for which robust stool 16S microbial sequencing data were available with paired blood plasma. We used liquid chromatography coupled mass spectrometry for directed detection of known and novel bioactive lipids[346,355] from FINRISK-2002 blood plasma. By identifying observable species units corresponding to unique microbes (see Methods), we can identify LC-MS features differentially abundant in individuals with higher levels of response-associated microbes (**Figure 3.1A**). We chose *Biffidobacterim longum* as a candidate ICB driver bacteria in this study, owing to the strong evidence for functional relevance of *B. longum* in Matson *et al*'s stool transfer experiment[246]. We detected 323 LC-MS features that met a robust false discovery correction cutoff as associated with *B. longum* prevalence in matched stool, of which 112 features were positively correlated (**Figure 3.1B**).

We tested the ICB response predictive value of these *B. longum* positively associated features in a cohort of advanced lung carcinoma patients treated with anti-PD1 IgG4 isotype antibody pembrolizumab and stereotactic radiation beam therapy (NCT02407171)[366]. Of the 112 LC-MS features measured in this cohort, one met statistical cutoff as a response-associated feature (**Figure 3.1C**). The LC-MS feature in question (Peak 1) was not identified in our library of 225 bioactive lipid standards[346]. Its response association appeared to be dichotomous; the *B. longum* associated metabolite was comparably elevated in patients with both stable and partial or complete response by RECIST 1.1 metrics[358] compared to progressive disease (**Figure 3.1D**).

Identifying the chemical structure of this candidate ICB response metabolite was necessary for testing functional relevance in greater detail. We therefore employed tandem mass spectrometry and chemical networking[356] against other metabolites in blood and chemical standards to aid in identifying chemically related metabolites. Significant structural matching to bile acid standards indicated Peak 1 was chemically related to glycine-conjugated dihydroxy bile acids (ex: glycochenodeoxycholic acid). Several isobaric metabolites with tandem mass spectral

similarity to bile acids were detected in blood plasma (**Figure 3.2A**), though none of these features were significantly associated with pembrolizumab response. We became interested in whether Peak 1 and its related bile acids were associated with anti-tumor response in other ICB regimens. Interestingly, we observed bile acid metabolites, specifically isobars of Peak 1, were positively associated with response in baseline blood plasma sampling of ipilimumab-treated melanoma patients (n = 60). A particularly strong association was observed for an isobar of Peak 1 we termed Peak 2 (**Figure 3.2B**). By tandem mass spectral deconvolution, we were able to putatively identify this class of bile acid metabolites as hexose conjugates, better known as bile acid glucosides (**Figure 3.2C**). Like glucuronides, glucosides are common conjugations to sterols and other cholesterol metabolites like bile acids[403,404], commonly believed to predominantly function as kinetic modulators of circulating bile acid levels through improved excretion[405]. While glucosidation of bile acids has not been reported as phenotypically distinct from other forms of sugar conjugation, bile acid glycosides have not undergone extensive characterization as signaling metabolites. We observe a ICB-predictive trend for four isobaric bile acid glucosides (**Figure 3.2D**). Of note, we observe no association for related bile acid glucuronides (**Figure 3.2E**) or n-acetyl glucosamides (**Figure 3.2F**).

The association between Peak 1 bile acid glucoside and *B. longum* observed in healthy individuals, and the context of pre-therapy predictive value in which Peak 1 was identified, led us to hypothesize that bile acid glucosides could impact systemic immunity in healthy individuals in a manner relevant to immune checkpoint blockade. In order to test this hypothesis, we measured bile acids and bile acid glucosides in 512 healthy individuals from the 500 Functional Genomes (500FG) cohort, for which peripheral immune cellularity of 80 distinct lymphoid and myeloid cell types are recorded[225]. Significant peripheral blood cellularity associations, particularly among cell types involved in immunological memory, were observed for Peak 1, Peak 2, and related bile acid metabolites (**Figure 3.3**). Peak 1 and Peak 2 bore strong positive correlations with central memory

and antigen-mature T-cell populations ($CD45RO^+$; $CD45RA^{--}$, $CD4/8^+$, $CD27^+$). Central memory T-cells, particularly $CD4^+$ $CD27^+$ memory T-cells in the periphery, have been positively linked to ICB responsiveness[406]; intratumoral memory T-cells also have positive response correlations when absent of anergy markers[171,396].

As we began to functionally characterize bile acid glucosides in systemic immunity, we became interested in the metabolism of bile acid glucosides and what we could glean from population-level human data with bile acid glucoside measurements. We utilized paired genomic and metabolomic information from FINRISK-2002 to identify genomic variants which associate strongly with bile acid glucoside abundance. We posited that genes relevant to the production of bile acid glucosides in humans would, when disrupted by a nonsynonymous mutation, have differential levels of bile acid glucosides in circulation. While neither Peak 1 nor Peak 2 were observed with statistically robust associations to any one polymorphism, glucosides of glycochenodeoxycholic acid and glycodeoxycholic acid significantly associated with polymorphisms in three genes (**Figure 3.4A-B**). Glycochenodeoxycholic acid glucoside bore a robust correlation with a missense mutation in the Solute Carrier Organic Anion Transporter Family Member 1B1 (SLCO1B1), a liver-restricted transported of estradiol glucuronides and drug glycosides, including statins[407,408]. Glycodeoxycholic acid glucoside was modestly associated with a missense mutation in the illeal-restricted SLC family member SLC10A2, a canonical bile acid transporter which mediates uptake from the gut[409,410], as well as an intronic mutation in maltase-glucoamylase (MGAM), an enzyme uncharacterized in bile acid metabolism.

MGAM is a brush border enzyme in the intestine which works in concert with sucrase-isomaltase and other sugar α-glucosidases to break down dietary starch[411]. Because the glucosyltransferase involved in adding a glucose to various bile acids in the liver is believed to act in concert with β-glucosidases[403,404], we hypothesized MGAM as an α-glucosidase may be important in the metabolism of bile acid glucosides. Of note, while MGAM has been predominantly

characterized as a brush border enzyme in the intestine, its tissue distribution is actually quite enriched in whole blood and bone marrow[412,413]. We therefore tested whether bile acid glucosides can be made via incubation with whole blood or peripheral blood mononuclear cells (PBMCs), in addition to the canonical production of bile acid glucosides from liver microsomes. Intriguingly, we found not only that bile acid glucosides could be made from both liver microsomes and PBMC cultures, but that the chromatographic profile of liver and PBMC-derived products were distinct (**Figure 3.4C**), indicating unique conjugation positions on the steroid ring of the bile acid. The possibility of lymphocyte-derived bile acid glucosides of unique chemistries is an observation which requires additional characterization, including phenotypic characterization in tissue-resident and tumor infiltrating lymphocytes.

Finally, we sought to understand the functional relevance of glucoside conjugation to bile acids as secondary messengers. To determine whether glucoside conjugation differentially impacted bioavailability of bile acid in circulation[405], we tested intravenous injection in mice of unconjugated chenodeoxycholic acid, glycochenodeoxycholic acid, and glycochenodeoxycholic acid glucoside and measured their relative abundance over time (**Figure 3.5**). There was no observed benefit or detriment to bioavailability conferred by glucoside conjugation, indicating any functional relevance to immune function of bile acid glucosides is likely not related to maintaining the circulating pool of bile acid.

Concluding Remarks

Altogether, our study represents a potential mechanism by which gut microbes may affect anti-tumor immunity and immune checkpoint response. *Bifidobacterium longum* levels were directly correlated to circulating bile acid glucosides, metabolic products of gut microbial enzymes and blood or liver glucosyltransferases. We found in ICB-treated individuals, bile acid glucosides positively correlated with response at baseline; in healthy individuals, they positively correlated with response-linked memory T-cell subsets.

This study does not directly address the function of bile acid glucosides in circulation. We found the glucoside on glycochenodeoxycholic acid does not considerably alter bioavailability, but have not linked glucose conjugation to any other relevant phenotype. Sterol glycosides have been reported as TLR4[414] or GPCR[415] agonists. Estradiol glucuronide may be an instructive model for considering bile acid glucosides; compared to unconjugated estradiol, estradiol glucuronide has a greatly decreased affinity of estrogen nuclear receptor and much higher for its GPCR analogue[415,416]. Bile acids are variable activators of the nuclear receptors FXR, LXR, and VDR[402], an effect which may be abrogated in favor of an unknown plasma membrane receptor interaction by bile acid glucosides.

Characterization of bile acid glucosides *in vivo* should take into consideration context and timing, especially in relationship to immune checkpoint blockade. Our data indicate bile acid glucosides are rapidly distributed and/or metabolized following administration, with a half-life of fewer than six hours. Studying immune fitness following bile acid glucoside administration, and the lag time to systemically observable effects on systemic immunity, may set the timing for bile acid glucoside administration for an immune checkpoint blockade study.

In conclusion, these data describe a microbiome-derived metabolite with immune checkpoint blockade response and systemic immune fitness correlates. The structure of this study may be mimicked to better understand the role of small molecule metabolites in mediating the diverse and often mechanistically unknown influences of the microbiome on human health.

Figures

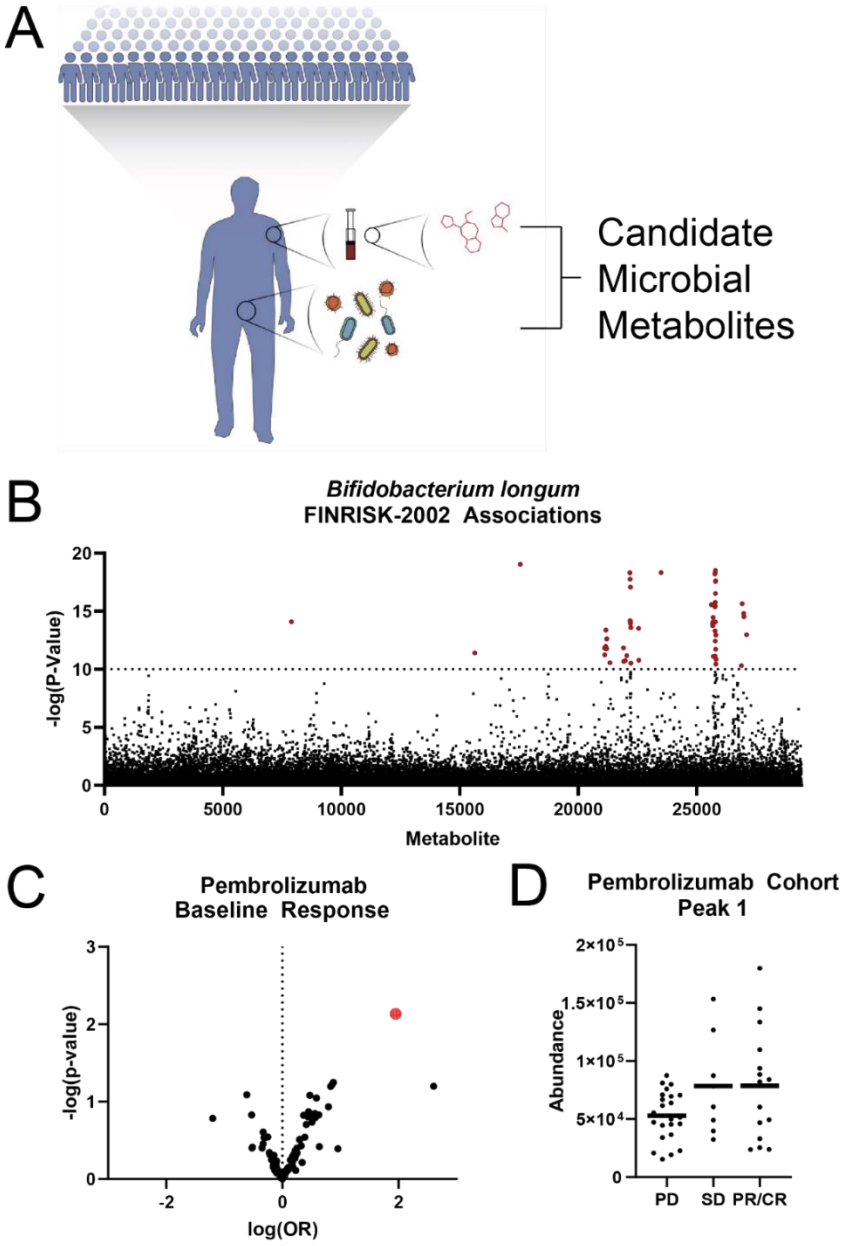

Figure 3.1: *Biffidobacterium longum* associated LC-MS features with pembrolizumab response association.

A) Schematic for detection of candidate microbially-influenced metabolites from matched 16S stool sequencing and peripheral blood plasma. B) Modified Manhattan plot of 29420 bioactive lipid LC-MS features detected blood plasma from FINRISK-2002 (n = 912), by association with *Biffidobacterium longum* matched OSU in stool. C) Volcano plot of 112 *B. longum* positively associated LC-MS features by baseline association to pembrolizumab response in NSCLC patients (n = 47). Red highlighted dot indicates Peak 1. D) Abundance of Peak 1 in pembrolizumab cohort baseline sampling.

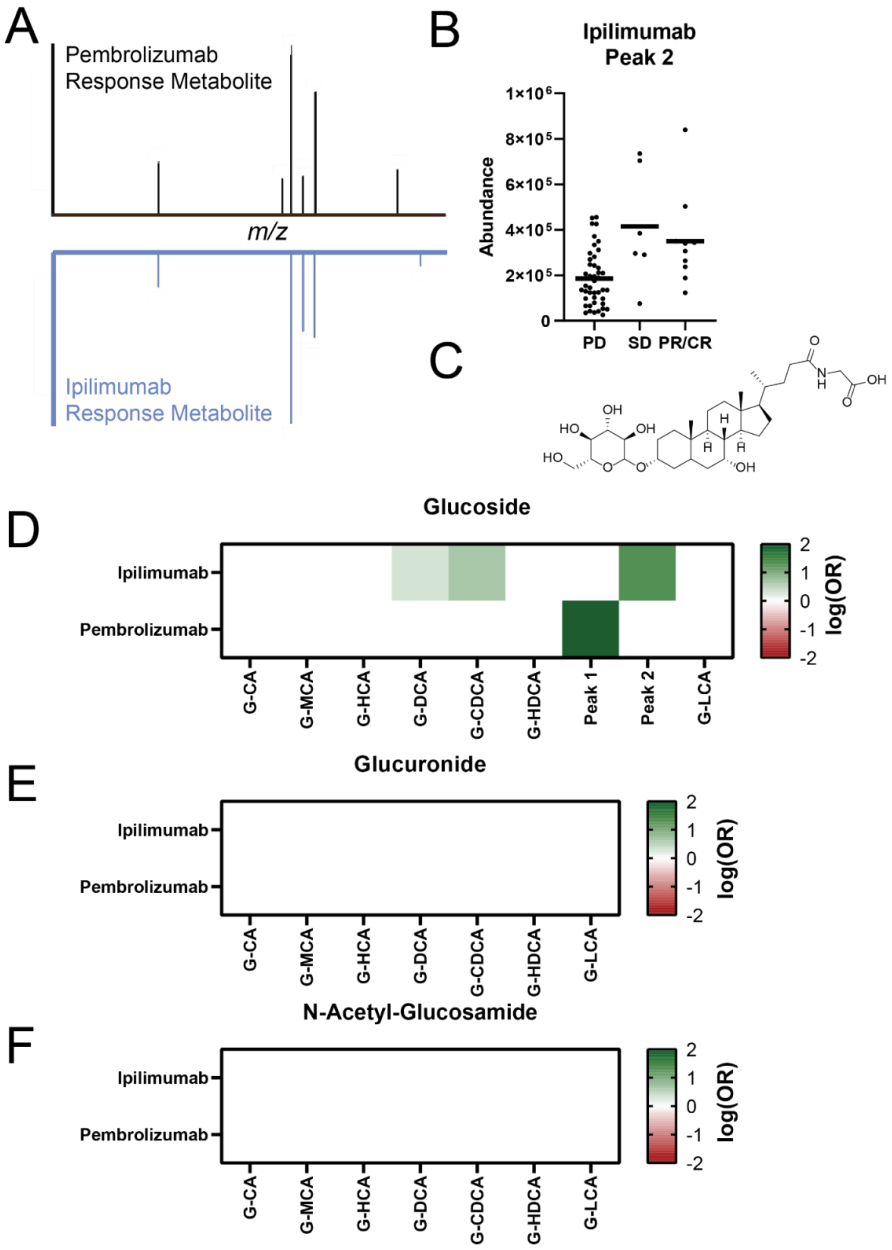

Figure 3.2: Identification of response-associated bile acid glucosides.

A) Tandem mass spectra of Peak 1 (top) and chemically related response metabolite (bottom) in ipilimumab-treated melanoma patients. B) Abundance of Peak 2 in ipilimumab-treated melanoma patients (n = 60). C) Structure of the dihydroxy bile acid glucoside glycochenodeoxycholic acid-3-glucoside. D-F) Natural logarithmic odds ratio for response in relationships with $p < 0.05$ in ipilimumab or pembrolizumab treated individuals for bile acid D) glucosides, E) glucuronides, and F) n-acetyl glucosamides.

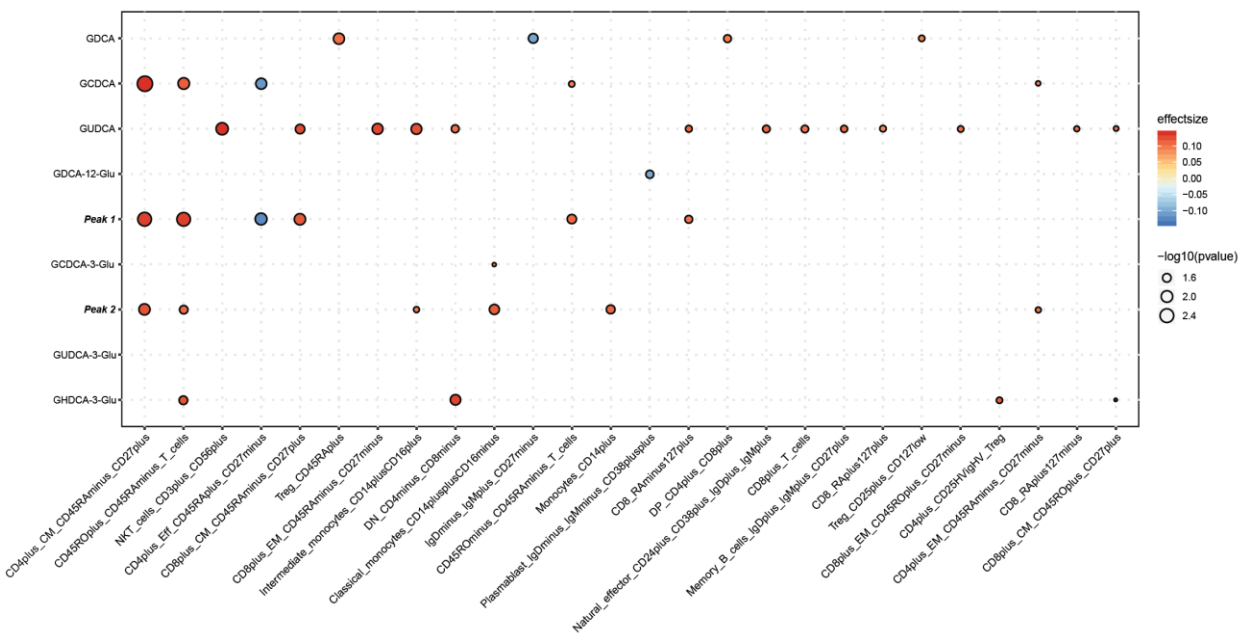

Figure 3.3: Bile acid glucosides associate with distinct immune cellularity profiles in healthy individuals.

Association between detected dihydroxy-, glycine-conjugated bile acids and bile acid glucosides in 500FG (n = 512) queried from 80 distinct lymphoid and myeloid PBMC populations. All immune cell populations listed had at least one relationship $p < 0.05$.

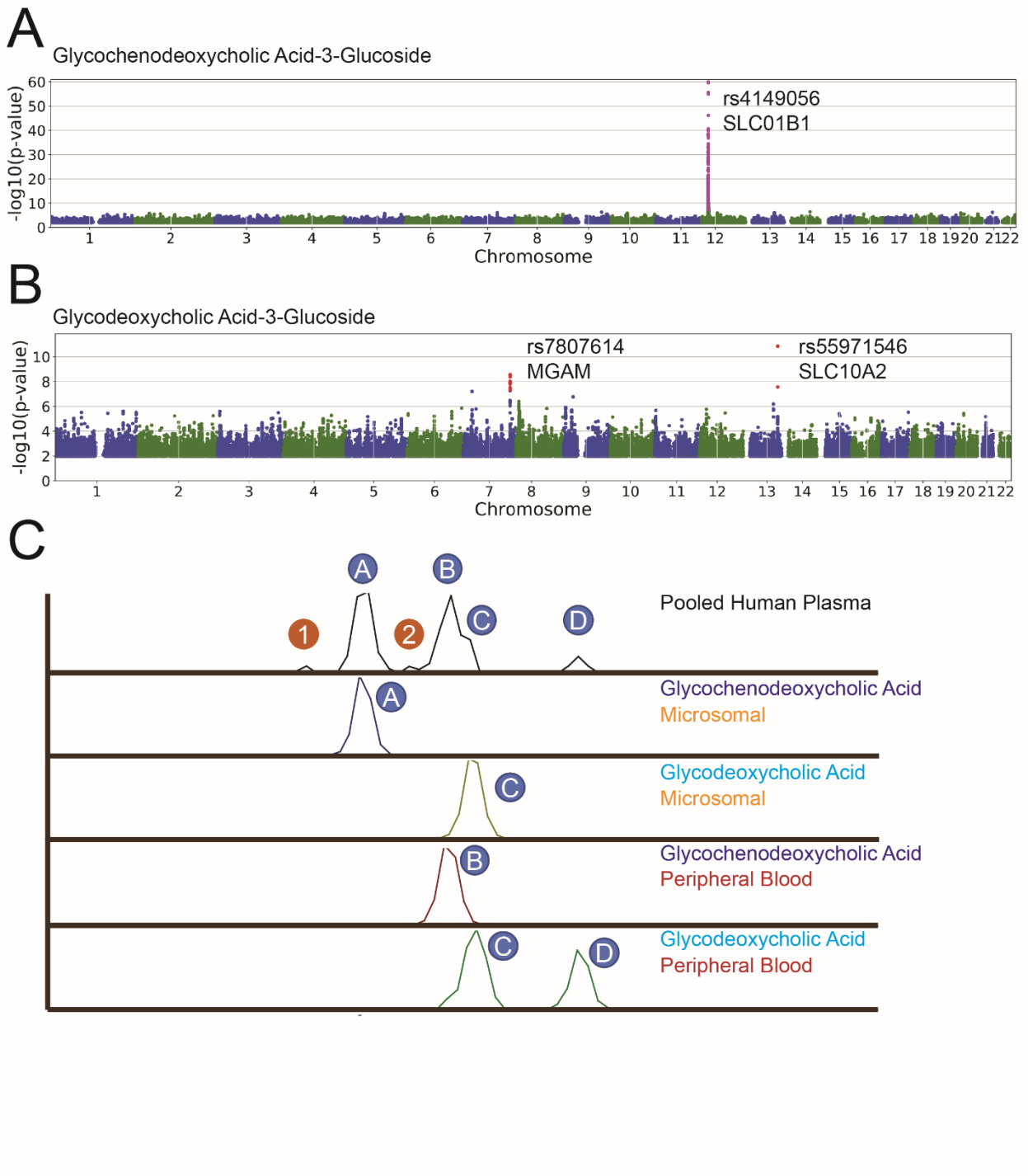

Figure 3.4: Circulating Bile Acid Glucoside Levels are Transporter and MGAM-dependent.

A-B) Manhattan plots of variant associations in FINRISK 2002 (n = 1285) and abundance in blood plasma of A) glycochenodeoxycholic acid-3-glucoside and B) glycodeoxycholic acid-3-glucoside. C) Chromatograms of bile acid glucosides in pooled blood plasma or from indicated incubations with microsomal fractions or PBMCs.

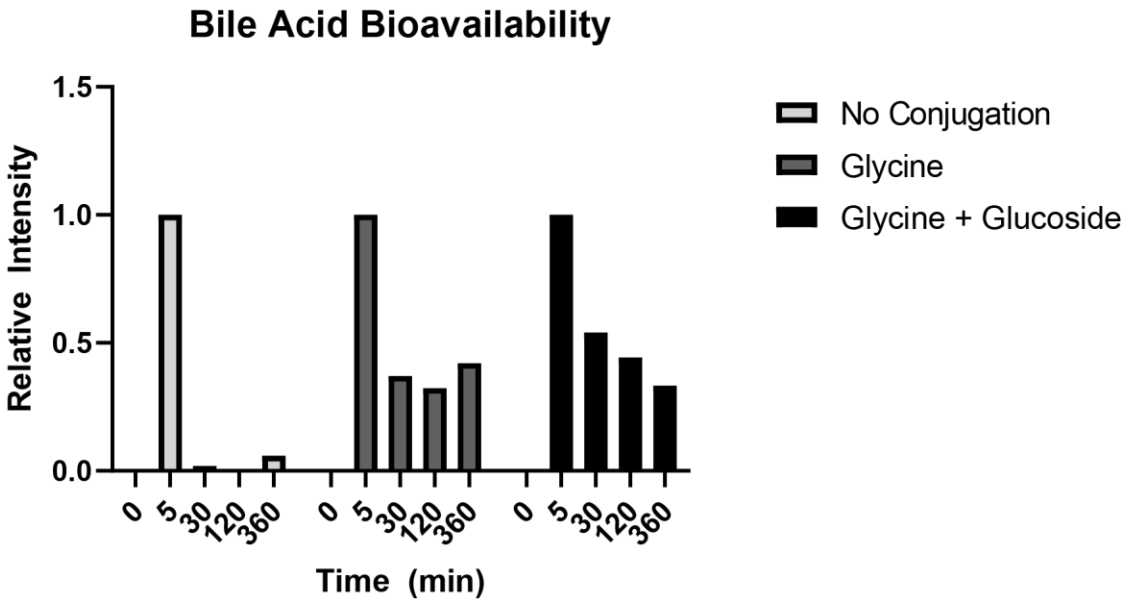

Figure 3.5: Glucoside conjugation does not increase blood retention of bile acid.

Abundance of chenodeoxycholic acid of indicated conjugation in peripheral blood plasma following tail vein intravenous administration. Data are relative to endogenous levels of indicated metabolite and normalized to the earliest time point measured.

Materials and Methods

Cohort Information. Archived and de-identified blood plasma samples were obtained in accordance with the institutional review boards of each institute (University of Southampton, Yale University).

FINRISK 16S Sequencing and OSU Designation. FINRISK-2002 sample handling, 16S sequencing and data handling, and identification of microbial species was performed as described previously[417].

Bioactive Lipid Directed LC-MS/MS. Data were acquired as described in Chapter 2. Briefly, Na-EDTA or heparin prepared blood samples were thawed from storage at -80°C overnight in light-free conditions at 4°C. All extractions were performed in 96-well format. 20uL of each sample were mixed with 80uL of -20°C ethanol containing 20 deuterated standards to precipitate protein and extract lipid content. Samples were vortexed at 4°C and 500rpm for 15 minutes and centrifuged for 10 minutes to sediment protein content. From each supernatant, 65uL were taken and mixed with 350uL water in an Axygen 500uL retention v-bottom 96 well plate. To improve extraction, an additional 65uL of -20°C ethanol was added gently to the protein pellet, vortexed gently by hand for 15 seconds, and added to the same well.

Complete extracted sample volumes were loaded onto a Phenomenex Strata-X 10mg/mL polymeric solid phase extraction (SPE) 96-well plate pre-washed stepwise with 600uL methanol, 600uL ethanol, and equilibrated with 900uL water. Following gravity elution from each SPE well, 600uL of 9:1 water:methanol were added as a wash, pulled through slowly at 5mmHg, and then increased to 20mmHg for 45 seconds to fully dry each SPE. Bound metabolites enriched for bioactive lipids were then eluted in 450uL ethanol into a fresh 500ul Axygen v-bottom plate. Sample eluate was dried in a vacuum concentrator at 40°C until completely dried, before adding 50uL per well of 75:20:5 water:methanol:acetonitrile containing 10uM CUDA as resuspension solvent. Sample plates were vortexed at 500 RPM for 10 minutes at 4°C to fully resuspend

metabolites, before transferring to 300uL glass inserts in a 96-well Greiner deep well plate and immediately sealed. Samples were then immediately analyzed via LC-MS/MS.

Directed, nontargeted liquid chromatography tandem mass spectrometry for the detection of bioactive lipid metabolites was performed as described previously355. LC-MS/MS was performed on a Thermo Vanquish UPLC system coupled to a Thermo QExactive Orbitrap mass spectrometer. Injection volume for each sample was 20uL onto a Phenomenex Kinetex C18 (1.7um particle size, 100 x 2.1 mm) column. Mobile phases were composed of; A: 70% water, 30% acetonitrile, 0.1% acetic acid, and B: 50% acetonitrile, 50% isopropanol, 0.02% acetic acid. Flow rate was a constant 0.375 mL/min, with gradient mobile phase as follows: 1% B from -1.00 minutes to 0.25 minutes, 1% to 55% B from 0.25 minutes to 5.00 minutes, 55% B to 99% B from 5.00 minutes to 5.50 minutes, and 99% B from 5.50 minutes to 7.00 minutes. Column temperature was 50°C, with a 50:25:25:0.1 water:acetonitrile:isopropanol:acetic acid needle was set to 5 seconds post-draw. Mass detection was performed with an equipped heated electrospray ionization (HESI) source with manually optimized source geometry355. Negative mode profile data was acquired for all samples, with sheath gas flow, aux gas flow, and sweep gas flow of 40, 15, and 2 units, respectively. Spray voltage was -3.5kV, and capillary and aux gas temperature were 265 and 350°C, respectively, with S-lens RF at 45. MS1 scan events were in a scan range of m/z 225-650, mass resolution of 17.5k, AGC of 1e6 and inject time of 50ms. To assist quantification and aligning intra- and inter-cohort chromatographic drift, tandem mass spectra were acquired using collision-induced dissociation (CID). Data independent acquisition (DIA) acquired in the following four mass windows: m/z 240.7–320.7, m/z 320.7–400.7, m/z 400.7–480.7, and m/z 480.7–560.7, with a mass resolution of 17.5, and AGC of 1e6, and an inject time of 40ms. Metabolite matching to LC-MS features was performed against an in-house library of bioactive lipids or by matching high quality tandem mass spectra against target features when identified.

LC-MS Data Handling. LC-MS peak identification was performed using deep neutral network-based classification as described previously391. Briefly, Thermo raw to mzXML file conversion was performed using MSconvert version 3.0.9393 (ProteoWizard), from which initial bulk LC-MS feature alignment was performed using in-house, R-based landmark identification and retention time correction. Chromatographic drift-corrected mzXML were then converted into composite raster image files including m/z and retention time windows bounding putative features. High-confidence features were then identified using a trained neutral network specific for this LC-MS/MS method. Semiquantitative comparisons of LC-MS features utilized peak height intensity values.

Bile Acid Glucoside Synthesis. Human liver microsome (Corning) bile acid glucoside reactions were performed with octyl-glucopyranoside as described previously[404]. Incubation in EDTA-whole blood or peripheral blood mononuclear cells were performed in an analogous manner, coincubating with maltose (Sigma) as a sugar donor.

Acknowledgements

Chapter 3 is in its entirety a manuscript in preparation, “Bile acid glucosides are predictors of immune checkpoint inhibitor response and promote anti-tumor immunity”, by Mathews, Ian T; Segota, Igor; Henglin, Mir; Mercader, Kysha; Tiwari, Saumya; Palmero, Amelia; Ding, Jeff; Dao, Khoi; Campbell, Allison; Cheng, Susan; Jain, Mohit; Sharma, Sonia.The dissertation author will be the primary author on this publication.

References

1 Ehrlich, P. Ueber den jetzigen Stand der Karzinomforschung [About the current State of Cancer Research]. *Ned Tijdschr Geneeskd* **5**, 273–290 (1909).

2 Billingham, R. E., Brent, L. & Medawar, P. B. Quantitative studies on tissue transplantation immunity. II. The origin, strength and duration of actively and adoptively acquired immunity. *Proc R Soc Lond B Biol Sci* **143**, 58-80, doi:10.1098/rspb.1954.0054 (1954).

3 Old, L. J. & Boyse, E. A. Immunology of Experimental Tumors. *Annu Rev Med* **15**, 167-186, doi:10.1146/annurev.me.15.020164.001123 (1964).

4 Burnet, M. Cancer; a biological approach. I. The processes of control. *Br Med J* **1**, 779-786, doi:10.1136/bmj.1.5022.779 (1957).

5 Thomas, L. & Lawrence, H. Cellular and humoral aspects of the hypersensitive states. *New York: Hoeber-Harper*, 529-532 (1959).

6 Burnet, F. M. The concept of immunological surveillance. *Prog Exp Tumor Res* **13**, 1-27, doi:10.1159/000386035 (1970).

7 Giunta, J. L. & Shklar, G. The effect of antilymphocyte serum on experimental hamster buccal pouch carcinogenesis. *Oral Surg Oral Med Oral Pathol* **31**, 344-353, doi:10.1016/0030-4220(71)90157-5 (1971).

8 Woods, D. A. Influence of antilymphocyte serum on DMBA induction of oral carcinomas. *Nature* **224**, 276-277, doi:10.1038/224276a0 (1969).

9 Defendi, V. & Roosa, R. A. The role of the thymus in carcinogenesis. *Wistar Inst Symp Monogr* **2**, 121-135 (1964).

10 Balner, H. & Dersjant, H. Neonatal thymectomy and tumor induction with methylcholanthrene in mice. *J Natl Cancer Inst* **36**, 513-521 (1966).

11 Grant, G. A. & Miller, J. F. Effect of neonatal thymectomy on the induction of sarcomata in C57 BL mice. *Nature* **205**, 1124-1125, doi:10.1038/2051124a0 (1965).

12 Kouri, R. & Nebert, D. Origins of Human Cancer. *by Hiatt, HH, Watson JD, and Winsten JA, Cold Spring Harbor Laboratory, University of Tokyo Press, Tokyo*, 811-835 (1977).

13 Heidelberger, C. Chemical carcinogenesis. *Annu Rev Biochem* **44**, 79-121, doi:10.1146/annurev.bi.44.070175.000455 (1975).

14 Stutman, O. Chemical carcinogenesis in nude mice: comparison between nude mice from homozygous matings and heterozygous matings and effect of age and carcinogen dose. *Journal of the National Cancer Institute* **62**, 353-358 (1979).

15 Stutman, O. Tumor development after 3-methylcholanthrene in immunologically deficient athymic-nude mice. *Science* **183**, 534-536 (1974).

16 Outzen, H. C., Custer, R. P., Eaton, G. J. & Prehn, R. T. Spontaneous and induced tumor incidence in germfree "nude" mice. *J Reticuloendothel Soc* **17**, 1-9 (1975).

17 Stutman, O. The Nude Mouse in Experimental and Clinical Research. *J. Fogh and B. Giovanella, Eds* **411** (1978).

18 Rygaard, J. & Povlsen, C. The mouse mutant nude does not develop spontaneous tumours. An argument against immunological surveillance. *Acta Pathologica Microbiologica Scandinavica Section B Microbiology and Immunology* **82**, 99-106 (1974).

19 Kaplan, D. H., Shankaran, V., Dighe, A. S., Stockert, E., Aguet, M., Old, L. J. & Schreiber, R. D. Demonstration of an interferon gamma-dependent tumor surveillance system in immunocompetent mice. *Proc Natl Acad Sci U S A* **95**, 7556-7561, doi:10.1073/pnas.95.13.7556 (1998).

20 Dighe, A. S., Richards, E., Old, L. J. & Schreiber, R. D. Enhanced in vivo growth and resistance to rejection of tumor cells expressing dominant negative IFN gamma receptors. *Immunity* **1**, 447-456, doi:10.1016/1074-7613(94)90087-6 (1994).

21 van den Broek, M. E., Kagi, D., Ossendorp, F., Toes, R., Vamvakas, S., Lutz, W. K., Melief, C. J., Zinkernagel, R. M. & Hengartner, H. Decreased tumor surveillance in perforin-deficient mice. *J Exp Med* **184**, 1781-1790, doi:10.1084/jem.184.5.1781 (1996).

22 Street, S. E., Trapani, J. A., MacGregor, D. & Smyth, M. J. Suppression of lymphoma and epithelial malignancies effected by interferon gamma. *J Exp Med* **196**, 129-134, doi:10.1084/jem.20020063 (2002).

23 Smyth, M. J., Thia, K. Y., Street, S. E., MacGregor, D., Godfrey, D. I. & Trapani, J. A. Perforin-mediated cytotoxicity is critical for surveillance of spontaneous lymphoma. *J Exp Med* **192**, 755-760, doi:10.1084/jem.192.5.755 (2000).

24 Street, S. E., Cretney, E. & Smyth, M. J. Perforin and interferon-gamma activities independently control tumor initiation, growth, and metastasis. *Blood* **97**, 192-197, doi:10.1182/blood.v97.1.192 (2001).

25 Herberman, R. B. & Rosenberg, E. B. Cellular cytotoxicity reactions to human leukemia associated antigens. *Bibl Haematol* **39**, 838-845, doi:10.1159/000427912 (1973).

26 Herberman, R. B., Hollinshead, A. C., Alford, T. C., McCoy, J. L., Halterman, R. H. & Leventhal, B. G. Delayed cutaneous hypersensitivity reactions to extracts of human tumors. *Natl Cancer Inst Monogr* **37**, 189-195 (1973).

27 Herberman, R. B. In vivo and in vitro assays of cellular immunity to human tumor antigens. *Fed Proc* **32**, 160-164 (1973).

28 Herberman, R. B., Nunn, M. E., Lavrin, D. H. & Asofsky, R. Effect of antibody to theta antigen on cell-mediated immunity induced in syngeneic mice by murine sarcoma virus. *J Natl Cancer Inst* **51**, 1509-1512, doi:10.1093/jnci/51.5.1509 (1973).

29 Lavrin, D. H., Herberman, R. B., Nunn, M. & Soares, N. In vitro cytotoxicity studies of murine sarcoma virus-induced immunity in mice. *J Natl Cancer Inst* **51**, 1497-1508, doi:10.1093/jnci/51.5.1497 (1973).

30 Glimcher, L., Shen, F. W. & Cantor, H. Identification of a cell-surface antigen selectively expressed on the natural killer cell. *J Exp Med* **145**, 1-9, doi:10.1084/jem.145.1.1 (1977).

31 Minato, N., Reid, L. & Bloom, B. R. On the heterogeneity of murine natural killer cells. *J Exp Med* **154**, 750-762, doi:10.1084/jem.154.3.750 (1981).

32 Ikuta, K., Hattori, M., Wake, K., Kano, S., Honjo, T., Yodoi, J. & Minato, N. Expression and rearrangement of the alpha, beta, and gamma chain genes of the T cell receptor in cloned murine large granular lymphocyte lines. No correlation with the cytotoxic spectrum. *J Exp Med* **164**, 428-442, doi:10.1084/jem.164.2.428 (1986).

33 Shinkai, Y., Lam, K.-P., Oltz, E. M., Stewart, V., Mendelsohn, M., Charron, J., Datta, M., Young, F., Stall, A. M. & Alt, F. W. RAG-2-deficient mice lack mature lymphocytes owing to inability to initiate V (D) J rearrangement. *Cell* **68**, 855-867 (1992).

34 Schuler, W., Weiler, I. J., Schuler, A., Phillips, R. A., Rosenberg, N., Mak, T. W., Kearney, J. F., Perry, R. P. & Bosma, M. J. Rearrangement of antigen receptor genes is defective in mice with severe combined immune deficiency. *Cell* **46**, 963-972, doi:10.1016/0092-8674(86)90695-1 (1986).

35 Falck, J., Coates, J. & Jackson, S. P. Conserved modes of recruitment of ATM, ATR and DNA-PKcs to sites of DNA damage. *Nature* **434**, 605-611, doi:10.1038/nature03442 (2005).

36 Shankaran, V., Ikeda, H., Bruce, A. T., White, J. M., Swanson, P. E., Old, L. J. & Schreiber, R. D. IFNγ and lymphocytes prevent primary tumour development and shape tumour immunogenicity. *Nature* **410**, 1107-1111 (2001).

37 O'Sullivan, T., Saddawi-Konefka, R., Vermi, W., Koebel, C. M., Arthur, C., White, J. M., Uppaluri, R., Andrews, D. M., Ngiow, S. F., Teng, M. W., Smyth, M. J., Schreiber, R. D. & Bui, J. D. Cancer immunoediting by the innate immune system in the absence of adaptive immunity. *J Exp Med* **209**, 1869-1882, doi:10.1084/jem.20112738 (2012).

38 Girardi, M., Oppenheim, D. E., Steele, C. R., Lewis, J. M., Glusac, E., Filler, R., Hobby, P., Sutton, B., Tigelaar, R. E. & Hayday, A. C. Regulation of cutaneous malignancy by γδ T cells. *Science* **294**, 605-609 (2001).

39 Dunn, G. P., Bruce, A. T., Ikeda, H., Old, L. J. & Schreiber, R. D. Cancer immunoediting: from immunosurveillance to tumor escape. *Nat Immunol* **3**, 991-998, doi:10.1038/ni1102-991 (2002).

40 Svane, I. M., Engel, A. M., Nielsen, M. B., Ljunggren, H. G., Rygaard, J. & Werdelin, O. Chemically induced sarcomas from nude mice are more immunogenic than similar sarcomas from congenic normal mice. *Eur J Immunol* **26**, 1844-1850, doi:10.1002/eji.1830260827 (1996).

41 Engel, A. M., Svane, I. M., Rygaard, J. & Werdelin, O. MCA sarcomas induced in scid mice are more immunogenic than MCA sarcomas induced in congenic, immunocompetent mice. *Scand J Immunol* **45**, 463-470, doi:10.1046/j.1365-3083.1997.d01-419.x (1997).

42 Thomas, L. On immunosurveillance in human cancer. *Yale J Biol Med* **55**, 329-333 (1982).

43 Birkeland, S. A., Storm, H. H., Lamm, L. U., Barlow, L., Blohme, I., Forsberg, B., Eklund, B., Fjeldborg, O., Friedberg, M., Frodin, L., Glattre, E., Halvorsen, S., Holm, N. V., Jakobsen, A., Jorgensen, H. E., Ladefoged, J., Lindholm, T., Lundgren, G. & Pukkala, E. Cancer risk after renal transplantation in the Nordic countries, 1964-1986. *Int J Cancer* **60**, 183-189, doi:10.1002/ijc.2910600209 (1995).

44 Penn, I. Posttransplant malignancies. *Transplant Proc* **31**, 1260-1262, doi:10.1016/s0041-1345(98)01987-3 (1999).

45 Gallagher, B., Wang, Z., Schymura, M. J., Kahn, A. & Fordyce, E. J. Cancer incidence in New York State acquired immunodeficiency syndrome patients. *Am J Epidemiol* **154**, 544-556, doi:10.1093/aje/154.6.544 (2001).

46 Sheil, A. G. Cancer after transplantation. *World J Surg* **10**, 389-396, doi:10.1007/BF01655298 (1986).

47 Penn, I. Malignant melanoma in organ allograft recipients. *Transplantation* **61**, 274-278, doi:10.1097/00007890-199601270-00019 (1996).

48 Pham, S. M., Kormos, R. L., Landreneau, R. J., Kawai, A., Gonzalez-Cancel, I., Hardesty, R. L., Hattler, B. G. & Griffith, B. P. Solid tumors after heart transplantation: lethality of lung cancer. *Ann Thorac Surg* **60**, 1623-1626, doi:10.1016/0003-4975(95)00120-4 (1995).

49 Chui, A., Koorey, D., Pathania, O., Rao, A., McCaughan, G. & Sheil, A. Polycystic disease: a rare indication for combined liver and kidney transplantation. *HONG KONG MEDICAL JOURNAL* **6**, 116-118 (2000).

50 Buell, J. F., Gross, T. G. & Woodle, E. S. Malignancy after transplantation. *Transplantation* **80**, S254-S264 (2005).

51 Bhat, M., Mara, K., Dierkhising, R. & Watt, K. D. S. Immunosuppression, Race, and Donor-Related Risk Factors Affect De novo Cancer Incidence Across Solid Organ Transplant Recipients. *Mayo Clin Proc* **93**, 1236-1246, doi:10.1016/j.mayocp.2018.04.025 (2018).

52 Kersey, J. H., Spector, B. D. & Good, R. A. Primary immunodeficiency diseases and cancer: the immunodeficiency-cancer registry. *Int J Cancer* **12**, 333-347, doi:10.1002/ijc.2910120204 (1973).

53 Mueller, B. U. & Pizzo, P. A. Cancer in children with primary or secondary immunodeficiencies. *J Pediatr* **126**, 1-10 (1995).

54 Ioachim, H. The opportunistic tumors of immune deficiency. *Advances in cancer research* **54**, 301-317 (1990).

55 Mayor, P. C., Eng, K. H., Singel, K. L., Abrams, S. I., Odunsi, K., Moysich, K. B., Fuleihan, R., Garabedian, E., Lugar, P., Ochs, H. D., Bonilla, F. A., Buckley, R. H., Sullivan, K. E., Ballas, Z. K., Cunningham-Rundles, C. & Segal, B. H. Cancer in primary immunodeficiency diseases: Cancer incidence in the United States Immune Deficiency Network Registry. *J Allergy Clin Immunol* **141**, 1028-1035, doi:10.1016/j.jaci.2017.05.024 (2018).

56 Ameratunga, R., Woon, S. T., Gillis, D., Koopmans, W. & Steele, R. New diagnostic criteria for common variable immune deficiency (CVID), which may assist with decisions to treat with intravenous or subcutaneous immunoglobulin. *Clin Exp Immunol* **174**, 203-211, doi:10.1111/cei.12178 (2013).

57 Gereige, J. D. & Maglione, P. J. Current Understanding and Recent Developments in Common Variable Immunodeficiency Associated Autoimmunity. *Front Immunol* **10**, 2753, doi:10.3389/fimmu.2019.02753 (2019).

58 Pulvirenti, F., Pecoraro, A., Cinetto, F., Milito, C., Valente, M., Santangeli, E., Crescenzi, L., Rizzo, F., Tabolli, S., Spadaro, G., Agostini, C. & Quinti, I. Gastric Cancer Is the Leading Cause of Death in Italian Adult Patients With Common Variable Immunodeficiency. *Front Immunol* **9**, 2546, doi:10.3389/fimmu.2018.02546 (2018).

59 Resnick, E. S., Moshier, E. L., Godbold, J. H. & Cunningham-Rundles, C. Morbidity and mortality in common variable immune deficiency over 4 decades. *Blood* **119**, 1650-1657, doi:10.1182/blood-2011-09-377945 (2012).

60 Gordon, I. O. & Freedman, R. S. Defective antitumor function of monocyte-derived macrophages from epithelial ovarian cancer patients. *Clin Cancer Res* **12**, 1515-1524, doi:10.1158/1078-0432.CCR-05-2254 (2006).

61 Griffith, T. S., Wiley, S. R., Kubin, M. Z., Sedger, L. M., Maliszewski, C. R. & Fanger, N. A. Monocyte-mediated tumoricidal activity via the tumor necrosis factor-related cytokine, TRAIL. *J Exp Med* **189**, 1343-1354, doi:10.1084/jem.189.8.1343 (1999).

62 Yeap, W. H., Wong, K. L., Shimasaki, N., Teo, E. C., Quek, J. K., Yong, H. X., Diong, C. P., Bertoletti, A., Linn, Y. C. & Wong, S. C. CD16 is indispensable for antibody-dependent cellular cytotoxicity by human monocytes. *Sci Rep* **6**, 34310, doi:10.1038/srep34310 (2016).

63 Yu, Y. R., Fong, A. M., Combadiere, C., Gao, J. L., Murphy, P. M. & Patel, D. D. Defective antitumor responses in CX3CR1-deficient mice. *Int J Cancer* **121**, 316-322, doi:10.1002/ijc.22660 (2007).

64 Hanna, R. N., Cekic, C., Sag, D., Tacke, R., Thomas, G. D., Nowyhed, H., Herrley, E., Rasquinha, N., McArdle, S., Wu, R., Peluso, E., Metzger, D., Ichinose, H., Shaked, I., Chodaczek, G., Biswas, S. K. & Hedrick, C. C. Patrolling monocytes control tumor metastasis to the lung. *Science* **350**, 985-990, doi:10.1126/science.aac9407 (2015).

65 Schmall, A., Al-Tamari, H. M., Herold, S., Kampschulte, M., Weigert, A., Wietelmann, A., Vipotnik, N., Grimminger, F., Seeger, W., Pullamsetti, S. S. & Savai, R. Macrophage and cancer cell cross-talk via CCR2 and CX3CR1 is a fundamental mechanism driving lung cancer. *Am J Respir Crit Care Med* **191**, 437-447, doi:10.1164/rccm.201406-1137OC (2015).

66 Franklin, R. A., Liao, W., Sarkar, A., Kim, M. V., Bivona, M. R., Liu, K., Pamer, E. G. & Li, M. O. The cellular and molecular origin of tumor-associated macrophages. *Science* **344**, 921-925 (2014).

67 Zhu, Y. P., Padgett, L., Dinh, H. Q., Marcovecchio, P., Blatchley, A., Wu, R., Ehinger, E., Kim, C., Mikulski, Z., Seumois, G., Madrigal, A., Vijayanand, P. & Hedrick, C. C. Identification of an Early Unipotent Neutrophil Progenitor with Pro-tumoral Activity in Mouse and Human Bone Marrow. *Cell Rep* **24**, 2329-2341 e2328, doi:10.1016/j.celrep.2018.07.097 (2018).

68 Yona, S., Kim, K. W., Wolf, Y., Mildner, A., Varol, D., Breker, M., Strauss-Ayali, D., Viukov, S., Guilliams, M., Misharin, A., Hume, D. A., Perlman, H., Malissen, B., Zelzer, E. & Jung, S. Fate mapping reveals origins and dynamics of monocytes and tissue macrophages under homeostasis. *Immunity* **38**, 79-91, doi:10.1016/j.immuni.2012.12.001 (2013).

69 Hashimoto, D., Chow, A., Noizat, C., Teo, P., Beasley, M. B., Leboeuf, M., Becker, C. D., See, P., Price, J., Lucas, D., Greter, M., Mortha, A., Boyer, S. W., Forsberg, E. C., Tanaka, M., van Rooijen, N., Garcia-Sastre, A., Stanley, E. R., Ginhoux, F., Frenette, P. S. & Merad, M. Tissue-resident macrophages self-maintain locally throughout adult life with minimal contribution from circulating monocytes. *Immunity* **38**, 792-804, doi:10.1016/j.immuni.2013.04.004 (2013).

70 Zhang, Q. W., Liu, L., Gong, C. Y., Shi, H. S., Zeng, Y. H., Wang, X. Z., Zhao, Y. W. & Wei, Y. Q. Prognostic significance of tumor-associated macrophages in solid tumor: a meta-analysis of the literature. *PLoS One* **7**, e50946, doi:10.1371/journal.pone.0050946 (2012).

71 Steidl, C., Lee, T., Shah, S. P., Farinha, P., Han, G., Nayar, T., Delaney, A., Jones, S. J., Iqbal, J., Weisenburger, D. D., Bast, M. A., Rosenwald, A., Muller-Hermelink, H. K., Rimsza, L. M., Campo, E., Delabie, J., Braziel, R. M., Cook, J. R., Tubbs, R. R., Jaffe, E. S., Lenz, G., Connors, J. M., Staudt, L. M., Chan, W. C. & Gascoyne, R. D. Tumor-associated macrophages and survival in classic Hodgkin's lymphoma. *N Engl J Med* **362**, 875-885, doi:10.1056/NEJMoa0905680 (2010).

72 Bohn, T., Rapp, S., Luther, N., Klein, M., Bruehl, T. J., Kojima, N., Aranda Lopez, P., Hahlbrock, J., Muth, S., Endo, S., Pektor, S., Brand, A., Renner, K., Popp, V., Gerlach, K., Vogel, D., Lueckel, C., Arnold-Schild, D., Pouyssegur, J., Kreutz, M., Huber, M., Koenig, J., Weigmann, B., Probst, H. C., von Stebut, E., Becker, C., Schild, H., Schmitt, E. & Bopp, T. Tumor immunoevasion via acidosis-dependent induction of regulatory tumor-associated macrophages. *Nat Immunol* **19**, 1319-1329, doi:10.1038/s41590-018-0226-8 (2018).

73 Corbet, C. & Feron, O. Tumour acidosis: from the passenger to the driver's seat. *Nat Rev Cancer* **17**, 577-593, doi:10.1038/nrc.2017.77 (2017).

74 Colegio, O. R., Chu, N. Q., Szabo, A. L., Chu, T., Rhebergen, A. M., Jairam, V., Cyrus, N., Brokowski, C. E., Eisenbarth, S. C., Phillips, G. M., Cline, G. W., Phillips, A. J. & Medzhitov, R. Functional polarization of tumour-associated macrophages by tumour-derived lactic acid. *Nature* **513**, 559-563, doi:10.1038/nature13490 (2014).

75 Mantovani, A., Allavena, P., Sica, A. & Balkwill, F. Cancer-related inflammation. *Nature* **454**, 436-444, doi:10.1038/nature07205 (2008).

76 Chong, H., Vodovotz, Y., Cox, G. W. & Barcellos-Hoff, M. H. Immunocytochemical localization of latent transforming growth factor-beta1 activation by stimulated macrophages. *J Cell Physiol* **178**, 275-283, doi:10.1002/(SICI)1097-4652(199903)178:3<275::AID-JCP1>3.0.CO;2-Q (1999).

77 Haque, A., Moriyama, M., Kubota, K., Ishiguro, N., Sakamoto, M., Chinju, A., Mochizuki, K., Sakamoto, T., Kaneko, N., Munemura, R., Maehara, T., Tanaka, A., Hayashida, J. N., Kawano, S., Kiyoshima, T. & Nakamura, S. CD206(+) tumor-associated macrophages promote proliferation and invasion in oral squamous cell carcinoma via EGF production. *Sci Rep* **9**, 14611, doi:10.1038/s41598-019-51149-1 (2019).

78 Takase, N., Koma, Y., Urakawa, N., Nishio, M., Arai, N., Akiyama, H., Shigeoka, M., Kakeji, Y. & Yokozaki, H. NCAM- and FGF-2-mediated FGFR1 signaling in the tumor microenvironment of esophageal cancer regulates the survival and migration of tumor-associated macrophages and cancer cells. *Cancer Lett* **380**, 47-58, doi:10.1016/j.canlet.2016.06.009 (2016).

79 Wang, R., Zhang, J., Chen, S., Lu, M., Luo, X., Yao, S., Liu, S., Qin, Y. & Chen, H. Tumor-associated macrophages provide a suitable microenvironment for non-small lung cancer invasion and progression. *Lung Cancer* **74**, 188-196, doi:10.1016/j.lungcan.2011.04.009 (2011).

80 Tamura, R., Tanaka, T., Yamamoto, Y., Akasaki, Y. & Sasaki, H. Dual role of macrophage in tumor immunity. *Immunotherapy* **10**, 899-909, doi:10.2217/imt-2018-0006 (2018).

81 Chen, X. J., Wu, S., Yan, R. M., Fan, L. S., Yu, L., Zhang, Y. M., Wei, W. F., Zhou, C. F., Wu, X. G., Zhong, M., Yu, Y. H., Liang, L. & Wang, W. The role of the hypoxia-Nrp-1 axis in the activation of M2-like tumor-associated macrophages in the tumor microenvironment of cervical cancer. *Mol Carcinog* **58**, 388-397, doi:10.1002/mc.22936 (2019).

82 Na, Y. R., Kwon, J. W., Kim, D. Y., Chung, H., Song, J., Jung, D., Quan, H., Kim, D., Kim, J. S., Ju, Y. W., Han, W., Ryu, H. S., Lee, Y. S., Hong, J. J. & Seok, S. H. Protein Kinase A Catalytic Subunit Is a Molecular Switch that Promotes the Pro-tumoral Function of Macrophages. *Cell Rep* **31**, 107643, doi:10.1016/j.celrep.2020.107643 (2020).

83 Giraudo, E., Inoue, M. & Hanahan, D. An amino-bisphosphonate targets MMP-9-expressing macrophages and angiogenesis to impair cervical carcinogenesis. *J Clin Invest* **114**, 623-633, doi:10.1172/JCI22087 (2004).

84 Du, R., Lu, K. V., Petritsch, C., Liu, P., Ganss, R., Passegue, E., Song, H., Vandenberg, S., Johnson, R. S., Werb, Z. & Bergers, G. HIF1alpha induces the recruitment of bone marrow-derived vascular modulatory cells to regulate tumor angiogenesis and invasion. *Cancer Cell* **13**, 206-220, doi:10.1016/j.ccr.2008.01.034 (2008).

85 Yin, Y., Yao, S., Hu, Y., Feng, Y., Li, M., Bian, Z., Zhang, J., Qin, Y., Qi, X., Zhou, L., Fei, B., Zou, J., Hua, D. & Huang, Z. The Immune-microenvironment Confers Chemoresistance of Colorectal Cancer through Macrophage-Derived IL6. *Clin Cancer Res* **23**, 7375-7387, doi:10.1158/1078-0432.CCR-17-1283 (2017).

86 Mills, C. D. Anatomy of a discovery: m1 and m2 macrophages. *Front Immunol* **6**, 212, doi:10.3389/fimmu.2015.00212 (2015).

87 Italiani, P. & Boraschi, D. From Monocytes to M1/M2 Macrophages: Phenotypical vs. Functional Differentiation. *Front Immunol* **5**, 514, doi:10.3389/fimmu.2014.00514 (2014).

88 Nahrendorf, M. & Swirski, F. K. Abandoning M1/M2 for a Network Model of Macrophage Function. *Circ Res* **119**, 414-417, doi:10.1161/CIRCRESAHA.116.309194 (2016).

89 Orecchioni, M., Ghosheh, Y., Pramod, A. B. & Ley, K. Corrigendum: Macrophage Polarization: Different Gene Signatures in M1(LPS+) vs. Classically and M2(LPS-) vs. Alternatively Activated Macrophages. *Front Immunol* **11**, 234, doi:10.3389/fimmu.2020.00234 (2020).

90 Savage, N. D., de Boer, T., Walburg, K. V., Joosten, S. A., van Meijgaarden, K., Geluk, A. & Ottenhoff, T. H. Human anti-inflammatory macrophages induce Foxp3+ GITR+ CD25+ regulatory T cells, which suppress via membrane-bound TGFbeta-1. *J Immunol* **181**, 2220-2226, doi:10.4049/jimmunol.181.3.2220 (2008).

91 Sica, A., Saccani, A., Bottazzi, B., Polentarutti, N., Vecchi, A., van Damme, J. & Mantovani, A. Autocrine production of IL-10 mediates defective IL-12 production and NF-kappa B activation in tumor-associated macrophages. *J Immunol* **164**, 762-767, doi:10.4049/jimmunol.164.2.762 (2000).

92 Allavena, P., Piemonti, L., Longoni, D., Bernasconi, S., Stoppacciaro, A., Ruco, L. & Mantovani, A. IL-10 prevents the differentiation of monocytes to dendritic cells but promotes their maturation to macrophages. *Eur J Immunol* **28**, 359-369, doi:10.1002/(SICI)1521-4141(199801)28:01<359::AID-IMMU359>3.0.CO;2-4 (1998).

93 Algarra, I., Collado, A. & Garrido, F. Altered MHC class I antigens in tumors. *Int J Clin Lab Res* **27**, 95-102, doi:10.1007/BF02912442 (1997).

94 Cabrera, T., Angustias Fernandez, M., Sierra, A., Garrido, A., Herruzo, A., Escobedo, A., Fabra, A. & Garrido, F. High frequency of altered HLA class I phenotypes in invasive breast carcinomas. *Hum Immunol* **50**, 127-134, doi:10.1016/0198-8859(96)00145-0 (1996).

95 Schumacher, T. N. & Schreiber, R. D. Neoantigens in cancer immunotherapy. *Science* **348**, 69-74, doi:10.1126/science.aaa4971 (2015).

96 King, D. P. & Jones, P. P. Induction of Ia and H-2 antigens on a macrophage cell line by immune interferon. *J Immunol* **131**, 315-318 (1983).

97 Basham, T. Y. & Merigan, T. C. Recombinant interferon-gamma increases HLA-DR synthesis and expression. *J Immunol* **130**, 1492-1494 (1983).

98 Cheney, E. E., Wise, E. L., Bui, J. D., Schreiber, R. D., Carayannopoulos, L. N., Spitzer, D., Zafirova, B., Polic, B., Shaw, A. S. & Markiewicz, M. A. A dual function of NKG2D ligands in NK-cell activation. *Eur J Immunol* **42**, 2452-2458, doi:10.1002/eji.201141849 (2012).

99 Bui, J. D., Carayannopoulos, L. N., Lanier, L. L., Yokoyama, W. M. & Schreiber, R. D. IFN-dependent down-regulation of the NKG2D ligand H60 on tumors. *J Immunol* **176**, 905-913, doi:10.4049/jimmunol.176.2.905 (2006).

100 Shiroishi, M., Tsumoto, K., Amano, K., Shirakihara, Y., Colonna, M., Braud, V. M., Allan, D. S., Makadzange, A., Rowland-Jones, S., Willcox, B., Jones, E. Y., van der Merwe, P. A., Kumagai, I. & Maenaka, K. Human inhibitory receptors Ig-like transcript 2 (ILT2) and ILT4 compete with CD8 for MHC class I binding and bind preferentially to HLA-G. *Proc Natl Acad Sci U S A* **100**, 8856-8861, doi:10.1073/pnas.1431057100 (2003).

101 Borrego, F., Ulbrecht, M., Weiss, E. H., Coligan, J. E. & Brooks, A. G. Recognition of human histocompatibility leukocyte antigen (HLA)-E complexed with HLA class I signal sequence-derived peptides by CD94/NKG2 confers protection from natural killer cell-mediated lysis. *J Exp Med* **187**, 813-818, doi:10.1084/jem.187.5.813 (1998).

102 Kren, L., Muckova, K., Lzicarova, E., Sova, M., Vybihal, V., Svoboda, T., Fadrus, P., Smrcka, M., Slaby, O., Lakomy, R., Vanhara, P., Krenova, Z. & Michalek, J. Production of immune-modulatory nonclassical molecules HLA-G and HLA-E by tumor infiltrating ameboid microglia/macrophages in glioblastomas: a role in innate immunity? *J Neuroimmunol* **220**, 131-135, doi:10.1016/j.jneuroim.2010.01.014 (2010).

103 Groh, V., Bahram, S., Bauer, S., Herman, A., Beauchamp, M. & Spies, T. Cell stress-regulated human major histocompatibility complex class I gene expressed in gastrointestinal epithelium. *Proc Natl Acad Sci U S A* **93**, 12445-12450, doi:10.1073/pnas.93.22.12445 (1996).

104 Wingren, A. G., Parra, E., Varga, M., Kalland, T., Sjogren, H. O., Hedlund, G. & Dohlsten, M. T Cell Activation Pathways: B7, LFA-3, and ICAM-1 Shape Unique T Cell Profiles. *Crit Rev Immunol* **37**, 463-481, doi:10.1615/CritRevImmunol.v37.i2-6.130 (2017).

105 Yang, J. J., Ye, Y., Carroll, A., Yang, W. & Lee, H. W. Structural biology of the cell adhesion protein CD2: alternatively folded states and structure-function relation. *Curr Protein Pept Sci* **2**, 1-17, doi:10.2174/1389203013381251 (2001).

106 Binder, C., Cvetkovski, F., Sellberg, F., Berg, S., Paternina Visbal, H., Sachs, D. H., Berglund, E. & Berglund, D. CD2 Immunobiology. *Front Immunol* **11**, 1090, doi:10.3389/fimmu.2020.01090 (2020).

107 Leitner, J., Herndler-Brandstetter, D., Zlabinger, G. J., Grubeck-Loebenstein, B. & Steinberger, P. CD58/CD2 Is the Primary Costimulatory Pathway in Human CD28-CD8+ T Cells. *J Immunol* **195**, 477-487, doi:10.4049/jimmunol.1401917 (2015).

108 Lo, D. J., Weaver, T. A., Stempora, L., Mehta, A. K., Ford, M. L., Larsen, C. P. & Kirk, A. D. Selective targeting of human alloresponsive CD8+ effector memory T cells based on CD2 expression. *Am J Transplant* **11**, 22-33, doi:10.1111/j.1600-6143.2010.03317.x (2011).

109 Kishimoto, T. K., Larson, R. S., Corbi, A. L., Dustin, M. L., Staunton, D. E. & Springer, T. A. The leukocyte integrins. *Adv Immunol* **46**, 149-182, doi:10.1016/s0065-2776(08)60653-7 (1989).

110 Monks, C. R., Freiberg, B. A., Kupfer, H., Sciaky, N. & Kupfer, A. Three-dimensional segregation of supramolecular activation clusters in T cells. *Nature* **395**, 82-86, doi:10.1038/25764 (1998).

111 Kaizuka, Y., Douglass, A. D., Varma, R., Dustin, M. L. & Vale, R. D. Mechanisms for segregating T cell receptor and adhesion molecules during immunological synapse formation in Jurkat T cells. *Proc Natl Acad Sci U S A* **104**, 20296-20301, doi:10.1073/pnas.0710258105 (2007).

112 Yi, J., Wu, X. S., Crites, T. & Hammer, J. A., 3rd. Actin retrograde flow and actomyosin II arc contraction drive receptor cluster dynamics at the immunological synapse in Jurkat T cells. *Mol Biol Cell* **23**, 834-852, doi:10.1091/mbc.E11-08-0731 (2012).

113 Dustin, M. L. The immunological synapse. *Cancer Immunol Res* **2**, 1023-1033, doi:10.1158/2326-6066.CIR-14-0161 (2014).

114 Comrie, W. A., Li, S., Boyle, S. & Burkhardt, J. K. The dendritic cell cytoskeleton promotes T cell adhesion and activation by constraining ICAM-1 mobility. *J Cell Biol* **208**, 457-473, doi:10.1083/jcb.201406120 (2015).

115 Benard, E., Nunes, J. A., Limozin, L. & Sengupta, K. T Cells on Engineered Substrates: The Impact of TCR Clustering Is Enhanced by LFA-1 Engagement. *Front Immunol* **9**, 2085, doi:10.3389/fimmu.2018.02085 (2018).

116 Valenzuela, H. F. & Effros, R. B. Divergent telomerase and CD28 expression patterns in human CD4 and CD8 T cells following repeated encounters with the same antigenic stimulus. *Clin Immunol* **105**, 117-125, doi:10.1006/clim.2002.5271 (2002).

117 Acuto, O. & Michel, F. CD28-mediated co-stimulation: a quantitative support for TCR signalling. *Nat Rev Immunol* **3**, 939-951, doi:10.1038/nri1248 (2003).

118 Schneider, H. & Rudd, C. E. Tyrosine phosphatase SHP-2 binding to CTLA-4: absence of direct YVKM/YFIP motif recognition. *Biochem Biophys Res Commun* **269**, 279-283, doi:10.1006/bbrc.2000.2234 (2000).

119 Sathish, J. G., Johnson, K. G., LeRoy, F. G., Fuller, K. J., Hallett, M. B., Brennan, P., Borysiewicz, L. K., Sims, M. J. & Matthews, R. J. Requirement for CD28 co-stimulation is lower in SHP-1-deficient T cells. *Eur J Immunol* **31**, 3649-3658, doi:10.1002/1521-4141(200112)31:12<3649::aid-immu3649>3.0.co;2-8 (2001).

120 Parry, R. V., Chemnitz, J. M., Frauwirth, K. A., Lanfranco, A. R., Braunstein, I., Kobayashi, S. V., Linsley, P. S., Thompson, C. B. & Riley, J. L. CTLA-4 and PD-1 receptors inhibit T-cell activation by distinct mechanisms. *Mol Cell Biol* **25**, 9543-9553, doi:10.1128/MCB.25.21.9543-9553.2005 (2005).

121 Chuang, E., Fisher, T. S., Morgan, R. W., Robbins, M. D., Duerr, J. M., Vander Heiden, M. G., Gardner, J. P., Hambor, J. E., Neveu, M. J. & Thompson, C. B. The CD28 and CTLA-4 receptors associate with the serine/threonine phosphatase PP2A. *Immunity* **13**, 313-322, doi:10.1016/s1074-7613(00)00031-5 (2000).

122 Rudd, C. E., Taylor, A. & Schneider, H. CD28 and CTLA-4 coreceptor expression and signal transduction. *Immunol Rev* **229**, 12-26, doi:10.1111/j.1600-065X.2009.00770.x (2009).

123 Collins, A. V., Brodie, D. W., Gilbert, R. J., Iaboni, A., Manso-Sancho, R., Walse, B., Stuart, D. I., van der Merwe, P. A. & Davis, S. J. The interaction properties of

costimulatory molecules revisited. *Immunity* **17**, 201-210, doi:10.1016/s1074-7613(02)00362-x (2002).

124 Qureshi, O. S., Zheng, Y., Nakamura, K., Attridge, K., Manzotti, C., Schmidt, E. M., Baker, J., Jeffery, L. E., Kaur, S., Briggs, Z., Hou, T. Z., Futter, C. E., Anderson, G., Walker, L. S. & Sansom, D. M. Trans-endocytosis of CD80 and CD86: a molecular basis for the cell-extrinsic function of CTLA-4. *Science* **332**, 600-603, doi:10.1126/science.1202947 (2011).

125 Brunet, J. F., Denizot, F., Luciani, M. F., Roux-Dosseto, M., Suzan, M., Mattei, M. G. & Golstein, P. A new member of the immunoglobulin superfamily--CTLA-4. *Nature* **328**, 267-270, doi:10.1038/328267a0 (1987).

126 Dariavach, P., Mattei, M. G., Golstein, P. & Lefranc, M. P. Human Ig superfamily CTLA-4 gene: chromosomal localization and identity of protein sequence between murine and human CTLA-4 cytoplasmic domains. *Eur J Immunol* **18**, 1901-1905, doi:10.1002/eji.1830181206 (1988).

127 Chen, L., Ashe, S., Brady, W. A., Hellstrom, I., Hellstrom, K. E., Ledbetter, J. A., McGowan, P. & Linsley, P. S. Costimulation of antitumor immunity by the B7 counterreceptor for the T lymphocyte molecules CD28 and CTLA-4. *Cell* **71**, 1093-1102, doi:10.1016/s0092-8674(05)80059-5 (1992).

128 Linsley, P. S., Greene, J. L., Tan, P., Bradshaw, J., Ledbetter, J. A., Anasetti, C. & Damle, N. K. Coexpression and functional cooperation of CTLA-4 and CD28 on activated T lymphocytes. *J Exp Med* **176**, 1595-1604, doi:10.1084/jem.176.6.1595 (1992).

129 Walunas, T. L., Lenschow, D. J., Bakker, C. Y., Linsley, P. S., Freeman, G. J., Green, J. M., Thompson, C. B. & Bluestone, J. A. CTLA-4 can function as a negative regulator of T cell activation. *Immunity* **1**, 405-413, doi:10.1016/1074-7613(94)90071-x (1994).

130 Leach, D. R., Krummel, M. F. & Allison, J. P. Enhancement of antitumor immunity by CTLA-4 blockade. *Science* **271**, 1734-1736, doi:10.1126/science.271.5256.1734 (1996).

131 Hodi, F. S., Mihm, M. C., Soiffer, R. J., Haluska, F. G., Butler, M., Seiden, M. V., Davis, T., Henry-Spires, R., MacRae, S., Willman, A., Padera, R., Jaklitsch, M. T., Shankar, S., Chen, T. C., Korman, A., Allison, J. P. & Dranoff, G. Biologic activity of cytotoxic T lymphocyte-associated antigen 4 antibody blockade in previously vaccinated metastatic melanoma and ovarian carcinoma patients. *Proc Natl Acad Sci U S A* **100**, 4712-4717, doi:10.1073/pnas.0830997100 (2003).

132 Ramagopal, U. A., Liu, W., Garrett-Thomson, S. C., Bonanno, J. B., Yan, Q., Srinivasan, M., Wong, S. C., Bell, A., Mankikar, S., Rangan, V. S., Deshpande, S., Korman, A. J. & Almo, S. C. Structural basis for cancer immunotherapy by the first-in-class checkpoint

inhibitor ipilimumab. *Proc Natl Acad Sci U S A* **114**, E4223-E4232, doi:10.1073/pnas.1617941114 (2017).

133 Phan, G. Q., Yang, J. C., Sherry, R. M., Hwu, P., Topalian, S. L., Schwartzentruber, D. J., Restifo, N. P., Haworth, L. R., Seipp, C. A., Freezer, L. J., Morton, K. E., Mavroukakis, S. A., Duray, P. H., Steinberg, S. M., Allison, J. P., Davis, T. A. & Rosenberg, S. A. Cancer regression and autoimmunity induced by cytotoxic T lymphocyte-associated antigen 4 blockade in patients with metastatic melanoma. *Proc Natl Acad Sci U S A* **100**, 8372-8377, doi:10.1073/pnas.1533209100 (2003).

134 Beck, K. E., Blansfield, J. A., Tran, K. Q., Feldman, A. L., Hughes, M. S., Royal, R. E., Kammula, U. S., Topalian, S. L., Sherry, R. M., Kleiner, D., Quezado, M., Lowy, I., Yellin, M., Rosenberg, S. A. & Yang, J. C. Enterocolitis in patients with cancer after antibody blockade of cytotoxic T-lymphocyte-associated antigen 4. *J Clin Oncol* **24**, 2283-2289, doi:10.1200/JCO.2005.04.5716 (2006).

135 Ribas, A. Clinical development of the anti-CTLA-4 antibody tremelimumab. *Semin Oncol* **37**, 450-454, doi:10.1053/j.seminoncol.2010.09.010 (2010).

136 Hodi, F. S., O'Day, S. J., McDermott, D. F., Weber, R. W., Sosman, J. A., Haanen, J. B., Gonzalez, R., Robert, C., Schadendorf, D., Hassel, J. C., Akerley, W., van den Eertwegh, A. J., Lutzky, J., Lorigan, P., Vaubel, J. M., Linette, G. P., Hogg, D., Ottensmeier, C. H., Lebbe, C., Peschel, C., Quirt, I., Clark, J. I., Wolchok, J. D., Weber, J. S., Tian, J., Yellin, M. J., Nichol, G. M., Hoos, A. & Urba, W. J. Improved survival with ipilimumab in patients with metastatic melanoma. *N Engl J Med* **363**, 711-723, doi:10.1056/NEJMoa1003466 (2010).

137 Schadendorf, D., Hodi, F. S., Robert, C., Weber, J. S., Margolin, K., Hamid, O., Patt, D., Chen, T. T., Berman, D. M. & Wolchok, J. D. Pooled Analysis of Long-Term Survival Data From Phase II and Phase III Trials of Ipilimumab in Unresectable or Metastatic Melanoma. *J Clin Oncol* **33**, 1889-1894, doi:10.1200/JCO.2014.56.2736 (2015).

138 Connolly, C., Bambhania, K. & Naidoo, J. Immune-Related Adverse Events: A Case-Based Approach. *Front Oncol* **9**, 530, doi:10.3389/fonc.2019.00530 (2019).

139 Nishimura, H., Nose, M., Hiai, H., Minato, N. & Honjo, T. Development of lupus-like autoimmune diseases by disruption of the PD-1 gene encoding an ITIM motif-carrying immunoreceptor. *Immunity* **11**, 141-151, doi:10.1016/s1074-7613(00)80089-8 (1999).

140 Marasco, M., Berteotti, A., Weyershaeuser, J., Thorausch, N., Sikorska, J., Krausze, J., Brandt, H. J., Kirkpatrick, J., Rios, P., Schamel, W. W., Kohn, M. & Carlomagno, T. Molecular mechanism of SHP2 activation by PD-1 stimulation. *Sci Adv* **6**, eaay4458, doi:10.1126/sciadv.aay4458 (2020).

141 Inaba, K., Witmer-Pack, M., Inaba, M., Hathcock, K. S., Sakuta, H., Azuma, M., Yagita, H., Okumura, K., Linsley, P. S., Ikehara, S., Muramatsu, S., Hodes, R. J. & Steinman, R. M. The tissue distribution of the B7-2 costimulator in mice: abundant expression on dendritic cells in situ and during maturation in vitro. *J Exp Med* **180**, 1849-1860, doi:10.1084/jem.180.5.1849 (1994).

142 Fife, B. T. & Bluestone, J. A. Control of peripheral T-cell tolerance and autoimmunity via the CTLA-4 and PD-1 pathways. *Immunol Rev* **224**, 166-182, doi:10.1111/j.1600-065X.2008.00662.x (2008).

143 Fanoni, D., Tavecchio, S., Recalcati, S., Balice, Y., Venegoni, L., Fiorani, R., Crosti, C. & Berti, E. New monoclonal antibodies against B-cell antigens: possible new strategies for diagnosis of primary cutaneous B-cell lymphomas. *Immunol Lett* **134**, 157-160, doi:10.1016/j.imlet.2010.09.022 (2011).

144 Terme, M., Ullrich, E., Aymeric, L., Meinhardt, K., Desbois, M., Delahaye, N., Viaud, S., Ryffel, B., Yagita, H., Kaplanski, G., Prevost-Blondel, A., Kato, M., Schultze, J. L., Tartour, E., Kroemer, G., Chaput, N. & Zitvogel, L. IL-18 induces PD-1-dependent immunosuppression in cancer. *Cancer Res* **71**, 5393-5399, doi:10.1158/0008-5472.CAN-11-0993 (2011).

145 Taube, J. M., Anders, R. A., Young, G. D., Xu, H., Sharma, R., McMiller, T. L., Chen, S., Klein, A. P., Pardoll, D. M., Topalian, S. L. & Chen, L. Colocalization of inflammatory response with B7-h1 expression in human melanocytic lesions supports an adaptive resistance mechanism of immune escape. *Sci Transl Med* **4**, 127ra137, doi:10.1126/scitranslmed.3003689 (2012).

146 Dong, H., Strome, S. E., Salomao, D. R., Tamura, H., Hirano, F., Flies, D. B., Roche, P. C., Lu, J., Zhu, G., Tamada, K., Lennon, V. A., Celis, E. & Chen, L. Tumor-associated B7-H1 promotes T-cell apoptosis: a potential mechanism of immune evasion. *Nat Med* **8**, 793-800, doi:10.1038/nm730 (2002).

147 Wing, K., Onishi, Y., Prieto-Martin, P., Yamaguchi, T., Miyara, M., Fehervari, Z., Nomura, T. & Sakaguchi, S. CTLA-4 control over Foxp3+ regulatory T cell function. *Science* **322**, 271-275, doi:10.1126/science.1160062 (2008).

148 Barber, D. L., Wherry, E. J., Masopust, D., Zhu, B., Allison, J. P., Sharpe, A. H., Freeman, G. J. & Ahmed, R. Restoring function in exhausted CD8 T cells during chronic viral infection. *Nature* **439**, 682-687, doi:10.1038/nature04444 (2006).

149 Ahmadzadeh, M., Johnson, L. A., Heemskerk, B., Wunderlich, J. R., Dudley, M. E., White, D. E. & Rosenberg, S. A. Tumor antigen-specific CD8 T cells infiltrating the tumor express high levels of PD-1 and are functionally impaired. *Blood* **114**, 1537-1544, doi:10.1182/blood-2008-12-195792 (2009).

150 Hellmann, M. D., Rizvi, N. A., Goldman, J. W., Gettinger, S. N., Borghaei, H., Brahmer, J. R., Ready, N. E., Gerber, D. E., Chow, L. Q., Juergens, R. A., Shepherd, F. A., Laurie, S. A., Geese, W. J., Agrawal, S., Young, T. C., Li, X. & Antonia, S. J. Nivolumab plus ipilimumab as first-line treatment for advanced non-small-cell lung cancer (CheckMate 012): results of an open-label, phase 1, multicohort study. *Lancet Oncol* **18**, 31-41, doi:10.1016/S1470-2045(16)30624-6 (2017).

151 Leighl, N. B., Hellmann, M. D., Hui, R., Carcereny, E., Felip, E., Ahn, M. J., Eder, J. P., Balmanoukian, A. S., Aggarwal, C., Horn, L., Patnaik, A., Gubens, M., Ramalingam, S. S., Lubiniecki, G. M., Zhang, J., Piperdi, B. & Garon, E. B. Pembrolizumab in patients with advanced non-small-cell lung cancer (KEYNOTE-001): 3-year results from an open-label, phase 1 study. *Lancet Respir Med* **7**, 347-357, doi:10.1016/S2213-2600(18)30500-9 (2019).

152 Villadolid, J. & Amin, A. Immune checkpoint inhibitors in clinical practice: update on management of immune-related toxicities. *Transl Lung Cancer Res* **4**, 560-575, doi:10.3978/j.issn.2218-6751.2015.06.06 (2015).

153 Dong, H., Zhu, G., Tamada, K., Flies, D. B., van Deursen, J. M. & Chen, L. B7-H1 determines accumulation and deletion of intrahepatic CD8(+) T lymphocytes. *Immunity* **20**, 327-336, doi:10.1016/s1074-7613(04)00050-0 (2004).

154 Ettinger, D. S., Wood, D. E., Akerley, W., Bazhenova, L. A., Borghaei, H., Camidge, D. R., Cheney, R. T., Chirieac, L. R., D'Amico, T. A., Dilling, T. J., Dobelbower, M. C., Govindan, R., Hennon, M., Horn, L., Jahan, T. M., Komaki, R., Lackner, R. P., Lanuti, M., Lilenbaum, R., Lin, J., Loo, B. W., Jr., Martins, R., Otterson, G. A., Patel, J. D., Pisters, K. M., Reckamp, K., Riely, G. J., Schild, S. E., Shapiro, T. A., Sharma, N., Stevenson, J., Swanson, S. J., Tauer, K., Yang, S. C., Gregory, K. & Hughes, M. NCCN Guidelines Insights: Non-Small Cell Lung Cancer, Version 4.2016. *J Natl Compr Canc Netw* **14**, 255-264, doi:10.6004/jnccn.2016.0031 (2016).

155 Coit, D. G., Thompson, J. A., Algazi, A., Andtbacka, R., Bichakjian, C. K., Carson, W. E., 3rd, Daniels, G. A., DiMaio, D., Fields, R. C., Fleming, M. D., Gastman, B., Gonzalez, R., Guild, V., Johnson, D., Joseph, R. W., Lange, J. R., Martini, M. C., Materin, M. A., Olszanski, A. J., Ott, P., Gupta, A. P., Ross, M. I., Salama, A. K., Skitzki, J., Swetter, S. M., Tanabe, K. K., Torres-Roca, J. F., Trisal, V., Urist, M. M., McMillian, N. & Engh, A. NCCN Guidelines Insights: Melanoma, Version 3.2016. *J Natl Compr Canc Netw* **14**, 945-958, doi:10.6004/jnccn.2016.0101 (2016).

156 Wolchok, J. D., Chiarion-Sileni, V., Gonzalez, R., Rutkowski, P., Grob, J. J., Cowey, C. L., Lao, C. D., Wagstaff, J., Schadendorf, D., Ferrucci, P. F., Smylie, M., Dummer, R., Hill, A., Hogg, D., Haanen, J., Carlino, M. S., Bechter, O., Maio, M., Marquez-Rodas, I., Guidoboni, M., McArthur, G., Lebbe, C., Ascierto, P. A., Long, G. V., Cebon, J., Sosman, J., Postow, M. A., Callahan, M. K., Walker, D., Rollin, L., Bhore, R., Hodi, F. S. & Larkin, J. Overall Survival with Combined Nivolumab and Ipilimumab in Advanced Melanoma. *N Engl J Med* **377**, 1345-1356, doi:10.1056/NEJMoa1709684 (2017).

157 Callahan, M. K., Kluger, H., Postow, M. A., Segal, N. H., Lesokhin, A., Atkins, M. B., Kirkwood, J. M., Krishnan, S., Bhore, R., Horak, C., Wolchok, J. D. & Sznol, M. Nivolumab Plus Ipilimumab in Patients With Advanced Melanoma: Updated Survival, Response, and Safety Data in a Phase I Dose-Escalation Study. *J Clin Oncol* **36**, 391-398, doi:10.1200/JCO.2017.72.2850 (2018).

158 Shoushtari, A. N., Friedman, C. F., Navid-Azarbaijani, P., Postow, M. A., Callahan, M. K., Momtaz, P., Panageas, K. S., Wolchok, J. D. & Chapman, P. B. Measuring Toxic Effects and Time to Treatment Failure for Nivolumab Plus Ipilimumab in Melanoma. *JAMA Oncol* **4**, 98-101, doi:10.1001/jamaoncol.2017.2391 (2018).

159 Pardoll, D. M. The blockade of immune checkpoints in cancer immunotherapy. *Nat Rev Cancer* **12**, 252-264, doi:10.1038/nrc3239 (2012).

160 Waldman, A. D., Fritz, J. M. & Lenardo, M. J. A guide to cancer immunotherapy: from T cell basic science to clinical practice. *Nat Rev Immunol*, doi:10.1038/s41577-020-0306-5 (2020).

161 Marin-Acevedo, J. A., Dholaria, B., Soyano, A. E., Knutson, K. L., Chumsri, S. & Lou, Y. Next generation of immune checkpoint therapy in cancer: new developments and challenges. *J Hematol Oncol* **11**, 39, doi:10.1186/s13045-018-0582-8 (2018).

162 Grosso, J. F., Kelleher, C. C., Harris, T. J., Maris, C. H., Hipkiss, E. L., De Marzo, A., Anders, R., Netto, G., Getnet, D., Bruno, T. C., Goldberg, M. V., Pardoll, D. M. & Drake, C. G. LAG-3 regulates CD8+ T cell accumulation and effector function in murine self- and tumor-tolerance systems. *J Clin Invest* **117**, 3383-3392, doi:10.1172/JCI31184 (2007).

163 Huang, C. T., Workman, C. J., Flies, D., Pan, X., Marson, A. L., Zhou, G., Hipkiss, E. L., Ravi, S., Kowalski, J., Levitsky, H. I., Powell, J. D., Pardoll, D. M., Drake, C. G. & Vignali, D. A. Role of LAG-3 in regulatory T cells. *Immunity* **21**, 503-513, doi:10.1016/j.immuni.2004.08.010 (2004).

164 Hemon, P., Jean-Louis, F., Ramgolam, K., Brignone, C., Viguier, M., Bachelez, H., Triebel, F., Charron, D., Aoudjit, F., Al-Daccak, R. & Michel, L. MHC class II engagement by its ligand LAG-3 (CD223) contributes to melanoma resistance to apoptosis. *J Immunol* **186**, 5173-5183, doi:10.4049/jimmunol.1002050 (2011).

165 Blackburn, S. D., Shin, H., Haining, W. N., Zou, T., Workman, C. J., Polley, A., Betts, M. R., Freeman, G. J., Vignali, D. A. & Wherry, E. J. Coregulation of CD8+ T cell exhaustion by multiple inhibitory receptors during chronic viral infection. *Nat Immunol* **10**, 29-37, doi:10.1038/ni.1679 (2009).

166 Grosso, J. F., Goldberg, M. V., Getnet, D., Bruno, T. C., Yen, H. R., Pyle, K. J., Hipkiss, E., Vignali, D. A., Pardoll, D. M. & Drake, C. G. Functionally distinct LAG-3 and PD-1 subsets on activated and chronically stimulated CD8 T cells. *J Immunol* **182**, 6659-6669, doi:10.4049/jimmunol.0804211 (2009).

167 Woo, S. R., Turnis, M. E., Goldberg, M. V., Bankoti, J., Selby, M., Nirschl, C. J., Bettini, M. L., Gravano, D. M., Vogel, P., Liu, C. L., Tangsombatvisit, S., Grosso, J. F., Netto, G., Smeltzer, M. P., Chaux, A., Utz, P. J., Workman, C. J., Pardoll, D. M., Korman, A. J., Drake, C. G. & Vignali, D. A. Immune inhibitory molecules LAG-3 and PD-1 synergistically regulate T-cell function to promote tumoral immune escape. *Cancer Res* **72**, 917-927, doi:10.1158/0008-5472.CAN-11-1620 (2012).

168 Fourcade, J., Sun, Z., Pagliano, O., Guillaume, P., Luescher, I. F., Sander, C., Kirkwood, J. M., Olive, D., Kuchroo, V. & Zarour, H. M. CD8(+) T cells specific for tumor antigens can be rendered dysfunctional by the tumor microenvironment through upregulation of the inhibitory receptors BTLA and PD-1. *Cancer Res* **72**, 887-896, doi:10.1158/0008-5472.CAN-11-2637 (2012).

169 Jin, H. T., Anderson, A. C., Tan, W. G., West, E. E., Ha, S. J., Araki, K., Freeman, G. J., Kuchroo, V. K. & Ahmed, R. Cooperation of Tim-3 and PD-1 in CD8 T-cell exhaustion during chronic viral infection. *Proc Natl Acad Sci U S A* **107**, 14733-14738, doi:10.1073/pnas.1009731107 (2010).

170 Johnston, R. J., Comps-Agrar, L., Hackney, J., Yu, X., Huseni, M., Yang, Y., Park, S., Javinal, V., Chiu, H., Irving, B., Eaton, D. L. & Grogan, J. L. The immunoreceptor TIGIT regulates antitumor and antiviral CD8(+) T cell effector function. *Cancer Cell* **26**, 923-937, doi:10.1016/j.ccell.2014.10.018 (2014).

171 Wang, B., Zhang, W., Jankovic, V., Golubov, J., Poon, P., Oswald, E. M., Gurer, C., Wei, J., Ramos, I., Wu, Q., Waite, J., Ni, M., Adler, C., Wei, Y., Macdonald, L., Rowlands, T., Brydges, S., Siao, J., Poueymirou, W., MacDonald, D., Yancopoulos, G. D., Sleeman, M. A., Murphy, A. J. & Skokos, D. Combination cancer immunotherapy targeting PD-1 and GITR can rescue CD8(+) T cell dysfunction and maintain memory phenotype. *Sci Immunol* **3**, doi:10.1126/sciimmunol.aat7061 (2018).

172 Sanmamed, M. F., Pastor, F., Rodriguez, A., Perez-Gracia, J. L., Rodriguez-Ruiz, M. E., Jure-Kunkel, M. & Melero, I. Agonists of Co-stimulation in Cancer Immunotherapy Directed Against CD137, OX40, GITR, CD27, CD28, and ICOS. *Semin Oncol* **42**, 640-655, doi:10.1053/j.seminoncol.2015.05.014 (2015).

173 Vezys, V., Penaloza-MacMaster, P., Barber, D. L., Ha, S. J., Konieczny, B., Freeman, G. J., Mittler, R. S. & Ahmed, R. 4-1BB signaling synergizes with programmed death ligand 1 blockade to augment CD8 T cell responses during chronic viral infection. *J Immunol* **187**, 1634-1642, doi:10.4049/jimmunol.1100077 (2011).

174 Liakou, C. I., Kamat, A., Tang, D. N., Chen, H., Sun, J., Troncoso, P., Logothetis, C. & Sharma, P. CTLA-4 blockade increases IFNgamma-producing CD4+ICOShi cells to shift the ratio of effector to regulatory T cells in cancer patients. *Proc Natl Acad Sci U S A* **105**, 14987-14992, doi:10.1073/pnas.0806075105 (2008).

175 Riley, J. L., Blair, P. J., Musser, J. T., Abe, R., Tezuka, K., Tsuji, T. & June, C. H. ICOS costimulation requires IL-2 and can be prevented by CTLA-4 engagement. *J Immunol* **166**, 4943-4948, doi:10.4049/jimmunol.166.8.4943 (2001).

176 Thorsson, V., Gibbs, D. L., Brown, S. D., Wolf, D., Bortone, D. S., Ou Yang, T. H., Porta-Pardo, E., Gao, G. F., Plaisier, C. L., Eddy, J. A., Ziv, E., Culhane, A. C., Paull, E. O., Sivakumar, I. K. A., Gentles, A. J., Malhotra, R., Farshidfar, F., Colaprico, A., Parker, J. S., Mose, L. E., Vo, N. S., Liu, J., Liu, Y., Rader, J., Dhankani, V., Reynolds, S. M., Bowlby, R., Califano, A., Cherniack, A. D., Anastassiou, D., Bedognetti, D., Mokrab, Y., Newman, A. M., Rao, A., Chen, K., Krasnitz, A., Hu, H., Malta, T. M., Noushmehr, H., Pedamallu, C. S., Bullman, S., Ojesina, A. I., Lamb, A., Zhou, W., Shen, H., Choueiri, T. K., Weinstein, J. N., Guinney, J., Saltz, J., Holt, R. A., Rabkin, C. S., Cancer Genome Atlas Research, N., Lazar, A. J., Serody, J. S., Demicco, E. G., Disis, M. L., Vincent, B. G. & Shmulevich, I. The Immune Landscape of Cancer. *Immunity* **48**, 812-830 e814, doi:10.1016/j.immuni.2018.03.023 (2018).

177 Ilieva, K. M., Correa, I., Josephs, D. H., Karagiannis, P., Egbuniwe, I. U., Cafferkey, M. J., Spicer, J. F., Harries, M., Nestle, F. O., Lacy, K. E. & Karagiannis, S. N. Effects of BRAF mutations and BRAF inhibition on immune responses to melanoma. *Mol Cancer Ther* **13**, 2769-2783, doi:10.1158/1535-7163.MCT-14-0290 (2014).

178 Wolchok, J. D., Kluger, H., Callahan, M. K., Postow, M. A., Rizvi, N. A., Lesokhin, A. M., Segal, N. H., Ariyan, C. E., Gordon, R. A., Reed, K., Burke, M. M., Caldwell, A., Kronenberg, S. A., Agunwamba, B. U., Zhang, X., Lowy, I., Inzunza, H. D., Feely, W., Horak, C. E., Hong, Q., Korman, A. J., Wigginton, J. M., Gupta, A. & Sznol, M. Nivolumab plus ipilimumab in advanced melanoma. *N Engl J Med* **369**, 122-133, doi:10.1056/NEJMoa1302369 (2013).

179 Liu, J., Lichtenberg, T., Hoadley, K. A., Poisson, L. M., Lazar, A. J., Cherniack, A. D., Kovatich, A. J., Benz, C. C., Levine, D. A., Lee, A. V., Omberg, L., Wolf, D. M., Shriver, C. D., Thorsson, V., Cancer Genome Atlas Research, N. & Hu, H. An Integrated TCGA Pan-Cancer Clinical Data Resource to Drive High-Quality Survival Outcome Analytics. *Cell* **173**, 400-416 e411, doi:10.1016/j.cell.2018.02.052 (2018).

180 Rizvi, N. A., Hellmann, M. D., Snyder, A., Kvistborg, P., Makarov, V., Havel, J. J., Lee, W., Yuan, J., Wong, P., Ho, T. S., Miller, M. L., Rekhtman, N., Moreira, A. L., Ibrahim, F., Bruggeman, C., Gasmi, B., Zappasodi, R., Maeda, Y., Sander, C., Garon, E. B., Merghoub, T., Wolchok, J. D., Schumacher, T. N. & Chan, T. A. Cancer immunology. Mutational landscape determines sensitivity to PD-1 blockade in non-small cell lung cancer. *Science* **348**, 124-128, doi:10.1126/science.aaa1348 (2015).

181 Rizvi, H., Sanchez-Vega, F., La, K., Chatila, W., Jonsson, P., Halpenny, D., Plodkowski, A., Long, N., Sauter, J. L., Rekhtman, N., Hollmann, T., Schalper, K. A., Gainor, J. F., Shen, R., Ni, A., Arbour, K. C., Merghoub, T., Wolchok, J., Snyder, A., Chaft, J. E., Kris, M. G., Rudin, C. M., Socci, N. D., Berger, M. F., Taylor, B. S., Zehir, A., Solit, D. B., Arcila, M. E., Ladanyi, M., Riely, G. J., Schultz, N. & Hellmann, M. D. Molecular Determinants of Response to Anti-Programmed Cell Death (PD)-1 and Anti-Programmed Death-Ligand 1 (PD-L1) Blockade in Patients With Non-Small-Cell Lung Cancer Profiled With Targeted Next-Generation Sequencing. *J Clin Oncol* **36**, 633-641, doi:10.1200/JCO.2017.75.3384 (2018).

182 Robbins, P. F., Lu, Y. C., El-Gamil, M., Li, Y. F., Gross, C., Gartner, J., Lin, J. C., Teer, J. K., Cliften, P., Tycksen, E., Samuels, Y. & Rosenberg, S. A. Mining exomic sequencing data to identify mutated antigens recognized by adoptively transferred tumor-reactive T cells. *Nat Med* **19**, 747-752, doi:10.1038/nm.3161 (2013).

183 Castle, J. C., Kreiter, S., Diekmann, J., Lower, M., van de Roemer, N., de Graaf, J., Selmi, A., Diken, M., Boegel, S., Paret, C., Koslowski, M., Kuhn, A. N., Britten, C. M., Huber, C., Tureci, O. & Sahin, U. Exploiting the mutanome for tumor vaccination. *Cancer Res* **72**, 1081-1091, doi:10.1158/0008-5472.CAN-11-3722 (2012).

184 Matsushita, H., Vesely, M. D., Koboldt, D. C., Rickert, C. G., Uppaluri, R., Magrini, V. J., Arthur, C. D., White, J. M., Chen, Y. S., Shea, L. K., Hundal, J., Wendl, M. C., Demeter, R., Wylie, T., Allison, J. P., Smyth, M. J., Old, L. J., Mardis, E. R. & Schreiber, R. D. Cancer exome analysis reveals a T-cell-dependent mechanism of cancer immunoediting. *Nature* **482**, 400-404, doi:10.1038/nature10755 (2012).

185 Chen, B., Khodadoust, M. S., Olsson, N., Wagar, L. E., Fast, E., Liu, C. L., Muftuoglu, Y., Sworder, B. J., Diehn, M., Levy, R., Davis, M. M., Elias, J. E., Altman, R. B. & Alizadeh, A. A. Predicting HLA class II antigen presentation through integrated deep learning. *Nat Biotechnol* **37**, 1332-1343, doi:10.1038/s41587-019-0280-2 (2019).

186 Yadav, M., Jhunjhunwala, S., Phung, Q. T., Lupardus, P., Tanguay, J., Bumbaca, S., Franci, C., Cheung, T. K., Fritsche, J., Weinschenk, T., Modrusan, Z., Mellman, I., Lill, J. R. & Delamarre, L. Predicting immunogenic tumour mutations by combining mass spectrometry and exome sequencing. *Nature* **515**, 572-576, doi:10.1038/nature14001 (2014).

187 Rooney, M. S., Shukla, S. A., Wu, C. J., Getz, G. & Hacohen, N. Molecular and genetic properties of tumors associated with local immune cytolytic activity. *Cell* **160**, 48-61, doi:10.1016/j.cell.2014.12.033 (2015).

188 DuPage, M., Mazumdar, C., Schmidt, L. M., Cheung, A. F. & Jacks, T. Expression of tumour-specific antigens underlies cancer immunoediting. *Nature* **482**, 405-409, doi:10.1038/nature10803 (2012).

189 Vonderheide, R. H. & Nathanson, K. L. Immunotherapy at large: the road to personalized cancer vaccines. *Nat Med* **19**, 1098-1100, doi:10.1038/nm.3317 (2013).

190 Friedlaender, A., Nouspikel, T., Christinat, Y., Ho, L., McKee, T. & Addeo, A. Tissue-Plasma TMB Comparison and Plasma TMB Monitoring in Patients With Metastatic Non-small Cell Lung Cancer Receiving Immune Checkpoint Inhibitors. *Front Oncol* **10**, 142, doi:10.3389/fonc.2020.00142 (2020).

191 San Lucas, F. A., Allenson, K., Bernard, V., Castillo, J., Kim, D. U., Ellis, K., Ehli, E. A., Davies, G. E., Petersen, J. L., Li, D., Wolff, R., Katz, M., Varadhachary, G., Wistuba, I., Maitra, A. & Alvarez, H. Minimally invasive genomic and transcriptomic profiling of visceral cancers by next-generation sequencing of circulating exosomes. *Ann Oncol* **27**, 635-641, doi:10.1093/annonc/mdv604 (2016).

192 Lu, H., Clauser, K. R., Tam, W. L., Frose, J., Ye, X., Eaton, E. N., Reinhardt, F., Donnenberg, V. S., Bhargava, R., Carr, S. A. & Weinberg, R. A. A breast cancer stem cell niche supported by juxtacrine signalling from monocytes and macrophages. *Nat Cell Biol* **16**, 1105-1117, doi:10.1038/ncb3041 (2014).

193 Theate, I., van Baren, N., Pilotte, L., Moulin, P., Larrieu, P., Renauld, J. C., Herve, C., Gutierrez-Roelens, I., Marbaix, E., Sempoux, C. & Van den Eynde, B. J. Extensive profiling of the expression of the indoleamine 2,3-dioxygenase 1 protein in normal and tumoral human tissues. *Cancer Immunol Res* **3**, 161-172, doi:10.1158/2326-6066.CIR-14-0137 (2015).

194 Rodriguez, P. C., Zea, A. H., DeSalvo, J., Culotta, K. S., Zabaleta, J., Quiceno, D. G., Ochoa, J. B. & Ochoa, A. C. L-arginine consumption by macrophages modulates the expression of CD3 zeta chain in T lymphocytes. *J Immunol* **171**, 1232-1239, doi:10.4049/jimmunol.171.3.1232 (2003).

195 Spranger, S., Spaapen, R. M., Zha, Y., Williams, J., Meng, Y., Ha, T. T. & Gajewski, T. F. Up-regulation of PD-L1, IDO, and T(regs) in the melanoma tumor microenvironment is driven by CD8(+) T cells. *Sci Transl Med* **5**, 200ra116, doi:10.1126/scitranslmed.3006504 (2013).

196 Van Allen, E. M., Miao, D., Schilling, B., Shukla, S. A., Blank, C., Zimmer, L., Sucker, A., Hillen, U., Foppen, M. H. G., Goldinger, S. M., Utikal, J., Hassel, J. C., Weide, B., Kaehler, K. C., Loquai, C., Mohr, P., Gutzmer, R., Dummer, R., Gabriel, S., Wu, C. J., Schadendorf, D. & Garraway, L. A. Genomic correlates of response to CTLA-4 blockade in metastatic melanoma. *Science* **350**, 207-211, doi:10.1126/science.aad0095 (2015).

197 Tumeh, P. C., Harview, C. L., Yearley, J. H., Shintaku, I. P., Taylor, E. J., Robert, L., Chmielowski, B., Spasic, M., Henry, G., Ciobanu, V., West, A. N., Carmona, M., Kivork, C., Seja, E., Cherry, G., Gutierrez, A. J., Grogan, T. R., Mateus, C., Tomasic, G., Glaspy, J. A., Emerson, R. O., Robins, H., Pierce, R. H., Elashoff, D. A., Robert, C. &

Ribas, A. PD-1 blockade induces responses by inhibiting adaptive immune resistance. *Nature* **515**, 568-571, doi:10.1038/nature13954 (2014).

198 Liang, Y., Lu, W., Zhang, X. & Lu, B. Tumor-infiltrating CD8+ and FOXP3+ lymphocytes before and after neoadjuvant chemotherapy in cervical cancer. *Diagn Pathol* **13**, 93, doi:10.1186/s13000-018-0770-4 (2018).

199 deLeeuw, R. J., Kost, S. E., Kakal, J. A. & Nelson, B. H. The prognostic value of FoxP3+ tumor-infiltrating lymphocytes in cancer: a critical review of the literature. *Clin Cancer Res* **18**, 3022-3029, doi:10.1158/1078-0432.CCR-11-3216 (2012).

200 Shi, L. Z., Wang, R., Huang, G., Vogel, P., Neale, G., Green, D. R. & Chi, H. HIF1alpha-dependent glycolytic pathway orchestrates a metabolic checkpoint for the differentiation of TH17 and Treg cells. *J Exp Med* **208**, 1367-1376, doi:10.1084/jem.20110278 (2011).

201 Michalek, R. D., Gerriets, V. A., Jacobs, S. R., Macintyre, A. N., MacIver, N. J., Mason, E. F., Sullivan, S. A., Nichols, A. G. & Rathmell, J. C. Cutting edge: distinct glycolytic and lipid oxidative metabolic programs are essential for effector and regulatory CD4+ T cell subsets. *J Immunol* **186**, 3299-3303, doi:10.4049/jimmunol.1003613 (2011).

202 Wang, Y. A., Li, X. L., Mo, Y. Z., Fan, C. M., Tang, L., Xiong, F., Guo, C., Xiang, B., Zhou, M., Ma, J., Huang, X., Wu, X., Li, Y., Li, G. Y., Zeng, Z. Y. & Xiong, W. Effects of tumor metabolic microenvironment on regulatory T cells. *Mol Cancer* **17**, 168, doi:10.1186/s12943-018-0913-y (2018).

203 Liu, D., Schilling, B., Liu, D., Sucker, A., Livingstone, E., Jerby-Arnon, L., Zimmer, L., Gutzmer, R., Satzger, I., Loquai, C., Grabbe, S., Vokes, N., Margolis, C. A., Conway, J., He, M. X., Elmarakeby, H., Dietlein, F., Miao, D., Tracy, A., Gogas, H., Goldinger, S. M., Utikal, J., Blank, C. U., Rauschenberg, R., von Bubnoff, D., Krackhardt, A., Weide, B., Haferkamp, S., Kiecker, F., Izar, B., Garraway, L., Regev, A., Flaherty, K., Paschen, A., Van Allen, E. M. & Schadendorf, D. Integrative molecular and clinical modeling of clinical outcomes to PD1 blockade in patients with metastatic melanoma. *Nat Med* **25**, 1916-1927, doi:10.1038/s41591-019-0654-5 (2019).

204 Sade-Feldman, M., Yizhak, K., Bjorgaard, S. L., Ray, J. P., de Boer, C. G., Jenkins, R. W., Lieb, D. J., Chen, J. H., Frederick, D. T., Barzily-Rokni, M., Freeman, S. S., Reuben, A., Hoover, P. J., Villani, A. C., Ivanova, E., Portell, A., Lizotte, P. H., Aref, A. R., Eliane, J. P., Hammond, M. R., Vitzthum, H., Blackmon, S. M., Li, B., Gopalakrishnan, V., Reddy, S. M., Cooper, Z. A., Paweletz, C. P., Barbie, D. A., Stemmer-Rachamimov, A., Flaherty, K. T., Wargo, J. A., Boland, G. M., Sullivan, R. J., Getz, G. & Hacohen, N. Defining T Cell States Associated with Response to Checkpoint Immunotherapy in Melanoma. *Cell* **175**, 998-1013 e1020, doi:10.1016/j.cell.2018.10.038 (2018).

205 Heidegger, S., Wintges, A., Stritzke, F., Bek, S., Steiger, K., Koenig, P. A., Gottert, S., Engleitner, T., Ollinger, R., Nedelko, T., Fischer, J. C., Makarov, V., Winter, C., Rad, R., van den Brink, M. R. M., Ruland, J., Bassermann, F., Chan, T. A., Haas, T. & Poeck, H.

RIG-I activation is critical for responsiveness to checkpoint blockade. *Sci Immunol* **4**, doi:10.1126/sciimmunol.aau8943 (2019).

206 Pozniak, J., Nsengimana, J., Laye, J. P., O'Shea, S. J., Diaz, J. M. S., Droop, A. P., Filia, A., Harland, M., Davies, J. R., Mell, T., Randerson-Moor, J. A., Muralidhar, S., Hogan, S. A., Freiberger, S. N., Levesque, M. P., Cook, G. P., Bishop, D. T. & Newton-Bishop, J. Genetic and Environmental Determinants of Immune Response to Cutaneous Melanoma. *Cancer Res* **79**, 2684-2696, doi:10.1158/0008-5472.CAN-18-2864 (2019).

207 Wang, H., Hu, S., Chen, X., Shi, H., Chen, C., Sun, L. & Chen, Z. J. cGAS is essential for the antitumor effect of immune checkpoint blockade. *Proc Natl Acad Sci U S A* **114**, 1637-1642, doi:10.1073/pnas.1621363114 (2017).

208 Li, T. & Chen, Z. J. The cGAS-cGAMP-STING pathway connects DNA damage to inflammation, senescence, and cancer. *J Exp Med* **215**, 1287-1299, doi:10.1084/jem.20180139 (2018).

209 Cauwels, A., Van Lint, S., Paul, F., Garcin, G., De Koker, S., Van Parys, A., Wueest, T., Gerlo, S., Van der Heyden, J., Bordat, Y., Catteeuw, D., Rogge, E., Verhee, A., Vandekerckhove, B., Kley, N., Uze, G. & Tavernier, J. Delivering Type I Interferon to Dendritic Cells Empowers Tumor Eradication and Immune Combination Treatments. *Cancer Res* **78**, 463-474, doi:10.1158/0008-5472.CAN-17-1980 (2018).

210 Wen, W. X. & Leong, C. O. Association of BRCA1- and BRCA2-deficiency with mutation burden, expression of PD-L1/PD-1, immune infiltrates, and T cell-inflamed signature in breast cancer. *PLoS One* **14**, e0215381, doi:10.1371/journal.pone.0215381 (2019).

211 Le, D. T., Uram, J. N., Wang, H., Bartlett, B. R., Kemberling, H., Eyring, A. D., Skora, A. D., Luber, B. S., Azad, N. S., Laheru, D., Biedrzycki, B., Donehower, R. C., Zaheer, A., Fisher, G. A., Crocenzi, T. S., Lee, J. J., Duffy, S. M., Goldberg, R. M., de la Chapelle, A., Koshiji, M., Bhaijee, F., Huebner, T., Hruban, R. H., Wood, L. D., Cuka, N., Pardoll, D. M., Papadopoulos, N., Kinzler, K. W., Zhou, S., Cornish, T. C., Taube, J. M., Anders, R. A., Eshleman, J. R., Vogelstein, B. & Diaz, L. A., Jr. PD-1 Blockade in Tumors with Mismatch-Repair Deficiency. *N Engl J Med* **372**, 2509-2520, doi:10.1056/NEJMoa1500596 (2015).

212 Overman, M. J., Lonardi, S., Wong, K. Y. M., Lenz, H. J., Gelsomino, F., Aglietta, M., Morse, M. A., Van Cutsem, E., McDermott, R., Hill, A., Sawyer, M. B., Hendlisz, A., Neyns, B., Svrcek, M., Moss, R. A., Ledeine, J. M., Cao, Z. A., Kamble, S., Kopetz, S. & Andre, T. Durable Clinical Benefit With Nivolumab Plus Ipilimumab in DNA Mismatch Repair-Deficient/Microsatellite Instability-High Metastatic Colorectal Cancer. *J Clin Oncol* **36**, 773-779, doi:10.1200/JCO.2017.76.9901 (2018).

213 Sinicrope, F. A. Lynch Syndrome-Associated Colorectal Cancer. *N Engl J Med* **379**, 764-773, doi:10.1056/NEJMcp1714533 (2018).

214 Zhang, T., Yu, H., Ni, C., Zhang, T., Liu, L., Lv, Q., Zhang, Z., Wang, Z., Wu, D., Wu, P., Chen, G., Wang, L., Wei, Q., Huang, J. & Wang, X. Hypofractionated stereotactic radiation therapy activates the peripheral immune response in operable stage I non-small-cell lung cancer. *Sci Rep* **7**, 4866, doi:10.1038/s41598-017-04978-x (2017).

215 Galluzzi, L., Buque, A., Kepp, O., Zitvogel, L. & Kroemer, G. Immunological Effects of Conventional Chemotherapy and Targeted Anticancer Agents. *Cancer Cell* **28**, 690-714, doi:10.1016/j.ccell.2015.10.012 (2015).

216 Pfirschke, C., Engblom, C., Rickelt, S., Cortez-Retamozo, V., Garris, C., Pucci, F., Yamazaki, T., Poirier-Colame, V., Newton, A., Redouane, Y., Lin, Y. J., Wojtkiewicz, G., Iwamoto, Y., Mino-Kenudson, M., Huynh, T. G., Hynes, R. O., Freeman, G. J., Kroemer, G., Zitvogel, L., Weissleder, R. & Pittet, M. J. Immunogenic Chemotherapy Sensitizes Tumors to Checkpoint Blockade Therapy. *Immunity* **44**, 343-354, doi:10.1016/j.immuni.2015.11.024 (2016).

217 Ribero, S., Stucci, L. S., Marra, E., Marconcini, R., Spagnolo, F., Orgiano, L., Picasso, V., Queirolo, P., Palmieri, G., Quaglino, P. & Bataille, V. Effect of Age on Melanoma Risk, Prognosis and Treatment Response. *Acta Derm Venereol* **98**, 624-629, doi:10.2340/00015555-2944 (2018).

218 Zhang, Q., Zhao, K., Shen, Q., Han, Y., Gu, Y., Li, X., Zhao, D., Liu, Y., Wang, C., Zhang, X., Su, X., Liu, J., Ge, W., Levine, R. L., Li, N. & Cao, X. Tet2 is required to resolve inflammation by recruiting Hdac2 to specifically repress IL-6. *Nature* **525**, 389-393, doi:10.1038/nature15252 (2015).

219 Jaiswal, S., Natarajan, P., Silver, A. J., Gibson, C. J., Bick, A. G., Shvartz, E., McConkey, M., Gupta, N., Gabriel, S., Ardissino, D., Baber, U., Mehran, R., Fuster, V., Danesh, J., Frossard, P., Saleheen, D., Melander, O., Sukhova, G. K., Neuberg, D., Libby, P., Kathiresan, S. & Ebert, B. L. Clonal Hematopoiesis and Risk of Atherosclerotic Cardiovascular Disease. *N Engl J Med* **377**, 111-121, doi:10.1056/NEJMoa1701719 (2017).

220 Leoni, C., Montagner, S., Rinaldi, A., Bertoni, F., Polletti, S., Balestrieri, C. & Monticelli, S. Dnmt3a restrains mast cell inflammatory responses. *Proc Natl Acad Sci U S A* **114**, E1490-E1499, doi:10.1073/pnas.1616420114 (2017).

221 Sano, S., Oshima, K., Wang, Y., Katanasaka, Y., Sano, M. & Walsh, K. CRISPR-Mediated Gene Editing to Assess the Roles of Tet2 and Dnmt3a in Clonal Hematopoiesis and Cardiovascular Disease. *Circ Res* **123**, 335-341, doi:10.1161/CIRCRESAHA.118.313225 (2018).

222 Souquette, A., Frere, J., Smithey, M., Sauce, D. & Thomas, P. G. A constant companion: immune recognition and response to cytomegalovirus with aging and implications for immune fitness. *Geroscience* **39**, 293-303, doi:10.1007/s11357-017-9982-x (2017).

223 Perrotta, F., Rocco, D., Vitiello, F., De Palma, R., Guerra, G., De Luca, A., Navani, N. & Bianco, A. Immune Checkpoint Blockade for Advanced NSCLC: A New Landscape for Elderly Patients. *Int J Mol Sci* **20**, doi:10.3390/ijms20092258 (2019).

224 Ter Horst, R., Jaeger, M., Smeekens, S. P., Oosting, M., Swertz, M. A., Li, Y., Kumar, V., Diavatopoulos, D. A., Jansen, A. F., Lemmers, H., Toenhake-Dijkstra, H., van Herwaarden, A. E., Janssen, M., van der Molen, R. G., Joosten, I., Sweep, F. C., Smit, J. W., Netea-Maier, R. T., Koenders, M. M., Xavier, R. J., van der Meer, J. W., Dinarello, C. A., Pavelka, N., Wijmenga, C., Notebaart, R. A., Joosten, L. A. & Netea, M. G. Host and Environmental Factors Influencing Individual Human Cytokine Responses. *Cell* **167**, 1111-1124 e1113, doi:10.1016/j.cell.2016.10.018 (2016).

225 Aguirre-Gamboa, R., Joosten, I., Urbano, P. C. M., van der Molen, R. G., van Rijssen, E., van Cranenbroek, B., Oosting, M., Smeekens, S., Jaeger, M., Zorro, M., Withoff, S., van Herwaarden, A. E., Sweep, F., Netea, R. T., Swertz, M. A., Franke, L., Xavier, R. J., Joosten, L. A. B., Netea, M. G., Wijmenga, C., Kumar, V., Li, Y. & Koenen, H. Differential Effects of Environmental and Genetic Factors on T and B Cell Immune Traits. *Cell Rep* **17**, 2474-2487, doi:10.1016/j.celrep.2016.10.053 (2016).

226 Stojan, G. & Petri, M. Epidemiology of systemic lupus erythematosus: an update. *Curr Opin Rheumatol* **30**, 144-150, doi:10.1097/BOR.0000000000000480 (2018).

227 Brito-Zeron, P., Kostov, B., Superville, D., Baughman, R. P., Ramos-Casals, M. & Autoimmune Big Data Study, G. Geoepidemiological big data approach to sarcoidosis: geographical and ethnic determinants. *Clin Exp Rheumatol* **37**, 1052-1064 (2019).

228 Simoni, Y., Becht, E., Fehlings, M., Loh, C. Y., Koo, S. L., Teng, K. W. W., Yeong, J. P. S., Nahar, R., Zhang, T., Kared, H., Duan, K., Ang, N., Poidinger, M., Lee, Y. Y., Larbi, A., Khng, A. J., Tan, E., Fu, C., Mathew, R., Teo, M., Lim, W. T., Toh, C. K., Ong, B. H., Koh, T., Hillmer, A. M., Takano, A., Lim, T. K. H., Tan, E. H., Zhai, W., Tan, D. S. W., Tan, I. B. & Newell, E. W. Bystander CD8(+) T cells are abundant and phenotypically distinct in human tumour infiltrates. *Nature* **557**, 575-579, doi:10.1038/s41586-018-0130-2 (2018).

229 Eckl-Dorna, J., Villazala-Merino, S., Linhart, B., Karaulov, A. V., Zhernov, Y., Khaitov, M., Niederberger-Leppin, V. & Valenta, R. Allergen-Specific Antibodies Regulate Secondary Allergen-Specific Immune Responses. *Front Immunol* **9**, 3131, doi:10.3389/fimmu.2018.03131 (2018).

230 Brahmer, J. R., Lacchetti, C., Schneider, B. J., Atkins, M. B., Brassil, K. J., Caterino, J. M., Chau, I., Ernstoff, M. S., Gardner, J. M., Ginex, P., Hallmeyer, S., Holter Chakrabarty, J., Leighl, N. B., Mammen, J. S., McDermott, D. F., Naing, A., Nastoupil, L. J., Phillips, T., Porter, L. D., Puzanov, I., Reichner, C. A., Santomasso, B. D., Seigel, C., Spira, A., Suarez-Almazor, M. E., Wang, Y., Weber, J. S., Wolchok, J. D., Thompson, J. A. & National Comprehensive Cancer, N. Management of Immune-Related Adverse

Events in Patients Treated With Immune Checkpoint Inhibitor Therapy: American Society of Clinical Oncology Clinical Practice Guideline. *J Clin Oncol* **36**, 1714-1768, doi:10.1200/JCO.2017.77.6385 (2018).

231 Curry, J. L., Reuben, A., Szczepaniak-Sloane, R., Ning, J., Milton, D. R., Lee, C. H., Hudgens, C., George, S., Torres-Cabala, C., Johnson, D., Subramanya, S., Wargo, J. A., Mudaliar, K., Wistuba, II, Prieto, V. G., Diab, A. & Tetzlaff, M. T. Gene expression profiling of lichenoid dermatitis immune-related adverse event from immune checkpoint inhibitors reveals increased CD14(+) and CD16(+) monocytes driving an innate immune response. *J Cutan Pathol* **46**, 627-636, doi:10.1111/cup.13454 (2019).

232 Yamamoto, N., Homma, S. & Millman, I. Identification of the serum factor required for in vitro activation of macrophages. Role of vitamin D3-binding protein (group specific component, Gc) in lysophospholipid activation of mouse peritoneal macrophages. *J Immunol* **147**, 273-280 (1991).

233 Sigmundsdottir, H., Pan, J., Debes, G. F., Alt, C., Habtezion, A., Soler, D. & Butcher, E. C. DCs metabolize sunlight-induced vitamin D3 to 'program' T cell attraction to the epidermal chemokine CCL27. *Nat Immunol* **8**, 285-293, doi:10.1038/ni1433 (2007).

234 Chen, S., Sims, G. P., Chen, X. X., Gu, Y. Y., Chen, S. & Lipsky, P. E. Modulatory effects of 1,25-dihydroxyvitamin D3 on human B cell differentiation. *J Immunol* **179**, 1634-1647, doi:10.4049/jimmunol.179.3.1634 (2007).

235 Lemire, J. M., Adams, J. S., Sakai, R. & Jordan, S. C. 1 alpha,25-dihydroxyvitamin D3 suppresses proliferation and immunoglobulin production by normal human peripheral blood mononuclear cells. *J Clin Invest* **74**, 657-661, doi:10.1172/JCI111465 (1984).

236 Rigby, W. F., Stacy, T. & Fanger, M. W. Inhibition of T lymphocyte mitogenesis by 1,25-dihydroxyvitamin D3 (calcitriol). *J Clin Invest* **74**, 1451-1455, doi:10.1172/JCI111557 (1984).

237 Muller, K. & Bendtzen, K. Inhibition of human T lymphocyte proliferation and cytokine production by 1,25-dihydroxyvitamin D3. Differential effects on CD45RA+ and CD45R0+ cells. *Autoimmunity* **14**, 37-43, doi:10.3109/08916939309077355 (1992).

238 Gorman, S., Kuritzky, L. A., Judge, M. A., Dixon, K. M., McGlade, J. P., Mason, R. S., Finlay-Jones, J. J. & Hart, P. H. Topically applied 1,25-dihydroxyvitamin D3 enhances the suppressive activity of CD4+CD25+ cells in the draining lymph nodes. *J Immunol* **179**, 6273-6283, doi:10.4049/jimmunol.179.9.6273 (2007).

239 Penna, G., Roncari, A., Amuchastegui, S., Daniel, K. C., Berti, E., Colonna, M. & Adorini, L. Expression of the inhibitory receptor ILT3 on dendritic cells is dispensable for induction of CD4+Foxp3+ regulatory T cells by 1,25-dihydroxyvitamin D3. *Blood* **106**, 3490-3497, doi:10.1182/blood-2005-05-2044 (2005).

240 Penna, G. & Adorini, L. 1 Alpha,25-dihydroxyvitamin D3 inhibits differentiation, maturation, activation, and survival of dendritic cells leading to impaired alloreactive T cell activation. *J Immunol* **164**, 2405-2411, doi:10.4049/jimmunol.164.5.2405 (2000).

241 Griffin, M. D., Lutz, W., Phan, V. A., Bachman, L. A., McKean, D. J. & Kumar, R. Dendritic cell modulation by 1alpha,25 dihydroxyvitamin D3 and its analogs: a vitamin D receptor-dependent pathway that promotes a persistent state of immaturity in vitro and in vivo. *Proc Natl Acad Sci U S A* **98**, 6800-6805, doi:10.1073/pnas.121172198 (2001).

242 Sun, N. Y., Chen, Y. L., Wu, W. Y., Lin, H. W., Chiang, Y. C., Chang, C. F., Tai, Y. J., Hsu, H. C., Chen, C. A., Sun, W. Z. & Cheng, W. F. Blockade of PD-L1 Enhances Cancer Immunotherapy by Regulating Dendritic Cell Maturation and Macrophage Polarization. *Cancers (Basel)* **11**, doi:10.3390/cancers11091400 (2019).

243 Vetizou, M., Pitt, J. M., Daillere, R., Lepage, P., Waldschmitt, N., Flament, C., Rusakiewicz, S., Routy, B., Roberti, M. P., Duong, C. P., Poirier-Colame, V., Roux, A., Becharef, S., Formenti, S., Golden, E., Cording, S., Eberl, G., Schlitzer, A., Ginhoux, F., Mani, S., Yamazaki, T., Jacquelot, N., Enot, D. P., Berard, M., Nigou, J., Opolon, P., Eggermont, A., Woerther, P. L., Chachaty, E., Chaput, N., Robert, C., Mateus, C., Kroemer, G., Raoult, D., Boneca, I. G., Carbonnel, F., Chamaillard, M. & Zitvogel, L. Anticancer immunotherapy by CTLA-4 blockade relies on the gut microbiota. *Science* **350**, 1079-1084, doi:10.1126/science.aad1329 (2015).

244 Gopalakrishnan, V., Spencer, C. N., Nezi, L., Reuben, A., Andrews, M. C., Karpinets, T. V., Prieto, P. A., Vicente, D., Hoffman, K., Wei, S. C., Cogdill, A. P., Zhao, L., Hudgens, C. W., Hutchinson, D. S., Manzo, T., Petaccia de Macedo, M., Cotechini, T., Kumar, T., Chen, W. S., Reddy, S. M., Szczepaniak Sloane, R., Galloway-Pena, J., Jiang, H., Chen, P. L., Shpall, E. J., Rezvani, K., Alousi, A. M., Chemaly, R. F., Shelburne, S., Vence, L. M., Okhuysen, P. C., Jensen, V. B., Swennes, A. G., McAllister, F., Marcelo Riquelme Sanchez, E., Zhang, Y., Le Chatelier, E., Zitvogel, L., Pons, N., Austin-Breneman, J. L., Haydu, L. E., Burton, E. M., Gardner, J. M., Sirmans, E., Hu, J., Lazar, A. J., Tsujikawa, T., Diab, A., Tawbi, H., Glitza, I. C., Hwu, W. J., Patel, S. P., Woodman, S. E., Amaria, R. N., Davies, M. A., Gershenwald, J. E., Hwu, P., Lee, J. E., Zhang, J., Coussens, L. M., Cooper, Z. A., Futreal, P. A., Daniel, C. R., Ajami, N. J., Petrosino, J. F., Tetzlaff, M. T., Sharma, P., Allison, J. P., Jenq, R. R. & Wargo, J. A. Gut microbiome modulates response to anti-PD-1 immunotherapy in melanoma patients. *Science* **359**, 97-103, doi:10.1126/science.aan4236 (2018).

245 Routy, B., Le Chatelier, E., Derosa, L., Duong, C. P. M., Alou, M. T., Daillere, R., Fluckiger, A., Messaoudene, M., Rauber, C., Roberti, M. P., Fidelle, M., Flament, C., Poirier-Colame, V., Opolon, P., Klein, C., Iribarren, K., Mondragon, L., Jacquelot, N., Qu, B., Ferrere, G., Clemenson, C., Mezquita, L., Masip, J. R., Naltet, C., Brosseau, S., Kaderbhai, C., Richard, C., Rizvi, H., Levenez, F., Galleron, N., Quinquis, B., Pons, N., Ryffel, B., Minard-Colin, V., Gonin, P., Soria, J. C., Deutsch, E., Loriot, Y., Ghiringhelli, F., Zalcman, G., Goldwasser, F., Escudier, B., Hellmann, M. D., Eggermont, A., Raoult, D., Albiges, L., Kroemer, G. & Zitvogel, L. Gut microbiome influences efficacy of PD-1-

based immunotherapy against epithelial tumors. *Science* **359**, 91-97, doi:10.1126/science.aan3706 (2018).

246 Matson, V., Fessler, J., Bao, R., Chongsuwat, T., Zha, Y., Alegre, M. L., Luke, J. J. & Gajewski, T. F. The commensal microbiome is associated with anti-PD-1 efficacy in metastatic melanoma patients. *Science* **359**, 104-108, doi:10.1126/science.aao3290 (2018).

247 Brennan, C. A. & Garrett, W. S. Gut Microbiota, Inflammation, and Colorectal Cancer. *Annu Rev Microbiol* **70**, 395-411, doi:10.1146/annurev-micro-102215-095513 (2016).

248 Ma, C., Han, M., Heinrich, B., Fu, Q., Zhang, Q., Sandhu, M., Agdashian, D., Terabe, M., Berzofsky, J. A., Fako, V., Ritz, T., Longerich, T., Theriot, C. M., McCulloch, J. A., Roy, S., Yuan, W., Thovarai, V., Sen, S. K., Ruchirawat, M., Korangy, F., Wang, X. W., Trinchieri, G. & Greten, T. F. Gut microbiome-mediated bile acid metabolism regulates liver cancer via NKT cells. *Science* **360**, doi:10.1126/science.aan5931 (2018).

249 Favara, D. M., Spain, L., Au, L., Clark, J., Daniels, E., Diem, S., Chauhan, D., Turajlic, S., Powell, N., Larkin, J. M. & Yousaf, N. Five-year review of corticosteroid duration and complications in the management of immune checkpoint inhibitor-related diarrhoea and colitis in advanced melanoma. *ESMO Open* **5**, doi:10.1136/esmoopen-2019-000585 (2020).

250 Verheijden, R. J., May, A. M., Blank, C. U., Aarts, M. J. B., van den Berkmortel, F., van den Eertwegh, A. J. M., de Groot, J. W. B., Boers-Sonderen, M. J., van der Hoeven, J. J. M., Hospers, G. A., Piersma, D., van Rijn, R. S., Ten Tije, A. J., van der Veldt, A. A. M., Vreugdenhil, G., van Zeijl, M. C. T., Wouters, M., Haanen, J., Kapiteijn, E. & Suijkerbuijk, K. P. M. Association of Anti-TNF with Decreased Survival in Steroid Refractory Ipilimumab and Anti-PD1-Treated Patients in the Dutch Melanoma Treatment Registry. *Clin Cancer Res* **26**, 2268-2274, doi:10.1158/1078-0432.CCR-19-3322 (2020).

251 Oh, D. Y., Cham, J., Zhang, L., Fong, G., Kwek, S. S., Klinger, M., Faham, M. & Fong, L. Immune Toxicities Elicted by CTLA-4 Blockade in Cancer Patients Are Associated with Early Diversification of the T-cell Repertoire. *Cancer Res* **77**, 1322-1330, doi:10.1158/0008-5472.CAN-16-2324 (2017).

252 Dubin, K., Callahan, M. K., Ren, B., Khanin, R., Viale, A., Ling, L., No, D., Gobourne, A., Littmann, E., Huttenhower, C., Pamer, E. G. & Wolchok, J. D. Intestinal microbiome analyses identify melanoma patients at risk for checkpoint-blockade-induced colitis. *Nat Commun* **7**, 10391, doi:10.1038/ncomms10391 (2016).

253 Wang, Y., Wiesnoski, D. H., Helmink, B. A., Gopalakrishnan, V., Choi, K., DuPont, H. L., Jiang, Z. D., Abu-Sbeih, H., Sanchez, C. A., Chang, C. C., Parra, E. R., Francisco-Cruz, A., Raju, G. S., Stroehlein, J. R., Campbell, M. T., Gao, J., Subudhi, S. K., Maru, D. M., Blando, J. M., Lazar, A. J., Allison, J. P., Sharma, P., Tetzlaff, M. T., Wargo, J. A. &

Jenq, R. R. Fecal microbiota transplantation for refractory immune checkpoint inhibitor-associated colitis. *Nat Med* **24**, 1804-1808, doi:10.1038/s41591-018-0238-9 (2018).

254 Turner, J. G., Rakhmilevich, A. L., Burdelya, L., Neal, Z., Imboden, M., Sondel, P. M. & Yu, H. Anti-CD40 antibody induces antitumor and antimetastatic effects: the role of NK cells. *J Immunol* **166**, 89-94, doi:10.4049/jimmunol.166.1.89 (2001).

255 Long, G. V., Dummer, R., Hamid, O., Gajewski, T. F., Caglevic, C., Dalle, S., Arance, A., Carlino, M. S., Grob, J. J., Kim, T. M., Demidov, L., Robert, C., Larkin, J., Anderson, J. R., Maleski, J., Jones, M., Diede, S. J. & Mitchell, T. C. Epacadostat plus pembrolizumab versus placebo plus pembrolizumab in patients with unresectable or metastatic melanoma (ECHO-301/KEYNOTE-252): a phase 3, randomised, double-blind study. *Lancet Oncol* **20**, 1083-1097, doi:10.1016/S1470-2045(19)30274-8 (2019).

256 Takahara, N., Kashiwagi, A., Nishio, Y., Harada, N., Kojima, H., Maegawa, H., Hidaka, H. & Kikkawa, R. Oxidized lipoproteins found in patients with NIDDM stimulate radical-induced monocyte chemoattractant protein-1 mRNA expression in cultured human endothelial cells. *Diabetologia* **40**, 662-670, doi:10.1007/s001250050731 (1997).

257 Chang, C. H., Qiu, J., O'Sullivan, D., Buck, M. D., Noguchi, T., Curtis, J. D., Chen, Q., Gindin, M., Gubin, M. M., van der Windt, G. J., Tonc, E., Schreiber, R. D., Pearce, E. J. & Pearce, E. L. Metabolic Competition in the Tumor Microenvironment Is a Driver of Cancer Progression. *Cell* **162**, 1229-1241, doi:10.1016/j.cell.2015.08.016 (2015).

258 Buck, M. D., Sowell, R. T., Kaech, S. M. & Pearce, E. L. Metabolic Instruction of Immunity. *Cell* **169**, 570-586, doi:10.1016/j.cell.2017.04.004 (2017).

259 Geiger, R., Rieckmann, J. C., Wolf, T., Basso, C., Feng, Y., Fuhrer, T., Kogadeeva, M., Picotti, P., Meissner, F., Mann, M., Zamboni, N., Sallusto, F. & Lanzavecchia, A. L-Arginine Modulates T Cell Metabolism and Enhances Survival and Anti-tumor Activity. *Cell* **167**, 829-842 e813, doi:10.1016/j.cell.2016.09.031 (2016).

260 Szefel, J., Danielak, A. & Kruszewski, W. J. Metabolic pathways of L-arginine and therapeutic consequences in tumors. *Adv Med Sci* **64**, 104-110, doi:10.1016/j.advms.2018.08.018 (2019).

261 Steggerda, S. M., Bennett, M. K., Chen, J., Emberley, E., Huang, T., Janes, J. R., Li, W., MacKinnon, A. L., Makkouk, A., Marguier, G., Murray, P. J., Neou, S., Pan, A., Parlati, F., Rodriguez, M. L. M., Van de Velde, L. A., Wang, T., Works, M., Zhang, J., Zhang, W. & Gross, M. I. Inhibition of arginase by CB-1158 blocks myeloid cell-mediated immune suppression in the tumor microenvironment. *J Immunother Cancer* **5**, 101, doi:10.1186/s40425-017-0308-4 (2017).

262 Munn, D. H., Shafizadeh, E., Attwood, J. T., Bondarev, I., Pashine, A. & Mellor, A. L. Inhibition of T cell proliferation by macrophage tryptophan catabolism. *J Exp Med* **189**, 1363-1372, doi:10.1084/jem.189.9.1363 (1999).

263 Belladonna, M. L., Puccetti, P., Orabona, C., Fallarino, F., Vacca, C., Volpi, C., Gizzi, S., Pallotta, M. T., Fioretti, M. C. & Grohmann, U. Immunosuppression via tryptophan catabolism: the role of kynurenine pathway enzymes. *Transplantation* **84**, S17-20, doi:10.1097/01.tp.0000269199.16209.22 (2007).

264 DiNatale, B. C., Murray, I. A., Schroeder, J. C., Flaveny, C. A., Lahoti, T. S., Laurenzana, E. M., Omiecinski, C. J. & Perdew, G. H. Kynurenic acid is a potent endogenous aryl hydrocarbon receptor ligand that synergistically induces interleukin-6 in the presence of inflammatory signaling. *Toxicol Sci* **115**, 89-97, doi:10.1093/toxsci/kfq024 (2010).

265 Mezrich, J. D., Fechner, J. H., Zhang, X., Johnson, B. P., Burlingham, W. J. & Bradfield, C. A. An interaction between kynurenine and the aryl hydrocarbon receptor can generate regulatory T cells. *J Immunol* **185**, 3190-3198, doi:10.4049/jimmunol.0903670 (2010).

266 Nguyen, N. T., Kimura, A., Nakahama, T., Chinen, I., Masuda, K., Nohara, K., Fujii-Kuriyama, Y. & Kishimoto, T. Aryl hydrocarbon receptor negatively regulates dendritic cell immunogenicity via a kynurenine-dependent mechanism. *Proc Natl Acad Sci U S A* **107**, 19961-19966, doi:10.1073/pnas.1014465107 (2010).

267 Pearce, E. L., Walsh, M. C., Cejas, P. J., Harms, G. M., Shen, H., Wang, L. S., Jones, R. G. & Choi, Y. Enhancing CD8 T-cell memory by modulating fatty acid metabolism. *Nature* **460**, 103-107, doi:10.1038/nature08097 (2009).

268 Araki, K., Turner, A. P., Shaffer, V. O., Gangappa, S., Keller, S. A., Bachmann, M. F., Larsen, C. P. & Ahmed, R. mTOR regulates memory CD8 T-cell differentiation. *Nature* **460**, 108-112, doi:10.1038/nature08155 (2009).

269 Chowdhury, P. S., Chamoto, K., Kumar, A. & Honjo, T. PPAR-Induced Fatty Acid Oxidation in T Cells Increases the Number of Tumor-Reactive CD8(+) T Cells and Facilitates Anti-PD-1 Therapy. *Cancer Immunol Res* **6**, 1375-1387, doi:10.1158/2326-6066.CIR-18-0095 (2018).

270 Dennis, E. A. & Norris, P. C. Eicosanoid storm in infection and inflammation. *Nat Rev Immunol* **15**, 511-523, doi:10.1038/nri3859 (2015).

271 Auch-Schwelk, W., Katusic, Z. S. & Vanhoutte, P. M. Thromboxane A2 receptor antagonists inhibit endothelium-dependent contractions. *Hypertension* **15**, 699-703, doi:10.1161/01.hyp.15.6.699 (1990).

272 Moncada, S., Herman, A. G., Higgs, E. A. & Vane, J. R. Differential formation of prostacyclin (PGX or PGI2) by layers of the arterial wall. An explanation for the anti-thrombotic properties of vascular endothelium. *Thromb Res* **11**, 323-344, doi:10.1016/0049-3848(77)90185-2 (1977).

273 Norris, P. C., Gosselin, D., Reichart, D., Glass, C. K. & Dennis, E. A. Phospholipase A2 regulates eicosanoid class switching during inflammasome activation. *Proc Natl Acad Sci U S A* **111**, 12746-12751, doi:10.1073/pnas.1404372111 (2014).

274 Morimoto, K., Shirata, N., Taketomi, Y., Tsuchiya, S., Segi-Nishida, E., Inazumi, T., Kabashima, K., Tanaka, S., Murakami, M., Narumiya, S. & Sugimoto, Y. Prostaglandin E2-EP3 signaling induces inflammatory swelling by mast cell activation. *J Immunol* **192**, 1130-1137, doi:10.4049/jimmunol.1300290 (2014).

275 Chan, M. M. & Moore, A. R. Resolution of inflammation in murine autoimmune arthritis is disrupted by cyclooxygenase-2 inhibition and restored by prostaglandin E2-mediated lipoxin A4 production. *J Immunol* **184**, 6418-6426, doi:10.4049/jimmunol.0903816 (2010).

276 Levy, B. D., Clish, C. B., Schmidt, B., Gronert, K. & Serhan, C. N. Lipid mediator class switching during acute inflammation: signals in resolution. *Nat Immunol* **2**, 612-619, doi:10.1038/89759 (2001).

277 Laidlaw, T. M. & Boyce, J. A. Aspirin-Exacerbated Respiratory Disease--New Prime Suspects. *N Engl J Med* **374**, 484-488, doi:10.1056/NEJMcibr1514013 (2016).

278 Lammermann, T., Afonso, P. V., Angermann, B. R., Wang, J. M., Kastenmuller, W., Parent, C. A. & Germain, R. N. Neutrophil swarms require LTB4 and integrins at sites of cell death in vivo. *Nature* **498**, 371-375, doi:10.1038/nature12175 (2013).

279 Huang, J. T., Welch, J. S., Ricote, M., Binder, C. J., Willson, T. M., Kelly, C., Witztum, J. L., Funk, C. D., Conrad, D. & Glass, C. K. Interleukin-4-dependent production of PPAR-gamma ligands in macrophages by 12/15-lipoxygenase. *Nature* **400**, 378-382, doi:10.1038/22572 (1999).

280 Samuelsson, B. Leukotrienes: mediators of immediate hypersensitivity reactions and inflammation. *Science* **220**, 568-575, doi:10.1126/science.6301011 (1983).

281 Harmon, G. S., Dumlao, D. S., Ng, D. T., Barrett, K. E., Dennis, E. A., Dong, H. & Glass, C. K. Pharmacological correction of a defect in PPAR-gamma signaling ameliorates disease severity in Cftr-deficient mice. *Nat Med* **16**, 313-318, doi:10.1038/nm.2101 (2010).

282 Zelenay, S., van der Veen, A. G., Bottcher, J. P., Snelgrove, K. J., Rogers, N., Acton, S. E., Chakravarty, P., Girotti, M. R., Marais, R., Quezada, S. A., Sahai, E. & Reis e Sousa, C. Cyclooxygenase-Dependent Tumor Growth through Evasion of Immunity. *Cell* **162**, 1257-1270, doi:10.1016/j.cell.2015.08.015 (2015).

283 Coulombe, F., Jaworska, J., Verway, M., Tzelepis, F., Massoud, A., Gillard, J., Wong, G., Kobinger, G., Xing, Z., Couture, C., Joubert, P., Fritz, J. H., Powell, W. S. & Divangahi, M. Targeted prostaglandin E2 inhibition enhances antiviral immunity through induction of type I interferon and apoptosis in macrophages. *Immunity* **40**, 554-568, doi:10.1016/j.immuni.2014.02.013 (2014).

284 Bottcher, J. P., Bonavita, E., Chakravarty, P., Blees, H., Cabeza-Cabrerizo, M., Sammicheli, S., Rogers, N. C., Sahai, E., Zelenay, S. & Reis, E. S. C. NK Cells Stimulate Recruitment of cDC1 into the Tumor Microenvironment Promoting Cancer Immune Control. *Cell* **172**, 1022-1037 e1014, doi:10.1016/j.cell.2018.01.004 (2018).

285 Liu, H., Xiong, X., Zhai, W., Zhu, T., Zhu, X., Zhu, Y., Peng, Y., Zhang, Y., Wang, J., Chen, H., Chen, Y. & Guo, A. Upregulation of Cytokines and Differentiation of Th17 and Treg by Dendritic Cells: Central Role of Prostaglandin E2 Induced by Mycobacterium bovis. *Microorganisms* **8**, doi:10.3390/microorganisms8020195 (2020).

286 Yan, J. J., Jung, J. S., Lee, J. E., Lee, J., Huh, S. O., Kim, H. S., Jung, K. C., Cho, J. Y., Nam, J. S., Suh, H. W., Kim, Y. H. & Song, D. K. Therapeutic effects of lysophosphatidylcholine in experimental sepsis. *Nat Med* **10**, 161-167, doi:10.1038/nm989 (2004).

287 Ojala, P. J., Hirvonen, T. E., Hermansson, M., Somerharju, P. & Parkkinen, J. Acyl chain-dependent effect of lysophosphatidylcholine on human neutrophils. *J Leukoc Biol* **82**, 1501-1509, doi:10.1189/jlb.0507292 (2007).

288 Kabarowski, J. H. G2A and LPC: regulatory functions in immunity. *Prostaglandins Other Lipid Mediat* **89**, 73-81, doi:10.1016/j.prostaglandins.2009.04.007 (2009).

289 Cencioni, M. T., Chiurchiu, V., Catanzaro, G., Borsellino, G., Bernardi, G., Battistini, L. & Maccarrone, M. Anandamide suppresses proliferation and cytokine release from primary human T-lymphocytes mainly via CB2 receptors. *PLoS One* **5**, e8688, doi:10.1371/journal.pone.0008688 (2010).

290 Chiurchiu, V., Leuti, A. & Maccarrone, M. Bioactive Lipids and Chronic Inflammation: Managing the Fire Within. *Front Immunol* **9**, 38, doi:10.3389/fimmu.2018.00038 (2018).

291 Drobnik, W., Liebisch, G., Audebert, F. X., Frohlich, D., Gluck, T., Vogel, P., Rothe, G. & Schmitz, G. Plasma ceramide and lysophosphatidylcholine inversely correlate with mortality in sepsis patients. *J Lipid Res* **44**, 754-761, doi:10.1194/jlr.M200401-JLR200 (2003).

292 El Alwani, M., Wu, B. X., Obeid, L. M. & Hannun, Y. A. Bioactive sphingolipids in the modulation of the inflammatory response. *Pharmacol Ther* **112**, 171-183, doi:10.1016/j.pharmthera.2006.04.004 (2006).

293 Liu, X., Moon, S. H., Jenkins, C. M., Sims, H. F. & Gross, R. W. Cyclooxygenase-2 Mediated Oxidation of 2-Arachidonoyl-Lysophospholipids Identifies Unknown Lipid Signaling Pathways. *Cell Chem Biol* **23**, 1217-1227, doi:10.1016/j.chembiol.2016.08.009 (2016).

294 Stark, G. R. How cells respond to interferons revisited: from early history to current complexity. *Cytokine & growth factor reviews* **18**, 419-423, doi:10.1016/j.cytogfr.2007.06.013 (2007).

295 Wu, J. & Chen, Z. J. Innate immune sensing and signaling of cytosolic nucleic acids. *Annu Rev Immunol* **32**, 461-488, doi:10.1146/annurev-immunol-032713-120156 (2014).

296 Dhanwani, R., Takahashi, M. & Sharma, S. Cytosolic sensing of immuno-stimulatory DNA, the enemy within. *Curr Opin Immunol* **50**, 82-87, doi:10.1016/j.coi.2017.11.004 (2018).

297 Pisetsky, D. S. The origin and properties of extracellular DNA: from PAMP to DAMP. *Clin Immunol* **144**, 32-40, doi:10.1016/j.clim.2012.04.006 (2012).

298 Crow, M. K., Olferiev, M. & Kirou, K. A. Type I Interferons in Autoimmune Disease. *Annu Rev Pathol* **14**, 369-393, doi:10.1146/annurev-pathol-020117-043952 (2019).

299 Lio, C. W., McDonald, B., Takahashi, M., Dhanwani, R., Sharma, N., Huang, J., Pham, E., Benedict, C. A. & Sharma, S. cGAS-STING Signaling Regulates Initial Innate Control of Cytomegalovirus Infection. *J Virol* **90**, 7789-7797, doi:10.1128/JVI.01040-16 (2016).

300 Belot, A., Wassmer, E., Twilt, M., Lega, J. C., Zeef, L. A., Oojageer, A., Kasher, P. R., Mathieu, A. L., Malcus, C., Demaret, J., Fabien, N., Collardeau-Frachon, S., Mechtouff, L., Derex, L., Walzer, T., Rice, G. I., Durieu, I. & Crow, Y. J. Mutations in CECR1 associated with a neutrophil signature in peripheral blood. *Pediatr Rheumatol Online J* **12**, 44, doi:10.1186/1546-0096-12-44 (2014).

301 Zavialov, A. V. & Engstrom, A. Human ADA2 belongs to a new family of growth factors with adenosine deaminase activity. *Biochem J* **391**, 51-57, doi:10.1042/BJ20050683 (2005).

302 Andreasyan, N. A., Hairapetyan, H. L., Sargisova, Y. G. & Mardanyan, S. S. ADA2 isoform of adenosine deaminase from pleural fluid. *FEBS Lett* **579**, 643-647, doi:10.1016/j.febslet.2004.11.109 (2005).

303 Novershtern, N., Subramanian, A., Lawton, L. N., Mak, R. H., Haining, W. N., McConkey, M. E., Habib, N., Yosef, N., Chang, C. Y., Shay, T., Frampton, G. M., Drake, A. C., Leskov, I., Nilsson, B., Preffer, F., Dombkowski, D., Evans, J. W., Liefeld, T., Smutko, J. S., Chen, J., Friedman, N., Young, R. A., Golub, T. R., Regev, A. & Ebert, B. L. Densely interconnected transcriptional circuits control cell states in human hematopoiesis. *Cell* **144**, 296-309, doi:10.1016/j.cell.2011.01.004 (2011).

304 Zhou, Q., Yang, D., Ombrello, A. K., Zavialov, A. V., Toro, C., Zavialov, A. V., Stone, D. L., Chae, J. J., Rosenzweig, S. D., Bishop, K., Barron, K. S., Kuehn, H. S., Hoffmann, P., Negro, A., Tsai, W. L., Cowen, E. W., Pei, W., Milner, J. D., Silvin, C., Heller, T., Chin, D. T., Patronas, N. J., Barber, J. S., Lee, C. C., Wood, G. M., Ling, A., Kelly, S. J., Kleiner, D. E., Mullikin, J. C., Ganson, N. J., Kong, H. H., Hambleton, S., Candotti, F., Quezado, M. M., Calvo, K. R., Alao, H., Barham, B. K., Jones, A., Meschia, J. F., Worrall, B. B., Kasner, S. E., Rich, S. S., Goldbach-Mansky, R., Abinun, M., Chalom, E., Gotte, A. C., Punaro, M., Pascual, V., Verbsky, J. W., Torgerson, T. R., Singer, N. G., Gershon, T. R., Ozen, S., Karadag, O., Fleisher, T. A., Remmers, E. F., Burgess, S. M., Moir, S. L., Gadina, M., Sood, R., Hershfield, M. S., Boehm, M., Kastner, D. L. & Aksentijevich, I. Early-onset stroke and vasculopathy associated with mutations in ADA2. *The New England journal of medicine* **370**, 911-920, doi:10.1056/NEJMoa1307361 (2014).

305 Zavialov, A. V., Yu, X., Spillmann, D., Lauvau, G. & Zavialov, A. V. Structural basis for the growth factor activity of human adenosine deaminase ADA2. *The Journal of biological chemistry* **285**, 12367-12377, doi:10.1074/jbc.M109.083527 (2010).

306 Lee, P. Y., Huang, Z., Hershfield, M. S. & Nigrovic, P. A. Analysis of peripheral blood ADA1 and ADA2 levels in children and adults. Response to: 'Total adenosine deaminase highly correlated with adenosine deaminase 2 activity in serum' by Gao et al. *Ann Rheum Dis*, doi:10.1136/annrheumdis-2020-217055 (2020).

307 Linden, J., Koch-Nolte, F. & Dahl, G. Purine Release, Metabolism, and Signaling in the Inflammatory Response. *Annu Rev Immunol* **37**, 325-347, doi:10.1146/annurev-immunol-051116-052406 (2019).

308 Szabados, E., Duggleby, R. G. & Christopherson, R. I. Metabolism of adenosine and deoxyadenosine by human erythrocytes and CCRF-CEM leukemia cells. *Int J Biochem Cell Biol* **28**, 1405-1415, doi:10.1016/s1357-2725(96)00080-5 (1996).

309 Smolenski, R. T., Kochan, Z., McDouall, R., Seymour, A. M. & Yacoub, M. H. Adenosine uptake and metabolism in human endothelial cells. *Adv Exp Med Biol* **370**, 435-438, doi:10.1007/978-1-4615-2584-4_94 (1994).

310 Jain, M., Nilsson, R., Sharma, S., Madhusudhan, N., Kitami, T., Souza, A. L., Kafri, R., Kirschner, M. W., Clish, C. B. & Mootha, V. K. Metabolite profiling identifies a key role for glycine in rapid cancer cell proliferation. *Science* **336**, 1040-1044, doi:10.1126/science.1218595 (2012).

311 Williams-Karnesky, R. L., Sandau, U. S., Lusardi, T. A., Lytle, N. K., Farrell, J. M., Pritchard, E. M., Kaplan, D. L. & Boison, D. Epigenetic changes induced by adenosine augmentation therapy prevent epileptogenesis. *J Clin Invest* **123**, 3552-3563, doi:10.1172/JCI65636 (2013).

312 Nilsson, R. & Jain, M. Simultaneous tracing of carbon and nitrogen isotopes in human cells. *Molecular bioSystems* **12**, 1929-1937, doi:10.1039/c6mb00009f (2016).

313 Huang, L., Kim, D., Liu, X., Myers, C. R. & Locasale, J. W. Estimating relative changes of metabolic fluxes. *PLoS Comput Biol* **10**, e1003958, doi:10.1371/journal.pcbi.1003958 (2014).

314 Chiappinelli, K. B., Strissel, P. L., Desrichard, A., Li, H., Henke, C., Akman, B., Hein, A., Rote, N. S., Cope, L. M., Snyder, A., Makarov, V., Budhu, S., Slamon, D. J., Wolchok, J. D., Pardoll, D. M., Beckmann, M. W., Zahnow, C. A., Merghoub, T., Chan, T. A., Baylin, S. B. & Strick, R. Inhibiting DNA Methylation Causes an Interferon Response in Cancer via dsRNA Including Endogenous Retroviruses. *Cell* **164**, 1073, doi:10.1016/j.cell.2015.10.020 (2016).

315 Canadas, I., Thummalapalli, R., Kim, J. W., Kitajima, S., Jenkins, R. W., Christensen, C. L., Campisi, M., Kuang, Y., Zhang, Y., Gjini, E., Zhang, G., Tian, T., Sen, D. R., Miao, D., Imamura, Y., Thai, T., Piel, B., Terai, H., Aref, A. R., Hagan, T., Koyama, S., Watanabe, M., Baba, H., Adeni, A. E., Lydon, C. A., Tamayo, P., Wei, Z., Herlyn, M., Barbie, T. U., Uppaluri, R., Sholl, L. M., Sicinska, E., Sands, J., Rodig, S., Wong, K. K., Paweletz, C. P., Watanabe, H. & Barbie, D. A. Tumor innate immunity primed by specific interferon-stimulated endogenous retroviruses. *Nat Med* **24**, 1143-1150, doi:10.1038/s41591-018-0116-5 (2018).

316 Gao, Z. W., Wang, X., Lin, F. & Dong, K. Total adenosine deaminase highly correlated with adenosine deaminase 2 activity in serum. *Ann Rheum Dis*, doi:10.1136/annrheumdis-2020-217007 (2020).

317 Khodadadi, I., Abdi, M., Ahmadi, A., Wahedi, M. S., Menbari, S., Lahoorpour, F. & Rahbari, R. Analysis of serum adenosine deaminase (ADA) and ADA1 and ADA2 isoenzyme activities in HIV positive and HIV-HBV co-infected patients. *Clin Biochem* **44**, 980-983, doi:10.1016/j.clinbiochem.2011.05.020 (2011).

318 Fernandez, E., Rodrigo, L., Riestra, S., Carcia, S., Gutierrez, F. & Ocio, G. Adenosine deaminase isoenzymes and neopterin in liver cirrhosis. *J Clin Gastroenterol* **30**, 181-186, doi:10.1097/00004836-200003000-00011 (2000).

319 Valadbeigi, S., Saghiri, R., Ebrahimi-Rad, M., Khatami, S. & Akhbari, H. Adenosine Deaminase Activity and HLA-DRB as Diagnostic Markers for Rheumatoid Arthritis. *Curr Rheumatol Rev* **15**, 44-49, doi:10.2174/1573397114666180406101239 (2019).

320 Ungerer, J. P., Oosthuizen, H. M., Retief, J. H. & Bissbort, S. H. Significance of adenosine deaminase activity and its isoenzymes in tuberculous effusions. *Chest* **106**, 33-37, doi:10.1378/chest.106.1.33 (1994).

321 Iwaki-Egawa, S., Yamamoto, T. & Watanabe, Y. Human plasma adenosine deaminase 2 is secreted by activated monocytes. *Biol Chem* **387**, 319-321, doi:10.1515/BC.2006.042 (2006).

322 Dale, N. & Frenguelli, B. G. Release of adenosine and ATP during ischemia and epilepsy. *Curr Neuropharmacol* **7**, 160-179, doi:10.2174/157015909789152146 (2009).

323 Sollevi, A. Cardiovascular effects of adenosine in man; possible clinical implications. *Prog Neurobiol* **27**, 319-349, doi:10.1016/0301-0082(86)90005-5 (1986).

324 Surendran, A., Aliani, M. & Ravandi, A. Metabolomic characterization of myocardial ischemia-reperfusion injury in ST-segment elevation myocardial infarction patients undergoing percutaneous coronary intervention. *Sci Rep* **9**, 11742, doi:10.1038/s41598-019-48227-9 (2019).

325 McDonough, A., Lee, R. V., Noor, S., Lee, C., Le, T., Iorga, M., Phillips, J. L. H., Murphy, S., Moller, T. & Weinstein, J. R. Ischemia/Reperfusion Induces Interferon-Stimulated Gene Expression in Microglia. *J Neurosci* **37**, 8292-8308, doi:10.1523/JNEUROSCI.0725-17.2017 (2017).

326 Vaupel, P. & Mayer, A. Hypoxia-Driven Adenosine Accumulation: A Crucial Microenvironmental Factor Promoting Tumor Progression. *Adv Exp Med Biol* **876**, 177-183, doi:10.1007/978-1-4939-3023-4_22 (2016).

327 Keyel, P. A. Dnases in health and disease. *Dev Biol* **429**, 1-11, doi:10.1016/j.ydbio.2017.06.028 (2017).

328 Carmona-Rivera, C., Khaznadar, S. S., Shwin, K. W., Irizarry-Caro, J. A., O'Neil, L. J., Liu, Y., Jacobson, K. A., Ombrello, A. K., Stone, D. L., Tsai, W. L., Kastner, D. L., Aksentijevich, I., Kaplan, M. J. & Grayson, P. C. Deficiency of adenosine deaminase 2 triggers adenosine-mediated NETosis and TNF production in patients with DADA2. *Blood* **134**, 395-406, doi:10.1182/blood.2018892752 (2019).

329 Barnes, B. J., Adrover, J. M., Baxter-Stoltzfus, A., Borczuk, A., Cools-Lartigue, J., Crawford, J. M., Dassler-Plenker, J., Guerci, P., Huynh, C., Knight, J. S., Loda, M., Looney, M. R., McAllister, F., Rayes, R., Renaud, S., Rousseau, S., Salvatore, S., Schwartz, R. E., Spicer, J. D., Yost, C. C., Weber, A., Zuo, Y. & Egeblad, M. Targeting potential drivers of COVID-19: Neutrophil extracellular traps. *The Journal of experimental medicine* **217**, doi:10.1084/jem.20200652 (2020).

330 Navon Elkan, P., Pierce, S. B., Segel, R., Walsh, T., Barash, J., Padeh, S., Zlotogorski, A., Berkun, Y., Press, J. J., Mukamel, M., Voth, I., Hashkes, P. J., Harel, L., Hoffer, V., Ling, E., Yalcinkaya, F., Kasapcopur, O., Lee, M. K., Klevit, R. E., Renbaum, P., Weinberg-Shukron, A., Sener, E. F., Schormair, B., Zeligson, S., Marek-Yagel, D., Strom, T. M., Shohat, M., Singer, A., Rubinow, A., Pras, E., Winkelmann, J., Tekin, M., Anikster, Y., King, M. C. & Levy-Lahad, E. Mutant adenosine deaminase 2 in a polyarteritis nodosa vasculopathy. *The New England journal of medicine* **370**, 921-931, doi:10.1056/NEJMoa1307362 (2014).

331 Markert, M. L. Purine nucleoside phosphorylase deficiency. *Immunodefic Rev* **3**, 45-81 (1991).

332 Ghodke-Puranik, Y., Dorschner, J. M., Vsetecka, D. M., Amin, S., Makol, A., Ernste, F., Osborn, T., Moder, K., Chowdhary, V., Eliopoulos, E., Zervou, M. I., Goulielmos, G. N., Jensen, M. A. & Niewold, T. B. Lupus-Associated Functional Polymorphism in PNP Causes Cell Cycle Abnormalities and Interferon Pathway Activation in Human Immune Cells. *Arthritis Rheumatol* **69**, 2328-2337, doi:10.1002/art.40304 (2017).

333 Ombrello, A. K., Qin, J., Hoffmann, P. M., Kumar, P., Stone, D., Jones, A., Romeo, T., Barham, B., Pinto-Patarroyo, G., Toro, C., Soldatos, A., Zhou, Q., Deuitch, N., Aksentijevich, I., Sheldon, S. L., Kelly, S., Man, A., Barron, K., Hershfield, M., Flegel, W. A. & Kastner, D. L. Treatment Strategies for Deficiency of Adenosine Deaminase 2. *The New England journal of medicine* **380**, 1582-1584, doi:10.1056/NEJMc1801927 (2019).

334 Yarilina, A. & Ivashkiv, L. B. Type I interferon: a new player in TNF signaling. *Curr Dir Autoimmun* **11**, 94-104, doi:10.1159/000289199 (2010).

335 Wang, N., Liang, H. & Zen, K. Molecular mechanisms that influence the macrophage m1-m2 polarization balance. *Frontiers in immunology* **5**, 614, doi:10.3389/fimmu.2014.00614 (2014).

336 Antoniewicz, M. R., Kelleher, J. K. & Stephanopoulos, G. Determination of confidence intervals of metabolic fluxes estimated from stable isotope measurements. *Metab Eng* **8**, 324-337, doi:10.1016/j.ymben.2006.01.004 (2006).

337 Postow, M. A., Sidlow, R. & Hellmann, M. D. Immune-Related Adverse Events Associated with Immune Checkpoint Blockade. *N Engl J Med* **378**, 158-168, doi:10.1056/NEJMra1703481 (2018).

338 Fennell, D. A., Summers, Y., Cadranel, J., Benepal, T., Christoph, D. C., Lal, R., Das, M., Maxwell, F., Visseren-Grul, C. & Ferry, D. Cisplatin in the modern era: The backbone of first-line chemotherapy for non-small cell lung cancer. *Cancer Treat Rev* **44**, 42-50, doi:10.1016/j.ctrv.2016.01.003 (2016).

339 Wilson, M. A. & Schuchter, L. M. Chemotherapy for Melanoma. *Cancer Treat Res* **167**, 209-229, doi:10.1007/978-3-319-22539-5_8 (2016).

340 Hellmann, M. D., Paz-Ares, L., Bernabe Caro, R., Zurawski, B., Kim, S. W., Carcereny Costa, E., Park, K., Alexandru, A., Lupinacci, L., de la Mora Jimenez, E., Sakai, H., Albert, I., Vergnenegre, A., Peters, S., Syrigos, K., Barlesi, F., Reck, M., Borghaei, H., Brahmer, J. R., O'Byrne, K. J., Geese, W. J., Bhagavatheeswaran, P., Rabindran, S. K., Kasinathan, R. S., Nathan, F. E. & Ramalingam, S. S. Nivolumab plus Ipilimumab in Advanced Non-Small-Cell Lung Cancer. *N Engl J Med*, doi:10.1056/NEJMoa1910231 (2019).

341 Krieg, C., Nowicka, M., Guglietta, S., Schindler, S., Hartmann, F. J., Weber, L. M., Dummer, R., Robinson, M. D., Levesque, M. P. & Becher, B. High-dimensional single-cell analysis predicts response to anti-PD-1 immunotherapy. *Nat Med* **24**, 144-153, doi:10.1038/nm.4466 (2018).

342 Goodman, A. M., Kato, S., Bazhenova, L., Patel, S. P., Frampton, G. M., Miller, V., Stephens, P. J., Daniels, G. A. & Kurzrock, R. Tumor Mutational Burden as an Independent Predictor of Response to Immunotherapy in Diverse Cancers. *Mol Cancer Ther* **16**, 2598-2608, doi:10.1158/1535-7163.MCT-17-0386 (2017).

343 Jacquelot, N., Roberti, M. P., Enot, D. P., Rusakiewicz, S., Ternes, N., Jegou, S., Woods, D. M., Sodre, A. L., Hansen, M., Meirow, Y., Sade-Feldman, M., Burra, A., Kwek, S. S., Flament, C., Messaoudene, M., Duong, C. P. M., Chen, L., Kwon, B. S., Anderson, A. C., Kuchroo, V. K., Weide, B., Aubin, F., Borg, C., Dalle, S., Beatrix, O., Ayyoub, M., Balme, B., Tomasic, G., Di Giacomo, A. M., Maio, M., Schadendorf, D., Melero, I., Dreno, B., Khammari, A., Dummer, R., Levesque, M., Koguchi, Y., Fong, L., Lotem, M., Baniyash, M., Schmidt, H., Svane, I. M., Kroemer, G., Marabelle, A., Michiels, S., Cavalcanti, A., Smyth, M. J., Weber, J. S., Eggermont, A. M. & Zitvogel, L. Predictors of responses to immune checkpoint blockade in advanced melanoma. *Nat Commun* **8**, 592, doi:10.1038/s41467-017-00608-2 (2017).

344 Topalian, S. L., Taube, J. M., Anders, R. A. & Pardoll, D. M. Mechanism-driven biomarkers to guide immune checkpoint blockade in cancer therapy. *Nat Rev Cancer* **16**, 275-287, doi:10.1038/nrc.2016.36 (2016).

345 Hodi, F. S., Chesney, J., Pavlick, A. C., Robert, C., Grossmann, K. F., McDermott, D. F., Linette, G. P., Meyer, N., Giguere, J. K., Agarwala, S. S., Shaheen, M., Ernstoff, M. S., Minor, D. R., Salama, A. K., Taylor, M. H., Ott, P. A., Horak, C., Gagnier, P., Jiang, J., Wolchok, J. D. & Postow, M. A. Combined nivolumab and ipilimumab versus ipilimumab alone in patients with advanced melanoma: 2-year overall survival outcomes in a multicentre, randomised, controlled, phase 2 trial. *Lancet Oncol* **17**, 1558-1568, doi:10.1016/S1470-2045(16)30366-7 (2016).

346 Watrous, J. D., Niiranen, T. J., Lagerborg, K. A., Henglin, M., Xu, Y. J., Rong, J., Sharma, S., Vasan, R. S., Larson, M. G., Armando, A., Mora, S., Quehenberger, O.,

Dennis, E. A., Cheng, S. & Jain, M. Directed Non-targeted Mass Spectrometry and Chemical Networking for Discovery of Eicosanoids and Related Oxylipins. *Cell Chem Biol* **26**, 433-442 e434, doi:10.1016/j.chembiol.2018.11.015 (2019).

347 Reinke, S. N., Gallart-Ayala, H., Gomez, C., Checa, A., Fauland, A., Naz, S., Kamleh, M. A., Djukanovic, R., Hinks, T. S. & Wheelock, C. E. Metabolomics analysis identifies different metabotypes of asthma severity. *Eur Respir J* **49**, doi:10.1183/13993003.01740-2016 (2017).

348 Takemura, M., Niimi, A., Matsumoto, H., Ueda, T., Yamaguchi, M., Matsuoka, H., Jinnai, M., Chung, K. F. & Mishima, M. Imbalance of endogenous prostanoids in moderate-to-severe asthma. *Allergol Int* **66**, 83-88, doi:10.1016/j.alit.2016.05.013 (2017).

349 Zhou, W., Goleniewska, K., Zhang, J., Dulek, D. E., Toki, S., Lotz, M. T., Newcomb, D. C., Boswell, M. G., Polosukhin, V. V., Milne, G. L., Wu, P., Moore, M. L., FitzGerald, G. A. & Peebles, R. S., Jr. Cyclooxygenase inhibition abrogates aeroallergen-induced immune tolerance by suppressing prostaglandin I2 receptor signaling. *J Allergy Clin Immunol* **134**, 698-705 e695, doi:10.1016/j.jaci.2014.06.004 (2014).

350 Maier, N. K., Leppla, S. H. & Moayeri, M. The cyclopentenone prostaglandin 15d-PGJ2 inhibits the NLRP1 and NLRP3 inflammasomes. *J Immunol* **194**, 2776-2785, doi:10.4049/jimmunol.1401611 (2015).

351 Ward-Caviness, C. K., Xu, T., Aspelund, T., Thorand, B., Montrone, C., Meisinger, C., Dunger-Kaltenbach, I., Zierer, A., Yu, Z., Helgadottir, I. R., Harris, T. B., Launer, L. J., Ganna, A., Lind, L., Eiriksdottir, G., Waldenberger, M., Prehn, C., Suhre, K., Illig, T., Adamski, J., Ruepp, A., Koenig, W., Gudnason, V., Emilsson, V., Wang-Sattler, R. & Peters, A. Improvement of myocardial infarction risk prediction via inflammation-associated metabolite biomarkers. *Heart* **103**, 1278-1285, doi:10.1136/heartjnl-2016-310789 (2017).

352 Patrono, C. & Baigent, C. Nonsteroidal anti-inflammatory drugs and the heart. *Circulation* **129**, 907-916, doi:10.1161/CIRCULATIONAHA.113.004480 (2014).

353 Arriola, E., Wheater, M. J., Warrier, A., Karydis, I. & Ottensmeier, C. H. H. Evaluation of the impact of infliximab use for the treatment of ipilimumab related diarrhoea on the outcome of patients with advanced melanoma. *Journal of Clinical Oncology* **33**, 9045-9045, doi:10.1200/jco.2015.33.15_suppl.9045 (2015).

354 Weber, J. S., Kahler, K. C. & Hauschild, A. Management of immune-related adverse events and kinetics of response with ipilimumab. *J Clin Oncol* **30**, 2691-2697, doi:10.1200/JCO.2012.41.6750 (2012).

355 Lagerborg, K. A., Watrous, J. D., Cheng, S. & Jain, M. High-Throughput Measure of Bioactive Lipids Using Non-targeted Mass Spectrometry. *Methods Mol Biol* **1862**, 17-35, doi:10.1007/978-1-4939-8769-6_2 (2019).

356 Watrous, J., Roach, P., Alexandrov, T., Heath, B. S., Yang, J. Y., Kersten, R. D., van der Voort, M., Pogliano, K., Gross, H., Raaijmakers, J. M., Moore, B. S., Laskin, J., Bandeira, N. & Dorrestein, P. C. Mass spectral molecular networking of living microbial colonies. *Proc Natl Acad Sci U S A* **109**, E1743-1752, doi:10.1073/pnas.1203689109 (2012).

357 Moolenaar, W. H. & Hla, T. SnapShot: Bioactive lysophospholipids. *Cell* **148**, 378-378 e372, doi:10.1016/j.cell.2012.01.013 (2012).

358 Eisenhauer, E. A., Therasse, P., Bogaerts, J., Schwartz, L. H., Sargent, D., Ford, R., Dancey, J., Arbuck, S., Gwyther, S., Mooney, M., Rubinstein, L., Shankar, L., Dodd, L., Kaplan, R., Lacombe, D. & Verweij, J. New response evaluation criteria in solid tumours: revised RECIST guideline (version 1.1). *Eur J Cancer* **45**, 228-247, doi:10.1016/j.ejca.2008.10.026 (2009).

359 Law, S. H., Chan, M. L., Marathe, G. K., Parveen, F., Chen, C. H. & Ke, L. Y. An Updated Review of Lysophosphatidylcholine Metabolism in Human Diseases. *Int J Mol Sci* **20**, doi:10.3390/ijms20051149 (2019).

360 Sevastou, I., Kaffe, E., Mouratis, M. A. & Aidinis, V. Lysoglycerophospholipids in chronic inflammatory disorders: the PLA(2)/LPC and ATX/LPA axes. *Biochim Biophys Acta* **1831**, 42-60, doi:10.1016/j.bbalip.2012.07.019 (2013).

361 Lu, L., Hu, C., Zhao, Y., He, L., Zhou, J., Li, H., Du, Y., Wang, Y., Wen, C., Han, X. & Fan, Y. Shotgun Lipidomics Revealed Altered Profiles of Serum Lipids in Systemic Lupus Erythematosus Closely Associated with Disease Activity. *Biomolecules* **8**, doi:10.3390/biom8040105 (2018).

362 Floegel, A., Stefan, N., Yu, Z., Muhlenbruch, K., Drogan, D., Joost, H. G., Fritsche, A., Haring, H. U., Hrabe de Angelis, M., Peters, A., Roden, M., Prehn, C., Wang-Sattler, R., Illig, T., Schulze, M. B., Adamski, J., Boeing, H. & Pischon, T. Identification of serum metabolites associated with risk of type 2 diabetes using a targeted metabolomic approach. *Diabetes* **62**, 639-648, doi:10.2337/db12-0495 (2013).

363 Wang-Sattler, R., Yu, Z., Herder, C., Messias, A. C., Floegel, A., He, Y., Heim, K., Campillos, M., Holzapfel, C., Thorand, B., Grallert, H., Xu, T., Bader, E., Huth, C., Mittelstrass, K., Doring, A., Meisinger, C., Gieger, C., Prehn, C., Roemisch-Margl, W., Carstensen, M., Xie, L., Yamanaka-Okumura, H., Xing, G., Ceglarek, U., Thiery, J., Giani, G., Lickert, H., Lin, X., Li, Y., Boeing, H., Joost, H. G., de Angelis, M. H., Rathmann, W., Suhre, K., Prokisch, H., Peters, A., Meitinger, T., Roden, M., Wichmann, H. E., Pischon, T., Adamski, J. & Illig, T. Novel biomarkers for pre-diabetes identified by metabolomics. *Mol Syst Biol* **8**, 615, doi:10.1038/msb.2012.43 (2012).

364 Borodulin, K., Tolonen, H., Jousilahti, P., Jula, A., Juolevi, A., Koskinen, S., Kuulasmaa, K., Laatikainen, T., Mannisto, S., Peltonen, M., Perola, M., Puska, P., Salomaa, V., Sundvall, J., Virtanen, S. M. & Vartiainen, E. Cohort Profile: The National FINRISK Study. *Int J Epidemiol*, doi:10.1093/ije/dyx239 (2017).

365 Bertrand, A., Kostine, M., Barnetche, T., Truchetet, M. E. & Schaeverbeke, T. Immune related adverse events associated with anti-CTLA-4 antibodies: systematic review and meta-analysis. *BMC Med* **13**, 211, doi:10.1186/s12916-015-0455-8 (2015).

366 Campbell, A. M., Herbst, R. S., Gettinger, S. N., Goldberg, S. B., Kluger, H. M., Chiang, A. C., Lilenbaum, R., Schalper, K. A., Sowell, R. T., Kaech, S. M. & Decker, R. H. Final results of a phase I prospective trial evaluating the combination of stereotactic body radiotherapy (SBRT) with concurrent pembrolizumab in patients with metastatic non-small cell lung cancer (NSCLC) or melanoma. *Journal of Clinical Oncology* **36**, 9099-9099, doi:10.1200/JCO.2018.36.15_suppl.9099 (2018).

367 Du, X., Liu, M., Su, J., Zhang, P., Tang, F., Ye, P., Devenport, M., Wang, X., Zhang, Y., Liu, Y. & Zheng, P. Uncoupling therapeutic from immunotherapy-related adverse effects for safer and effective anti-CTLA-4 antibodies in CTLA4 humanized mice. *Cell Res*, doi:10.1038/s41422-018-0012-z (2018).

368 Chassaing, B., Aitken, J. D., Malleshappa, M. & Vijay-Kumar, M. Dextran sulfate sodium (DSS)-induced colitis in mice. *Curr Protoc Immunol* **104**, Unit 15 25, doi:10.1002/0471142735.im1525s104 (2014).

369 Poritz, L. S., Garver, K. I., Green, C., Fitzpatrick, L., Ruggiero, F. & Koltun, W. A. Loss of the tight junction protein ZO-1 in dextran sulfate sodium induced colitis. *J Surg Res* **140**, 12-19, doi:10.1016/j.jss.2006.07.050 (2007).

370 Okayasu, I., Hatakeyama, S., Yamada, M., Ohkusa, T., Inagaki, Y. & Nakaya, R. A novel method in the induction of reliable experimental acute and chronic ulcerative colitis in mice. *Gastroenterology* **98**, 694-702, doi:10.1016/0016-5085(90)90290-h (1990).

371 Perez-Ruiz, E., Minute, L., Otano, I., Alvarez, M., Ochoa, M. C., Belsue, V., de Andrea, C., Rodriguez-Ruiz, M. E., Perez-Gracia, J. L., Marquez-Rodas, I., Llacer, C., Alvarez, M., de Luque, V., Molina, C., Teijeira, A., Berraondo, P. & Melero, I. Prophylactic TNF blockade uncouples efficacy and toxicity in dual CTLA-4 and PD-1 immunotherapy. *Nature* **569**, 428-432, doi:10.1038/s41586-019-1162-y (2019).

372 Wang, F., Yin, Q., Chen, L. & Davis, M. M. Bifidobacterium can mitigate intestinal immunopathology in the context of CTLA-4 blockade. *Proc Natl Acad Sci U S A* **115**, 157-161, doi:10.1073/pnas.1712901115 (2018).

373 Dieleman, L. A., Ridwan, B. U., Tennyson, G. S., Beagley, K. W., Bucy, R. P. & Elson, C. O. Dextran sulfate sodium-induced colitis occurs in severe combined immunodeficient mice. *Gastroenterology* **107**, 1643-1652, doi:10.1016/0016-5085(94)90803-6 (1994).

374 Chen, C., Shah, Y. M., Morimura, K., Krausz, K. W., Miyazaki, M., Richardson, T. A., Morgan, E. T., Ntambi, J. M., Idle, J. R. & Gonzalez, F. J. Metabolomics reveals that hepatic stearoyl-CoA desaturase 1 downregulation exacerbates inflammation and acute colitis. *Cell Metab* **7**, 135-147, doi:10.1016/j.cmet.2007.12.003 (2008).

375 Li, S., Sullivan, N. L., Rouphael, N., Yu, T., Banton, S., Maddur, M. S., McCausland, M., Chiu, C., Canniff, J., Dubey, S., Liu, K., Tran, V., Hagan, T., Duraisingham, S., Wieland, A., Mehta, A. K., Whitaker, J. A., Subramaniam, S., Jones, D. P., Sette, A., Vora, K., Weinberg, A., Mulligan, M. J., Nakaya, H. I., Levin, M., Ahmed, R. & Pulendran, B. Metabolic Phenotypes of Response to Vaccination in Humans. *Cell* **169**, 862-877 e817, doi:10.1016/j.cell.2017.04.026 (2017).

376 Bakker, O. B., Aguirre-Gamboa, R., Sanna, S., Oosting, M., Smeekens, S. P., Jaeger, M., Zorro, M., Vosa, U., Withoff, S., Netea-Maier, R. T., Koenen, H., Joosten, I., Xavier, R. J., Franke, L., Joosten, L. A. B., Kumar, V., Wijmenga, C., Netea, M. G. & Li, Y. Integration of multi-omics data and deep phenotyping enables prediction of cytokine responses. *Nat Immunol* **19**, 776-786, doi:10.1038/s41590-018-0121-3 (2018).

377 Li, Y., Oosting, M., Smeekens, S. P., Jaeger, M., Aguirre-Gamboa, R., Le, K. T., Deelen, P., Ricano-Ponce, I., Schoffelen, T., Jansen, A. F., Swertz, M. A., Withoff, S., van de Vosse, E., van Deuren, M., van de Veerdonk, F., Zhernakova, A., van der Meer, J. W., Xavier, R. J., Franke, L., Joosten, L. A., Wijmenga, C., Kumar, V. & Netea, M. G. A Functional Genomics Approach to Understand Variation in Cytokine Production in Humans. *Cell* **167**, 1099-1110 e1014, doi:10.1016/j.cell.2016.10.017 (2016).

378 Schalper, K. A., Carleton, M., Zhou, M., Chen, T., Feng, Y., Huang, S. P., Walsh, A. M., Baxi, V., Pandya, D., Baradet, T., Locke, D., Wu, Q., Reilly, T. P., Phillips, P., Nagineni, V., Gianino, N., Gu, J., Zhao, H., Perez-Gracia, J. L., Sanmamed, M. F. & Melero, I. Elevated serum interleukin-8 is associated with enhanced intratumor neutrophils and reduced clinical benefit of immune-checkpoint inhibitors. *Nat Med* **26**, 688-692, doi:10.1038/s41591-020-0856-x (2020).

379 Zhang, J. & Bai, C. Elevated Serum Interleukin-8 Level as a Preferable Biomarker for Identifying Uncontrolled Asthma and Glucocorticosteroid Responsiveness. *Tanaffos* **16**, 260-269 (2017).

380 Kain, V. & Halade, G. V. Role of neutrophils in ischemic heart failure. *Pharmacol Ther* **205**, 107424, doi:10.1016/j.pharmthera.2019.107424 (2020).

381 Rashidi, F., Rashidi, A., Golmohamadi, A., Hoseinzadeh, E., Mohammadi, B., Mirzajani, H., Kheiri, M. & Jamshidi, P. Does absolute neutrophilia predict early congestive heart

failure after acute myocardial infarction? A cross-sectional study. *South Med J* **101**, 19-23, doi:10.1097/SMJ.0b013e31815d3e11 (2008).

382 Franssen, C. F., Huitema, M. G., Muller Kobold, A. C., Oost-Kort, W. W., Limburg, P. C., Tiebosch, A., Stegeman, C. A., Kallenberg, C. G. & Tervaert, J. W. In vitro neutrophil activation by antibodies to proteinase 3 and myeloperoxidase from patients with crescentic glomerulonephritis. *J Am Soc Nephrol* **10**, 1506-1515 (1999).

383 Charles, L. A., Caldas, M. L., Falk, R. J., Terrell, R. S. & Jennette, J. C. Antibodies against granule proteins activate neutrophils in vitro. *J Leukoc Biol* **50**, 539-546, doi:10.1002/jlb.50.6.539 (1991).

384 Lin, P., Welch, E. J., Gao, X. P., Malik, A. B. & Ye, R. D. Lysophosphatidylcholine modulates neutrophil oxidant production through elevation of cyclic AMP. *J Immunol* **174**, 2981-2989, doi:10.4049/jimmunol.174.5.2981 (2005).

385 Pavan, A., Calvetti, L., Dal Maso, A., Attili, I., Del Bianco, P., Pasello, G., Guarneri, V., Aprile, G., Conte, P. & Bonanno, L. Peripheral Blood Markers Identify Risk of Immune-Related Toxicity in Advanced Non-Small Cell Lung Cancer Treated with Immune-Checkpoint Inhibitors. *Oncologist* **24**, 1128-1136, doi:10.1634/theoncologist.2018-0563 (2019).

386 Nakaya, A., Kurata, T., Yoshioka, H., Takeyasu, Y., Niki, M., Kibata, K., Satsutani, N., Ogata, M., Miyara, T. & Nomura, S. Neutrophil-to-lymphocyte ratio as an early marker of outcomes in patients with advanced non-small-cell lung cancer treated with nivolumab. *Int J Clin Oncol* **23**, 634-640, doi:10.1007/s10147-018-1250-2 (2018).

387 Tang, Z., Xiong, D., Song, J., Ye, M., Liu, J., Wang, Z., Zhang, L. & Xiao, X. Antitumor Drug Combretastatin-A4 Phosphate Aggravates the Symptoms of Dextran Sulfate Sodium-Induced Ulcerative Colitis in Mice. *Front Pharmacol* **11**, 339, doi:10.3389/fphar.2020.00339 (2020).

388 Diao, N., Zhang, Y., Chen, K., Yuan, R., Lee, C., Geng, S., Kowalski, E., Guo, W., Xiong, H., Li, M. & Li, L. Deficiency in Toll-interacting protein (Tollip) skews inflamed yet incompetent innate leukocytes in vivo during DSS-induced septic colitis. *Sci Rep* **6**, 34672, doi:10.1038/srep34672 (2016).

389 Frasch, S. C., McNamee, E. N., Kominsky, D., Jedlicka, P., Jakubzick, C., Zemski Berry, K., Mack, M., Furuta, G. T., Lee, J. J., Henson, P. M., Colgan, S. P. & Bratton, D. L. G2A Signaling Dampens Colitic Inflammation via Production of IFN-gamma. *J Immunol* **197**, 1425-1434, doi:10.4049/jimmunol.1600264 (2016).

390 Barber, M. N., Risis, S., Yang, C., Meikle, P. J., Staples, M., Febbraio, M. A. & Bruce, C. R. Plasma lysophosphatidylcholine levels are reduced in obesity and type 2 diabetes. *PLoS One* **7**, e41456, doi:10.1371/journal.pone.0041456 (2012).

391 Kantz, E. D., Tiwari, S., Watrous, J. D., Cheng, S. & Jain, M. Deep Neural Networks for Classification of LC-MS Spectral Peaks. *Anal Chem* **91**, 12407-12413, doi:10.1021/acs.analchem.9b02983 (2019).

392 Krause, P., Zahner, S. P., Kim, G., Shaikh, R. B., Steinberg, M. W. & Kronenberg, M. The tumor necrosis factor family member TNFSF14 (LIGHT) is required for resolution of intestinal inflammation in mice. *Gastroenterology* **146**, 1752-1762 e1754, doi:10.1053/j.gastro.2014.02.010 (2014).

393 Sharma, P. & Allison, J. P. Dissecting the mechanisms of immune checkpoint therapy. *Nat Rev Immunol* **20**, 75-76, doi:10.1038/s41577-020-0275-8 (2020).

394 Amaral, T., Schulze, M., Sinnberg, T., Nieser, M., Martus, P., Battke, F., Garbe, C., Biskup, S. & Forschner, A. Are Pathogenic Germline Variants in Metastatic Melanoma Associated with Resistance to Combined Immunotherapy? *Cancers (Basel)* **12**, doi:10.3390/cancers12051101 (2020).

395 Bremnes, R. M., Busund, L. T., Kilvaer, T. L., Andersen, S., Richardsen, E., Paulsen, E. E., Hald, S., Khanehkenari, M. R., Cooper, W. A., Kao, S. C. & Donnem, T. The Role of Tumor-Infiltrating Lymphocytes in Development, Progression, and Prognosis of Non-Small Cell Lung Cancer. *J Thorac Oncol* **11**, 789-800, doi:10.1016/j.jtho.2016.01.015 (2016).

396 Gide, T. N., Quek, C., Menzies, A. M., Tasker, A. T., Shang, P., Holst, J., Madore, J., Lim, S. Y., Velickovic, R., Wongchenko, M., Yan, Y., Lo, S., Carlino, M. S., Guminski, A., Saw, R. P. M., Pang, A., McGuire, H. M., Palendira, U., Thompson, J. F., Rizos, H., Silva, I. P. D., Batten, M., Scolyer, R. A., Long, G. V. & Wilmott, J. S. Distinct Immune Cell Populations Define Response to Anti-PD-1 Monotherapy and Anti-PD-1/Anti-CTLA-4 Combined Therapy. *Cancer Cell* **35**, 238-255 e236, doi:10.1016/j.ccell.2019.01.003 (2019).

397 Garrett, W. S. Immune recognition of microbial metabolites. *Nat Rev Immunol* **20**, 91-92, doi:10.1038/s41577-019-0252-2 (2020).

398 Chun, E., Lavoie, S., Fonseca-Pereira, D., Bae, S., Michaud, M., Hoveyda, H. R., Fraser, G. L., Gallini Comeau, C. A., Glickman, J. N., Fuller, M. H., Layden, B. T. & Garrett, W. S. Metabolite-Sensing Receptor Ffar2 Regulates Colonic Group 3 Innate Lymphoid Cells and Gut Immunity. *Immunity* **51**, 871-884 e876, doi:10.1016/j.immuni.2019.09.014 (2019).

399 Bachem, A., Makhlouf, C., Binger, K. J., de Souza, D. P., Tull, D., Hochheiser, K., Whitney, P. G., Fernandez-Ruiz, D., Dahling, S., Kastenmuller, W., Jonsson, J., Gressier, E., Lew, A. M., Perdomo, C., Kupz, A., Figgett, W., Mackay, F., Oleshansky, M., Russ, B. E., Parish, I. A., Kallies, A., McConville, M. J., Turner, S. J., Gebhardt, T. & Bedoui, S. Microbiota-Derived Short-Chain Fatty Acids Promote the Memory Potential of

Antigen-Activated CD8(+) T Cells. *Immunity* **51**, 285-297 e285, doi:10.1016/j.immuni.2019.06.002 (2019).

400 Jenkins, B. J., Seyssel, K., Chiu, S., Pan, P. H., Lin, S. Y., Stanley, E., Ament, Z., West, J. A., Summerhill, K., Griffin, J. L., Vetter, W., Autio, K. J., Hiltunen, K., Hazebrouck, S., Stepankova, R., Chen, C. J., Alligier, M., Laville, M., Moore, M., Kraft, G., Cherrington, A., King, S., Krauss, R. M., de Schryver, E., Van Veldhoven, P. P., Ronis, M. & Koulman, A. Odd Chain Fatty Acids; New Insights of the Relationship Between the Gut Microbiota, Dietary Intake, Biosynthesis and Glucose Intolerance. *Sci Rep* **7**, 44845, doi:10.1038/srep44845 (2017).

401 Ramirez-Perez, O., Cruz-Ramon, V., Chinchilla-Lopez, P. & Mendez-Sanchez, N. The Role of the Gut Microbiota in Bile Acid Metabolism. *Ann Hepatol* **16**, s15-s20, doi:10.5604/01.3001.0010.5494 (2017).

402 Jia, W., Xie, G. & Jia, W. Bile acid-microbiota crosstalk in gastrointestinal inflammation and carcinogenesis. *Nat Rev Gastroenterol Hepatol* **15**, 111-128, doi:10.1038/nrgastro.2017.119 (2018).

403 Matern, H. & Matern, S. Formation of bile acid glucosides and dolichyl phosphoglucose by microsomal glucosyltransferases in liver, kidney and intestine of man. *Biochim Biophys Acta* **921**, 1-6, doi:10.1016/0005-2760(87)90163-9 (1987).

404 Matern, H., Fiebig, H. H. & Matern, S. Glycoside conjugation in microsomes from hepatic and renal carcinoma of man. *Hepatology* **7**, 931-936, doi:10.1002/hep.1840070523 (1987).

405 Wietholtz, H., Marschall, H. U., Reuschenbach, R., Matern, H. & Matern, S. Urinary excretion of bile acid glucosides and glucuronides in extrahepatic cholestasis. *Hepatology* **13**, 656-662 (1991).

406 Takeuchi, Y., Tanemura, A., Tada, Y., Katayama, I., Kumanogoh, A. & Nishikawa, H. Clinical response to PD-1 blockade correlates with a sub-fraction of peripheral central memory CD4+ T cells in patients with malignant melanoma. *Int Immunol* **30**, 13-22, doi:10.1093/intimm/dxx073 (2018).

407 Kameyama, Y., Yamashita, K., Kobayashi, K., Hosokawa, M. & Chiba, K. Functional characterization of SLCO1B1 (OATP-C) variants, SLCO1B1*5, SLCO1B1*15 and SLCO1B1*15+C1007G, by using transient expression systems of HeLa and HEK293 cells. *Pharmacogenet Genomics* **15**, 513-522, doi:10.1097/01.fpc.0000170913.73780.5f (2005).

408 Moyer, A. M., de Andrade, M., Faubion, S. S., Kapoor, E., Dudenkov, T., Weinshilboum, R. M. & Miller, V. M. SLCO1B1 genetic variation and hormone therapy in menopausal women. *Menopause* **25**, 877-882, doi:10.1097/GME.0000000000001109 (2018).

409 Xiao, L. & Pan, G. An important intestinal transporter that regulates the enterohepatic circulation of bile acids and cholesterol homeostasis: The apical sodium-dependent bile acid transporter (SLC10A2/ASBT). *Clin Res Hepatol Gastroenterol* **41**, 509-515, doi:10.1016/j.clinre.2017.02.001 (2017).

410 Kemis, J. H., Linke, V., Barrett, K. L., Boehm, F. J., Traeger, L. L., Keller, M. P., Rabaglia, M. E., Schueler, K. L., Stapleton, D. S., Gatti, D. M., Churchill, G. A., Amador-Noguez, D., Russell, J. D., Yandell, B. S., Broman, K. W., Coon, J. J., Attie, A. D. & Rey, F. E. Genetic determinants of gut microbiota composition and bile acid profiles in mice. *PLoS Genet* **15**, e1008073, doi:10.1371/journal.pgen.1008073 (2019).

411 Quezada-Calvillo, R., Sim, L., Ao, Z., Hamaker, B. R., Quaroni, A., Brayer, G. D., Sterchi, E. E., Robayo-Torres, C. C., Rose, D. R. & Nichols, B. L. Luminal starch substrate "brake" on maltase-glucoamylase activity is located within the glucoamylase subunit. *J Nutr* **138**, 685-692, doi:10.1093/jn/138.4.685 (2008).

412 Thul, P. J. & Lindskog, C. The human protein atlas: A spatial map of the human proteome. *Protein Sci* **27**, 233-244, doi:10.1002/pro.3307 (2018).

413 Wu, C., Jin, X., Tsueng, G., Afrasiabi, C. & Su, A. I. BioGPS: building your own mash-up of gene annotations and expression profiles. *Nucleic Acids Res* **44**, D313-316, doi:10.1093/nar/gkv1104 (2016).

414 Lewis, S. S., Hutchinson, M. R., Frick, M. M., Zhang, Y., Maier, S. F., Sammakia, T., Rice, K. C. & Watkins, L. R. Select steroid hormone glucuronide metabolites can cause toll-like receptor 4 activation and enhanced pain. *Brain Behav Immun* **44**, 128-136, doi:10.1016/j.bbi.2014.09.004 (2015).

415 Zucchetti, A. E., Barosso, I. R., Boaglio, A. C., Basiglio, C. L., Miszczuk, G., Larocca, M. C., Ruiz, M. L., Davio, C. A., Roma, M. G., Crocenzi, F. A. & Pozzi, E. J. G-protein-coupled receptor 30/adenylyl cyclase/protein kinase A pathway is involved in estradiol 17ss-D-glucuronide-induced cholestasis. *Hepatology* **59**, 1016-1029, doi:10.1002/hep.26752 (2014).

416 Coldham, N. G., Dave, M., Sivapathasundaram, S., McDonnell, D. P., Connor, C. & Sauer, M. J. Evaluation of a recombinant yeast cell estrogen screening assay. *Environ Health Perspect* **105**, 734-742, doi:10.1289/ehp.97105734 (1997).

417 Palmu, J., Salosensaari, A., Havulinna, A. S., Cheng, S., Inouye, M., Jain, M., Salido, R. A., Sanders, K., Brennan, C., Humphrey, G. C., Sanders, J. G., Vartiainen, E., Laatikainen, T., Jousilahti, P., Salomaa, V., Knight, R., Lahti, L. & Niiranen, T. J. Association Between the Gut Microbiota and Blood Pressure in a Population Cohort of 6953 Individuals. *J Am Heart Assoc*, e016641, doi:10.1161/JAHA.120.016641 (2020).